NARROW LINEWIDTH, DIODE LASER PUMPED, SOLID STATE LASERS

Nigel R. Gallaher

A Thesis Submitted for the Degree of PhD
at the
University of St Andrews

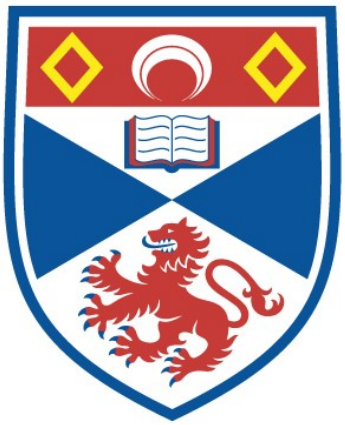

1994

Narrow Linewidth, Diode Laser Pumped, Solid State Lasers

Thesis submitted for the degree of Doctor of Philosophy to the University of St. Andrews

by

Nigel R. Gallaher B.Sc.

J. F. Allen Physics Research Laboratories

Department of Physics & Astronomy

University of St. Andrews

North Haugh

St. Andrews, Fife

Scotland

ProQuest LLC.
789 East Eisenhower Parkway
P.O. Box 1346
Ann Arbor, MI 48106 – 1346

TL
B460

Declaration

I, Nigel R. Gallaher, hereby certify that this thesis has been composed by myself, that it is a record of my own work, and that it has not been accepted in partial or complete fulfilment of any other degree or professional qualification.

Signed Date 21 Sept. 1993

I was admitted to the Faculty of Science of the University of St. Andrews under Ordinance General No 12 on 1st October, 1987 and as a candidate for the degree of Ph.D. on 1st October, 1987

Signed Date 21 Sept. 1993

I hereby certify that the candidate has fulfilled the conditions of the Resolution and Regulations appropriate to the Degree of Ph.D.

Signature of Supervisor Date 21 Sept. 1993

Copyright

ACKNOWLEDGEMENTS

I am indebted to many people for their assistance in the completion of this work, namely my research supervisor Professor Malcolm Dunn for his encouragement and patient proof-reading of this thesis, Dr. Bruce Sinclair for his helpful suggestions and infectious enthusiasm for physics, and Dr. Bill Sleat for imparting some of his vast knowledge and experience in the "art" of electronics.

I must also thank Dr. David Tunstall and Dr. Ian Firth for the loan of some essential pieces of apparatus, and Newport Research Corporation for providing the high performance Supercavity mirrors used in this work.

The assistance of the technical support staff in the electronics workshop and mechanical workshop is greatly appreciated with special thanks going to Mr. Jimmy Lindsay for manufacturing the laser cavities and optics mounts so skilfully.

Finally, I owe a great debt of gratitude to my wife, Dr. Yueping Liu for the support, encouragement and above all friendship, she has provided.

Financial support was given by the Science and Engineering Council.

ABSTRACT

The design, construction, evaluation and development of an all solid state, narrow linewidth laser source is presented. The narrow linewidth laser system was based on a miniature standing wave Nd:YAG laser cavity, end-pumped with 100mW of 809nm light from a fibre coupled GaAlAs diode laser array. This basic CW laser generated up to 30mW at 1064nm in a single, diffraction limited transverse mode (TEM_{00}) but multi-longitudinal mode output beam. The laser had a pump power threshold of 24mW and an optical to optical slope efficiency of 39%. A simple rate equation based numerical model of this laser was developed to allow various design parameters such as length of Nd:YAG gain medium and amount of output coupling to be optimised. Excellent agreement between the numerical model predictions of the output power as a function of input pump power and experimental data from the optimised multi-longitudinal mode laser was obtained.

To restrict this laser to operate on a single longitudinal mode, twisted cavity mode and intracavity etalon, mode selecting techniques were investigated. Both methods were found to produce reliable single mode laser operation and resulted in output powers at the 10mW level.

The relative free running frequency stability between a pair of single longitudinal mode diode laser pumped Nd:YAG lasers was investigated. By isolating these lasers from environmental noise using a small, custom built anechoic chamber the linewidth of the optical heterodyne signal between the two free running lasers was reduced from tens of megahertz to around 10kHz measured on a millisecond time scale. Further improvement in linewidth was achieved by actively locking the laser frequency to a novel ultra high finesse ($\mathcal{F}$~12,500, free spectral range ~500MHz) spherical mirror Fabry-Perot reference interferometer using the technique of Pound-Drever locking. The locked laser displayed a maximum frequency deviation of only 1kHz from the centre of

the reference cavity transmission and a frequency noise spectral density of ~20Hz/$\sqrt{\text{Hz}}$ at 1kHz.

In one of the first reported demonstrations of an all solid state injection seeded laser system, this single frequency laser was used to injection seed a diode laser array, transversely pumped, Q-switched Nd:YAG laser to produce 0.25mJ, 35ns pulses in a single longitudinal, single transverse mode beam.

Preliminary results on injection locking between two single frequency diode laser pumped Nd:YAG laser are also reported. A novel frequency stabilisation scheme based on resonant optical feedback locking is proposed and some preliminary experimental work on this technique is presented.

Contents

Chapter 3

Chapter 4

Chapter 1

INTRODUCTION

1.1 Diode Pumped Solid State Lasers

Many exciting fields of research in optoelectronics, such as coherent optical communications[1,2,3,4,5,6], LIDAR remote sensing[7,8,9,10,11], gravitational wave detectors[12,13,14], laser isotope separation[15,16,17,18] and the next generation of optical frequency standards[19,20,21,22,23,24] based on laser cooled[25,26,27,28] atoms or ions, rely on lasers with extremely narrow linewidth outputs. Progress in many of these areas has been hindered , however, due to the technical difficulties encountered in producing reliable laser sources having the necessary degree of frequency stability. With the recent revolution in diode laser pumped solid state laser technology, highly efficient and compact all solid-state laser sources are now available which display unprecedented levels of frequency stability. This has stimulated research in the field of ultra-stable lasers and made the development of coherent optical sources a far less daunting prospect.

The underlying design philosophy behind diode laser pumped solid state laser technology is the replacement of conventional flash lamp pump sources by highly efficient, robust and long lived semiconductor diode lasers. The resulting hybrid all solid-state or holosteric (from the Greek meaning wholly solid) laser acquires many of the most desirable qualities of the diode laser pump. Modern high power diode lasers are extremely reliable and have useful lifetimes in excess of 10^4 hours, typically two orders of magnitude longer than high performance gas discharge lamps currently used for laser excitation. The overall conversion efficiency of electrical energy into useful light energy in a semiconductor diode laser is also far superior to its flash lamp counterpart and commonly approaches 50%. In end-pumped diode laser pumped solid state laser geometry the partial spatial coherence of the diode laser emission allows the pump beam to be tightly focused enabling excellent spatial overlap between the pump light and cavity mode of the

solid state laser and selective excitation of the TEM_{00} cavity mode. Through temperature tuning effects of the diode laser emission wavelength it is also possible to achieve excellent spectral coincidence between the pump wavelength and a strong absorption band in the solid state gain medium. This results in optical-optical conversion efficiency in the holosteric laser as high as 30-40% and overall electrical to optical or "wall plug" efficiency approaching 20%. In comparison, a good flash pumped systems will have a wall plug efficiency in the region of only 5%.

Such high conversion efficiencies in diode pumped lasers means that waste heat production in the solid state gain medium is minimised and so forced air or water cooling of the gain medium is often unnecessary. As well as simplifying laser design, the absence of any forced cooling of the laser greatly reduces the technical noise (mechanical vibrations and acoustic noise) in the laser head resulting in excellent free running frequency stability. Diode pumped solid state laser systems can in general be made extremely compact and robust and so can be easily isolated from the environment, further improving their free running stability performance. For instance, diode pumped solid state lasers have been demonstrated with free running, short term linewidths in the region of a few kilohertz[29,30,31,32,33]. With the application of the advanced frequency stabilisation technique of Pound-Drever locking[34], this already narrow linewidth can be dramatically reduced to the millihertz level[35,36,37]. In contrast, conventional flash lamp pumped solid state lasers have intrinsic linewidths typically in the region of 30-40 MHz. Even under active frequency control, these lasers have only achieved linewidth down to 100-200 kHz[38,39].

Diode laser pumping not only harnesses the attractive features of the diode laser pump source itself but also overcomes many of the drawbacks, such as limited output power, poor beam quality and broad linewidth, encountered when using high power diode lasers directly as a primary laser source . The holosteric approach offers access to higher output powers by providing a convenient means of multiplexing the outputs from several diode laser pumps and by exploiting the energy storage capabilities of solid state gain media

through Q-switching techniques. High output powers in diffraction-limited beams opens up many opportunities in efficient nonlinear frequency conversion processes such as frequency doubling[40,41,42,43], sum frequency mixing[44] and more recently, efficient and widely tunable all solid state optical parametric oscillators (OPOs)[45,46,47]. This and the wide variety of other solid state gain materials, which can be pumped by diode lasers, provide access to wavelength regions difficult to reach with today's diode lasers.

This holosteric approach to laser design was in fact proposed back in 1963 by Newman[48] shortly after the invention of the semiconductor diode laser. Even at this early stage in the history of laser development, many of the advantages of an all solid state laser system were already apparent. The first successful demonstration of a diode laser pumped solid state laser was performed by Keyes and Quist[49] in 1964, using a GaAs diode laser to optically pump U:CaF_2 operating at 4K. Despite this early demonstration of the diode pumped solid state laser principle and other subsequent demonstrations over the course of the late 1960s[50,51,52] and 1970s[53,54,55,56] progress was slow and experiments achieved little more than proof of principle status. Realisation of the full potential of diode pumped solid state lasers was hampered at this stage by the lack of development in the newly emerging field of semiconductor diode lasers. These early pump sources tended to be unreliable and the optical output power they could deliver was limited to only a few milliwatts. Another limitation to the practicality of these early diode pumped solid state lasers was the need for cryogenic cooling of the semiconductor diode lasers and frequently of the solid state gain medium also, in order to reduce laser threshold and to achieve spectral overlap of the diode laser emission and the absorption bands of the solid state gain medium through temperature tuning effects.

The true launch of the diode pumped solid state laser era came in the mid 1980's with the maturation of semiconductor diode laser fabrication techniques and the publication in 1985 by Zhou et al[57] describing the first truly practical diode pumped solid state laser system. The device consisted of a 5mm long rod of Nd:YAG, the ends of which had been suitably coated to form the laser cavity mirrors. This miniature Nd:YAG cavity was

longitudinally pumped by a single stripe GaAs/GaAlAs laser delivering 10-40mW of optical power depending on the particular make of the diode laser used. Although the output power from the diode pumped solid state laser was comparatively modest at around a few milliwatts, this simple laser displayed an excellent optical-optical slope efficiency of 25% and unprecedented levels of overall electrical-optical efficiency and free running frequency stability of 6.5% and sub-10kHz over 0.3sec respectively.

Since this pioneering demonstration of the potential of diode pumped solid state laser technology, progress has been made both in the development of the semiconductor diode laser pump sources and in diode pumped solid state laser design and performance. This is evident from the almost bewildering number of publications in these areas and the extensive review articles appearing in the scientific press[58,59,60,61]. The performance of diode pumped solid state lasers is continuing to be extended with, for instance, electrical-optical (wall plug) efficiency as high as 15.8%[62] being reported in a Nd:YAG laser as well as ever increasing output power. For example Tidwell et al[63] demonstrated 60W cw output in a TEM_{00} mode from an end-pumped Nd:YAG laser. Single frequency output at the 15W level has been achieved by Golla et al[64] using the technique of injection locking. Diode pumped solid state laser technology has impinged on all areas of laser engineering from cw devices exhibiting ultranarrow linewidth, through high power Q-switched systems[65,66] to mode-locked ultrashort pulse lasers[67]. Not only have diode pumped solid state lasers fulfilled expectations of efficiency, size, reliability and frequency stability but the technology has also stimulated much activity in laser engineering itself. Many innovative laser systems have been developed to better exploit the advantages of new diode laser arrays, bars and stacks. For example, the tightly folded resonator or TFR laser[68] efficiently couples the light from a high power diode laser by coinciding multiple bounces of the laser mode inside a slab of gain medium with the individual stripes of a laser diode bar. Other novel schemes for multiplexing several pump sources have utilised lenses[69,70], optical fibres by for example forming individual fibre pigtail from separate laser diodes into a single circular apertured fibre bundle[71] or coupling pump light from many fibre pigtailed laser diodes into the gain rod through evanescent wave coupling[72]. In

the field of single frequency holosteric lasers a particularly noteworthy and highly successful laser design is the monolithic NonPlanar Ring Oscillator (NPRO) invented by Kane et al[73] and subsequently modified by Trutna et al[74]. In this unidirectional ring laser all the elements of the intracavity optical isolator are embodied in the monolithic gain medium itself. The ring path is defined by four reflectors, three of which are provided by total internal reflection within the gain medium. A concave multilayer dielectric mirror used at oblique incidence acts as a partial polariser as well as the fourth cavity reflector. A magnetic field applied to the Faraday active gain medium forms the nonreciprocal (direction dependent) rotator whilst the reciprocal (direction independent) rotation is generated by the out-of-plane total internal reflections in the crystal[75]. The dimensions of monolithic device are typically 5×4×2mm. The NPRO laser has proved ideal for diode laser pumping, capable of high output power (0.91W)[76] and excellent free running frequency stability (3-10kHz)[77,78] and has become a successful commercial product[79]. Fast piezoelectric frequency tuning has also been demonstrated in monolithic[80] and two-piece[81] diode pumped NPRO devices as well as NPRO operation at other wavelengths (1.319 and 1.338μm)[24] and in other materials such as neodymium doped gadolinium gallium garnet (Nd:GGG)[82]

The Nd:YAG solid state gain medium used by Zhou et al in the first demonstration of the new generation of diode pumped solid state lasers has remained the most common laser gain medium in such devices to date and indeed is the material used in the lasers described in this thesis. Since the first demonstration of laser action in Nd:YAG in 1964[83], the material has established itself as the most widely used and perhaps most versatile solid state laser medium. For the purpose of laser diode pumping the Nd^{3+} laser active ion is ideally suited because its strong absorption bands at around 809nm coincide well with the emission wavelengths accessible to high power GaAs and GaAlAs diode lasers. The YAG host lattice for this ion has many attractive mechanical and optical properties for a laser material. YAG can be grown relatively easily and in large quantities with excellent optical quality. The robustness of the crystal is adequate to withstand

commercial cutting and polishing techniques and allows the fabrication of small rods, cubes, rhombs and other more exotic geometry used in diode pumped laser systems.

Finally, the thermal conductivity of Nd:YAG is high. Whilst this feature is perhaps of little concern in low power laser diode pumped systems because of the small thermal load on the laser rod, it is an important consideration in high power systems where thermal lensing and even fracturing of the laser rods are major problems[84]. A more comprehensive discussion of the mechanical, optical and lasing properties of Nd:YAG can be found in, for example, Koechner[85] and Zverev et al[86].

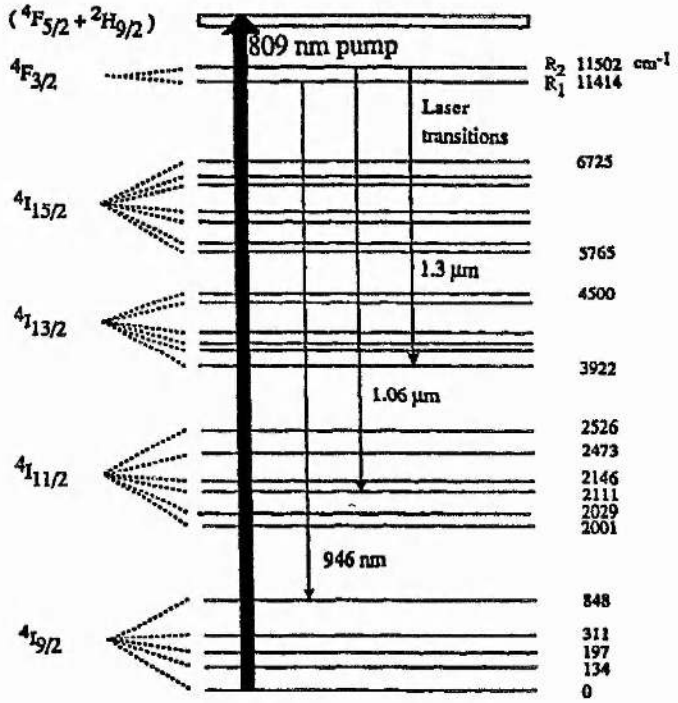

Figure 1.1. Energy Level Diagram of Nd:YAG

A simplified energy level diagram illustrating the salient features of Nd:YAG is shown in figure 1.1. The room temperature transition from $^4F_{3/2} \rightarrow {}^4I_{11/2}$ at ~1064nm emission has the highest gain of all transitions in Nd:YAG and consequently is the most frequently used in both flashlamp pumped and laser diode pumped systems. Other Nd:YAG transitions have been demonstrated in laser diode pumped systems namely $^4F_{3/2} \rightarrow {}^4I_{13/2}$ at the important optical fibre communications wavelength of 1300nm and the quasi-three level system lasing from $^4F_{3/2} \rightarrow {}^4I_{9/2}$ at 946 nm. Frequency doubling of these three

transitions is relatively straight forward resulting in red (750nm), green (532nm) and blue (473nm) light. As well as providing useful source for high density optical data storage[87] there is the possibility of producing an all solid state white light laser source for use in high definition colour projection.

Rapid progress is continuing to be made on all fronts in the field of holosteric lasers. The diode laser pump sources are constantly being improved to give ever higher output powers in better quality beams and over an increasing range of emission wavelengths[88,89]. New nonlinear materials are being developed and existing material growth techniques are being improved opening up more opportunities in nonlinear frequency conversion. New solid state gain materials are also being developed for use in diode pumped lasers such as the self-frequency doubling Neodymium Yttrium Aluminium Borate (NYAB) laser[90] or widely tunable vibronic gain media such as Cr:Alexandrite[91], Cr:$LiSrAlF_6$ [92], Cr:$LiCaAlF_6$ [93] and Cr:$LiSrGaF_6$ [94]. This wavelength diversity coupled with the extraordinary frequency stability possible with holosteric lasers means that widely tunable coherent optical sources are now a practical reality.

1.2 Thesis Outline

Chapter 2 contains a brief overview of the remarkable advance made in diode laser technology starting from the basic single emitter device through to the very high power one and two dimensional arrays and fibre coupled devices available today. The particular fibre coupled diode laser array used to end pump the Nd:YAG lasers in this thesis is also described and a full characterisation of its optical properties is provided.

The design, construction and evaluation of the basic end-pumped, multi-longitudinal mode Nd:YAG laser is described in Chapter 3. The important question of mode overlap between pump and cavity beams for reliable TEM_{00} operation of the Nd:YAG laser was investigated together with the determination of the optimum level of output coupling required for maximum laser output power. To characterise the laser performance, optical

to optical slope efficiency measurements were made and the transverse and longitudinal mode behaviour of the Nd:YAG laser output was also investigated. A simple rate equation based numerical model of an end-pumped solid laser was developed and used to study the effect of altering various design parameters, such as Nd:YAG rod length and output coupling, on the performance of the solid state laser. A comparison between the laser behaviour predicted by this model and the experimental data obtained from the system is also presented.

The next step in the refinement of the basic Nd:YAG laser source was to improve its longitudinal mode characteristics from multimode to single mode operation. The basic causes of multi-longitudinal mode operation in lasers are discussed and various methods of mode control are reviewed in Chapter 4. Mode selection by intracavity etalon and by twisted mode were deemed the most appropriate techniques to apply to the open cavity Nd:YAG laser described in the previous chapter. These two mode selection techniques were investigated experimentally using the diode end-pumped Nd:YAG laser and the relative merits and difficulties encountered with these two systems were described.

In Chapter 5 the numerous environmental and fundamental factors which influence the free-running frequency stability of a solid state laser are considered. This section also charts the gradual improvement in the passive, relative frequency stability of two cw end-pumped single mode holosteric lasers through modifications in cavity design and acoustic isolation. The emphasis here was on reducing the short term laser linewidth in order to ease the demands on bandwidth and gain of any electronic servo loop to be used for further active frequency stabilisation.

To achieve additional line narrowing of the diode laser pumped Nd:YAG laser output spectrum active frequency stabilisation techniques had to be considered. Chapter 6 introduces the general principles of active laser frequency stabilisation and reviews some of the most common techniques available. Particular attention is paid to the Pound-Drever method of frequency stabilisation as this was the technique applied to the lasers in this work. A phasor model of the Pound-Drever stabiliser is presented which provides useful

insight into the operation of this system. This is followed by a more rigorous mathematical description. The chapter concludes with a discussion of the ultimate limit of active stabilisation in reducing laser linewidth.

Following on from this theoretical analysis of active frequency stabilisation, Chapter 7 describes the experimental implementation of the Pound-Drever frequency stabiliser of the diode pumped Nd:YAG laser. Include here was design, construction and characterisation of the ultra high finesse (F~12,000) optical reference cavity together with details of the wide bandwidth piezoceramic transducer used to modify the laser frequency. The level of frequency stabilisation achieved with this system was assessed and the limitations of the particular servo loop design used were identified.

One area where frequency stabilised CW lasers are used is in axial mode selection (injection seeding) and frequency control (injection locking) of higher power pulsed and CW laser oscillators by injected signal. Chapter 8 describes experimental work in the use of the narrow linewidth, CW, end-pumped holosteric laser as a "master oscillator" for injection seeding a Q-switched transversely pumped holosteric laser and some preliminary studies of its use for injection locking a second CW, end pumped holosteric laser. The novel use of resonant optical feedback locking as a method for frequency stabilising diode laser pumped Nd:YAG lasers is also proposed. Finally, in chapter 9, the accomplishments of the current work are summarised.

1.3 References

1 Yamamoto Y., Kimura T., "Coherent Optical Fibre Transmission System", IEEE J. Quant. Elec. **QE-17**(6) 919 (1981)

2 Kazovsky L. G., "Balanced Phase-Locked Loops For Optical Homodyne Receivers: Performance Analyis, Design Considerations And Laser Linewidth", J. Lightwave Tech. **LT-4**(2) 182 (1986)

3 Lucente M., Kintzer E. S., Alexander S. B., Fujimoto J. G., Chan V. W. S., "Coherent optical communication with injection-locked high-power semiconductor laser array", Electron. Lett., **25**(17), 1112 (1989)

4 Wallmeroth K., Wandernoth B., Franz J., Meier H., Schorp B., "Towards a Coherent Optical Free-Space Communication System", Electron. Lett. **26** (9), 572 (1990)

5 Heilmann R., Kuschel J., "Absolute frequency Locking of Diode Pumped Nd:YAG Laser For Application in Free-Space Optical Communication", Elec. Lett. **29**(9) 810 (1993)

6 Cheng E., "Diode-Pumped Lasers Can Communicate in Space", Laser Focus World **27**(7) 99 (1991)

7 Byer R. L., Gustafson E. K., Trebino R., "Tunable Solid State Lasers For Remote Sensing", Springer Verlag (1985)

8 Hess R. V., Brockman P., Bair C. H., Barnes J. C., Byuik C. E., Buoncristiani A. M., Magee C. J., "Developement in Tunable Solid State Lasers With High Spectral Purity, High Efficiency and Long Lifetime For Differential Absorption LIDAR", SPIE Laser Radar Technology And Applications **663** 14 (1986)

9 Kane T. J., Kozlovsky W. J., Byer R. L., "Coherent Laser Radar at 1.06μm Using Nd:YAG Lasers", Opt. Lett. **12**(4) 239 (1987)

10 Lutz H., Armandillo E., "Laser-Based Remote Sensing From Space", ESA Bulletin no.66 pps73-79 May (1991)

11 Moody S. E., "Evaluation of Laser Technologies For On-Aircraft Wind Shear Detection", SPIE Laser Radar II **783** 124 (1987)

12 Weber J., "The Detection of Gravitational Waves", Sci. Am. **224** 22 (1971)

13 Davies P. C. W., "The Search For Gravity Waves", Cambridge University Press (1980)

14 Kerr G., "Experimental Developments Towards a Long-Baseline Laser Interferometric Gravitational Radiation Detector", Ph.D. Thesis, University of Glasgow (1986)

15 Letokhov V. S., Moore C. B., "Laser Isotope Separation (Review)", Sov. J. Quant. Elec. **6**(2) 129 (1976)

16 Letokhov V. S., Moore C. B., "Laser Isotope Separation (Review) II", Sov. J. Quant. Elec. **6**(3) 259 (1976)

17 Moore C. B., "The Application of Lasers to Isotope Separation", Acc. Chem. Res., **6** 323 (1973)

18 Zare R. N., "Laser Separation of Isotopes", Sci. Am. **236**(2) 86 (1977)

19 Bollinger J. J., Prestage J. D., Itano W. M., Wineland D. J., "Laser-Cooled-Atomic Frequency Standard", Phys. Rev. Lett. **54**(10) 1000 (1985)

20 Thompson R. C., Barwood G. P., Gill P., "Progress Towards an Optical Frequency Standard Based on Ion Traps", Appl. Phys. B **46** 87 (1988)

21 Barwood G. P., Bell A. S., Gill P., Klein H. A., "Trapped Yb^+ as a Potential Optical Frequency Standard", 4th Symposium on Frequency Standards and Metrology, Ancona, Italy (1988)

22 Blatt R., Gill P., Thompson R. C., "Current Perspectives on the Physics of Trapped Ions", J. Mod. Opt. **39**(2) 193 (1992)

23 Prestage J. D., Tjoelker R. L., Dick G. J., Maleki L., "Ultra-Stable Hg^+ Trapped Ion Frequency Standard", J. Mod. Opt. **39**(2) 221 (1992)

24 Arie A., Gustafson E. K., Byer R. L., "Frequency Stabilised Diode Laser Pumped Solid State Lasers: Optical Clocks of the Future", Optics and Photonics News pps 43-44 December (1992)

25 Prodan J., Migdall A., Phillips W. D., So I., Metcalf H., Dalibard J., "Stopping Atoms With Laser Light", Phys. Rev. Lett. **54**(10) 992 (1985)

26 Phillips W. D., Metcalf H., "Cooling And Trapping Atoms", Sci. Am. **256**(3) 36 (1987)

27 Wineland D. J., "Laser Cooling", Physics Today pps 34-40 June (1987)

28 Cohen-Tannoudji C. N., Phillips W. D., "New Mechanisms For Laser Cooling", Physics Today pps 33-40 October (1990)

29 Zhou B., Kane T. J., Dixon G. J., Byer R. L., "Efficient, Frequency Stable Laser Diode Pumped Nd:YAG Laser", Opt. Lett. **10**(2) 62 (1985)

30 Kane T. J., Nilsson A. C., Byer R. L., "Frequency Stability and Offset Locking of a Laser Diode Pumped Nd:YAG Monolithic Nonplanar Ring Oscillator", Opt. Lett. **12**(3) 175 (1987)

31 Kane T. J., Kozlovsky W. J., Byer R. L., "Coherent Laser Radar at 1.06μm Using Nd:YAG Lasers", Opt. Lett. **12**(4) 239 (1987)

32 Bush S. P., Güngör A., Davis C. C., "Studies of the Coherence Properties of a Diode Pumped Nd:YAG Ring Laser", Appl. Phys. Lett. **53**(8) 646 (1988)

33 Nachman P., Munch J., Yee R., "Diode Pumped, Frequency Stable, Tunable, Continuous Wave Nd:Glass Laser", IEEE J. Quant. Elect. **26**(2) 317 (1990)

34 Drever R. W. P., Hall J. L., Kowalski F. V., Hough J., Ford G. M., Munley A. J., Ward H., "Laser Phase and Frequency Stabilization Using an Optical Resonator", Appl. Phys. B **31** 97 (1983)

35 Shoemaker D., Brillet A., Nary Man C., Crégut O., Kerr G., "Frequency Stabilised Laser Diode Pumped Nd:YAG Laser", Opt. Lett. **14**(12) 609 (1989)

36 Day T., Gustafson E. K., Byer R. L., "Sub-Hertz Relative Frequency Stabilisation of Two Diode Laser Pumped Nd:YAG Lasers Locked to a Fabry-Perot Interferometer", IEEE J. Quant. Elec. **28**(4) 1106 (1992)

37 Uehara N., Ueda K-I., "193mHz Beat Linewidth of Frequency Stabilised Laser Diode Pumped Nd:YAG Ring Lasers", Opt. Lett. **18**(7) 505 (1993)

38 Peng K C, Wu L A, Kimble H J, "Frequency-stabilised Nd:YAG laser with high output power", Appl. Opt. **24** (7), 938 (1985)

39 Sun Y L, Byer R L, "Submegahertz frequency-stabilized Nd:YAG oscillator", Opt. Lett. **7**(9), 408 (1982)

40 Risk W. P., Lenth W., "Room-Temperature, Continuous-Wave, 946nm Nd:YAG Laser Pumped By Laser-Diode Arrays And Intracavity Frequency Doubled To 475nm", Opt. Lett., **12**(12) 993 (1988)

41 Burnham R., Hays A. D., "High Power Diode Array Pumped Frequency Doubled CW Nd:YAG Laser", Opt. Lett. **14**(1) 27 (1989)

42 Marshall L. R., Kaz A. D., Burnham R. L., "3W Continuous Wave Diode Pumped 532nm Laser", Opt. Lett. **17**(16) 1110 (1992)

43 Marshall L. R., Hays A. D., Kaz A., Burnham R. L., "Intracavity Doubled Mode-Locked And CW Diode Pumped Lasers", IEEE J. Quant. Elec. **28**(4) 1158 (1992)

44 Risk W. P., Baumert C. J., Bjorkland G. C., Schellenberg F. M., Lenth W., "Generation Of Blue Light By Intracavity Frequency Mixing of The Laser And Pump Radiation of a Miniature Neodymium:Yttrium Aluminium Garnet Laser", Appl. Phys. Lett. **52**(2) 85 (1988)

45 Malcolm G. P. A., Ebrahimzadeh M., Ferguson A. I., "Efficient Frequency Conversion of Mode-Locked Diode-Pumped Lasers and Tunable All-Solid-State Laser Sources", IEEE J. Quant. Elec. **28**(4) 1172 (1992)

46 Cui Y., Dunn M. H., Norrie C. J., Sibbett W., Sinclair B. D., Tang Y., Terry J. A. C., "All-Solid-State Optical Parametric Oscillator For The Visible", Opt. Lett. **17**(9) 646 (1992)

47 Cui Y., Withers D. E., Rae C. F., Norrie C. J., Tang Y., Sinclair B. D., Sibbett W., Dunn M. H., "Widely Tunable All-Solid-State Optical Parametric Oscillator For The Visible And Near Infrared", Opt. Lett. **18**(2) 122 (1993)

48 Newman R., "Excitation of Nd Fluorecence in $CaWO_4$ by Recombination Radiation in GaAs", J. Appl. Phys. **34**(2) 437 (1963)

49 Keyes R. J., Quist T. M., "Injection Luminescent Pumping of $CaF_2:U^{3+}$ With GaAs Diode Lasers", Appl.Phys. Lett. **4** 50 (1964)

50 Ochs S. A., Pankove J. I., "Injection-Luminescence Pumping of a $CaF_2:Dy^{2+}$ Laser", Proc. IEEE **52** 713 (1964)

51 Ross M., "YAG Laser Operation by Semiconductor Laser Pumping", Proc. IEEE **56** 196 (1968)

52 Allen R. B., Scalise S. J., "Continuous Operation of a YAlG:Nd Laser by Injection Luminescent Pumping", Appl. Phys. Lett., **14** 188 (1969)

53 Danielmeyer H. G., Ostermayer F. W., "Diode-Pump-Modulated Nd:YAG Laser", J. Appl. Phys. **43**(6) 2911 (1972)

54 Rosenkrantz I. J., "GaAs Diode-Pumped Nd:YAG Laser", J. Appl. Phys. **43**(11) 4603 (1972)

55 Chinn S. R., Hong H. Y-P., Pierce J. W., "Spiking Oscillations in Diode-Pumped NdP_5O_{14} and $NdAl_3(BO_3)_4$ Lasers", IEEE J. Quant. Elec. **QE-12**(3) 189 (1976)

56 Ostermayer F. W., "LED End-Pumped Nd:YAG Lasers", IEEE J. Quant. Elec. **QE-13**(1) 1 (1977)

57 Zhou B., Kane T. J., Dixon G. J., Byer R. L., "Efficient, Frequency-Stable Laser Diode Pumped Nd:YAG Laser", Opt. Lett. **10**(2) 62 (1985)

58 Byer R. L., "Diode Laser-Pumped Solid State Lasers", Science **239**(2) 742 (1988)

59 Fan T. Y., Byer R. L., "Diode Laser-Pumped Solid State Lasers", IEEE J. Quant. Elec. **24**(6) 895 (1988)

60 Hughes D. W., Barr J. R. M., "Laser Diode Pumped Solid State Lasers", J. Phys. D: Appl. Phys. **25** 563 (1992)

61 Special Issue on Diode-Pumped Solid-State Lasers, IEEE J. Quant. Elec. **28**(4) 940 (1992)

62 Fields R. A., Birnbaum M., Fincher C. L., "Highly Efficient Nd:YVO_4 Diode-Laser End-Pumped Laser", Appl. Phys. Lett. **51** 1885 (1987)

63 Tidwell S. C., Seamans J. F., Bowers M. S., "Highly Efficient 60-W TEM_{00} cw Diode-End-Pumped Nd:YAG Laser", Opt. Lett. **18**(2) 116 (1993)

64 Golla D., Freitag I., Zellmer H., Schone W., Kropke I., Welling H., "15W Single-Frequency Operation of a CW, Diode Laser-Pumped Nd:YAG Ring Laser", Opt. Comm. **98**(1,2,3) 86 (1993)

65 Kasinski J. J., Hughes W., DiBiase D., Bournes P., Burnham R., "One Joule Output From a Diode-Array-Pumped Nd:YAG Laser with Side-Pumped Rod Geometry", IEEE J. Quant. Elec. **28**(4) 977 (1992)

66 Holder L. E., Kennedy C., Long L., "One Joule Per Q-Switched Pulse Diode-Pumped Laser", IEEE J. Quant. Elec. **28**(4) 986 (1992)

67 Malcolm G. P. A., Ferguson A. I., "Mode-Locking of Diode Laser-Pumped Solid-State Lasers", Opt. Quant. Elec. **24** 705 (1992)

68 Baer T. M., Head D. F., Gooding P., Kintz G. J., Hutchison S., "Performance of Diode Pumped Nd:YAG and Nd:YLF Lasers in a Tightly Folded Resonator Configuration", IEEE J. Quant. Elec. **28**(4) 1131 (1992)

69 Fan T. Y., Sanchez A., DeFeo W. E., "Scalable, End-Pumped, Diode-Laser-Pumped Laser", Opt. Lett. **14**(19) (1989)

70 Leger J. R., Goltsos W. C., "Geometrical Transformation of Linear Diode-Laser Arrays for Longitudinal Pumping of Solid-State Lasers", IEEE J. Quant. Elec. **28**(4) 1088 (1992)

71 Berger J., Welch D. F., Streifer W., Scifres D. R., Hoffman N. J., Smith J. J., Radecki D., "Fibre-Bundle Coupled, Diode End-Pumped Nd:YAG Laser", Opt. Lett. **13**(4) 306 (1988)

72 Howerton P. H., Cordray D. M., "Diode-Pumped Amplifier/Laser Using Leaky Wave Fibre Coupling : An Evalution", IEEE J. Quant. Elec. **28**(4) 1081 (1992)

73 Kane T. J., Byer R. L., " Monolithic, Unidirectional Single-Mode Nd:YAG Laser", Opt. Lett. **10**(2) 65 (1985)

74 Trutna W. R., Donald D. K., Nazarathy M., "Unidirectional Diode Laser Pumped Nd:YAG Ring Laser with a Small Magnetic Field", Opt. Lett. 12(4) 248 (1987)

75 Nilsson A. C., Gustafson E. K., Byer R. L., "Eigenpolarization Theory of Monolithic Nonplanar Ring Oscillators", IEEE J. Quant. Elec. **25**(4) 767 (1989)

76 Cheng E. A. P., Kane T. J., "High Power Single Mode Diode Pumped Nd:YAG Laser Using a Monolithic Nonplanar Ring Resonator"' Opt. Lett. **16**(7) 478 (1991)

77 Kane T. J., Nilsson A. C., Byer R. L., "Frequency Stability and Offset Locking of a Laser Diode Pumped Nd:YAG Monolithic Nonplanar Ring Oscillator", Opt. Lett. **12**(3) 175 (1987)

78 Bush S. P., Gungor A., Davis C. C., "Studies of the Coherence Properties of a Diode Pumped Nd:YAG Ring Laser", Appl. Phys. Lett. **53**(8) 646 (1988)

79 Series 200, 500mW output power diode pumped ring laser - Lightwave Electronics, California, USA (1990).

80 Kane T. J., Cheng E. A. P., "Fast Frequency Tuning and Phase Locking of Diode Pumped Nd:YAG Ring Laser", Opt. Lett. **13**(11) 970 (1988)

81 Trutna W. R., Donald D. K., "Two-Piece Piezoelectrically Tuned Single Mode Nd:YAG Ring Laser", Opt. Lett. **15**(7) 369 (1990)

82 Day T., Nilsson A. C., Fejer M. M., Farinas A. D., Gustafson E. K., Nabors C. D., Byer R. L., "30Hz Linewidth, Diode Laser Pumped, Nd:GGG Nonplanar Ring Oscillators by Active Stabilization", Elec. Lett. **25**(13) 810 (1989)

83 Geusic J. K., Marcos H. M., Von Utert L. G., "Laser Oscillations in Nd-Doped Yttrium Aluminium, Yttrium Gallium and Gadolinium Garnets", Appl. Phys. Lett. **4**(10) 182 (1964)

84 Basu S., Byer R. L., "Average Power Limits of Diode-Laser-Pumped Solid State Lasers", Appl. Opt. **29**(12) 1765 (1990)

85 Koechner W., "Solid State Laser Engineering", Springer Verlag, 2nd Eddition (1976)

86 Zverev G. M., Golyaev Y. D., Shalaev E. A., Shokin A. A., "Neodymium Activated Yttrium-Aluminium Garnet (YAG:Nd) Lasers", J. Sov. Las. Res. **8**(3) 189 (1987)

87 Oka M., Kubota S., "Second-Harmonic Generation Green Laser for Higher-Density Optical Disks", Jpn. J. Appl. Phys. **31**(pt.1, no.2B) 513 (1992)

88 Wang C. A., Groves S. H., "New Materials For Diode Laser Pumping of Solid State Lasers", IEEE J. Quant. Elec. **28**(4) 942 (1992)

89 Endriz J. G., Vakili M., Browder G. S., De Vito M., Haden J. M., Harnagel G. L., Plano W. E., Sakamoto M., Welch D. F., Willing S., Worland D. P., Yao H. C., "High Power Diode Laser Arrays", IEEE J. Quant. Elec. **28**(4) 952 (1992)

90 Hemmati H., "Diode Pumped Self-Frequency Doubled Neodymium Yttrium Aluminium Borate (NYAB) Laser", IEEE J. Quant. Elec. **28**(4) 1169 (1992)

91 Scheps R., Gately B., Mayers J. F., Krasinski J. S., Heller D. F., "Alexandrite Laser Pumped by Semiconductor Lasers", Appl. Phys. Lett. **56**(23) 2288 (1990)

92 Scheps R., Mayers J. F., Serreze H. B., Rosenberg A., Morris R. C., Long M., "Diode Pumped Cr:$LiSrAlF_6$ Lasers", Opt. Lett. **16**(11) 820 (1991)

93 Scheps R., "Cr:$LiCaAlF_6$ Laser Pumped by Visible Laser Diodes", IEEE J. Quant. Elec. **27**(8) 1968 (1991)

94 Scheps R., "Laser-Diode-Pumped Cr:$LiSrGaF_6$", IEEE J. Photon Tech. Lett. **4**(6) 548 (1992)

Chapter 2

DIODE LASER PUMPS FOR SOLID STATE LASERS

2.1 Introduction

Of key importance to the recent advances in diode laser pumped solid state laser technology has been the remarkable progress made in the development of high power, highly efficient and reliable semiconductor diode lasers. In the field of high power diode lasers research, much of the interest has focused on devices fabricated from ternary alloys of $Ga_{1-x}Al_xAs$. This family of laser diodes emit in the near infra-red region of the spectrum with wavelengths ranging from 640-900nm. This wavelength range spans the absorption pump bands of several important laser active ions (e.g. Nd^{3+}, Ho^{3+}, Er^{3+}) used in many common solid state laser hosts[1,2,3,4,5].

The highest output powers reported to date for GaAlAs diode lasers have been achieved using integrated linear arrays of diode lasers and hybrid two dimensional stacks of such arrays. For instance, CW power levels over 100W from a 1cm wide linear array have been reported[6]. Peak output powers have been pushed even higher by operating diode laser arrays in a long pulse, low duty factor mode to give over 210W peak power from a single 1cm wide array and over 3kW peak power at around 810nm from a 1cm × 1cm two-dimensional stack[7].

2.2 Single Emitter Diode Laser Design

The basic building block for the newest generation of high power arrays is a GaAlAs gain-guided Single Quantum Well, Separate Confinement Heterostructure (SQW-SCH). The internal structure of such a device, illustrated in figure2.1, consists of several thin

crystalline layers of GaAlAs epitaxially grown on a GaAs substrate. The device derives its name from the fact that the electrical carriers and the optical field generated are confined vertically within the device by different layers of the diode laser structure. At the centre of the device is a two dimensional quantum well active region formed by a very thin (typically 10nm) layer of undoped GaAlAs sandwiched between thicker (~40nm) quantum confinement layers of larger band gap (higher Al content) undoped GaAlAs. Above and below these layers forming the quantum well are the p and n-doped layers of GaAlAs. A final capping layer of heavily doped p-type GaAs is deposited on the top of the semiconductor stack to enable ohmic contacts to be formed on the device.

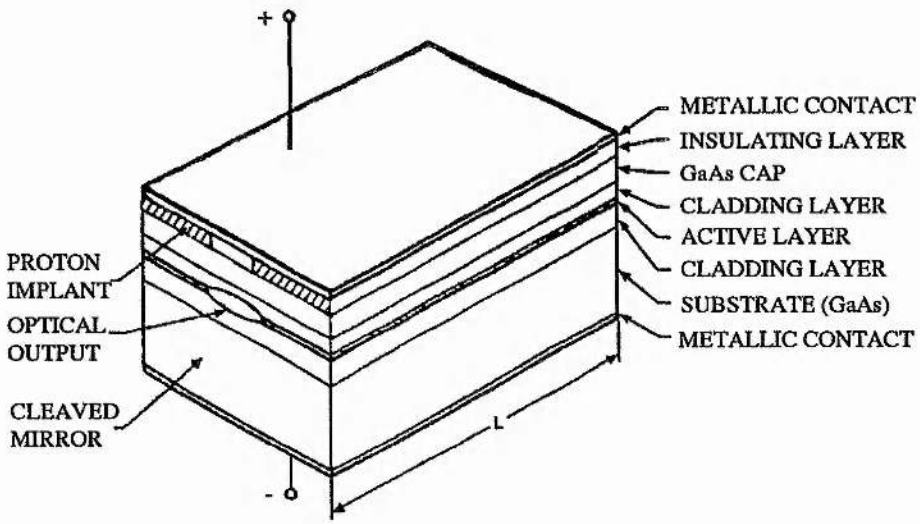

Figure 2.1. Internal structure of a single quantum-well GaAlAs diode laser.

As constructed, there is no structure in the device to give lateral confinement of electrical carriers or the optical field. Instead, the width of the active region in this dimension is defined by restricting current flow to a narrow channel through the structure. Channelling of the drive current is achieved by leaving only a narrow, well defined strip of high electrical conductivity material on the surface contacting layer and rendering the remainder of this layer electrically insulating by proton bombardment.

With the application of a suitable external voltage to this stripe contact the pn junction of the diode laser becomes forward biased causing electrons and holes to be

injected into the active region from the n and p-doped semiconductor layers respectively. These injected carriers become trapped in the quantum well layer by potential barriers (heterobarriers) at the layer boundaries thus establishing the "population inversion" required for laser action.

Photons generated by the subsequent radiative recombination of these holes and electrons experience strong vertical confinement within the device due to variations in the refractive index of the different semiconductor layers. The optical slab-waveguide formed by these layers has an effective emitting aperture of typically 300-500nm in height. By comparison, optical confinement in the plane of the device is much weaker. In this dimension the width of the optical mode is constrained by the high optical loss suffered in the regions of unpumped semiconductor bounding the active stripe. The width of this so called "gain guided" optical mode is of the order of 5μm for narrow stripe devices. Because of the large difference in optical confinement in the planes parallel to and perpendicular to the diode junction the optical mode emitted from the diode laser is highly astigmatic but can nevertheless be focused to a diffraction limited spot by suitable cylindrical optics.

The final element required to achieve laser action in the device is optical feedback. This is provided by Fresnel reflection of the lasing mode at the cleaved ends of the semiconductor crystal. Since GaAlAs has a high refractive index, typically around 3.6, the reflectivity of the semiconductor/air interface is over 30%. In general diode lasers exhibit very large optical gain per unit length and so the relatively low amount of optical feedback provided by the cleaved crystal facets is usually adequate to sustain oscillation. However, for ultimate output power performance from high power diode lasers the reflectivity of the end facets is often modified by the application of dielectric coatings. Usually a high reflectivity (>95%) coating is deposited on the rear facet whilst an anti-reflection (AR) coating layer is applied to the front facet to reduce its reflectivity to less than 5%.

2.2.1 Wavelength Output

The wavelength of the radiation emitted from a diode laser is determined by the bandgap energy of the active region. For GaAlAs devices the laser emission lies in the near infrared part of the spectrum varying from ~640 to ~900nm depending on the exact composition of the device. Whilst coarse wavelength tuning of the diode laser is achieved during the construction stage by choosing the appropriate Aluminium content, fine wavelength adjustment of the finished device is achieved by varying its operating temperature. The emission wavelength shifts at a rate of ~0.3nm/°C due to temperature related changes in the bandgap energy[8]. The operating temperature of the diode laser can be conveniently and precisely controlled by a thermoelectric (Peltier) device enabling the wavelength of the diode laser output to be matched to the absorption bands of many solid state laser materials resulting in highly efficient pumping.

2.2.2 Maximum Output Power

The maximum optical power available from a diode laser is generally limited by the emission area of the crystal facet and in the case of single, narrow active stripe devices, CW powers as high as 425mW from a 3.1μm wide active region have been demonstrated[9]. Under such operating conditions the optical power density at the diode laser facets is extremely high (of the order of a few megawatts/cm^2) and operating lifetimes are short. For GaAlAs devices, if the optical power density at the facet exceeds ~6MW/cm^2, enough localised heating occurs due to non-radiative recombination of carriers that the mirror facets melt in a catastrophic thermal runaway process[10]. To obtain a reasonably long working lifetime >10^4 hours it is necessary to operate diode lasers at 20 to 30% of the catastrophic mirror damage limit and so the output of commercially available single stripe devices is rated at around 50mW.

To reach higher output powers from diode lasers it is therefore necessary to increase the effective facet area to keep the optical power density within safe limits. In practice, however, it is found that increasing the emitter width of a single stripe to over ~10μm can lead to laser oscillation on many incoherent, unstable filaments[11,2]. This filamentary lasing results from an interaction between the optical field and the injected carriers in the active region giving rise to self-focusing of the lasing mode. In a region of high optical field strength within the active stripe, there is correspondingly stronger stimulated recombination of carriers. Associated with this reduced carrier density is an increase in the refractive index in that region and so the lasing filament produces its own optical waveguide. This situation is, however, potentially unstable since there are neighbouring regions of high, undepleted gain. If these high gain regions are wide enough they may be able to support lasing of other filaments. Since such filaments lase essentially independently, their outputs are uncorrelated giving rise to a far-field beam divergence far greater than the diffraction limit. Such uncontrolled filamentary lasing is also potentially hazardous as localised regions of high power density can occur resulting in premature failure of the device. Despite the problems associated with these devices, very high powers have been achieved from single broad area diode lasers. For instance, a 600μm wide stripe GaAlAs broad area laser has been operated up to 5W CW output power[12] and an InGaAsP/GaAs 100μm wide stripe device displayed 5.3W CW output[13].

2.3 High Power Diode Laser Arrays

2.3.1 Diode Laser Arrays and Bars

The solution to the problems of reliable high power emission, scalability and to some extent beam coherence has been to integrate several narrow stripe diode lasers onto a common substrate. See figure 2.2. This apparently simple approach has only become practical comparatively recently due to developments in Molecular Beam Epitaxy (MBE) and Metal-Organic Chemical Vapour Deposition (MOCVD) crystal growth

techniques and advances in photolithographic processes. These sophisticated epitaxial growth systems are capable of the very fine compositional control necessary to grow the multilayer diode laser structure and are also able to produce relatively large areas of semiconductor of high uniformity.

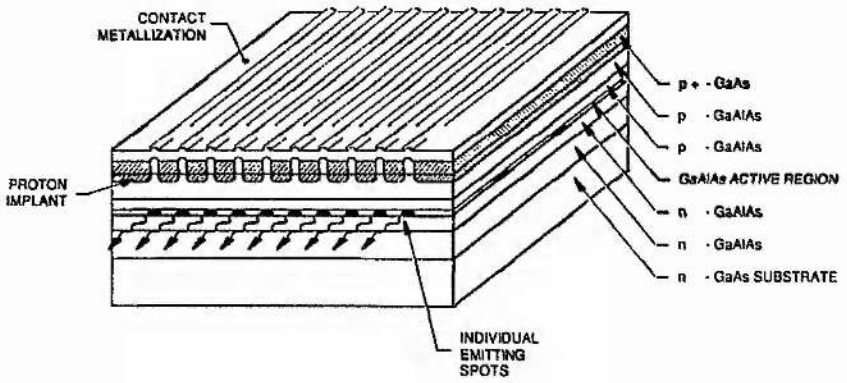

Figure 2.2. Schematic of a high power laser diode array.

As with the single stripe device described above, the multiple active stripes are defined on the diode laser wafer by proton bombardment of the surface layer. If these active stripes are defined sufficiently close together then lateral leakage of optical radiation can cause evanescent coupling of optical modes in adjacent emitters resulting in coherence of the output beam across the array facet. Ideally the array of emitters should phase-lock with zero phase difference between neighbouring stripes to generate a single lobed, diffraction limited far field radiation pattern. In practice, however, due to high optical loss between stripes, the lowest threshold mode of operation for the array tends to be that with adjacent stripes locked in anti-phase resulting in a dual lobed emission. For the purposes of pumping solid state lasers this coherent dual lobed radiation pattern may in fact be detrimental to laser performance because of the nonuniform pumping of the solid state gain medium. For this reason, in many commercially produced devices, the degree of phase locking across the array is relaxed so the intensity profile of the far field emission pattern in the plane of the diode junction is more uniform although several times the diffraction limit in width. In the plane perpendicular to the diode junction, the output beam remains diffraction limited[8].

The maximum output power characteristics of these arrays scale approximately linearly with the number of emitters in the array up to total array widths of the order of 400μm. However, as the width of the array becomes significantly greater than the laser cavity length, Amplified Spontaneous Emission (ASE) and even transverse lasing can occur across the array causing instability and reduced output power in the desired lasing mode. Such parasitic optical interactions across the array can be suppressed by etching grooves periodically along the length of the device[14]. In this way, very large arrays, known as diode laser bars, have been fabricated. At present practical processing considerations limit laser bar widths to a maximum of 1cm. Such a 1cm wide bar, with a total active aperture size of 7200μm, has been operated up to a 122W CW before failing catastrophically[6].

Although the maximum output power for this device was limited by catastrophic melting of the diode laser facet, under CW operating conditions it is more usual for the maximum output power to be limited by heat dissipation in the diode junction. Excessive heat build up in the diode laser manifests itself as a reversible roll-off in output power with increasing drive current[15,4]. By operating the array in a long pulse (~250μs), low repetition rate (~100Hz) mode known as quasi-CW operation, over-heating of the diode junction can be avoided and the peak output power is limited only by the catastrophic failure level.

2.3.2 Two Dimensional Diode Laser Stacks

Yet higher output powers can be attained by combining the outputs of many individual diode laser arrays or bars. Diode laser bars can be conveniently stacked to form large two dimensional arrays suitable for side pumping solid state laser rods or slabs. Care must be exercised when selecting bar elements for a two dimensional stack. The bars chosen must have similar light vs current characteristics and spectral outputs in order to achieve relatively uniform intensity output from the emitting face and an overall spectral emission narrow enough for efficient pumping of solid state laser materials. The major drawback with the stack geometry is the difficulty in removing waste heat even

when operating the array quasi-CW. To maintain high brightness output from the stack, bars are mounted close together and so waste heat can usually only be removed from the rear surface. Various stack architectures have been developed to improve heat dissipation including the use of impingement coolers[16] or synthetic diamond heat spreaders mounted on silicon microchannel coolers[17].

2.3.3 Fibre Coupled Diode Laser Arrays

An alternative method of multiplexing diode laser arrays to achieve high powers is to couple the output from individual diode laser arrays or bars into multimode optical fibres and form these fibres into tightly packed bundles[18]. Although the need for accurate alignment of the optical fibres to the diode laser arrays adds an extra element of complexity to the packaging of the device (and subsequent increase in production costs), fibre coupling offers several advantages over two dimensional stacks for high power operation. For instance, fibre coupling enables:

1. the diode laser arrays to be physically separated easing the problem of waste heat removal.

2. the arrays to be individually temperature tuned for best spectral matching of pump radiation into absorption bands of solid state laser materials. This relaxes the tolerances on spectral matching of diode laser array emission compared with the high degree of spectral and electrical matching required for two dimensional stacks.

3. the diode laser arrays and their associated hardware (current drive units, temperature controllers, heatsinks, etc) to be located remotely from the solid state laser. This enables complete electrical isolation of the laser head and offers the possibility of a more compact laser head design.

4. scalability to higher powers by simply adding more fibre coupled arrays.

5. easy replacement of damaged diode laser arrays.

6. circular optical output. Fibre optic coupling can be a useful way of circularising the highly astigmatic, elliptical output beam of a diode laser array. Linear-to-circular fibre bundles have also been used successfully to combine the individual laser array elements of a multiple array, 1cm wide, diode laser bar into a circular output format[4]

However, fibre coupled arrays exhibit a lower overall electrical to optical efficiency due to quite high coupling losses incurred because of the mismatch between the elliptical output mode shape of the diode laser array and the guided modes of the optical fibre. The optical brightness (optical power per unit area per unit solid angle) of a fibre coupled array is also significantly less than that obtained directly from the array because of the larger emitting area of the fibre end. To illustrate this, a standard diode laser array emitting 500mW from a 100μm × 0.5μm aperture into an elliptical mode with FWHM divergence of 40° in the major axis and 10° in the minor axis has an optical brightness approaching 5MW/cm^{-2}-sr. in contrast, a commercially available fibre coupled version of the same array exhibits an optical brightness of only 11kW/cm^{-2}-sr assuming a typical coupling efficiency of 50% into a 100μm diameter core, 0.3 N.A. optical fibre. Significant improvements in optical brightness can be achieved by using a smaller diameter fibre flared into an elliptical cross-section at one end. The elliptically shaped fibre end, butt coupled to the diode array offers a good match to the array's elliptical output greatly improving coupling efficiency. The optical brightness at the output end of a multimode fibre is given by the expression

$$\text{optical Brightness} = \frac{\text{Power}}{\text{Area of fibre end} \times \text{Solid angle of fibre emission}}$$

$$= \frac{P}{\{\pi r\,(\text{N.A.})\}^2} \qquad (2.1)$$

where P is the optical power from fibre, r equals the fibre core radius and (N.A.) is the numerical aperture of the fibre. From equation (2.1) it can be seen that the brightness is inversely proportional to the square of the fibre core radius so it is obviously advantageous to taper the fibre core to a small size.

Using this approach Chang-Hasnain and co-workers[19] at Spectra Diode Laboratories have demonstrated coupling efficiencies in excess of 80% for a 100μm wide diode array coupled into a 140μm × 22μm elliptically ended fibre tapered to a circular exit aperture of 50μm diameter. The maximum output power from the fibre reached 850mW CW corresponding to an optical brightness from the fibre end of 150kW/(cm^{-2} sr).

2.4 Other Areas In High Power Diode Laser Research

Although edge emitting GaAlAs phased array technology is currently proving a very successful route to high output power, long lifetime semiconductor diode lasers, many other routes to high output powers from diode laser devices are also being explored.

For instance, diode laser arrays are now being developed which emit an output beam perpendicular to the surface of the device as opposed to the more conventional edge emission. Since these surface emitting lasers are not constrained to emit from an exposed edge of the semiconductor, they can be grown anywhere on the substrate enabling one and two dimensional integrated arrays to be fabricated on a single substrate. The problem of waste heat removal which currently plagues edge emitting, high power linear arrays, bars and two dimensional stacks may be eased in the surface emitting geometry as heat can be removed directly through the whole area of the substrate. At present there are three basic configurations of surface emitting devices; vertical cavity lasers[20,21], 45° deflectors[22,23,24] and grating surface emitters[25,26,27,28].

Efforts are also being made to improve the beam quality from high power diode laser arrays. A number of promising diode laser geometries are emerging that have

successfully generated coherent high power emission such as Y-junction coupled arrays[29,30,31], injection locked arrays[32,33], hybrid and monolithically integrated Master Oscillator/Power Amplifiers (MOPA)[34,35,36,37,38] devices and arrays of resonant antiguides[39,40,41,42,43,44].

High power diode laser technology is also being applied to other families of semiconductor lasers to provide high power devices operating at alternative wavelengths. Of particular note has been the development of high power strained layer quantum well InGaAs diode lasers emitting in the 910 - 980nm region of the spectrum[45,8,46] for pumping Erbium doped optical fibre amplifiers in long distance optical communication networks[47]. Also, high power diode laser arrays operating in the red visible part of the spectrum (660-680nm)[48,49] are now available and are of considerable interest as pump sources for new vibronic solid state laser gain media such as Cr:Alexandrite[50], Cr:$LiSrAlF_6$ [51], Cr:$LiCaAlF_6$ [52] and Cr:$LiSrGaF_6$ [53].

The wavelength range accessible from diode lasers is also being extended to longer and shorter wavelengths through the development of new semiconductor alloys and diode lasers architectures. The wavelength range now covered by the semiconductor diode laser family extends from 30μm in the mid infra-red generated from PbSnSe lead salt diode lasers down to 447nm from the new cryogenically cooled ZnSe/ZnMgSSe Multiple Quantum Well devices[54,55,56,57].

Given the large spectral coverage possible from diode lasers and the progress being made in the areas of diode laser technology and solid state laser medium research, in particular tunable vibronic systems, there is tremendous potential for developments in the field of diode laser pumped solid state lasers.

2.5 Characterisation of the Pump Diode Laser

In this work, the laser diode array used to end-pump the Nd:YAG laser is a GaAlAs quantum well device (model SDL-2422-42) having a gain guided, double heterojunction

structure. This device, manufactured by Spectra Diode Labs, is packaged in a TO-3 style canister and comes complete with an internal thermo-electric cooler (TEC) and a photodiode for optical output power monitoring. Laser emission is via a fused silica multimode, step index optical fibre pigtail of dimensions 100μm core diameter , 140μm cladding diameter and effective numerical aperture N.A.=0.3. Close coupling of this fibre to the emitting facet of the laser diode array is specified to provide approximately 50% coupling efficiency resulting in a net maximum optical output power of 100mW from the fibre end.

2.5.1 Fibre Pigtail Output.

The multimode optical fibre scrambles the spatial mode pattern of the laser diode array resulting in a spatially incoherent but temporally coherent optical emission. The output from the fibre has a circularly symmetric, approximately flat topped intensity profile emerging as a 20° full width at half maximum (FWHM) diverging light cone as shown in figure 2.3.

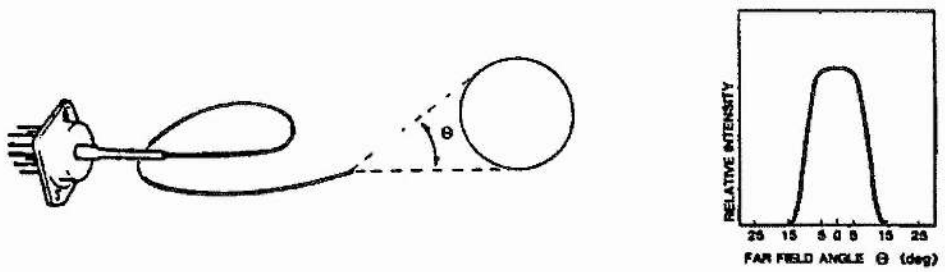

Figure 2.3. Intensity emission pattern from a fibre coupled laser diode array (diagram from Ref.8).

2.5.2 Laser Diode Drivers.

Commercial laser diode drivers (Spectra Diode Labs SDL800) were used to power the CW laser diode arrays. These drivers can provide DC currents up to 1 Amp and may be operated in either a Current Control (constant diode current) or in a Light Control (constant light output from the laser diode array) mode. The driver unit also contains

thermo-electric cooler (TEC) control circuitry to enable temperature control of the laser diode over the range -20°C - +40°C to an accuracy of ±1°C.

2.5.3 Output Power Vs Current Characteristics.

Figure 2.4 shows the light versus current characteristics for the laser diode taken at diode temperatures of 0°C and 25°C. Below threshold the device behaves as a low efficiency Light Emitting Diode (LED) generating only incoherent spontaneous emission. As lasing threshold current is exceeded however, the optical power emitted from the laser diode array increases in a rapid, linear fashion with increasing input current.

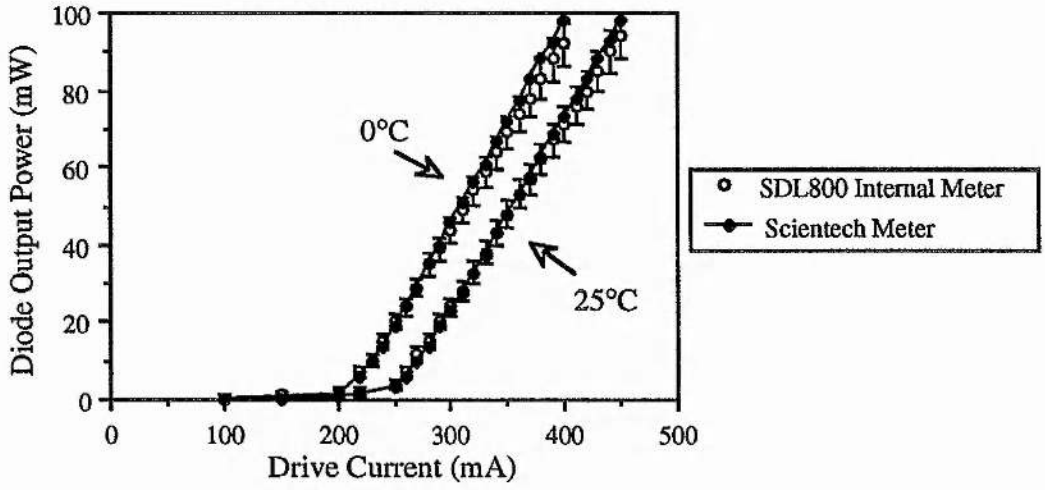

Figure 2.4. Output power as a function of drive current for one of the diode laser arrays. Optical power measurements were made using the laser diode's internal power meter and with an external Scientech power meter.

It can also be seen from figure 2.4 that there is a dependence of laser threshold current on device temperature. This change in threshold current with temperature can be approximated by the exponential function[8]

$$(\text{threshold at } T_2) = (\text{threshold at } T_1)\exp[(T_2 - T_1)/T_0] \qquad (2.2)$$

where T_0 is known as the threshold temperature coefficient. For GaAlAs devices, T_0 lies typically in the range 120 - 190K, the exact value depending on the material quality and

structure of the device. For the data in figure 2.4, T_0 is approximately 150K. The increase in threshold current with increasing temperature is due in part to the increased energy spread of the carriers injected in to the active region.

2.5.4 Spectral Characteristics.

The spectral characteristics of the laser diode array output were studied using a Monospek 1000, 1 metre monochromator calibrated to the 632.8nm and 1064nm laser transitions of a HeNe and a Nd:YAG laser respectively. The highly divergent laser emission from the fibre pigtail was focused onto the input slit of the monochromator by means of a ×10 microscope objective. Transmission through the monochromator was monitored by a large area silicon photodiode (mounted at the monochromator output slit) coupled to an amplifier and chart recorder.

Mode Structure.

A typical output spectrum from the laser diode array is shown in figure 2.5. The device oscillates simultaneously on several (typically 5-10) longitudinal modes contained within a ≈2nm envelope. These modes are adjacent longitudinal modes of the Fabry-Perot laser cavity and are separated in wavelength by the laser cavity's free spectral range $\Delta\lambda$ given by (see Ref.8)

$$\Delta\lambda \approx \frac{\lambda^2}{2nL\cdot(1.25)} \tag{2.3}$$

where λ = operating wavelength (810nm), n = effective refractive index of the active region (≈2.86) and L = laser cavity length. The factor (1.25) is included to account for dispersion in the layered structure of the diode. From the spectrum illustrated in figure 2.5 the mode spacing is 0.34nm and so equation (2.3) indicates a cavity length, L, of 270μm for this device. The spectral width of the individual longitudinal modes is specified in the manufacturers literature to be 10MHz - 5GHz depending on the power in the mode.

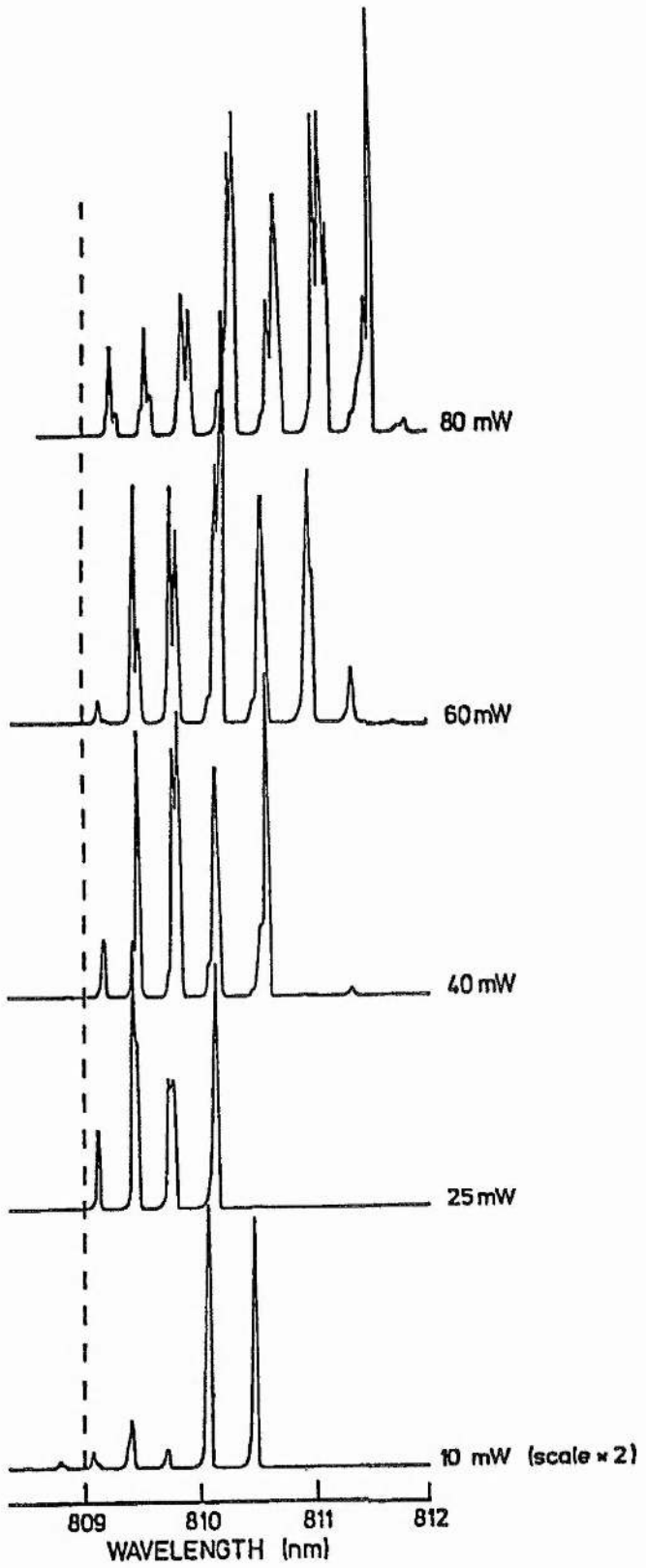

Figure 2.5. Diode laser emission spectra at different output powers.

As well as oscillating on several longitudinal modes, the laser diode array supports oscillation of lateral modes across the evanescently coupled active stripes. It is the presence of these lateral modes or "supermodes"[58] which is responsible for the clearly visible substructure superimposed on the spectrum in figure 2.5.

Mode Structure as a Function of Power.

Figure 2.5 shows emission spectra of the laser array for various optical output powers. As might be expected, the number of oscillating modes tends to increase with increasing output power. The envelope of the diode laser emission spectrum also shifts towards longer wavelengths with increasing drive current probably due to an increasing temperature differential between the laser diode chip and the temperature controlled heatsink.

Temperature Tuning.

The tunability of the laser diode output wavelength was investigated. Spectra of the laser output were recorded for various laser diode temperatures in the range 0°C - 30°C whilst maintaining a constant laser output power of 50mW. The primary tuning characteristic indicated by this data (see figure 2.6) is that the 2nm wide wavelength envelope of the laser diode emission shifts at a rate of ~0.23nm/°C. This effect is caused by temperature related changes in the bandgap energy. Figure 2.6 also shows that the wavelength of any one longitudinal mode has a much smaller temperature dependence, changing by only ~0.06nm/°C. This tuning of the individual mode frequencies is related to thermal expansion of the laser diode cavity and temperature dependant variations of the refractive index of the active region.

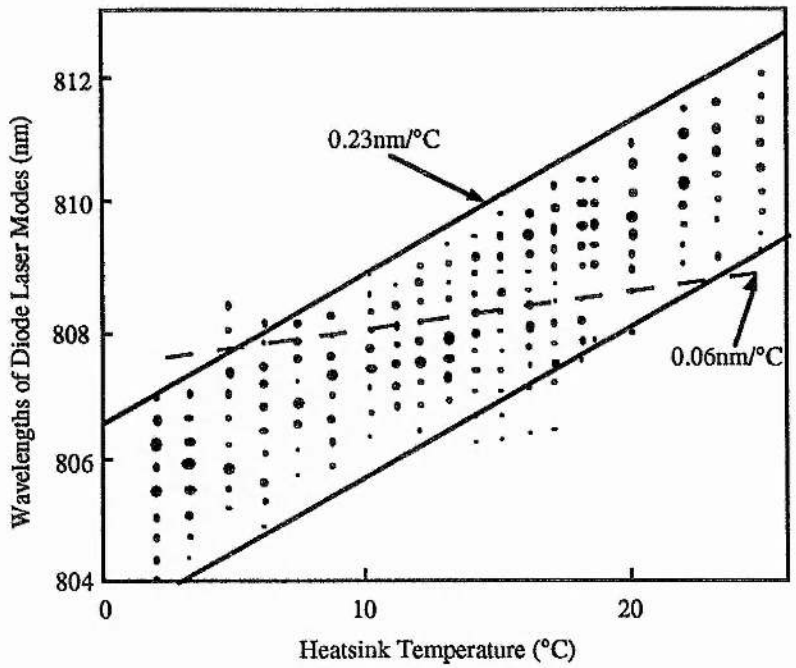

(a)

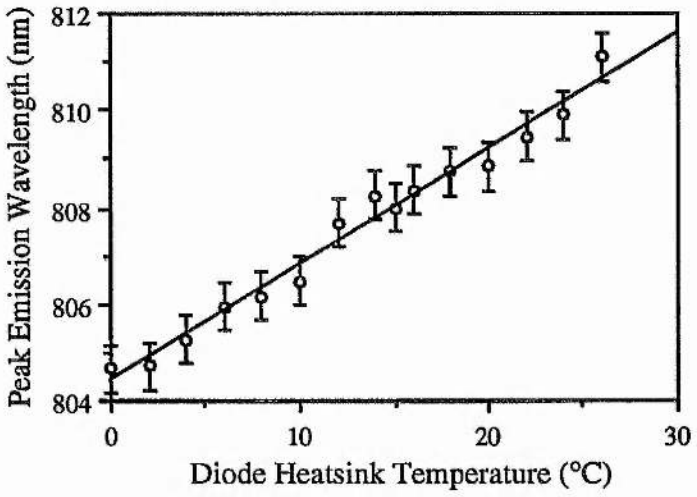

(b)

Figure 2.6. Temperature tuning of the diode laser array. (a) Here, the measured wavelengths of each individual diode laser mode is indicated, with the size of the marker corresponding (approximately) to the relative strength of the mode. (b) The wavelength of the peak in diode laser output as a function of temperature. The total diode laser output power from the fibre was 50mW for each graph.

2.6 References

1 Streifer W., Burnham R. D., Paoli T. L., Scifres D. R., "Phased Array Diode Lasers", Laser Focus **20**(6) 100 (1984)

2 Cross P. S., Jacobs R. R., Scifres D. R., "Dynamite Diodes", Photon. Spec. **18**(9) 79 (1984)

3 Cross P. S., Harnagel G. L., Streifer W., Scifres D. R., Welch D. F., "Ultra-High Power Semiconductor Diode Laser Arrays", Science **237**(9) 1305 (1987)

4 Striefer W., Scifres D. R., Harnagel G. L., Welch D. F., Berger J., Sakamoto M., "Advances in Diode Laser Pumps", IEEE J. Quant. Elec. **24**(6) 883 (1988)

5 Endriz J. G., Vakili M., Browder G. S., DeVito M., Haden J. M., Harnagel G. L., Plano W. E., Sakamoto M., Welch D. F., Willing S., "High Power Diode Laser Arrays", IEEE J. Quant. Elec. **28**(4) 952 (1992)

6 Sakamoto M., Endriz J. G., Scifres D. R., "120W CW Output Power From Monolithic AlGaAs (800nm) Laser Diode Array Mounted on Diamond Heatsink", Elec. Lett. **28**(2) 197 (1992)

7 Welch D. F., Mehuys D., Parke R., Nam D., Waarts R., Harnagel G., Endriz J., Scifres D., "High Power, Two-Dimensional Laser Array", Technical Digest volume 8 from Conference on Lasers and Electro-Optics (1991), (Optical Society Of America, Washington D.C. 1991) paper CWE5

8 "Laser Diode Operator's Manual and Technical Notes", Spectra Diode Labs, San Jose, California, (1989)

9 Jaeckel H., Bona G. L., Buchmann P., Meier H. P., Vettiger P., Kozlovsky W. J., Lenth W., "Very high power (425mW) AlGaAs SQW-Grinsch Ridge laser with

frequency doubled output (41mW at 428nm)", IEEE J. Quant. Elect. **27** (6), 1560 (1991)

10 Henry C. H., "Catastrophic Damage of $Al_xGa_{1-x}As$ Double Heterostructure Laser Material", J. Appl. Phys. **50**(5) 3721 (1979)

11 Thompson G. H. B., "Physics of Semiconductor Laser Devices", John Wiley and Sons LTD., U.K., (1985) ISBN 0-471-27685-5,pp 331-346

12 Yamanaka H., Iwamoto K., Yamaguchi N., Honda K., Mamine T., Kojima C., "Progress in Super High Power Laser Diodes With a Broad Area Structure", Technical Digest volume 7 from Conference on Lasers an Electro-Optics (1990), (Optical Society of America, Washington D.C. 1990) paper CFA2

13 Garbuzov D. Z., Antonishkis N. Y., Bondareu A. D., Gulakov A. B., Zhigulin S. N., Katsavets N. I., Kochergin A. V., Rafailov E. U., "High Power 0.8μm InGaAsP-GaAs SCH SQW Laser", IEEE J. Quant. Elec. **27**(6) 1531 (1991)

14 Harnagel G. L., Cross P. S., Scifres D. R., Welch D. F., Lennon C. R., Worland D. P., Birnham R. D., "High-Power Quasi-CW Monolithic Laser Diode Linear Arrays", Appl. Phys. Lett. **49**(21) 1418 (1986)

15 Welch D. F., Chan B., Streifer W., Scifres D. R., "High-Power, 8W CW, Single-Quantum-Well Laser Diode Array", Elec. Lett. **24**(2) 113 (1988)

16 Spectra Diode Laboratories technical note "Laser Diode Array Designs for the NOSC High Efficiency Advances Solid State Laser" April 1991.

17 Mundinger D., Beach R., Benett W., Solarz R., Sperry V., Ciarlo D., "High Average Power Edge Emitting Laser Diode-Array on Silicon Microchannel Coolers", Appl. Phys. Lett. **57**(21) 2172 (1990)

18 Berger J., Welch D. F., Streifer W., Scifres D. R., Hoffman N. J., Smith J. J., Rodechi D., "Fibre Coupled, End-Pumped Nd:YAG Laser", Opt. Lett. **13**(4) 306 (1988)

19 Chang-Hasnain C., Worland D. P., scifres D. R., "High-Intensity Fibre-Coupled Diode-Laser Array", Elec. Lett. **22**(2) 65 (1986)

20 Scherer A., Jewell J. L., Lee Y. H., Harbison J. P., Florez L. T., "Fabrication of Microlasers and Microresonator Optical Switches", Appl. Phys. Lett. **55**(26) 2724 (1989)

21 Yoo H. J., Scherer A., Harbison J. P., Florez L. T., Paek E. G., Van Der Gaag B. P., Hayes J. R., Von Lehmen A., Kwon Y. S., "Fabrication of a 2-Dimensional Phased-Array of Vertical-Cavity Surface-Emitting Lasers", Appl. Phys. Lett. **56**(13) 1198 (1990)

22 Liau Z. L., Walpole J. N., "Surface Emitting GaInAsP-InP Laser with Low Threshold Current and High Efficiency", Appl. Phys. Lett. **46** 115 (1985)

23 Roux R., "Monolithic Pump Lasers Emerge From Lab", Laser Focus World **27**(4) 27 (1991)

24 Jansen M., Yang J. J., Heflinger L., Ou S. S., Sergant M., Haung J., Wilcox J., "Coherent Operation of Injection-Locked Monolithic Surface-Emitting Diode-Laser Arrays", Appl. Phys. Lett. **54**(26) 2634 (1989)

25 Parke R., Waarts R., Welch D. F., Hardy A., Streifer W., "High Efficiency, High Uniformity, Grating Coupled Surface Emitting Lasers", Elec. Lett. **26**(2) 125 (1990)

26 Evans G. A., Carlson N. W., Hammer J. M., Lurie M., Butler J. K., Palfrey S. L., Amantea R., Carr L. A., Hawrylo F. Z., James E. A., Kaiser C. J., Kirk J. B.,

Reichert W. F., Chinn S. R., Shealy J. R., Zory P. S., "Coherent, Monolithic Two-Dimensional (10×10) Laser Arrays Using Grating Surface Emission", Appl. Phys. Lett. **53** 2123 (1988)

27 Evans G. A., Carlson N. W., Hammer J. M., Lurie M., Butler J. K., Pa;frey S. L., Amantea R., Carr L. A., Hawrylo F. Z., James E. A., Kaiser C. J., Kirk J. B., Reichert W. F., "Two-Dimensional Coherent Laser Arrays Using Grating Surface Emission", IEEE J. Quant. Elec. **25**(6) 1525 (1989)

28 Evans G. A., Carlson N. W., Bour D. P., Lurie M., "14W Peak Power Grating Surface Emitting Laser Array", Elec. Lett. **26**(17) 1381 (1990)

29 Streifer W., Welch D. F., Cross P. S., Scifres D. R., "Y-Junction Semiconductor Laser Arrays", IEEE J. Quant. Elec. **QE-23**(6) 744-756 (1987)

30 Chinn S. R., "Analysis of a Laser Phased-Array Using a Distributed Y-Junction Analogue", IEEE J. Quant. Elec. **24**(4) 687 (1988)

31 Whiteaway J. E. A., Moule D. J., Clements S. J., "Tree Array Lasers", Elec. Lett. **25**(12) 779 (1989)

32 Leger J. R., Swanson G. J., VeldKamp W. B., "Coherent Beam Addition of GaAlAs Lasers by Binary Phase Gratings", Appl. Phys. Lett. **48**(14) 888 (1986)

33 Brewer L. R., "Highly Coherent Injection-Locked Laser Diode-Arrays", Appl. Opt. **30**(3) 317 (1991)

34 Welch D. F., Waarts R., Mehuys D., Parke R., Scifres D., Craig R., Sreifer D., "High-Power, Diffraction Limited, Monolithically Integrated Master Oscillator Power Amplifier", Appl. Phys. Lett. **57**(20) 2054 (1990)

35 Botez D., "Performance of Semiconductor Lasers Continues to Improve", Laser Focus World **27**(2) 29 (1991)

36 Goldberg L., Weller J. F., Mehuys D., Welch D. F., Cross P. S., Scifres D.R., "12W Broad Area Semiconductor Amplifier with Diffration Limited Optical Output", Elec. Lett. **27**(11) 927 (1991)

37 Welch D. F., Parke R., Mehuys D., Hardy A., Lang R., Obrien S., Scifres S., "1.1W CW, Diffraction-Limited Operation of a Monolithically Integrated Flared-Amplifier Master Oscillator Power-Amplifier", Elec. Lett. **28**(21) 2011 (1992)

38 Mehuys D., Welch D. F., Goldberg L., "2.0W CW, Diffraction-Limited Tapered Amplifier With Diode Injection", Elec. Lett., **28**(21) 1944 (1992)

39 Botez D., Mawst L. J., Hayashida P., Peterson G., Roth T. J., "High-Power, Diffraction-Limited-Beam Operation From Phase-Locked Diode Laser Arrays of Closely Spaced Leaky Waveguides (Antiguides)", Appl. Phys. Lett. **53**(6) 464 (1988)

40 Mawst L. J., Botez D., Roth T. J., Peterson G., Yang J. J., "Diffraction Coupled, Phase-Locked Arrays of Antiguided, Quantum-Well Lasers Grown by Metalorganic Chemical Vapour Deposition", Elec. Lett. **24**(15) 958 (1988)

41 Botez D., Mawst L. J., Peterson G. L., Roth T. J., "Phase-Locked Arrays of Antiguides - Modal Content and Discrimination", IEEE J. Quant. Elec. **26**(3) 482 (1990)

42 Botez D., Jansen M., Mawst L. J., Peterson G., Roth T. J., "Watt-Range, Coherent, Uniphase Powers From Phase-Locked Arrays of Antiguided Diode-Lasers", Appl. Phys. Lett. **58**(19) 2070 (1991)

43 Botez D., "ROW Laser Array Produces Watts of Coherent Power", Laser Focus World **27**(10) 105 (1991)

44 Zmudzinski C., Mawst L. J., Botez D., "1W Diffraction-Limited-Beam Operation of a Resonant-Optical-Waveguide Diode Laser Arrays at 0.98μm" Elec. Lett. **28**(16) 1543 (1992)

45 Laidig W. D., Lin Y. F., Caldwell P. J., "Properties of $In_xGa_{1-x}As$-GaAs Strained Layer Quantum-Well-Heterostructure Injection Lasers", J. Appl. Phys. **57**(1) 33 (1985)

46 Zmudzinski C., Mawst L. J., Botez D., "1W Diffraction-Limited-Beam Operation of a Resonant-Optical-Waveguide Diode Laser Arrays at 0.98μm" Elec. Lett. 28(16) 1543 (1992)

47 Shimizu M., Horiguchi M., Yamada M., Nishi I., Noda J., Takeshita A. Okayasu M., Uehara S., Sugita E., "Compact and Highly Efficient Fibre Amplifier Modules Pumped by a 0.98μm Laser Diode", J. Lightwave Tech. **9**(2) 291 (1991)

48 Haden J. M., Nam D. W., Welch D. F., Endriz J. G., "High Power, 60W Quasi-CW, Visible Laser Diode Array", Elec. Lett. **28**(5) 451 (1992)

49 Serreze H. B., Harding C. M., "100W 671nm Visible Laser Diode Array", Elec. Lett. **28**(23) 2115 (1992)

50 Scheps R., Gately B., Mayers J. F., Krasinski J. S., Heller D. F., "Alexandrite Laser Pumped by Semiconductor Lasers", Appl. Phys. Lett. **56**(23) 2288 (1990)

51 Scheps R., Mayers J. F., Serreze H. B., Rosenberg A., Morris R. C., Long M., "Diode Pumped Cr:$LiSrAlF_6$ Lasers", Opt. Lett. **16**(11) 820 (1991)

52 Scheps R., "Cr:$LiCaAlF_6$ Laser Pumped by Visible Laser Diodes", IEEE J. Quant. Elec. **27**(8) 1968 (1991)

53 Scheps R., "Laser-Diode-Pumped Cr:LiSrGaF$_6$", IEEE J. Photon Tech. Lett. **4**(6) 548 (1992)

54 Colles M. J., Pidgeon C. R. ,"Tunable Lasers", Rep. Prog. Phys. **38**(3) 435 (1975)

55 Thompson G. H. B., "Physics of Semiconductor Laser Devices", John Wiley and Sons (1980)

56 Hecht J., "The Laser Guide Book", McGraw-Hill (1986)

57 Okuyama H., Miyajima T., Morinaga Y., Hei F., Ozawa M., Akimoto K., "ZnSe/ZnMgSSe Blue Laser Diode", Elec. Lett. **28**(19) 1798 (1992)

58 Verdeyen J. T., "Laser Electronics", Prentice-Hall Inc., 2nd Edition (1989)

Chapter 3

CHARACTERISATION AND MODELLING OF THE Nd:YAG HOLOSTERIC LASER

3.1 Nd:YAG Laser Cavity Design

The structure of the holosteric laser is similar to the experimental systems developed by, for example, Sipes[1], Berger et al[2] and to some commercial systems such as the Spectra-Physics model 7900 fibre coupled Nd:YAG laser. The laser had a plano-concave resonator containing a 5mm long, 3mm diameter Nd:YAG rod. The pumped end of the Nd:YAG rod was dichroically coated to form a highly transmitting window for the pump wavelength (T>85% at 809nm) and a high reflectivity mirror at the lasing wavelength (R>99.5% at 1064nm). The opposite end of the laser rod was slightly wedged to prevent etalon effects and was also antireflection coated for 1064nm light to reduce intracavity losses. Output coupling was by means of a 1-1.5% transmission concave mirror with a typical radius of curvature of 50mm. This output mirror was mounted on a two axis gimbal mount and a linear translation stage to allow the mirrors to be aligned and the cavity length to be optimised. The end-pumped laser cavity is illustrated in figure 3.1.

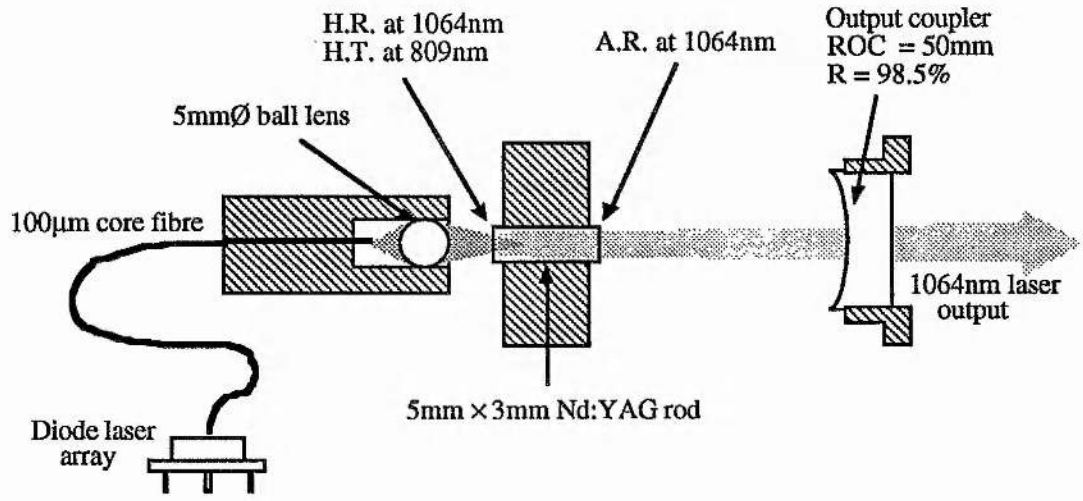

Figure 3.1. Schematic diagram of the open cavity, end-pumped holosteric laser.

3.2 Pump Light Delivery System

The diode laser array's fibre optic pigtail and a focusing element were aligned and clamped in a "V" groove machined between two aluminium blocks. This pump assembly was mounted on a three axis linear translation unit to facilitate accurate spatial positioning of the pump beam with respect to the end of the Nd:YAG rod.

In order to focus the highly divergent (~14° half cone) output beam from the 100μm core, N.A.=0.3 fibre pigtail, the focusing element was required to have a large numerical aperture. The focusing element used was a single, antireflection coated, 5mm diameter ball lens (Melles Griot model 06LMS205). The optimum focused spot size for the pump beam was found by varying the fibre end - ball lens separation whilst monitoring the Nd:YAG laser output power. A fibre - lens separation of between 2mm and 3mm corresponding to a pump spot radius of around 70μm gave best results for a laser mode waist of about 60μm. The tolerance on the exact pump beam spot size was not too critical as the Nd:YAG laser output power could also be maximised by adjusting the laser cavity length to optimise the mode overlap and divergence of the pump and laser beams.

The use of a single large numerical aperture lens for focusing the pump light meant that spherical aberration played an important role in determining the pump beam profile inside the Nd:YAG rod. To investigate these aberration effects the fibre - ball lens pair were modelled using a computer based ray tracing analysis. The end face of the fibre was divided into 1000 elements and from each of these elements a 14° half angle cone of rays was propagated through the lens and into the laser rod. The power density at any point inside the laser rod could then be calculated by dividing the rod into many elements and counting the number of rays passing through each element at that point. An example of a contour plot generated by this model showing the pump power density distribution inside the rod is shown in figure 3.2. From this figure it can be seen that the lens aberrations actually have the beneficial effect of softening the pump beam focus within the rod thus improving the spatial overlap of the pump beam to the low divergence laser mode.

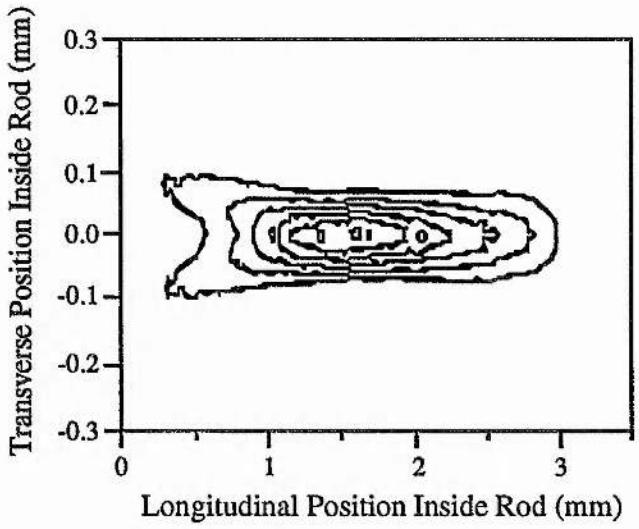

Figure 3.2. Contour plot of the pump density within the Nd:YAG rod in the absence of any absorption. The fibre-ball lens separation was 2mm and the lens-rod distance was 3mm.

Since it was not possible to measure experimentally the pump power distribution inside the laser rod directly, the only way of checking the accuracy of the computer model was to set the rod refractive index value to 1 and to compare the data generated to free space pump beam profile measurements made using a scanning pinhole (12μm diameter) and photodiode arrangement. The results are compared in figure 3.3 and show a reasonable agreement between experiment and model.

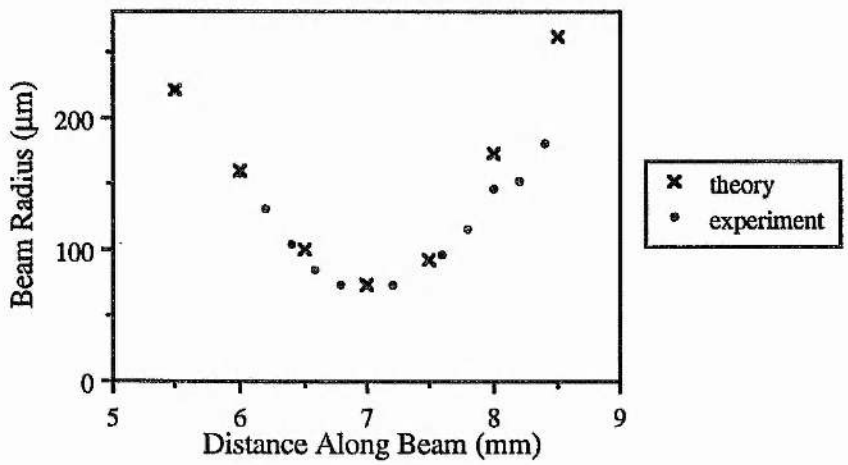

Figure 3.3. Comparison of the experimental and theoretical pump beam divergence in air. The beam radius was taken to be the beam half width at the $1/e^2$ intensity point.

3.3 Spectroscopic Study of Nd:YAG

To determine the overlap of the emission wavelength of the diode laser and the absorption profile of the Nd:YAG laser rod, a spectroscopic analysis of the Nd:YAG sample was carried out. The transmission spectrum of the 5mm long Nd:YAG crystal was recorded using a Monospek 1 metre scanning monochromator with an incandescent lamp as a white light source. This optical transmission data was then converted into units of absorptivity per unit length normalised to the black body emission spectrum of the incandescent lamp. This converted data is displayed in figure 3.4 together with the typical 2nm wide emission band from the multi-longitudinal mode laser diode for comparison. The 2nm emission band of the diode laser is too broad to be matched completely into the maximum absorption peak of the Nd:YAG. Using a single frequency high power diode laser would offer a better spectral overlap with the maximum Nd:YAG absorption and so could improve pumping efficiency.

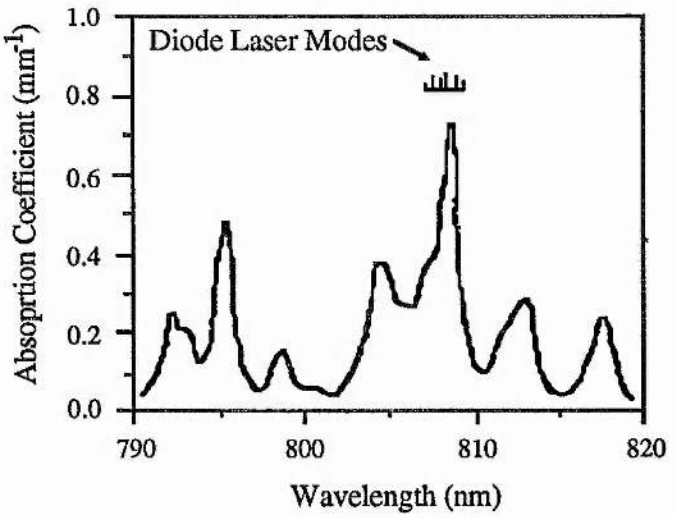

Figure 3.4. Absorption spectrum of 1% doped Nd:YAG. For comparison the ~2nm wide diode laser array emission spectrum is also shown.

3.4 Measurement Of Pump Light Transmission Through an Nd:YAG Laser Rod

To obtain more direct data on the absorption of the diode laser emission in the Nd:YAG rod the diode laser output was passed through the crystal and the transmitted optical power recorded as a function of diode heatsink temperature (i.e.. mean emission wavelength). See figure 3.5. In comparison with figure 3.4, much of the fine spectral absorption detail of the Nd:YAG sample has been lost due to the relatively broad diode laser wavelength emission smearing out the sharper absorption features of the Nd:YAG.

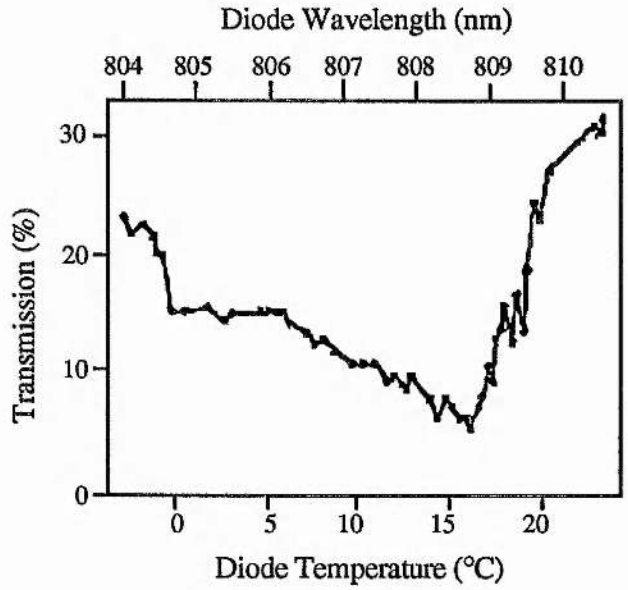

Figure 3.5. Transmission of the diode laser pump light through a 5mm long Nd:YAG rod plotted as a function of the diode laser heatsink temperature/output wavelength. Output power from the fibre coupled diode laser was 100mW from the end of the fibre.

From figure 3.5 the maximum absorption of pump radiation in the laser crystal occurs at a diode heatsink temperature of ~16±0.5°C corresponding to a wavelength emission from the diode laser array centred on ~808.7nm. At this pump wavelength approximately 95% of the diode laser emission was absorbed in the 5mm long sample of Nd:YAG.

3.5 Optimum Output Coupling

For any laser oscillator there is an optimum amount of output coupling which gives the maximum power extraction from the resonator. If the amount of output coupling is too small, the power circulating in the resonator will be high but only a small portion of this power can leak from the cavity to form a useful output. If, on the other hand, too much light is coupled from the cavity, the overall cavity losses will exceed the available gain and laser threshold will not be reached. Between these too extremes exists an amount of output coupling for which the power extracted from the laser is a maximum.

In an attempt to determine the optimum output coupling for the diode pumped Nd:YAG laser, the laser output power was recorded as a function of pump power for a selection of cavity end mirrors of differing reflectivities. This data, plotted in figure 3.6, indicated an optimum output coupling of around 1%. However, this method for determining the optimum output coupling was rather unsatisfactory since the laser output power could only be determined for a few discrete values of mirror reflectivity and the laser had to be realigned for each separate end mirror. A true comparison of the output

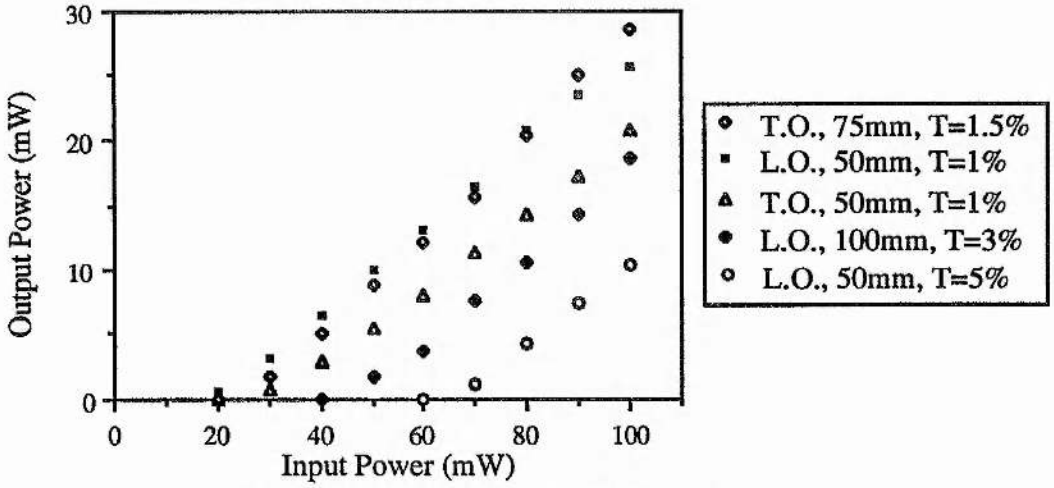

Figure 3.6. Optical to optical slope efficiency data from the Nd:YAG holosteric laser for a variety of output coupler mirrors. L.O. - Laser Optik, T.O. - Tech. Optics.

power data for the different mirrors used was also not possible because of the inconsistencies in the mirror radii of curvature. The different mirror curvatures gave rise to different spot sizes within the Nd:YAG rod which in turn influenced the power output from the laser.

To obtain more detailed information on the effect of output coupling on laser output power for this system, some form of continuously variable output coupler was required. To achieve this, the end cavity mirror was replaced by a 100mm radius of curvature, high reflectivity (>99.9%) mirror and a 2mm thick fused silica glass plate was inserted into the cavity at close to Brewster's angle to act as the output coupler[3]. The insertion of this glass plate constrained the laser to oscillate on one linear polarisation. By rotating the glass plate around Brewster's angle, the Fresnel reflectivity of the surface of the glass plate could be varied from zero to a few percent for that polarisation state.

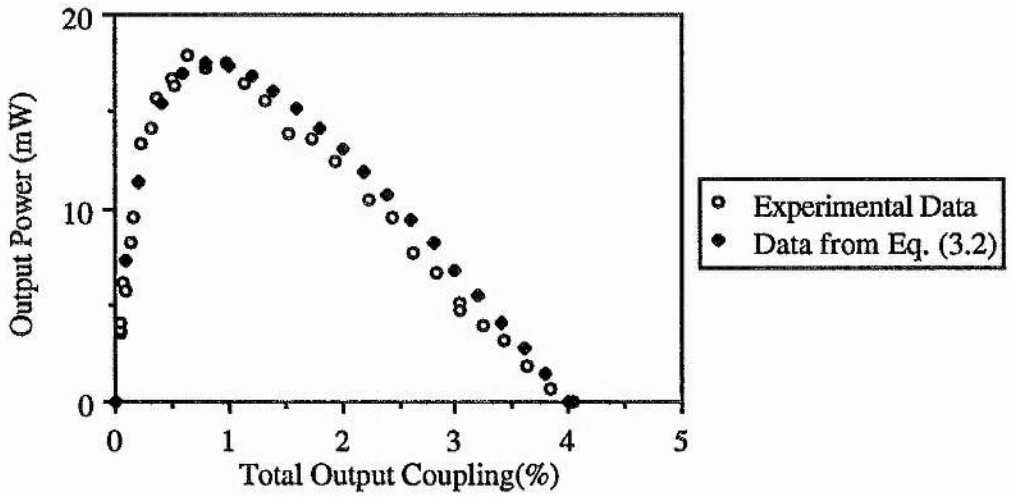

Figure 3.7 Laser output power as a function of output coupling.

In figure 3.7 the total output power from the laser (measured from both sides of the intracavity plate and through the cavity end mirror) has been plotted as a function of the total percentage of output coupling (i.e.. reflectivity of intracavity plate plus cavity end mirror transmission). From this graph it can be seen that the maximum laser output power was achieved for an output coupling of (0.8±0.2)%. The data on this graph also gives an indication of the parasitic losses within the laser cavity by making use of the expression[4]

$$\beta_p = \frac{\beta_{opt}^2}{\beta_{max} - 2\beta_{opt}} \tag{3.1}$$

where β_p = parasitic loss

β_{opt} = optimum output coupling ((0.8±0.2)% in this case)

β_{max} = output coupling at which lasing ceases. (4.0 ± 0.1% in this case)

Equation (3.1) gives a value of 0.27% for the parasitic losses in this holosteric Nd:YAG laser.

The laser output power as a function of output coupling anticipated by theory is given by[4]

$$I_{out} = \beta_{oc}\left[\frac{\beta_p + \beta_{max}}{\beta_p + \beta_{oc}} - 1\right]\frac{I_{sat}}{2} \tag{3.2}$$

where β_{oc} = output coupling

I_{sat} = saturation intensity.

Using the experimentally derived values for β_p, β_{opt} and β_{max} in the above equation the predicted behaviour of the laser output power as a function of output coupling was plotted together with the experimental data in figure 3.7. Although the form of the experimental and theoretical data plotted on this graph can be seen to be in good agreement, the value of I_{sat} required to achieve this fit is 4.7kWcm^{-2} which is somewhat larger than the accepted value of around 1kWcm^{-2}. (See for instance reference[5]).

In order to rule out inconsistencies in the Fresnel reflectivity values as a possible source of error in this measured value for I_{sat}, the ratio of the power coupled out of the laser cavity by the high reflectivity output coupler together with the calculated values of Fresnel reflectivity were used to determine the output power transmission of the output coupler in the following expression:

$$T = \frac{R_f}{1-R_f} \cdot \frac{I_t}{I_f} \tag{3.3}$$

where T = optical power transmission coefficient of high reflectivity cavity end mirror

R_f = Fresnel reflectivity of intracavity glass plate

I_t = optical power transmitted through cavity end mirror

I_f = optical power reflected from Fresnel plate.

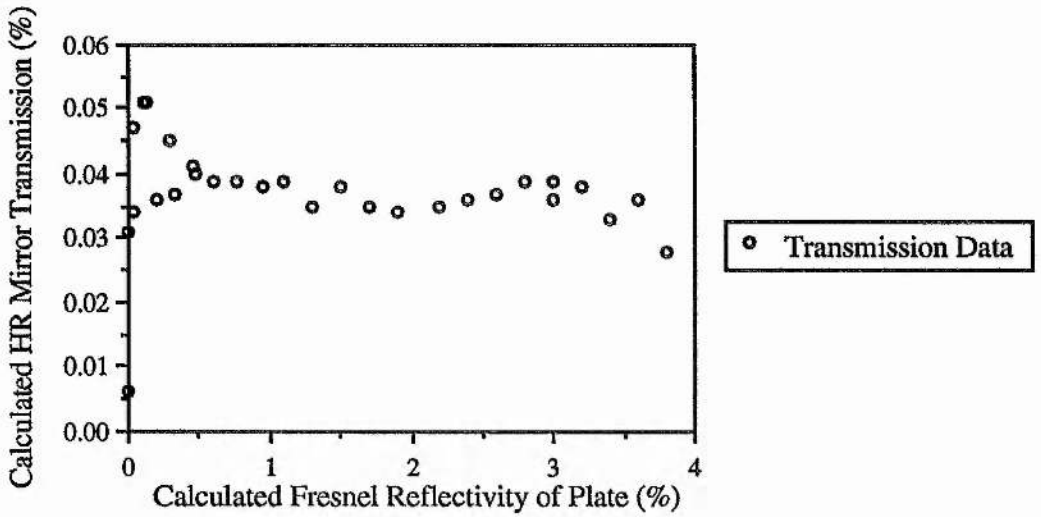

Figure 3.8. Transmission data for the high reflectivity laser output coupler calculated for each value of Fresnel reflectivity of the intracavity plate. The results show good consistency.

The percentage power transmission of the end mirror was plotted against R_f, the calculated Fresnel reflectivity of the glass plate as shown on figure 3.8. The mean percentage transmission calculated for the high reflectivity cavity end mirror was 0.038%. The consistency of the calculated values for this transmission plotted in figure 3.8 indicate that the Fresnel reflectivity values calculated for the intracavity glass plate are reliable. As might be expected, the greatest deviation from the mean for these value of T occurs when the amount of power reflected out of the cavity by the glass plate is very small i.e. when the glass plate is near Brewster's angle or at angle which gives the maximum tolerable reflectivity for which lasing can be sustained. At these two extremes, the fractional error in measuring the small amounts of power coupled from the cavity becomes significant.

3.6 Transverse Mode Quality

The excellent spatial overlap of the pump mode volume and the lasing mode in the Nd:YAG gain medium possible in the end pumped laser geometry allows selective excitation of the TEM_{00} cavity mode. Thus the laser can be made to oscillate on the fundamental transverse cavity mode without the need for insertion of lossy intracavity transverse mode defining elements.

To test the purity of the transverse mode output from the holosteric laser, the transverse intensity profile of the laser beam was measured. Light intensity measurements were recorded using an apertured (100μm diameter pinhole) silicon photodiode as it was scanned across the beam on a precision micrometer translation stage. A typical beam profile from such an experiment is illustrated in figure 3.9. The experimental data shows an excellent fit to a Gaussian curve also plotted in this figure indicating that the laser was operating on a single transverse TEM_{00} mode.

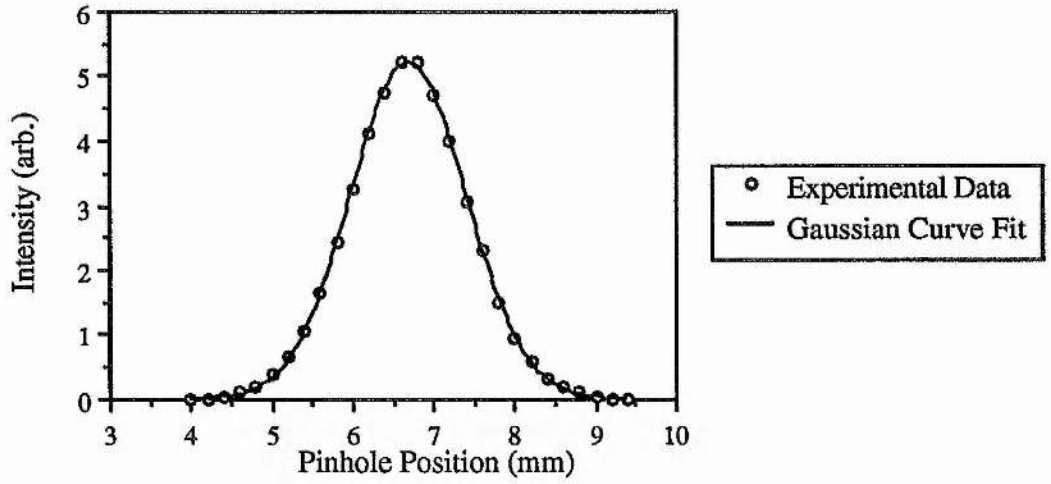

Figure 3.9. Transverse mode profile of the Nd:YAG laser output showing TEM_{00} operation.

As a further check on the transverse mode quality of the laser output, the beam divergence was measured and compared with the theoretically predicted divergence of the TEM_{00} mode computed from the geometry of the laser cavity. Figure 3.10 shows experimental values of the laser beam radius (the distance from the centre of the beam to

the position where the beam intensity has fallen to $1/e^2$ of the peak value) recorded at various distances from the laser output mirror. The resonator parameters for this Nd:YAG laser were measured to be; Nd:YAG crystal length = 5mm, intracavity air space = 42mm, cavity end mirror radius of curvature = 50mm.

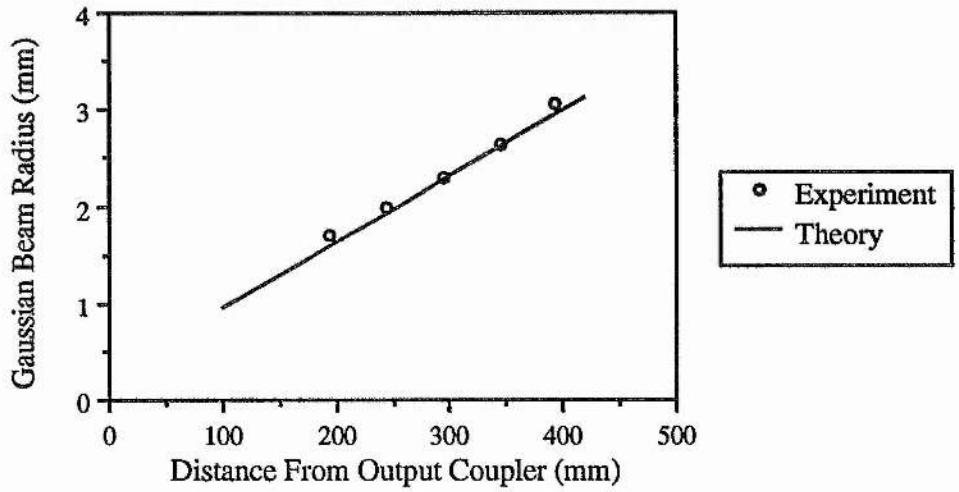

Figure 3.10. Comparison of the experimentally observed divergence of the holosteric laser output beam with that predicted by theory.

From these parameters, the expected propagation of the TEM_{oo} mode was calculated using conventional Gaussian beam optics theory. See figure 3.10. It is worth noting that the concave/plano glass substrate of the laser output coupler mirror acted as a diverging lens and this effect had to be included in the calculation. From figure 3.10 the good match between the experimental beam divergence data and the predicted values further indicate that the laser was operating on the fundamental TEM_{oo} cavity mode.

3.7 Output Spectrum of the Nd:YAG Holosteric Laser

The Fabry-Perot type, standing wave resonator used for the end-pumped holosteric laser exhibits resonances at regularly spaced frequency intervals $\Delta\nu_{fsr}$. $\Delta\nu_{fsr}$ is termed the free spectral range of the cavity and has the value

$$\Delta\nu_{fsr} = \frac{c}{2L} \tag{3.4}$$

where c = speed of light in vacuum

L = optical path length of laser cavity.

Why and how many of these cavity resonances or longitudinal modes oscillate in the laser is determined by the nature of the laser gain medium and the exact geometry of the laser. This topic will be discussed in more detail in Chapter 4.

The frequency spacing, $\Delta\nu_{fsr}$, of the end-pumped Nd:YAG holosteric laser, with its approximately 50mm long cavity, was around 3GHz. In terms of wavelength, this frequency interval corresponds to a wavelength separation of $\Delta\lambda \approx 11.3$pm, somewhat below the resolution limit of conventional prism or diffraction grating monochromators. The resolution necessary to observe individual longitudinal modes of the laser can be achieved using a scanning, plane-parallel Fabry-Perot interferometer and so such a device was constructed to enable investigation of the longitudinal mode structure of the laser.

The Fabry-Perot interferometer was constructed from two plane mirrors, both coated to give 3% optical power transmission. The rear surface of each mirror substrate was antireflection coated to reduce spurious etaloning effects within the substrate. One mirror was mounted on standard, commercial micrometer mounts allowing translation of the mirror along the optical axis of the interferometer and also angular adjustment in two perpendicular planes. The second mirror was mounted on a piezo electric transducer (Photon Control model ASM 18). This transducer had three independently controllable channels allowing fine angular adjustment of the mirror.

A small area ($1mm^2$) silicon photodiode placed on the output side of the Fabry-Perot interferometer was used to monitor the intensity of the central Fabry-Perot fringe as the interferometer was scanned through several free spectral ranges. The photodiode signal, after suitable amplification, was displayed on a Hammeg 208 digital storage oscilloscope

scanned synchronously with the ramp voltage driving the Fabry-Perot piezo transducer. In this way, a static display of the transmission through the scanning Fabry-Perot interferometer could be obtained on the oscilloscope, digitally stored and subsequently down loaded to an XY chart recorder for analysis.

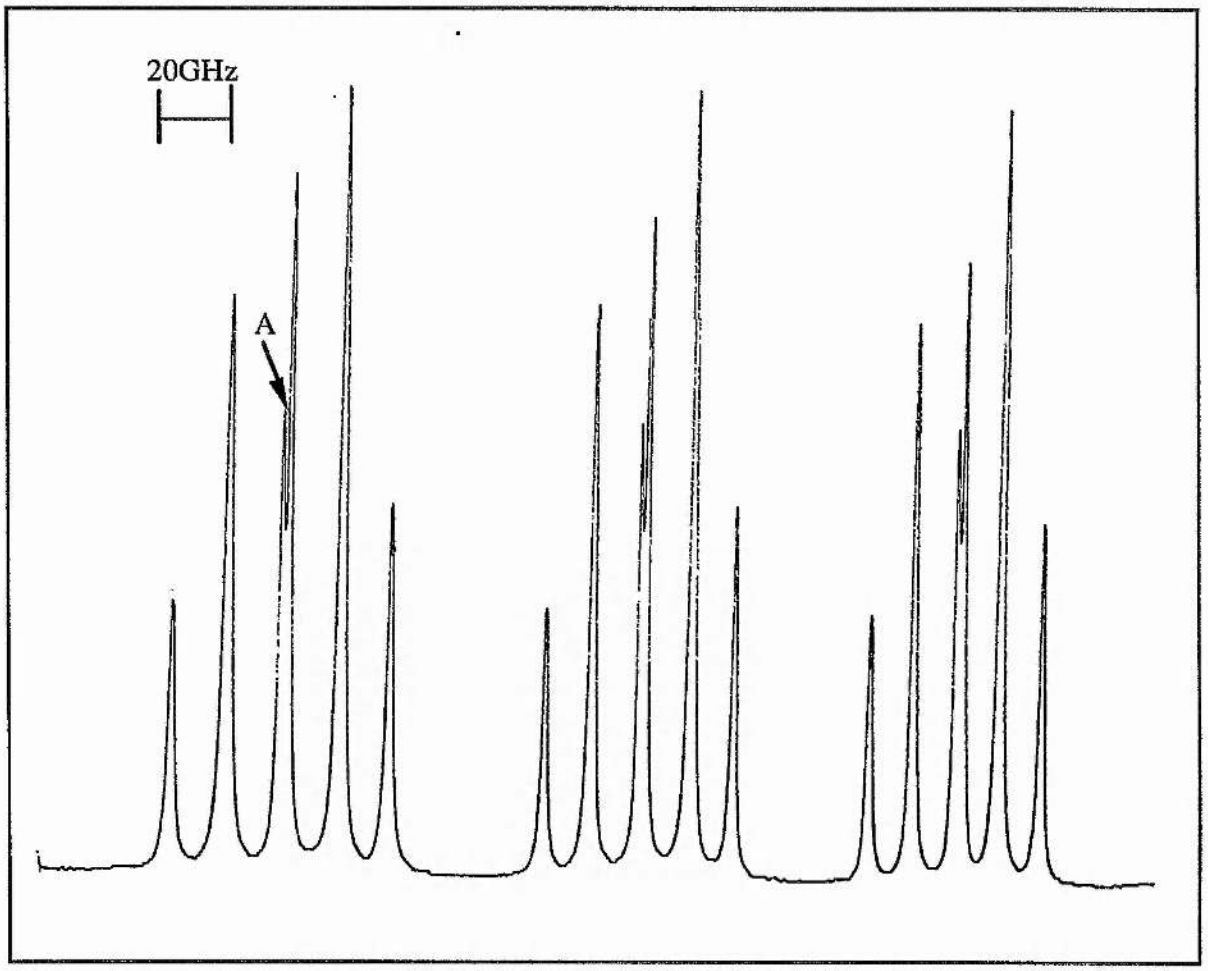

Figure 3.11. The output frequency spectrum of the holosteric laser displayed on a scanning Fabry-Perot interferometer. The closely spaced modes at A are adjacent longitudinal modes separated by 2.34GHz.

Using this interferometer system, the output spectrum of the laser was recorded. See figure 3.11. This figure displays approximately three free spectral ranges of the scanning Fabry-Perot interferometer transmission and clearly shows the laser operating on 6 longitudinal modes. The two very closely spaced modes (marked A) visible in the centre of each mode spectrum are separated in frequency by 2.34GHz and correspond to two adjacent longitudinal modes of the laser cavity. The more widely spaced modes in figure

3.11 are separated by around 6 or 7 free spectral ranges of the laser cavity as a result of spatial hole burning in the laser gain medium (see section 4.2.2). In figure 3.11 it is just discernible that the group of modes displayed in each free spectral range become closer together for increasing voltage applied to the interferometer piezo transducer. This indicates that the movement of the scanning mirror was some nonlinear function of the applied voltage.

The physical separation, Δx, between equivalent peaks from adjacent free spectral range orders of the Fabry-Perot interferometer were measured from figure 3.11 and plotted against the mean displacement, $\underline{x}$, of each pair of modes from the origin, $x = 0$. In this case, the origin was arbitrarily defined as the left-most peak on figure 3.11. Values

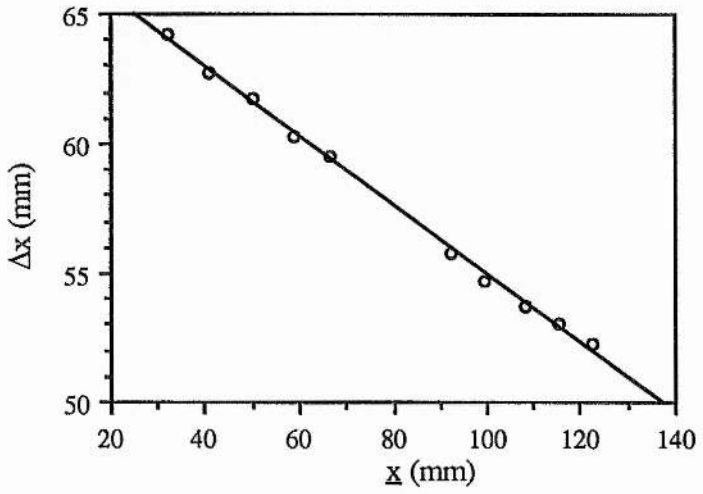

Figure 3.12. Linearisation calibration for the scanning Fabry-Perot interferometer.

of Δx were plotted against $\underline{x}$ (see figure 3.12) and a regression analysis applied to determine the form of the best fit curve. For this data a good fit was obtained with the straight line function

$$\Delta x = a + b\underline{x} \tag{3.5}$$

where $a = 68.324$

$b = -0.134$

Frequency spacings, $\delta\nu$, of modes on figure 3.11 physically separated by a distance δx could then be calculated using

$$\frac{\delta\nu}{\delta x} = \frac{\Delta\nu_{fsr}}{\Delta x} = \frac{\Delta\nu_{fsr}}{a + bx} \tag{3.6}$$

The c/2L free spectral range, $\Delta\nu_{fsr}$, of the Fabry-Perot interferometer was evaluated by measuring the mirror separation, L, using a travelling microscope.

3.8 Optical to Optical Slope Efficiency

The 1064nm laser output power was measured as a function of the input optical pump power from the fibre coupled laser diode array. The Nd:YAG laser emission was passed through a "black glass" filter (Schott glass RG1000) to remove any background pump radiation before being measured using a calibrated photodiode optical power meter (Newport). Corresponding values for the optical pump power supplied to the Nd:YAG laser were recorded from the calibrated readout on the diode laser driver.

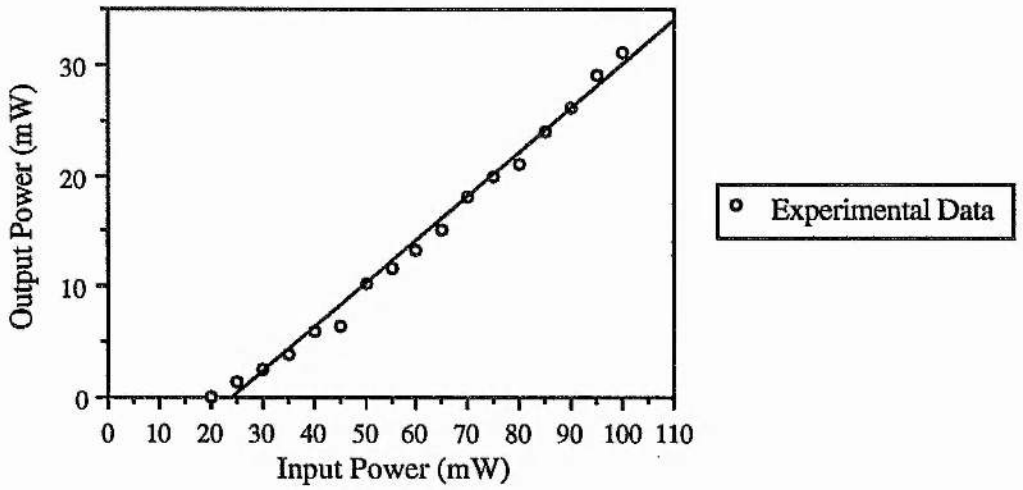

Figure 3.13 Output power at 1064nm plotted against input pump power at 809nm for the Nd:YAG holosteric laser showing an optical to optical slope efficiency of 39%.

As described in section 2.5.4 the emission wavelength from the diode laser array was dependent on its output power. So to obtain a true slope efficiency measurement it was necessary to compensate for this wavelength shift by adjusting the diode laser array heat sink temperature to maximise the Nd:YAG laser output at each level of pump power. The optical to optical slope efficiency data displayed in figure 3.13 was for a 5mm long, 1% doped Nd:YAG rod fabricated at GEC Hirst Research Centre and coated by Laser Optik (Germany). The output coupler used for the laser had a 75mm radius of curvature and an optical power reflectivity of 98.5%. From figure 3.13 the Nd:YAG laser threshold was 24mW and its slope efficiency was 39%.

3.9 Rate Equation Model of the 1064nm Nd:YAG Laser

To assess the performance of the cw, end pumped Nd:YAG holosteric laser and to gain insight into its operation, a rate equation based model of the laser was developed. In contrast to previously published models of end pumped, cw solid state laser[6,7] the converging/diverging profile of the focused pump beam has been taken into consideration.

The salient features of the Nd:YAG energy levels are illustrated in figure 3.14

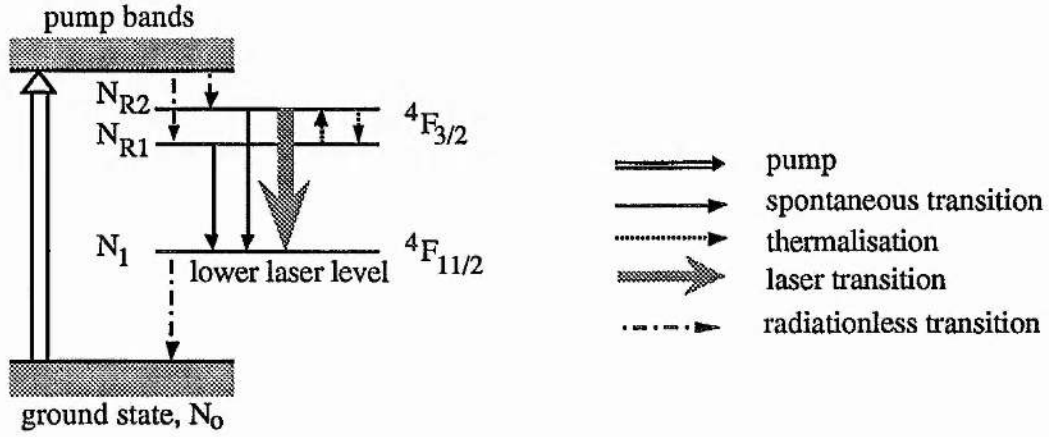

Figure 3.14. Energy level diagram for the four level 1064nm Nd:YAG laser.

From the well documented data on transition rates between participating energy levels of the 1064nm Nd:YAG laser the following assumptions can be safely made;

a) since the fluorescence quantum efficiency of the $^4F_{3/2}$ upper laser level is greater than 99.5% the approximation can be made that all ions optically pumped into the pump bands relax into the metastable $^4F_{3/2}$ upper laser multiplet. This nonradiative relaxation process is rapid taking times of the order of ~10^{-8}s.(See reference 8),

b) the relative population densities N_{R1} and N_{R2} of the two sublevels of the $^4F_{3/2}$ band remains constant due to rapid thermally induced transitions between the two sublevels. The fraction f_2 of the total $^4F_{3/2}$ population density residing in the upper sublevel is calculated from the Boltzmann distribution law to be 40%[5] at room temperature. The population density of this sublevel can be expressed as

$$N_{R2} = f_2(N_{R1}+N_{R2}) \tag{3.7}$$

c) Nd^{3+} ion lifetimes in the $^4I_{11/2}$ lower laser level are very short, typically < 10^{-8}s, and so the population density in the level is assumed to be insignificant.

3.9.1 Rate Equation Analysis

The dynamic behaviour of the population densities in the various energy levels of the system under the influence of optical pumping can be described by the following three rate equations;

$$\frac{dN_0}{dt} = -R + \frac{N_{R2}}{\tau} + \frac{N_{R1}}{\tau} + \frac{2^*I_L\sigma_s}{h\nu_L} \cdot N_{R2} \tag{3.8}$$

$$\frac{dN_{R2}}{dt} = R - \frac{N_{R2}}{\tau} - \frac{2^*I_L\sigma_s}{h\nu_L} \cdot N_{R2} - K_{21}N_{R2} + K_{12}N_{R1} \tag{3.9}$$

$$\frac{dN_{R1}}{dt} = -\frac{N_{R1}}{\tau} + K_{21}N_{R2} - K_{12}N_{R1} \tag{3.10}$$

where R = pump rate (excitations per unit volume per second)

τ = spontaneous emission lifetime

I_L = irradiance of intracavity circulating laser light assumed equal in both directions

σ_s = stimulated emission cross-section

K_{ij} = thermalisation coefficients for transitions between the levels R_1 and R_2

The factor of 2^* in the stimulated emission terms of equations (3.8) and (3.9) accounts for depletion of the upper laser level population by the two counter-propagating waves present in the linear laser cavity. The pumping rate R need only appear in one of equations (3.9) or (3.10) because of the rapid redistribution of population densities within the upper laser manifold to their thermal equilibrium values.

Under steady state conditions the populations of the various levels remains constant and so setting d/dt=0, equations (3.9) and (3.10) can be combined to form an expression for the steady state or saturated population inversion

$$N_{R2} = \frac{f_2 R\tau}{1 + \frac{2f_2\sigma_s\tau I_L}{h\nu_L}} \tag{3.11}$$

Now, under optical pumping by a spectrally narrow source such as a diode laser, each pump photon absorbed by the laser active ions will induce a transition of an ion in the ground state to an excited state in the pump band. In the case of diode laser pumping at around 809nm, this pump band is formed from the $^4F_{5/2}$ and the $^2H_{9/2}$levels. From this pump band the ion de-excites rapidly until it reaches the metastable upper laser level. Thus every absorbed pump photon contributes an excited ion to the upper laser level. The pump rate R is the number of such excitations per unit volume per second and so can be written

$$R = \frac{1}{h\nu_p} \cdot \frac{dI_p}{dz} \tag{3.12}$$

where I_p = pump light intensity

ν_p = pump light frequency

h = Planck's constant

But the axial decay in the pump intensity dI_p/dz can be expressed in terms of more readily measurable quantities

$$dI_p = I_p \sigma_A N_0 dz \tag{3.13}$$

where σ_A = absorption cross-section

N_0 = ground state population density

Since, from the initial assumptions, all the laser active ions will reside only in the ground state and the $^4F_{3/2}$ doublet excited state for any appreciable length of time, the total Nd ion. dopant density, N_T, is

$$N_T = N_0 + N_{R1} + N_{R2} \tag{3.14}$$

Thus equation (3.13) becomes

$$\frac{dI_p}{dz} = I_p \sigma_A (N_T - N_{R1} - N_{R2}) \tag{3.15}$$

Returning now to the expression for the population inversion (3.11) and substituting for the pump rate R using (3.12) and (3.15) the steady state population inversion can be written

$$N_{R2} = \frac{N_T}{\frac{h\nu_p}{f_2 I_p \sigma_A \tau} + 2\frac{I_L \nu_p \sigma_s}{I_p \nu_L \sigma_A} + \frac{1}{f_2}} \tag{3.16}$$

Recall that the ultimate goal of this model is to predict laser output powers under various conditions of pumping, parasitic losses, output coupling, etc. In the above equation the values of all the elements are known with the exception of N_{R2} and the desired quantity I_L, the steady state intracavity intensity. In order to arrive at a value for I_L a final piece of fundamental laser physics is brought into play. That is, under steady state,

cw, lasing conditions the round trip gain must equal the round trip losses. Equivalently, the single pass gain (γ) and loss (δ) coefficients must be equal. From the well known laser gain equation

$$\frac{dI_L}{dz} = N_{R2}\sigma_s I_L = \gamma I_L \tag{3.17}$$

the single pass saturated gain coefficient γ can be calculated from the integral

$$\gamma = \int N_{R2}\sigma_s dz \tag{3.18}$$

evaluated over the length of the laser rod. (Note that the fractional single pass gain $G=e^{\gamma}$. Equating this to the single pass loss coefficient δ

$$\delta = \frac{1}{2}\left(\eta + \log_e \frac{1}{R_1 R_2}\right) \tag{3.19}$$

where η = round trip loss coefficient = $e^{-\beta_p}$

β_p = fractional parasitic loss

R_1, R_2 = power reflectivities of the cavity end mirrors

gives

$$\int N_{R2}\sigma_s dz = \frac{1}{2}\left(\eta + \log_e \frac{1}{R_1 R_2}\right) \tag{3.20}$$

If N_{R2} is substituted from (3.16), the intracavity intensity I_L is the only unknown in the equation. To evaluate I_L an iterative process is adopted. Using an estimated initial value for I_L the integral in (3.20) is solved numerically and the resulting single pass gain coefficient, γ, compared with the loss coefficient δ. The value of I_L is then modified and the integration process is performed again. This continues until, after several iterations, γ equals δ.

3.9.2 Numerical Evaluation of Integrated Single Pass Saturated Gain

The computation of the saturated gain γ, integrated along the length of the gain medium (equation 3.18) was performed by dividing the length of the rod into a large number of elemental slices and calculating γ for each slice consecutively. To enhance the realism of the model the nonuniform intensity profiles of both the laser beam and the pump beam were considered by further subdividing each disc-like slice of the laser rod into a series of concentric annuli as shown in figure 3.15.

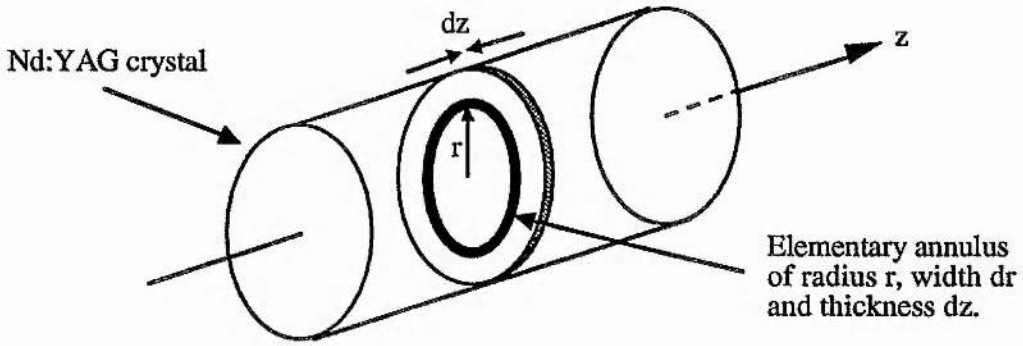

Figure 3.15. Sectioning the Nd:YAG rod for numerical integration.

The transverse intensity profile of the laser beam was taken to be a TEM_{00} Gaussian mode. From Gaussian beam propagation calculations the divergence of the laser beam over the typical 5mm length of the gain medium is negligible and so for the purposes of the computer model the laser beam radius was assumed to be constant. In the case of the pump beam the intensity profile was approximated by either a cylindrically symmetric top

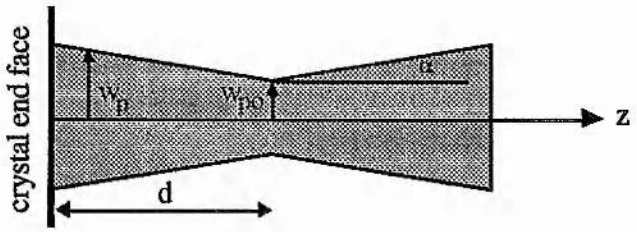

Figure 3.16. Focusing geometry of the pump beam along the rod.

hat or triangular profile. Focusing of the pump beam was accounted for by specifying a minimum pump beam radius, w_{po}, at a position d within the rod together with a divergence angle, α as shown in figure 3.16. The pump beam radius, $w_p(z)$, at any position along the laser rod is thus given by

$$w_p = w_{po} + |z-d| \tan(\alpha) \tag{3.21}$$

Starting with an estimated value for the intracavity laser beam intensity, I_L, the intensity of the laser and pump beams are calculated in each annulus of the first disc-like section of the rod. These intensity values are converted into powers and summed over all the annuli making up that slice to give total laser beam and pump beam powers exiting that slice. These optical powers are then redistributed over the Gaussian and top hat (or triangular) beam profiles of appropriate radius for the laser and pump beams respectively entering the next slice. This assumption that the laser and pump beams maintain their spatial profiles along the rod can, at least in the case of the laser beam, be justified. In this case cavity diffraction losses help to maintain the Gaussian beam profile over many round trips of the cavity.

After integrating over the entire volume of the laser rod in this manner, the total power of the laser beam, $P_{Lmax}(final)$, exiting the rod is compared with that entering the rod, $P_{Lmax}(initial)$, in order to calculate the gain coefficient, γ, for a single pass of the laser rod.

$$\gamma = \ln\left(\frac{P_{Lmax}(final)}{P_{Lmax}(initial)}\right) \approx \frac{P_{Lmax}(final) - P_{Lmax}(initial)}{P_{Lmax}(initial)} \tag{3.22}$$

This computed value for single pass gain is compared with the known value for single pass cavity loss. If these values differ then the initial intensity of the saturating laser beam entering the rod is altered appropriately and the integration process repeated. After a number of such iterations a value for the steady state intracavity intensity is found which saturates the gain down to equal the cavity losses. The laser output power can then finally be calculated from

$$P_{out} = (1-R_2)\, P_{Lmax}(final) \qquad (3.23)$$

where R_2 = power reflectivity of the laser output coupler.

3.9.3 Results

Results from this model of the end-pumped, Nd:YAG holosteric laser were generated using FORTRAN computer code written by A. Wray[9]. The laser parameters used in the calculations are summarised in table 3.1.

TABLE 3.1

maximum pump power	100mW
pump beam divergence in laser rod	5°
pump beam waist	70μm
pump beam waist position in laser rod	700μm (from plane end)
Nd:YAG laser beam waist	90μm
laser rod length	5mm
laser rod refractive index	1.82
pump power transmission through dichroic coating	84%
1064nm power reflectivity of output coupler	98.5%
parasitic cavity losses	0.3%
Nd atom concentration in laser rod	1.4×10^{20}atoms cm^{-3}
Nd:YAG absorption cross-section at 809nm	5.4×10^{-20} cm^2
Nd:YAG stimulated emission cross-section at 1064nm	8.1×10^{-19} cm^2
upper laser level lifetime	230μs

Figure 3.17(a) shows the optical to optical slope efficiency data predicted by the computer model using both top-hat and triangular pump beam profiles. Overlaid on this graph are experimental slope efficiency data from the bread-boarded Nd:YAG holosteric laser showing excellent correlation between measured and modelled results.

The model has also proved useful for examining the effects of gain medium length on laser output power. Under full pump power conditions the laser output power was calculated as a function of Nd:YAG length. See figure 3.17(b). This data indicates that the laser rod length could be reduced to 3mm without significant loss in output power but also that no major penalty is paid in terms of reabsorption loss by the longer 5mm rods currently used. From the point of view of single longitudinal mode operation from the Nd:YAG holosteric laser it is also worth noting from this graph that reasonable output powers (~15mW) may be obtained from very short monolithic Nd:YAG rod cavities around 1mm or less in length.

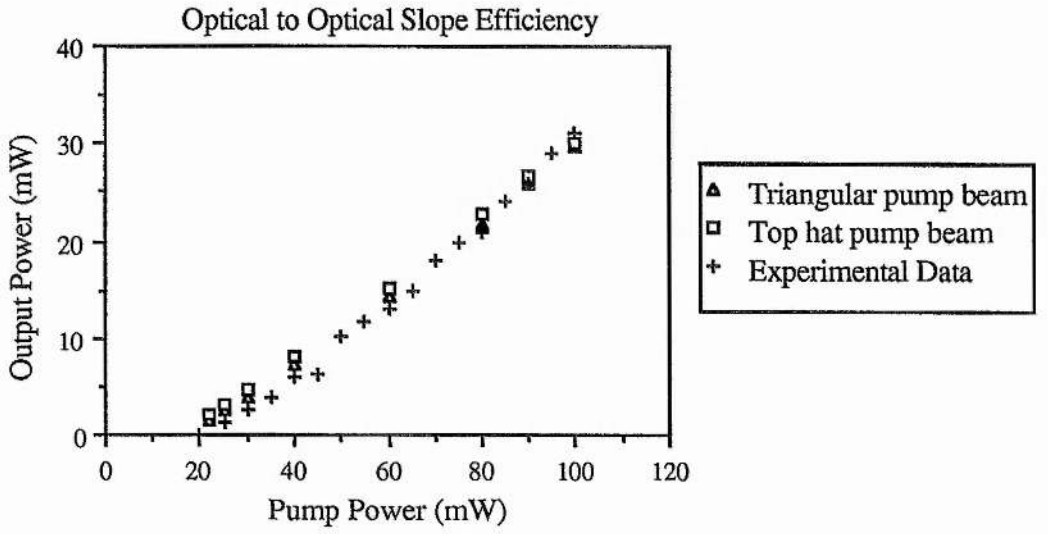

(a)

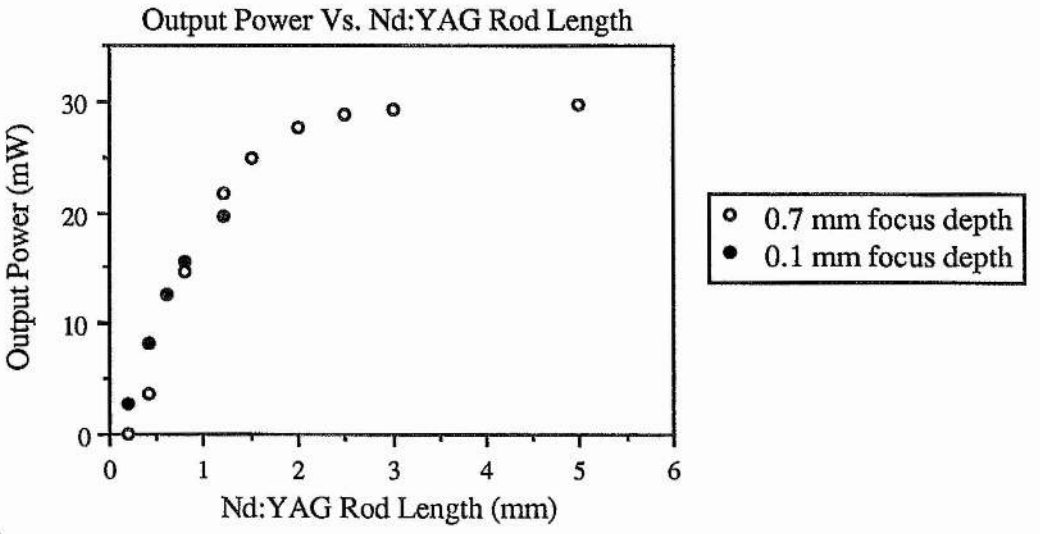

(b)

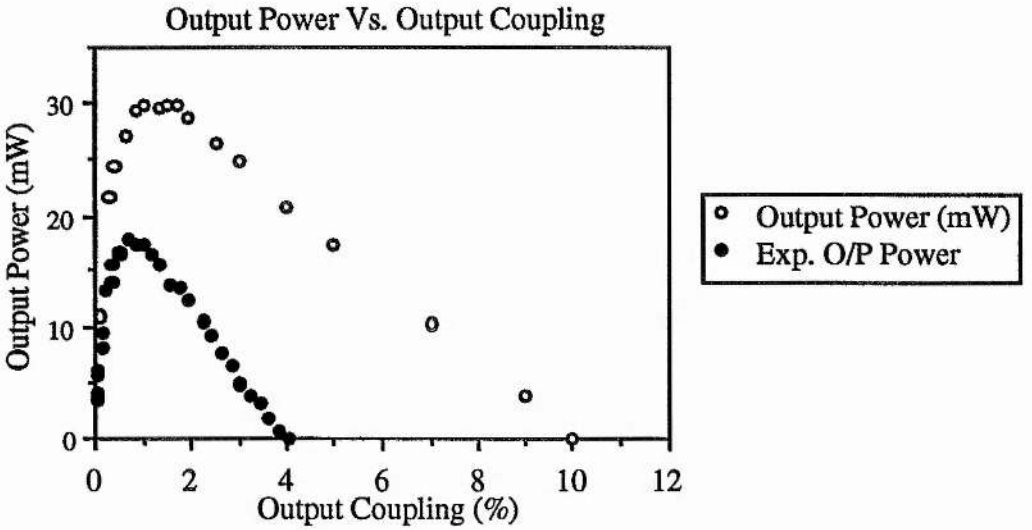

(c)

Figure 3.17. Results from the computer model of the end-pumped, 1064nm Nd:YAG holosteric laser

To check the optimum output coupling for the laser the model was used to calculate the output power as a function of output coupling as shown in figure 3.17(c). The experimental data from section 3.5, also shown on this graph, has the same functional form as that predicted by the model but with much reduced output powers. The discrepancy between the data from modelling and those from the experiments in this case results from the particular laser configuration required by the experiment. As described in section 3.5 the laser used in the output power versus output coupling experiment contained a variable angle, intracavity glass plate as the output coupler. The inclusion of this intracavity plate degraded the performance of the laser somewhat by increasing parasitic losses through absorption scattering and polarisation discrimination effects. Consequently even the slope efficiency of this laser would also have disagreed with the computer model. Despite these differences the optimum output coupling of 1.5% predicted by the model is not substantially different from the experimental data.

3.10 References

1 Sipes D. L., "Highly Efficient Neodymium: Yttrium Aluminium Garnet Laser End-Pumped by a Semiconductor Laser Array", Appl. Phys. Lett. **47**(2) 74 (1985)

2 Berger J., Welch D. F., Sicfres D. R., Streifer W., Cross P. S., "High Power, High Efficiency Neodymium: Yttrium Aluminium Garnet Laser End-Pumped by a Laser Diode Array", Appl. Phys. Lett. **51**(16) 1212 (1987)

3 Heard H. G., "Laser Parameter Measurement Handbook", John Wiley and Sons (1968)

4 Siegman A. E., "Lasers", University Science Books (1986)

5 Koechner W., "Solid-State Laser Engineering", Springer-Verlag (1988)

6 Fan T. Y., Byer R. L., "Modeling and cw Operation of a Quasi-Three-Level 946nm Nd:YAG Laser", IEEE J. Quant. Elec. **QE-23**(5) 605 (1987)

7 Risk W. P., "Modeling of Longitudinally Pumped Solid-State Lasers Exhibiting Reabsorption Losses", J. Opt. Soc. Am. B **5**(7) 1412 (1988)

8 Zverev G. M., Golyaev Y. D., Shalaev E. A.,Shokin A. A., "Neodymium Activated Yttrium Aluminium Garnets", J. Sov. Las. Res. **8**(3) 189 (1987)

9 Wray A., "Modelling of Laser Diode Pumped Nd:YAG Microlasers", Summer research project, University of St. Andrews, Scotland, (1988)

Chapter 4

LONGITUDINAL MODE SELECTION

4.1 Introduction.

The spectral output from most laser sources, although narrow, is far from being monochromatic. Instead, lasers tend to operate on several closely spaced, discrete frequencies simultaneously. In order to progress towards the production of a single frequency laser system, the mechanisms responsible for this more common multifrequency behaviour of lasers must be addressed to enable frequency selection methods to be found. In this chapter these issues will be briefly reviewed together with a detailed discussion of the design and implementation of the single frequency holosteric Nd:YAG lasers.

4.2 Line Broadening and Mode Competition Effects.

There are two main factors which determine the multifrequency nature of a laser's output. These are;

1) the broadening process determining the spectral lineshape function of the gain medium and whether the optical gain profile of the lasing material is *homogeneously* or *inhomogeneously* broadened,

2) the geometry of the laser resonator.

In principle, the laser gain medium is capable of sustaining oscillations at any optical frequency within its gain profile for which optical gain exceeds the losses in the feedback system. The feedback required for oscillation is often provided by an optical cavity enclosing the gain medium. Such cavities exhibit strong, low-loss resonances, called

longitudinal modes, at regularly spaced, discrete frequencies determined by the geometry of the resonator. The frequency spacing between consecutive longitudinal cavity modes is known as the cavity free spectral range, $\Delta\nu_{fsr}$ and has the value

$$\Delta\nu_{fsr} = c/P \tag{4.1}$$

where P is the round trip optical path length of the cavity. For optical cavities of a practical size the frequency spacing of these longitudinal modes is often much smaller than the overall gain bandwidth supported by the laser medium. Thus many low-loss optical modes of the cavity exist within the laser gain bandwidth, all having the potential to oscillate. The number of these modes that actually reach oscillation threshold is determined by how strongly they compete for the available gain.

4.2.1 Inhomogeneously Broadened Gain Profiles.

In certain types of laser gain media, line shape broadening processes are present which modify the emitted optical transition frequency of each laser active centre within the laser material by different degrees. The overall effect of this collection of individually shifted transition frequencies is to broaden the total gain profile of the laser transition. The laser transitions of such materials are said to be inhomogeneously broadened.

Optical radiation passing through an inverted, inhomogeneously broadened gain medium will interact only with those laser active centres having resonance frequencies close to, or coinciding with, the frequency of the incident radiation. The spectral distribution of optical gain will thus become depleted in the vicinity of the frequency of the optical field, forming a depression or "hole" in the laser gain profile. The remaining laser active centres take no part in this interaction and so their available gain remains unused. This process of spectrally selective gain saturation is referred to as spectral hole burning. This process enables lasers having inhomogeneously broadened gain profiles to oscillate on several longitudinal modes, each mode receiving gain from its own spectral group or ensemble of inverted laser active centres.

4.2.2 Homogeneously Broadened Gain Profiles.

In laser materials exhibiting an ideal homogeneously broadened gain profile all the laser active centres in the material will posses identical absorption and emission characteristics. Thus, from a simplistic view point, the presence of an electromagnetic field oscillating at just one optical frequency within the laser cavity will interact with all the laser active centres resulting in complete saturation across the bandwidth of the available optical gain. Due to the removal of all the available gain by the oscillating mode, other potential modes will be suppressed and the laser will oscillate only on one frequency. In practice, however, this is rarely found to be the case and so most real homogeneously broadened laser systems oscillate on more than one frequency. The reason for this multifrequency output from homogeneously broadened laser transitions is spatial hole burning and will be explored in the following section.

Spatial Hole Burning.

As discussed in the previous section, lasers with homogeneously broadened active media should, in theory, oscillate on a single axial mode of the resonant cavity. The reason that this is often not found in practice is due to the presence of a spatial modulation of the laser gain known as spatial hole burning.

A commonly used laser resonator configuration is the Fabry-Perot interferometer. In such cavities the superposition of two counter-propagating optical fields of equal frequency produces a standing wave field distribution within the resonator. Along the resonator's optical axis, this standing wave displays periodically spaced regions of zero field amplitude (nodes) separated by regions where the field is a maximum (antinodes). Consecutive nodes in this spatially modulated field are separated by a distance corresponding to one half of the optical wavelength. If such a standing wave optical field exists within a pumped laser active material it causes the population inversion to be

preferentially depleted in the regions of largest field amplitude through stimulated emission processes. In the nodal planes of the standing wave, however, there is no optical field to interact with the population inversion and so the optical gain in these regions remains intact. In this way, the population inversion and hence the laser gain becomes spatially modulated with maximum population inversion at the nodal planes of the optical field and minima at the field antinodes. See figure 4.1

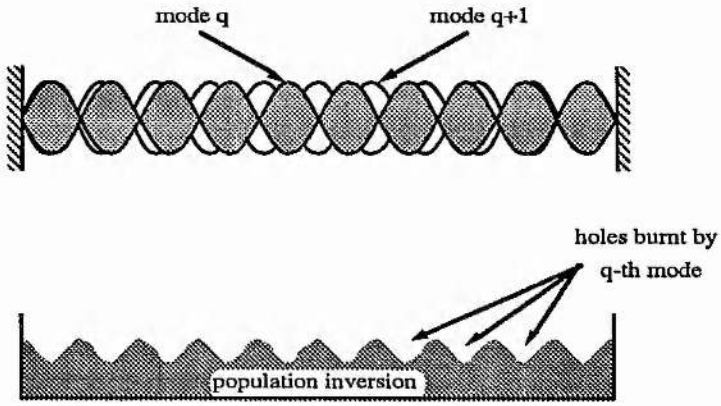

Figure 4.1. Spatial hole burning.

A second cavity mode whose standing wave field has antinodes coinciding with the regions of unsaturated gain may experience enough gain to oscillate in the cavity. Because this secondary resonating mode interacts essentially with a different spatial group of laser active centres from the primary mode, there is little or no gain competition between these modes and both can oscillate simultaneously. By this process it may be possible for several longitudinal modes to oscillate even in a homogeneously broadened laser medium.

In the absence of any other frequency dependent losses in the resonator, the output spectrum from the laser suffering spatial hole burning will depend on the length of the active medium, its position within the resonator and the strength and uniformity of the pumping.

The frequency spacing between simultaneously oscillating spatial hole burning modes in a homogeneously broadened laser medium can be estimated using a simple spatial hole burning model as follows. Figure 4.2 illustrates the laser geometry being considered.

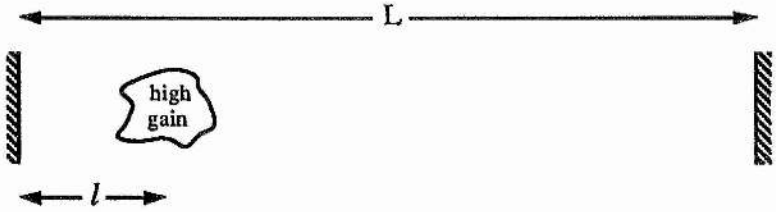

Figure 4.2 Effect of gain position on spatial hole burning.

The overall optical path length between the cavity end mirrors is given by L. Inside the cavity is a region of high optical gain positioned a distance l from the left hand cavity mirror. This region of high gain may be caused by the presence of a small piece of uniformly pumped active medium or perhaps due to a localised region of strong pumping within the laser gain element.

Consider now two spatial hole burning cavity modes with the highest probability for oscillation in this cavity. If the axial mode number of these two modes is q_1 and q_2 respectively then the wavelengths of each mode will be

$$\lambda_1 = \frac{2L}{q_1} \tag{4.2}$$

$$\lambda_2 = \frac{2L}{q_2} \tag{4.3}$$

For these two modes to be able to oscillate simultaneously the field of one standing wave must exploit the regions of undepleted gain left by the other standing wave field. To achieve this, the two oscillating modes must be $\pi/2$ radians out of phase by the time they reach the gain region at l so that an antinode of one standing wave coincides with the node of the other standing wave.

The boundary conditions of the resonant cavity dictate that the field of each cavity mode has a node at the cavity end mirrors. So, taking the initial phase of each of the two oscillating modes to be zero at the left hand mirror, the phase, ϕ, of each wave at point l in the cavity will be

$$\phi_1 = \frac{2\pi l}{\lambda_1} \tag{4.4}$$

$$\phi_2 = \frac{2\pi l}{\lambda_2} \tag{4.5}$$

As stated above the phase difference, $\Delta\phi$, between these two waves must be $\pi/2$ in the gain region. So

$$\Delta\phi = \phi_2 - \phi_1 = \frac{\pi}{2} \tag{4.6}$$

From 4.4 and 4.5 this becomes

$$\frac{\lambda_1 - \lambda_2}{\lambda_1\lambda_2} = \frac{1}{4l} \tag{4.7}$$

Substituting for λ_1 and λ_2, equation 4.7 gives

$$q_2 - q_1 = \frac{L}{2l} \tag{4.8}$$

the axial mode spacing of the spatial hole burning modes. Since adjacent cavity modes are separated in frequency by the cavity free spectral range, $\Delta\nu_{fsr}$, equation 4.8 can be re-expressed as a frequency difference, $\Delta\nu_{\text{spatial hole burning}}$

$$\Delta\nu_{\text{spatial hole burning}} = \Delta\nu_{fsr} \times (q_2 - q_1)$$

$$= \frac{c}{4l} \tag{4.9}$$

From equation 4.9 it can be seen that positioning the gain at the centre of the cavity (i.e. l =L/2) means that adjacent spatial hole burning modes correspond to adjacent axial modes of the cavity, separated in frequency by the cavity free spectral range, $\Delta\nu_{fsr}$=c/2L.This is the situation illustrated in figure 4.1. However, in the case of an end pumped holosteric laser, the gain medium is often situated at one end of the cavity so adjacent spatial hole burning modes will in general be several axial modes apart. Also in

the end pumped holosteric laser system the optical pumping of the laser rod tends to be nonuniform with a region of higher gain existing in the focus of the pump beam. The spatial hole burning mode spacing will therefore be dependent on the pump beam focus position.

4.3 Mode Selection by Manipulation of Laser Parameters

4.3.1 Short Cavities

Single longitudinal mode operation of a standing wave laser can be achieved by shortening the cavity length, L, to the point where the c/2L longitudinal mode spacing exceeds the oscillation bandwidth[1,2,3,4]. This ensures that only one cavity resonance exists within the laser gain bandwidth at any one time. The drawback with this system is that the physical constraint placed on the cavity length for single frequency operation restricts the length of the gain medium which can fit within the cavity. This will ultimately limit the maximum power available from the laser. The restricted cavity length may also exclude the use of other intracavity elements such as polarisers or nonlinear crystals.

4.3.2 Laser Operation Close To Threshold

Alternatively, single mode operation can be obtained by operating the laser just above oscillation threshold. Provided the laser gain curve is not too broad and/or the longitudinal mode spacing is not too small, most lasers can be made to operate on a single mode by reducing the gain (or increasing the cavity losses) until only one longitudinal mode remains within the reduced oscillation bandwidth envelope[5,6]. Again this technique produces single mode laser output at the expense of greatly reduced output power. Also because the lasing mode is only just above threshold the output power can be unstable.

4.4 Interferometric Mode Selectors.

In this class of mode selection, single mode operation of the laser is accomplished by using some additional interferometric device which gives strong frequency dependent loss either outside or inside the laser cavity. This group of mode selectors can loosely be subdivided into extracavity frequency filters, intracavity frequency filters or resonant reflector types.

4.4.1 External Frequency Filters

A simplistic approach to obtaining single frequency output from a laser is to pass its multifrequency output through some form of external optical frequency filter. The small intermodal frequency separation of the multi-longitudinal mode laser output (typically only tens or hundreds of megahertz) prohibits the use of spatially dispersing prism or grating filters. A more practical alternative is to use a short Fabry–Perot bandpass filter. The requirements for such a filter are

a) the frequency width of the filter pass band must be less than the laser mode spacing so that only one mode is transmitted by the filter.

b) the free spectral range of the filtering cavity must be greater than the frequency span over which the laser shows net optical gain. This ensures that only one filter pass band exists within the oscillating bandwidth of the laser.

c) the filter should have zero intensity transmission between consecutive resonance orders of the Fabry-Perot filter.

The first of these requirements is primarily set by the reflectivity of the filter cavity mirrors while the second requirement is fulfilled by judicious choice of the mirror separation. To satisfy the final requirement of the mode selecting filter, the mirrors must be of excellent optical quality to prevent excessive transmission losses caused by scattering and absorption. To maintain a Gaussian profile mode on transmission through

the filter and to avoid spurious filter transmissions due to higher order transverse modes of the passive cavity, the TEM_{00} mode of the laser output must be spatially matched to the fundamental transverse mode volume of the filter cavity using appropriate optics. A further complication of this method of mode selection is that the laser frequencies not transmitted by the filter are reflected back towards the laser. This necessitates insertion of an optical diode between the laser and the filter cavity to prevent this optical feedback from reaching the laser where it would cause intensity and frequency instabilities.

While this method of choosing a single mode from a multimode laser output spectrum has been used successfully[7] it is often advantageous to suppress unwanted modes within the laser itself. Intracavity mode selection techniques are often found to provide stronger suppression of unwanted frequencies in the laser output since they need only provide enough intracavity loss to counteract the gain available to the undesired frequencies. Also, by allowing only one longitudinal mode to oscillate within the cavity, gain competition is eliminated often resulting in more power being funnelled into that single mode compared to the power in the same mode under multimode oscillation conditions. An additional advantage of preventing multimode laser oscillation is that intensity and frequency instabilities in the laser output, due to cross-talk between simultaneously oscillating longitudinal modes, are greatly reduced.

4.4.2 Resonant Reflectors

This method of mode selection involves replacing one or more of the laser cavity mirrors by a composite mirror containing stacked etalons (coated or uncoated) or beamsplitter, mirror combinations. These multielement reflectors form resonant interferometric structures, the frequency dependent optical field amplitude and phase reflectivity of which can be tailored to give a narrow region of high reflectivity necessary to maintain oscillation of the laser on one frequency only. A useful summary of the various features and merits of the different structures can be found in reference [8] together

with an extensive range of references concerning theoretical and experimental work on these devices.

The main drawback of the resonant reflector technique is its extreme sensitivity to disturbances in the local environmental such as mechanical vibrations and fluctuations in temperature or pressure. Relative movements, on a subwavelength scale, between reflector elements in the cavity will have a major influence on the cavity losses. Thus this technique is unattractive for use in lasers requiring high frequency and intensity stability but can be a useful form of mode selection and output coupling in high gain, high power laser systems because of their high resistance to optical damage.

4.4.3 Intracavity Tilted Etalon

The intracavity tilted etalon is one of the most favoured methods of laser mode control because of its relative simplicity, tunability, low insertion loss for the selected mode and stability. The etalon itself is simply a plane-parallel Fabry-Perot interferometer formed between two air spaced plane reflectors or by reflections between the polished surfaces of an optically transparent solid. Tilting the etalon surfaces away from the perpendicular to the optic axis of the laser cavity effectively decouples the two resonators, preventing the etalon from forming a resonant reflector with the laser cavity mirrors. See figure 4.3. Thus the etalon acts only as a band pass filter within the laser resonator.

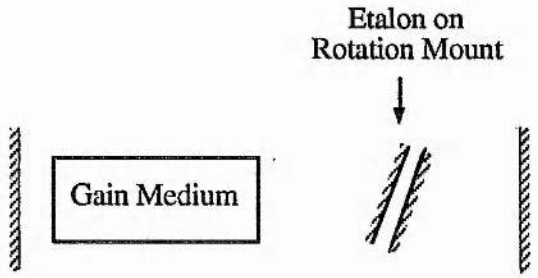

Figure 4.3. Schematic of an etalon mode selector in a laser cavity.

Expressions for the transmission and reflection characteristics of the Fabry-Perot etalon are well established . See for instance reference 9. In the absence of any scattering or absorption losses within the etalon, these expressions can be written as follows;

$$\text{Etalon Transmission Coefficient} = \frac{I_t}{I_i} = \frac{1}{1+F\sin^2(\delta/2)} \tag{4.10}$$

$$\text{Etalon Reflection Coefficient} = \frac{I_r}{I_i} = \frac{F\sin^2(\delta/2)}{1+F\sin^2(\delta/2)} \tag{4.11}$$

where

F = Coefficient of Finesse $= \frac{4R}{(1-R)^2}$

R = Power reflectivity of etalon mirrors (both equal in this case)

δ = Phase shift between consecutive round trips of etalon cavity $= \frac{2\pi}{\lambda} \cdot 2nd\cos\theta$

λ = free space wavelength

n = refractive index of etalon spacer

d = physical separation of etalon mirrors

θ = internal angle between the light rays in the etalon and the etalon normal.

For small angles the external angle of incidence is given by $\theta' \approx n\theta$.

I_i, I_t, I_r are the incident, transmitted and reflected intensities respectively.

Maxima in the etalon transmission occur when $\delta/2 = m\pi$; m is an integer. i.e.

$$\left(\frac{I_t}{I_i}\right)_{max} \text{ when } 2nd\cos\left(\frac{\theta'}{n}\right) = m\lambda \tag{4.12}$$

Thus from equation (4.12) the band pass wavelength, λ, can easily be tuned by varying the tilt angle θ' or by changing the optical thickness of the etalon, nd, by for example changing the etalon temperature. In the case of optical thickness tuning, the shift $\Delta\nu$ in the etalon resonance frequency for a change in optical thickness $\Delta(nd)$ is

$$\Delta\nu = \nu\frac{\Delta(nd)}{nd} \tag{4.13}$$

For tilt tuning of the etalon transmission the frequency shift for a given value of external tilt angle θ' is given by

$$\Delta\nu = \nu_o \frac{\theta'^2}{2} \qquad \text{for small } \theta' \tag{4.14}$$

where ν_o is the etalon resonance frequency for $\theta=0$. Thus from equation (4.14) the resonance frequency tuning characteristics of a tilted etalon are independent from the etalon thickness.

Losses

For etalons with low reflectivity surfaces (<20% - 30%)[10] the most significant loss mechanism is beam walk-off. Under conditions of normal incidence the reflection coefficient for monochromatic light incident on a resonant etalon will be zero at resonance. See equation (4.11). This is because the portion of the incident beam directly reflected from the first etalon surface is exactly cancelled, through destructive interference, by the multiple reflections from the second surface of the etalon. However, in the case of the tilted intracavity etalon, the combination of the small intracavity laser beam diameter and the tilt angle of the etalon means that the series of back reflected beams from the etalon surfaces no longer overlap completely. Perfect destructive interference of these reflected waves cannot occur and so some of the incident power will be reflected out of the cavity.

An approximate analytical expression describing this cavity round trip power loss due to the tilted etalon has been derived by Leeb[11]. In this derivation the round trip loss is determined by correlating a Gaussian approximation of the beam profile distorted by the etalon with the initial Gaussian beam profile. For etalon induced intracavity power losses of a few percent or less the round trip power loss, l_t, is given by

$$l_t \approx \frac{2R}{(1-R)^2} \cdot \left(\frac{2d}{w} \tan\theta' \cos\theta\right)^2 \tag{4.15}$$

where w=Gaussian beam radius at the etalon. In most practical circumstances, the tilt angle will be small ($\theta<0.1$ radian) and so equation 4.15 can be further simplified to

$$l_t \approx \frac{2R}{(1-R)^2} \cdot \left(\frac{2d\theta}{w}\right)^2 \qquad ;\theta<0.1 \text{ radian} \tag{4.16}$$

Equation (4.16) implies that the tilt losses of the etalon can be minimised by keeping the tilt angle as small as possible and by locating the intracavity etalon where the beam radius is at its largest.

For etalons with higher reflectivity surfaces another loss mechanism becomes significant. This is optical power loss due to scattering and absorption in the etalon mirrors and can be expressed as[12]

$$l_{sa} \approx \frac{4A}{(1-R)} \tag{4.17}$$

for one round trip of the laser cavity. The power loss factor caused by scattering and absorption in the etalon mirrors is given by A.

Intracavity Etalon Design Criteria[12,13]

As with the extracavity Fabry-Perot etalon mode selector discussed earlier, the frequency gain bandwidth, $\Delta\nu_{gain}$, of the laser sets a lower limit on the free spectral range, $\Delta\nu_{fsr}$, of the intracavity etalon. To ensure that only one etalon transmission maximum lies within the laser gain

$$\Delta\nu_{fsr} > \Delta\nu_{gain} \tag{4.18}$$

Therefore, the maximum etalon thickness, d, which can be tolerated is

$$d < \frac{c}{2n\Delta\nu_{gain}} \tag{4.19}$$

The other design parameter of the etalon which can be optimised is the etalon mirror reflectivity. For a fixed optical path length between the etalon mirrors the reflectivity determines how quickly the etalon transmission, T, rolls off from its peak value with changing frequency. In order that the laser operates only on a single axial mode the etalon

transmission loss experienced by all the unwanted axial laser modes, away from the etalon resonance, must be sufficient to take these modes below oscillation threshold. Expressing this mathematically, to suppress the unwanted laser cavity modes the following inequality must be satisfied:

$$T(\nu)G(\nu) < 1 \tag{4.20}$$

where

$G(\nu)$ = residual single pass gain factor for the secondary axial mode with the highest probability for oscillation,

$T(\nu)$ = etalon transmission for the most likely secondary axial mode.

For small etalon tilt angles ($\theta<0.1$ radian) the etalon transmission for some optical frequency an amount $\delta\nu$ away from the etalon resonance frequency, ν_o, can be found from equation 4.10 to be

$$T(\nu_o + \delta\nu) \approx \frac{1}{1+ F\left(\frac{2\pi nd\delta\nu}{c}\right)^2} \tag{4.21}$$

In order to suppress all the unwanted axial modes of the laser equation 4.20 must be satisfied, so

$$\frac{R}{(1-R)^2} > (G-1)\left(\frac{c}{4\pi nd\delta\nu}\right)^2 \tag{4.22}$$

which defines the minimum required reflectivity of the etalon mirrors. The frequency difference, $\delta\nu$, between the lasing mode and the second most likely longitudinal mode to oscillate will be some integer multiple, q, of the laser cavity free spectral range, c/2L. Thus equation 4.22 becomes

$$\frac{R}{(1-R)^2} > (G-1)\left(\frac{L}{2\pi ndq}\right)^2 \tag{4.23}$$

where L is the optical path length of the laser cavity.

The two inequalities of equations 4.19 and 4.23 only define boundaries for the etalon thickness and reflectivity respectively. To optimise these two parameters the loss introduced by the etalon must also be considered. The parameter with the most significant influence on the etalon tilt and scatter losses is the etalon mirror power reflectivity, R. As the etalon mirror reflectivity increases the etalon induced intracavity losses become larger. To minimise these losses then, the lowest possible etalon mirror reflectivity should be used. From equation (4.23) this in turn dictates that the etalon thickness, d, is maximised.

4.5 Elimination of Spatial Hole Burning

The mode selection techniques discussed so far work essentially by discarding the available optical power in all but one cavity longitudinal mode. For lasers with homogeneously broadened gain media, whose multi longitudinal mode operation is predominantly due to spatial hole burning, this is a very wasteful method of mode selection since there are spatial regions of untapped gain within the laser medium. A more efficient approach to single frequency operation of such lasers is to eliminate the spatial hole burning so that all the lasers active centres can contribute to the laser output.

Various techniques are available to eliminate spatial hole burning and these techniques will be described in the following sections.

4.5.1 Relative Motion of Active Medium and the Laser Cavity

Spatial hole burning of the laser active medium in a standing wave resonator can be prevented from occurring by physically moving the laser medium and standing wave field relative to each other. Danielmeyer et al[14] demonstrated single frequency output from a flash lamp pumped Nd:YAG laser by moving the Nd:YAG rod along the axis of the linear optical resonator. In their experiment the elliptical pump chamber containing the Nd:YAG rod was suspended on an air cushion on an optical rail and moved at a velocity of $10cms^{-1}$ to obtain up to 1.2W of single frequency laser output. Although capable of high output

powers, the inherent lack of mechanical stability of such a system makes it unattractive for lasers requiring a high degree of intensity and frequency stability.

A more elegant way to implement this method of preventing spatial hole burning is to fix both the laser crystal and the optical resonator but move the standing wave optical field. The spatial position of the nodes and antinodes of the standing wave optical field can be modulated by using an intracavity electro-optic phase modulator to modulate the optical path length of the laser cavity. However, to maintain a constant frequency output from the laser the overall optical path length of the cavity must remain constant. This requires that a second intracavity electro-optic phase modulator is placed at the opposite side of the laser crystal and driven in antiphase to the first modulator.[15]

4.5.2 Twisted Mode Cavity

In contrast with the previously described technique for eliminating spatial hole burning, the twisted mode[16,17,18,19] approach has the attraction of being a purely passive technique. The twisted mode lasers contains three intracavity polarising elements the function of which is to generate a circularly polarised standing wave within the laser crystal. This circularly polarised standing wave is the "twisted mode" of the cavity from which the technique derives its name. The time averaged intensity of the twisted mode in the gain medium turns out to be spatially uniform along the optic axis of the cavity and so no spatial hole burning in the gain medium occurs.

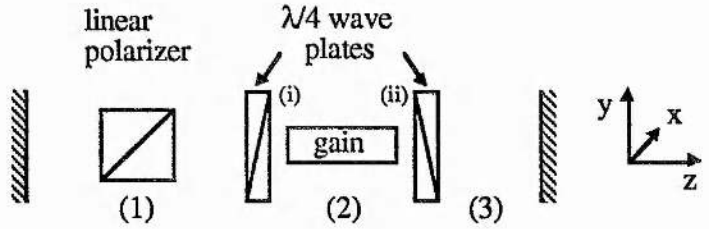

Figure 4.4 The basic components of a twisted mode laser.

Figure 4.4 shows schematically the various optical elements of a twisted mode laser cavity. The cavity contains two quarter wave plates, one at either end of the laser rod. A

linear polariser, usually in the form of a Brewster's angle plate, is also incorporated at one end of the cavity and orientated so that its plane of incidence lies at 45° to the fast axis of the neighbouring waveplate. Although the relative angle between the fast axes of the quarter wave plates is not critical in the elimination of spatial hole burning in the gain medium[16], in practice the plates are usually orientated such that the fast axes are perpendicular. As well as being a much simpler system to analyse mathematically, this particular geometry tends to make the mechanical alignment of all the intracavity polarising elements easier.

To understand the influence of the various elements of the twisted mode laser on the polarisation of the optical field as it propagates round the resonator, consider a plane polarised electromagnetic wave commencing from position (1) and travelling initially to the right along the positive z-direction. See figure 4.4. The plane of polarisation of the wave is defined by the linear polarising element and lies at 45° to the x and y axes. Thus the wave can be written in component form as

$$E_{x1} = E_0 \cos(kz-\omega t)$$

$$E_{y1} = E_0 \cos(kz-\omega t) \qquad (4.24)$$

where $k = 2\pi/\lambda$ is the propagation constant of the wave and $\omega = 2\pi\nu$ is its angular frequency. For convenience the x and y coordinate axes have been defined to coincide with the axes of the wave plates.

On passing through the first quarter wave plate (i) a relative phase shift of $\pi/2$ radians is introduced between the x and y components of the E field. So, in region (2)

$$E_{x2} = E_0 \cos(kz-\omega t-\pi/2)$$

$$E_{y2} = E_0 \cos(kz-\omega t) \qquad (4.25)$$

which is just a left circularly polarised travelling wave. The second quarter wave plate, with its fast axis perpendicular to that of the first wave plate, compensates for the $\pi/2$

phase shift between the components of the wave and returns the wave to a plane polarised state. The plane of polarisation is the same as that in region (1). In region (3) then, the wave is described by

$$E_{x3} = E_0 \cos(kz-\omega t-\pi/2)$$

$$E_{y3} = E_0 \cos(kz-\omega t-\pi/2) \qquad (4.26)$$

After being reflected from the cavity end mirror and experiencing a second passage through quarter wave plate (ii) the now counter propagating wave entering the laser rod will be

$$E_{x4} = E_0 \cos\{k(2L-z)-\omega t-\pi/2\}$$

$$E_{y4} = E_0 \cos\{k(2L-z)-\omega t-\pi\} \qquad (4.27)$$

where L is the single pass optical path length of the laser cavity. This describes a right circularly polarised wave travelling in the negative z-direction through the laser rod. Continuing through the cavity the wave traverses wave plate (i) for the second time which has the effect of returning the wave to its original plane polarised state. Thus, after one cavity round trip the polarisation of the wave is returned to its original state and so for frequencies where the overall round trip phase shift is some integer multiple of 2π, this cavity will exhibit resonant behaviour.

From the point of view of eliminating spatial hole burning the important feature to note is the form of the x and y components of the optical field in the region between the wave plates. Summing the counter propagating components of the wave in this region gives

$$E_{x2} + E_{x4} = E_x = 2E_0 \sin(kL-\omega t)\cdot\cos(kL-kz)$$

$$E_{y2} + E_{y4} = E_y = 2E_0 \sin(kL-\omega t)\cdot\sin(kL-kz) \qquad (4.28)$$

This can be interpreted as either two orthogonal, linearly polarised standing waves oscillating in phase but spatially displaced from each other along the z-axis by $\lambda/4$ or as a circularly polarised standing wave.

The intensity, I, of this circularly polarised standing wave is proportional to the square of the magnitude of the electric field vector represented the components E_x and E_y.

$$I \propto E_x^2 + E_y^2 = 4E_0^2 \sin^2(kL-\omega t) \tag{4.29}$$

As can be seen from this equation the intensity of the optical field within the laser rod is independent of position along the optic axis, z , and is therefore spatially uniform throughout the gain medium. Thus there is no spatial hole burning in the gain and the laser will oscillate on a single longitudinal mode of the cavity.

It is worth pointing out that an alternative self-consistent mode can be excited in this cavity by rotating the plane of polarisation of the linear polariser by 90°. This mode will exhibit the opposite handedness of circular polarisation within the laser rod from the previously described case. The intracavity linear polariser thus plays an important role in selecting just one of the two possible twisted modes of the cavity. Without the linear polariser the laser is likely to display instabilities in its output polarisation and intensity as these two modes compete for the available gain.

The above analysis can easily be used to examine the case where the fast axes of the two quarter wave plates are aligned. Again the resulting intensity along the axis of the laser rod is uniform and so the laser will oscillate on a single cavity mode but the linear polarisation states at either end of the laser cavity will be orthogonal.

4.5.3 Ring Cavity

An alternative approach in the elimination of spatial hole burning is to prevent standing waves from occurring by physically separating the two counter-propagating waves. This can be done by replacing the conventional linear laser cavity with a ring geometry

arrangement. The ring laser structure can support pure travelling waves which can run independently in one or both of two distinct counter-propagation directions. For a ring laser containing a homogeneously broadened gain medium the travelling wave should saturate the gain medium uniformly, with no spatial hole burning along the optical axis, resulting in bistable unidirectional mode operation. However, unavoidable back scattering of radiation from intracavity components can cause cross coupling into the counter-propagation mode which, together with mode competition effects such as self- and cross-saturation of the gain, may lead to bidirectional laser oscillation or mode hopping between counter-propagating modes.

The desired stable unidirectional laser operation can be enforced by a variety of techniques such as back reflections from an external mirror[20] or the use of an intracavity acousto-optic modulator[21,22]. The most common technique used to select unidirectional ring oscillation is the inclusion of a nonreciprocal optical isolator inside the ring cavity. The optical isolator normally consists of a Faraday rotator, a half wave plate and a linear polariser. For one propagation direction the polarization rotation caused by the Faraday rotator and by the half wave plate cancel resulting in a low loss cavity round trip for the linearly polarised mode defined by the polariser. For the opposite direction of propagation the induced polarization rotations are additive and so the rotated plane polarised mode experiences higher loss on passing through the polariser. Many examples of single frequency dye and solid state ring lasers utilising this type of unidirectional device can be found in the literature[23,24]. The technique has also been used successfully on Nd:YAG holosteric lasers[25,26,27] but in these cases the Nd:YAG rod itself, which has a small Verdet constant, was placed in a magnetic field to provide the Faraday rotation.

A particularly elegant implementation of the intracavity unidirectional device is the monolithic NonPlanar Ring Oscillator (NPRO) invented by Kane et al[28] and subsequently modified by Trutna et al[29]. In this device all the elements of the intracavity optical isolator are embodied in the monolithic gain medium itself. The ring path is defined by four reflectors, three of which are provided by total internal reflection within the gain medium.

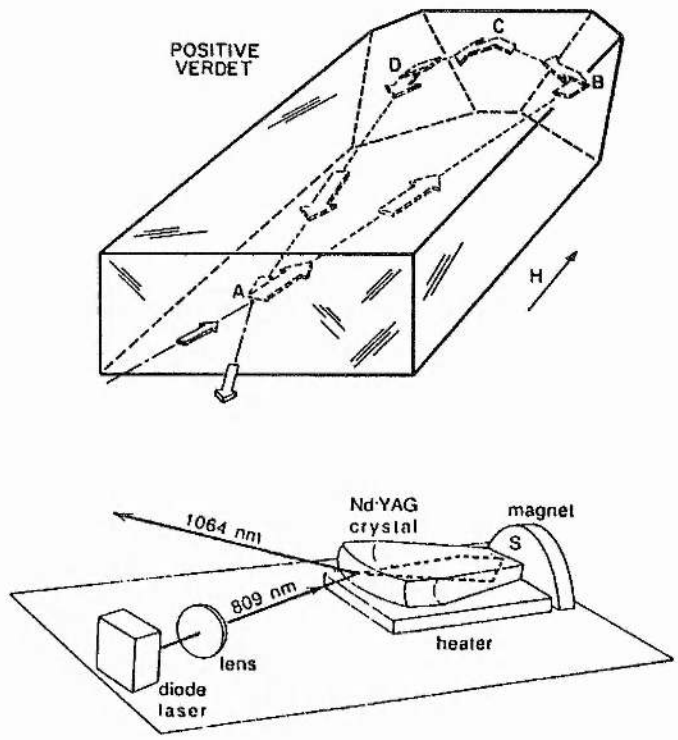

Figure 4.5. (a) a close-up view of the NPRO laser cavity showing the ring path taken by the laser beam inside the solid state gain medium. Surface A is the dielectric coated curved output coupler. This surface also acts as a partial polariser. Nonreciprocal polarisation rotation is produced within the device by applying a magnetic field, H, to the Faraday active gain material whilst reciprocal polarisation rotation occurs from the out-of-plane total internal reflections at B, C and D. (Diagram from ref. 28)
(b) A schematic of a diode laser pumped NPRO laser.(Diagram from ref.30)

A concave multilayer dielectric mirror used at oblique incidence acts as a partial polariser as well as the fourth cavity reflector. A magnetic field applied to the Faraday active gain medium forms the nonreciprocal (direction dependent) rotator whilst the reciprocal (direction independent) rotation is generated by the out-of-plane total internal reflections in the crystal[31]. The dimensions of monolithic device are typically 5×4×2mm. See figure 4.5. The NPRO laser has proved ideal for diode laser pumping, capable of high output power (0.91W)[32] and excellent free running frequency stability (3-10kHz)[33,34] and has become a successful commercial product[35]. Fast piezoelectric frequency tuning has also been demonstrated in monolithic[36] and two-piece[37] diode pumped NPRO devices as well as NPRO operation at other wavelengths (1.319 and 1.338μm)[24] and in other materials (Nd:GGG)[38]. The NPRO design is however, limited to Faraday active laser materials and

can only be operated in CW or gain switched modes since there is no access to the cavity for modulators, Q-switches or nonlinear crystals.

4.6 Experimental Implementation of Etalon Mode Selection

Of the wide variety of selection techniques available the intracavity etalon technique was one of the most appealing for use in the holosteric Nd:YAG laser because of its effectiveness and simplicity.

4.6.1 Optimum Etalon for the Holosteric Laser

Following the design criteria laid down in section 4.4.3, intracavity mode selecting etalons were designed for a typical end-pumped Nd:YAG holosteric laser. The parameters of the laser were as follows;

cavity optical path length, L = 40mm,
longitudinal mode spacing, $\Delta\nu_{fsr}$ = 3.75GHz,
bandwidth supporting laser action, $\Delta\nu_{gain} \leq 100$ GHz,
residual single pass gain = 1.25% (i.e. G = 1.0125).

For the etalon to prevent all unwanted longitudinal modes from oscillating it must provide at least enough loss to account for the difference between the unsaturated and saturated gain for those modes. A value for this residual gain was estimated using the data from the optimum output coupling experiment described in section 3.5. Referring to the experimental output coupling data in figure 3.7, this residual round trip gain corresponds to the difference between the maximum output coupling loss at which lasing just ceases (4% in this case) and the output coupling loss under normal lasing conditions (1.5% for this laser). Thus the residual round trip gain is approximately 2.5% giving a single pass value of1.25%. It is worth noting that this will be an over estimate of the actual residual

gain since in this calculation no account was taken of the frequency dependence of the gain curve and also of any hole burning effects which act to slightly reduced the unsaturated gain level.

From equation (4.19) the maximum tolerable thickness, d, for a solid fused silica etalon of refractive index n = 1.45 was calculated to be $d \leq 1.03$mm. Experimental work on the multimode holosteric lasers showed that the frequency separation of the lasing mode and the next most likely spatial hole burning mode was at least 5 free spectral ranges of the laser cavity. For single longitudinal mode operation of the laser the transmission losses of the etalon must therefore overwhelm the residual single pass gain for this secondary mode 5 cavity modes distant from the lasing mode. The minimum etalon mirror reflectivity, R, required to achieve this was calculated from equation (4.23) with the integer q set to 5. In this case the minimum required reflectivity, R, was found to be only 0.89%. However, to guarantee suppression of all but one of the longitudinal modes the etalon transmission losses should exceed the residual single pass gain even for the cavity mode adjacent to the lasing mode. Setting q=1 in equation (4.23) then gives a required etalon reflectivity value R>16.02%.

The Airy functions for a 1.03mm thick fused silica etalon of reflectivity R=0.89% and 16.02% respectively have been plotted in figure 4.6 over a frequency range spanning the gain bandwidth. For comparison, the Airy transmission function for an uncoated fused silica etalon (Fresnel reflectivity R=3.4%) has also been shown. The 1.25% loss level required to prevent lasing in the holosteric laser has also been indicated on the graph to show that these etalons are of the minimum reflectivity required to suppress all modes more than 5 and 1 free spectral ranges of the laser cavity from the lasing mode respectively.

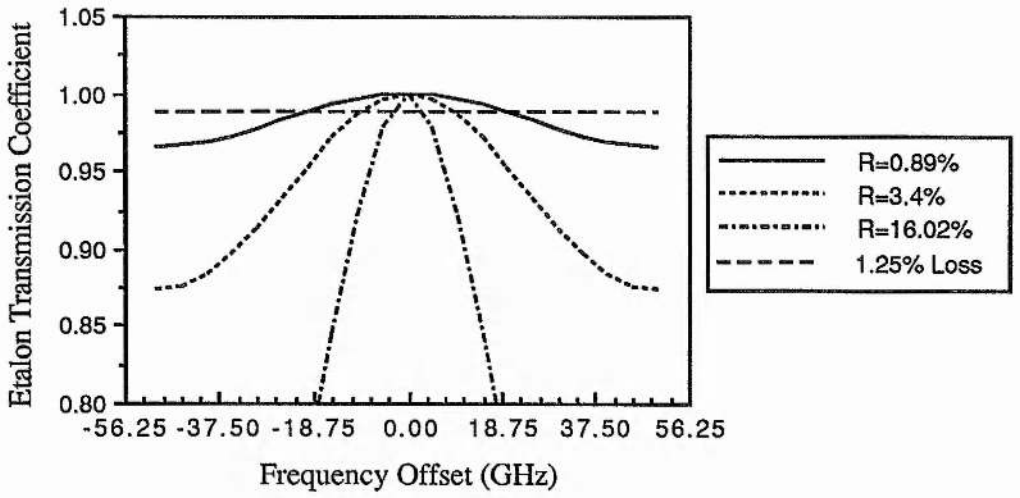

Figure 4.6. Transmission functions for the intracavity etalons. The minor tick marks on the frequency axis represent the axial modes of the laser cavity whilst the major ticks correspond to axial modes favoured through spatial hole burning. The frequency range spans the 100GHz gain bandwidth of the laser.

4.6.2 Results from the Nd:YAG Laser with Intracavity Etalon Mode Selector

The calculation shown above indicated that if the inherent mode selecting property of the spatial hole burning process in the multimode holosteric laser was exploited then a solid fused silica etalon of maximum thickness $d \leq 1.03$mm and with minimum mirror power reflectivity of $R \geq 0.89\%$ would be adequate for single mode selection in the laser. Since the Fresnel power reflectivity of 3.4% for a fused silica - air interface exceeds this minimum reflectivity requirement (see figure 4.6), solid uncoated fused silica etalons were chosen for mode control of the holosteric laser.

A variety of etalons ranging in thickness from 0.12mm up to 2mm were tried in the open cavity of the bread-boarded holosteric laser to assess their effectiveness for longitudinal mode selection. Each etalon was mounted in turn on a galvanometer (General Scanning Inc.) controlled by a General Scanning Inc. A-102 Driver Amplifier to enable

fine tilt tuning of the etalon transmission frequency. The results for the intracavity etalons tried are summarised in table 4.1.

Table 4.1

Etalon Thickness	Etalon Free Spectral Range	Description of Etalon	Maximum Possible Pump Power for SLM Operation	SLM Laser Output Power	Comments
0.12mm	862.1GHz	Microscope cover slip (Chance Propper Ltd. No.0)	50mW	4.3mW	very difficult to get SLM operation
0.17mm	608.5GHz	Microscope cover slip (Chance Propper Ltd. No.1)	55mW	1mW	very difficult to get SLM operation
0.20mm	517.2GHz	Fused silica etalon (CVI)	80mW	6mW	required large etalon tilt angle
0.23mm	449.8GHz	Microscope cover slip (Chance Propper Ltd. No.2)	46mW	4.6mW	required large etalon tilt angle
0.50mm	206.9GHz	Fused silica etalon (ICOS)	90mW	12mW	reliable SLM operation at this pump power
1.00mm	103.4GHz	Fused silica etalon (ICOS)	100mW	10 - 15mW	reliable SLM operation
1.00mm	103.4GHz	Microscope slide	100mW	1mW	low output power due to poor optical quality of the glass
2.00mm	51.7GHz	Fused silica etalon (CVI)	90mW	2.3mW	required large etalon tilt angle

These results can easily be understood by referring to figure 4.7 in which the Airy function for each etalon have been plotted. The curves have been plotted over a frequency range of 100GHz corresponding to the lasing bandwidth of the holosteric laser and the frequency axis has been calibrated so that each minor division represents an axial mode of the laser cavity while each major division represents an axial mode favoured through spatial hole burning. Also indicated on this graph is the level of additional single pass loss required in the laser to prevent oscillation under full pump power conditions.

For the uncoated etalons less than 1mm thick, the etalon transmission as a function of frequency does not roll off rapidly enough to prevent other spatial hole burning modes

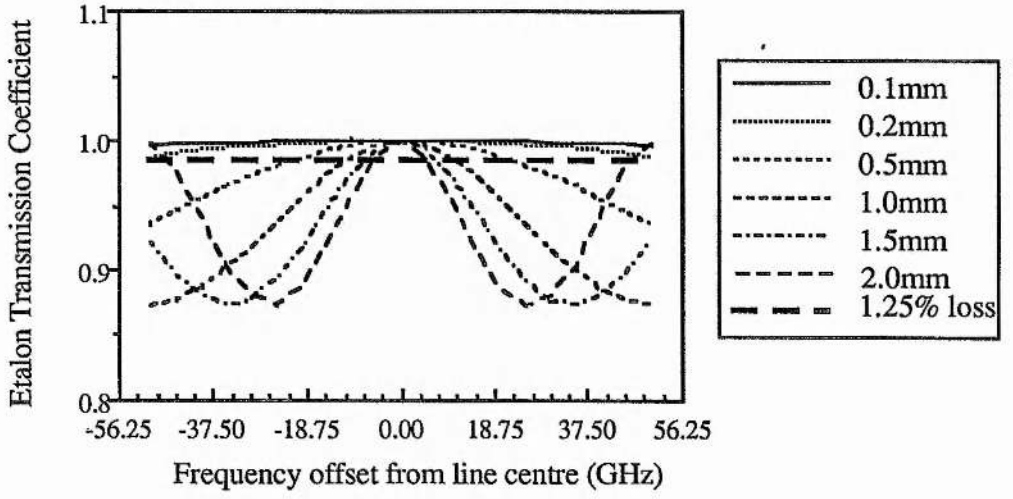

Figure 4.7 Transmission functions for various uncoated fused silica etalons.

from reaching oscillation threshold. Figure 4.8a for instance shows the output spectrum of the laser containing the 0.5mm thick intracavity etalon. This shows the laser oscillating on three longitudinal modes where the intermodal frequency spacing is dictated by spatial hole burning but where the frequency range over which oscillation can occur is governed by the etalon transmission. As table 4.1 indicates operation could only be achieved with intracavity etalons of thickness less than 1mm if the available laser gain was reduced by decreasing the pump power.

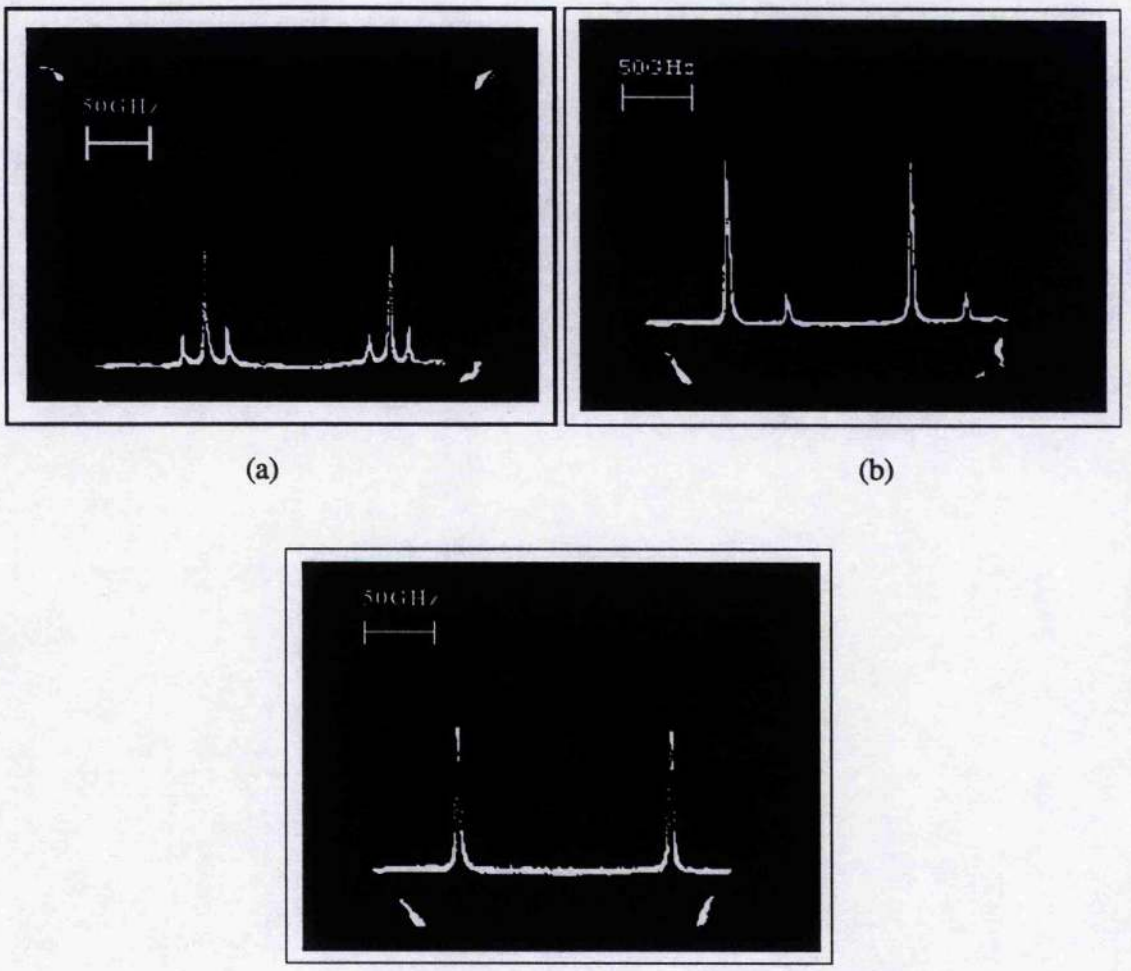

(a) (b)

(c)

Figure 4.8 Longitudinal mode output from the holosteric laser containing (a) a 0.5mm thick, (b) 2mm thick and (c) 1mm thick uncoated fused silica intracavity etalon.

In the case of the uncoated etalons greater than 1mm thick the etalon transmission rolls off quickly enough to suppress spatial hole burning modes adjacent to the lasing mode but unfortunately rolls back on again within the lasing bandwidth. With these thicker intracavity etalons the laser again oscillated on more than one longitudinal mode with the frequency separation of the lasing modes being determined by the free spectral range of the etalon. This is illustrated in figure 4.8b which shows the output spectrum of the holosteric laser containing a 2mm thick uncoated fused silica intracavity etalon. The laser oscillated on 2 cavity modes (49±3)GHz apart corresponding to the free spectral range of the etalon. As predicted by the theoretical analysis and confirmed by the results shown in

table 4.1, the 1mm etalon gave the best mode selection performance (see figure 4.8(c)) with laser output power routinely in excess of 10mW.

4.6.3 Polarisation Splitting

For the purpose of monitoring the single mode output from the holosteric laser a 50mm, 1.5GHz free spectral range scanning confocal interferometer was constructed as illustrated in figure 4.9.

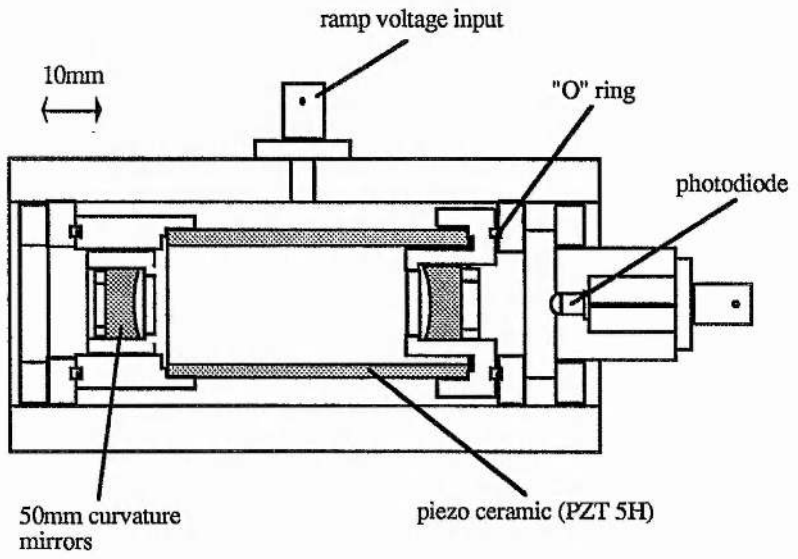

Figure 4.9. The 50mm, 1.5GHz free spectral range scanning confocal interferometer.

Frequency scanning of the interferometer was accomplished by amplifying the ramp voltage signal from an oscilloscope and applying this high voltage ramp signal to the piezoceramic tube separating the two interferometer mirrors. The output from the photodiode monitoring the transmission of the interferometer was passed through a transimpedence amplifier and displayed on the oscilloscope.

Using this interferometer it was occasionally observed that the "single" longitudinal mode of the holosteric laser was apparently split into two closely spaced modes. A typical scanning confocal interferometer trace illustrating this behaviour is shown in figure 4.10. From the interferometer trace the frequency splitting between the two peaks was around

40MHz, too small to be due to adjacent longitudinal modes or even adjacent transverse modes which were separated by some 3.75GHz and 1.3GHz respectively for this cavity. To check that the double modes observed on the interferometer were not from overlapping orders of the interferometer the beat frequency between the modes was measured using a fast silicon avalanche photodiode (Hero Electronics BPW28) with a bandwidth of 3GHz and an rf spectrum analyser (Hewlett Packard model 70001A Mainframe). The beat frequency observed using this technique was found to range from 37MHz for a laser pump power of 100mW down to 29MHz when the pump power was reduced to 50mW thus confirming the original frequency splitting measurement made using the interferometer.

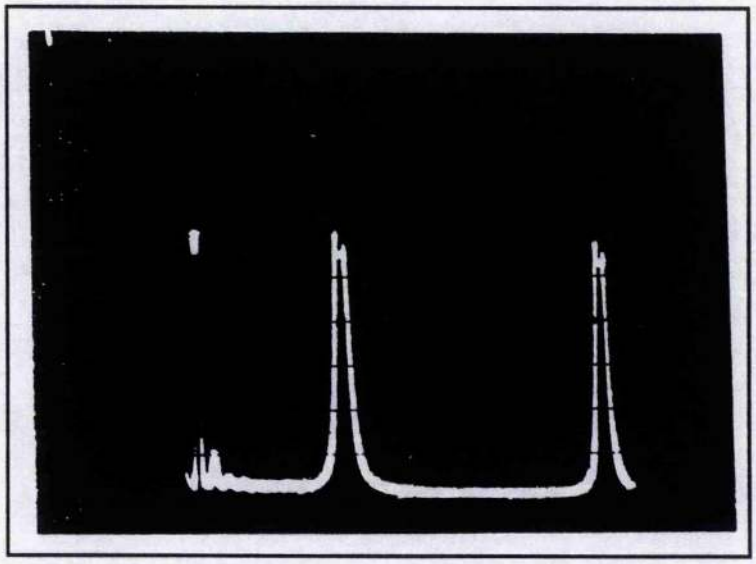

Figure 4.10. Polarisation splitting of the holosteric laser longitudinal mode spectrum. The main peaks are separated by the interferometer free spectral range (1.5GHz). The two closely spaced peaks are only 37MHz apart.

Similar frequency splitting of the longitudinal modes in holosteric Nd:YAG lasers has been reported by other workers[39,40] and has been attributed to nondegenerate orthogonal linear polarisation modes of the laser cavity due to stress induced birefringence in the Nd:YAG crystal. This cause was confirmed in the end-pumped holosteric laser by passing the laser output through a linear polarising cube. As the polariser was rotated one half of the double peak on the scanning confocal interferometer trace was seen to disappear and

the ~40MHz optical beat signal monitored on the rf spectrum analyser decreased by 25dB. Rotating the polariser through 90° selected the other peak on the interferometer trace indicating that the two modes were orthogonally polarised.

Some workers have used the stress induced birefringence of the Nd:YAG crystal to define the polarization state of the laser output. They have found that one of the two linear polarization states can be selectively excited by aligning the polarization plane with the linearly polarised pump radiation from the diode array. However, in the case of the fibre coupled diode laser pump array this method of polarization selection was not possible as the pump light emitted from the fibre was unpolarised. Instead polarization control of the Nd:YAG laser output was achieved by inserting a fused silica plate, orientated at Brewster's angle, into the laser cavity. The Brewster plate was only 0.2mm thick to minimise the amount of elliptisity induced in the laser beam profile. When the laser output was passed through a linear polarising cube extinction ratios of up to 455:1 were recorded showing that the laser output was strongly linearly polarised. With the holosteric laser operating multi-longitudinal mode insertion of the intracavity Brewster plate reduced the laser output power by typically 2mW from its original 15mW level. The addition of the longitudinal mode selecting etalon reduced the linearly polarised, single longitudinal mode output power of the laser to the 7-10mW range.

4.6.4 Frequency Tuning

The output frequency of the holosteric laser could be scanned by altering the optical path length of the cavity via the piezo mounted output mirror. With the etalon position unaltered the single mode laser output could be tuned over approximately 3.75GHz, corresponding to a free spectral range of the cavity, before mode hoping occurred. See figure 4.11.

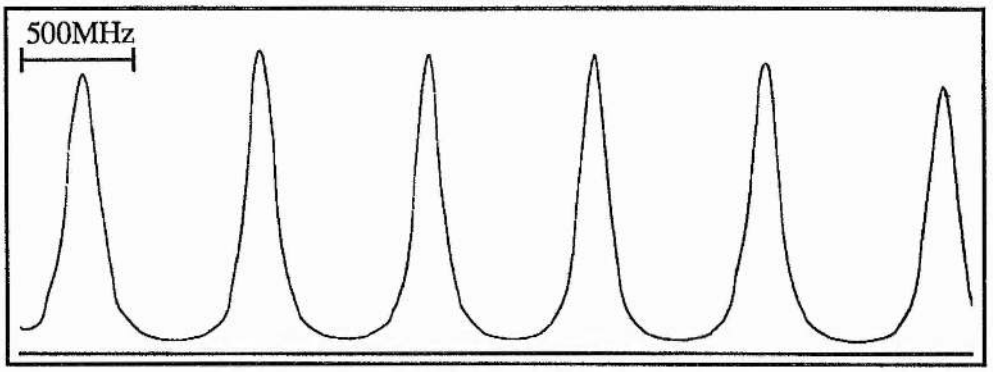

Figure 4.11. Transmission of the holosteric laser output through a 100mm, $\Delta\nu_{fsr}$=750MHz static confocal interferometer showing single mode frequency tuning of the laser output over ~3.75GHz.

By scanning the etalon angle in sympathy with the changing cavity length it should be possible to extend this single mode tuning range to cover most of the 100GHz gain bandwidth of the laser. The ramp voltage used to scan the laser cavity length can also be used to synchronously drive the etalon galvanometer. But, since the transmission frequency of the intracavity etalon changes as the square of its tilt angle (see equation 4.14) the ramp voltage to the galvanometer must first be passed through a square root circuit to give a linear scan of the etalon transmission frequency[41]. An alternative method for synchronously tuning the intracavity etalon is to apply a small modulation to the etalon angle and use phase sensitive detection to derive an error signal for servo locking the etalon angle to maximise the laser output power[40].

4.7 The Diode Laser Pumped Twisted Mode Laser

Although the intracavity etalon mode selector proved successful in generating single longitudinal mode operation of the diode pumped Nd:YAG laser, the need to have a movable element (the etalon) inside the laser cavity made the system less desirable for use in an ultra-frequency-stable laser. The more complex twisted mode technique for mode selection, described in section 4.5.2, was an attractive alternative offering the possibility of being built into a compact, mechanically stable laser cavity containing no moving components. This technique had the added advantage of potentially having a higher

efficiency by eliminating spatial hole burning in the gain medium. Because of these advantages, a second diode pumped laser was constructed incorporating the twisted mode system. Details of the design, construction and operation of this laser are described in the following sections.

4.7.1 Optical Components

The basic elements of the end pumped, twisted mode, holosteric laser are shown schematically in figure 4.12. The pump module, consisting of a 100mW, fibre coupled diode laser array and 5mm diameter spherical focusing lens was similar to that used for the end pumped holosteric laser system described in Chapter 3. Since space between the pump light focusing optic and the end of the Nd:YAG rod was limited to approximately 3mm this restricted the choice of the intracavity quarter wave plates for this twisted mode cavity design.

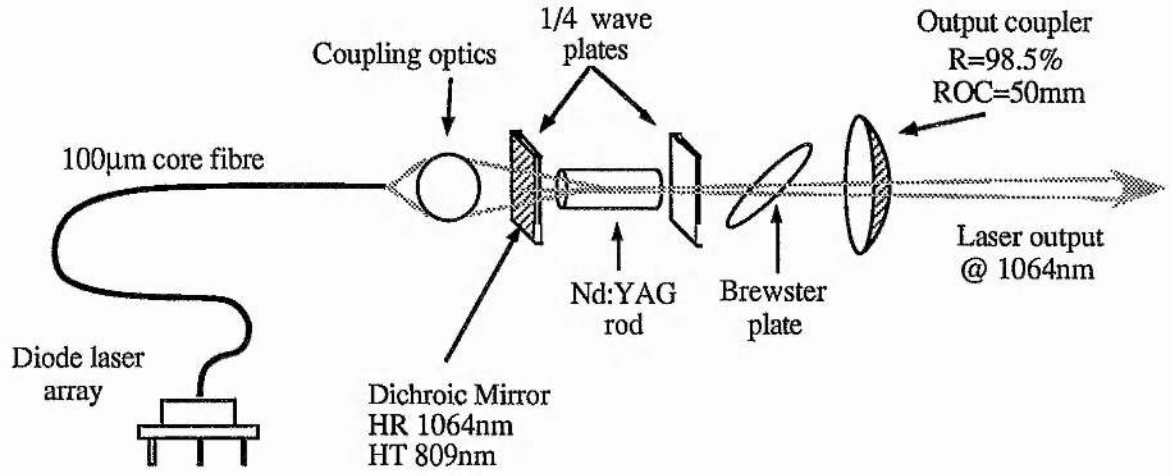

Figure 4.12 The optical components of the twisted mode holosteric laser.

Whilst zero order quarter wave plates would have been the preferred choice in terms of retardation stability with temperature, the physical thickness (typically ≥ 2mm) of commercially available zero order plates precluded their use in this design. For this reason low order quartz quarter wave plates were used. These plates, supplied by Isle Optics (UK), were 10mm × 10mm × ≈148μm and exhibited a retardation of 5λ/4. The very low

order of these wave plates meant that the temperature sensitivity of their retardation was similar to that of zero order wave plates.

As a further space saving measure, the wave plate at the pump end of the laser cavity was coated on one surface with a dielectric coating to form a high reflector mirror for the lasing wavelength of 1.064μm and a highly transmitting window for the pump light at 809nm. With the exception of the Brewster's angle plate, all other intracavity surfaces were antireflection coated to reduce intracavity losses and reduce laser threshold.

As discussed in section 4.5.2 two orthogonal linear polarisation states are possible within the twisted mode laser cavity. To select just one of these linearly polarised modes a 1mm thick, 12.5mm diameter fused silica plate set at Brewster's angle was incorporated in the cavity.

A standard Laseroptik 50mm radius of curvature, concave mirror with an optical power transmission of 1.5% for light at 1.064μm was used as the laser output coupler. The rear, plain surface of the BK7 mirror substrate was wedged and antireflection coated to prevent spurious etalon effects within the mirror substrate.

4.7.2 Mechanical Design

The conventional orientation of the optical elements used in a twisted mode laser is to have the fast axes of the two quarter wave plates rotated by 90° with respect to each other and at 45° to the plane of polarisation selected by the Brewster's angle plate. See section 4.5.2. The square (10mm × 10mm) format of the quarter wave plates with the fast axis of the wave plate along the diagonal of the plate suggested a laser cavity design in which the orientation of the intracavity elements was preset. Such a scheme was attractive primarily from the point of view of good mechanical stability but had the added advantages of compactness and low cost since it eliminated the need for expensive and bulky commercial positioning and rotation stages.

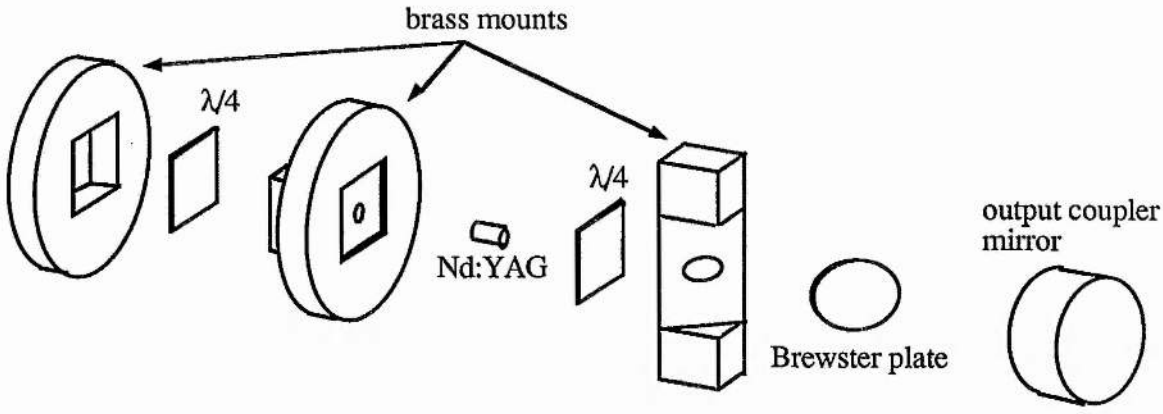

Figure 4.14. An exploded view of the pre-aligned twisted mode laser.

The design for mounting the two quarter wave plates, Nd:YAG rod and the Brewster's angle plate is shown in an exploded view in figure 4.14. The metal pieces holding these intracavity components were made from brass since this material is easy to machine accurately. The quarter wave plates were held in place by compression between the metal holders. To prevent damage to the wave plates, the plates were cushioned between "washers" cut from thin P.T.F.E. tape. A nylon tipped set screw was used to gently clamp the Nd:YAG rod whilst the fused silica plate was bonded to the Brewster's angle brass wedge using an acetone soluble adhesive (CRYSTALBOND 509 adhesive - Aremco Products Inc. Melting point approx. 120°C).

The output coupler mirror was mounted on a commercial mirror mount to facilitate alignment of the optical cavity. The mirror mount used was a Photon Control MICROPOINT 25. This type of mount is carved from a solid block of spring steel and was chosen for its good mechanical stability. A tubular piezo ceramic element was included in the output coupler assembly to provide fine control of the laser cavity length and hence laser output frequency.

The multimode optical fibre used to pipe the pump light from the diode laser array to the laser head, together with the 5mm diameter spherical focusing lens were clamped between the two halves of a cylindrical aluminium block. Groves cut along the centre of each half of the aluminium cylinder were uses to locate and align the optical fibre and the

ball lens. See figure 4.13. A rubber "O"-ring was glued around the circumference of this cylindrical block at the light output end to form a gimbal bearing about which the angle of the pump beam could be pivoted. Finally the pump module, the holder containing the wave plates, Nd:YAG rod and Brewster plate, and the output coupler were all mounted inside an aluminium tube.

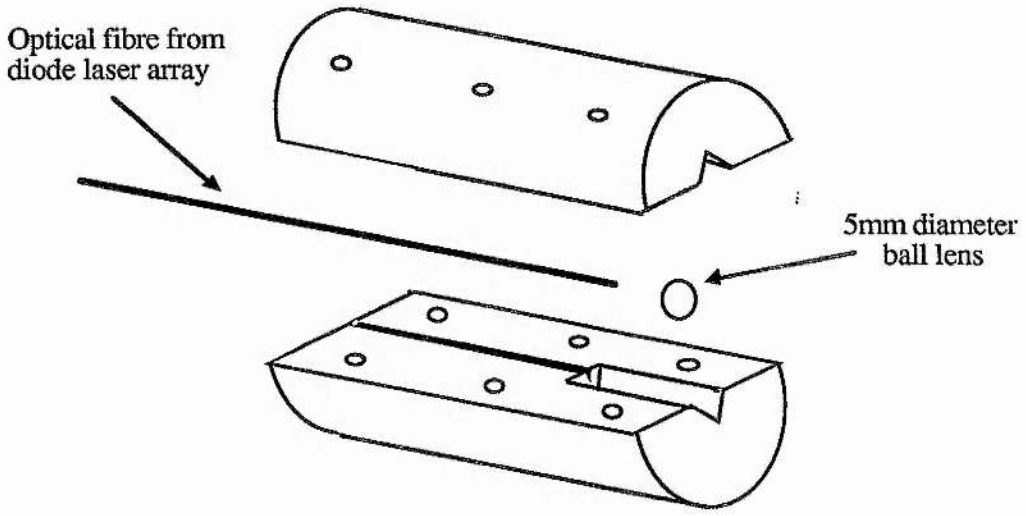

Figure 4.13. An exploded view of the pump module housing the optical fibre and focusing lens.

4.7.3 Characterisation of the Twisted Mode Holosteric Laser

A. Output Power and Slope Efficiency

When pumped with 100mW of 809nm light from the fibre coupled diode laser array (Spectra Diode Labs. model SDL-2422-H2) the twisted mode laser generated 7.3mW of single longitudinal mode, 1.064μm laser output in a TEM_{00} beam. The single longitudinal mode output power from the Nd:YAG laser was recorded as a function of pump power. See figure 4.15.

Because the wavelength emission of the diode laser shifted to longer wavelengths with increasing output power (see section 2.5.4) the diode laser temperature had to be adjusted for each measurement in order to temperature tune the diode laser wavelength back to the maximum absorption band in the Nd:YAG laser rod. The optical to optical slope efficiency

of the twisted mode laser was thus measured to be (10±0.2)% with a threshold of (24.4±1.5mW). In theory, with the elimination of spatial hole burning in the gain medium, the single frequency output power should have been comparable to the multi-longitudinal mode output power (~30mW for this laser). The relatively low output power achieved in practice could be accounted for by the increase in intracavity loss caused by the large number of intracavity elements (16 surfaces per cavity round trip) and by residual birefringence in the Nd:YAG rod disrupting the desired polarisation state of the lasing mode between the two quarter wave plates.

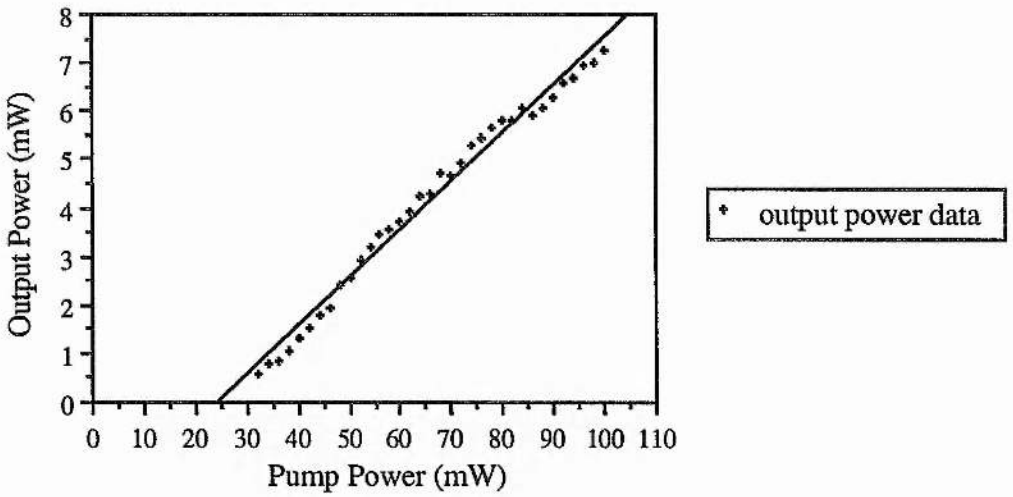

Figure 4.15 Optical to optical slope efficiency of the twisted mode laser.

B. Spectral Output and Frequency Tuning Performance

The longitudinal mode structure of the diode pumped, twisted mode, Nd:YAG laser was studied using a 1.5GHz free spectral range scanning confocal interferometer in conjunction with a scanning plane-parallel Fabry-Perot interferometer with a free spectral range of 100GHz. The plane-parallel Fabry-Perot interferometer, with its large free spectral range, provided an unambiguous display of the laser modes whilst the confocal interferometer with its higher resolution was used to check for finer spectral detail.

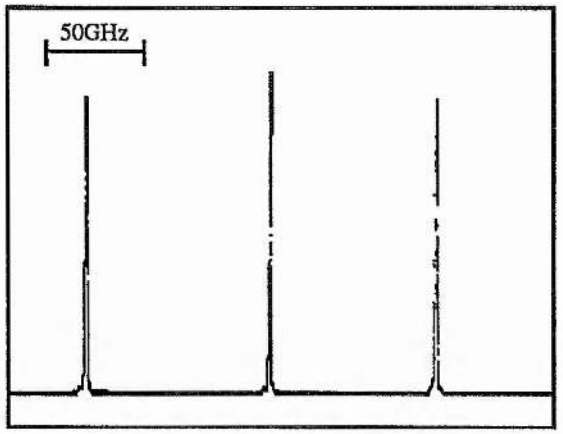

Figure 4.16. Scanning plane-parallel Fabry-Perot interferometer trace showing single longitudinal mode operation of the twisted mode holosteric laser.

A typical transmission trace from the scanning Fabry-Perot interferometer showing single longitudinal mode operation of the twisted mode laser is shown in figure 4.16. The laser could maintain this single longitudinal mode output for approximately one hour before thermal drifting of the laser cavity length and consequently drifting of the laser mode frequency resulted in the single mode operation giving way to laser oscillation on two or more longitudinal modes.

To investigate the axial mode behaviour and frequency tuning characteristics of the unstabilised twisted mode laser further, the laser cavity length was manually scanned by changing the voltage applied to the piezoceramic mount of the laser output coupler. At best single longitudinal mode output of the twisted mode laser could be maintained over a tuning range of 1.5GHz at the full pump power of 100mW before giving way to multi-longitudinal mode operation. More typically, however, the laser would tune on a single mode for ~750MHz. This first mode was then joined by a second axial mode and these two mode would continue to scan for ~750MHz. The first mode would then die out leaving only the second axial mode as the laser cavity length was gradually altered.

The double axial mode output of the laser is illustrated on the scanning plane-parallel Fabry-Perot interferometer trace of figure 4.17(a).

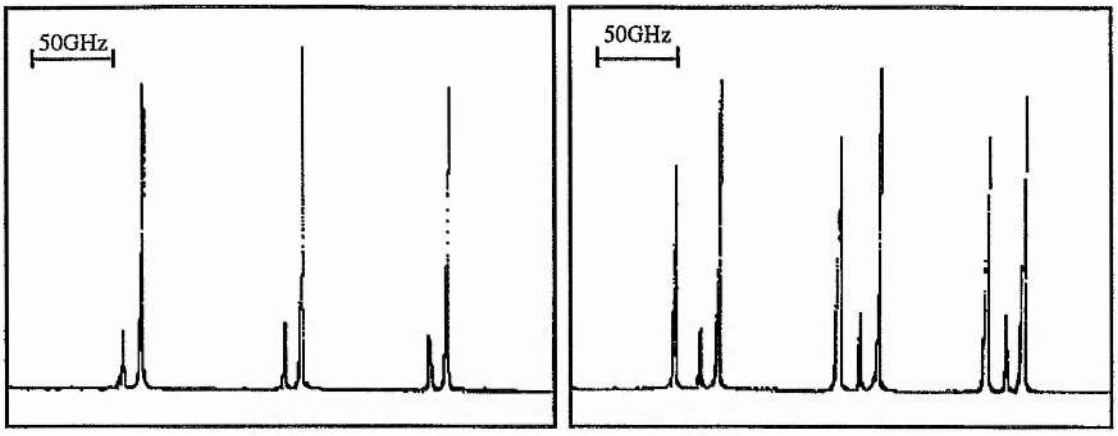

(a) (b)

Figure 4.17. Scanning Fabry-Perot interferometer traces shown the twisted mode laser oscillating on (a) two and (b) three longitudinal modes.

After compensating for the nonlinear frequency scan of the interferometer (see section 3.7) the two axial modes were found to be separated by (11.3±0.3)GHz. This frequency spacing corresponded to 3 free spectral ranges of the ~40mm optical path length laser cavity ($\Delta\nu_{fsr}$~3.75GHz). Occasionally the twisted mode laser would oscillate on 3 axial modes as shown in figure 4.17(b). In this particular case, the modes were spaced by 4 and 3 free spectral ranges of the laser cavity.

C. Spatial Hole Burning in the Twisted Mode Laser

The fact that the twisted mode laser was capable of multi-longitudinal mode oscillation indicates that there was some residual spatial hole burning occurring within the Nd:YAG gain medium. Similar multi-longitudinal mode operation in twisted mode lasers has been observed by other workers[42] but appears to have gone unpublished in the open literature.

The existence of spatial hole burning in the twisted mode laser suggested that the light field inside the laser rod was not perfectly circularly polarised. A number of factors may have contributed to this departure from pure circular polarization such as; birefringence in the Nd:YAG rod or in the dielectric coatings, retardation errors in the quarter wave plates, or misorientation of the intracavity polarising elements. Of these factors the most likely

and most easily addressed causes of spatial hole burning are birefringence in the Nd:YAG rod and misorientation of the intracavity polarising elements.

Birefringence in Nd:YAG

Although Nd:YAG is in theory an optically isotropic solid, Nd:YAG crystals can exhibit some birefringence if subjected to mechanical stress. This stress can be inherent in the crystal having been "frozen" in during the growth process, or can be caused by external sources such as clamping screws or nonuniform thermal loading[43]. As an illustration of the inherent optical anisotropy present in commercially grown Nd:YAG, figure 4.18 shows a section from a 300mm diameter Nd:YAG boule placed between crossed linear polarisers and back-lit by a white light source. The boule exhibits the bright central core and bright stress flares radiating from the centre typical of all Nd:YAG boules grown by the Czochralski method[23]. This stress pattern is caused by inhomogeneous Nd^{3+} ion concentration resulting in nonuniform thermal expansion coefficients within the volume of the boule.

Figure 4.18. This photograph shows the white light transmission of a Nd:YAG boule place between crossed linear polarisers. The characteristic strain flares are clearly visible. The circular hole in the top right hand corner of the boule is where a laser rod has been cut out.

Obviously the presence of such inherent birefringence in the gain medium of a twisted mode laser would have an adverse effect on the polarization state of the light in the laser and so the procurement of high quality Nd:YAG material is an essential consideration when constructing a twisted mode laser.

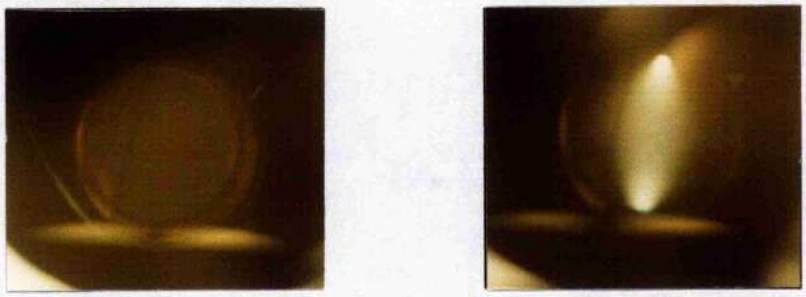

(a) (b)

Figure 4.19. A high quality, birefringence free Nd:YAG laser rod (3mm Ø × 5mm long) is shown here, viewed between crossed polarisers. (a) In the absence of mechanical stress no strain flares can be seen. (b) When pressure is applied to the rod by means of a nylon tipped clamping screw (entering from the top of the picture) the rod exhibits stress induced birefringence.

However, even with high quality, birefringence-free Nd:YAG it is still possible to induce birefringence by applying mechanical pressure to the laser rod. This behaviour is demonstrated in figure 4.19. Figure 4.19(a) is a photograph of a 3mm diameter × 5mm long Nd:YAG laser rod positioned between crossed linear polarisers. The rod is made from high quality Nd:YAG material and shows no optical anisotropy. In figure 4.19(b) the same rod is shown but this time a small amount of pressure is applied to the top of the rod by means of a nylon tipped set screw. Stress induced birefringence is clearly visible in this case. This method of securing the Nd:YAG laser rod in the holosteric laser was commonly used in earlier cavity designs but because of the stress induced birefringence it can cause, this mounting method should be avoided for the polarisation sensitive twisted mode laser.

New Twisted Mode Cavity Design

To investigate the sensitivity of the twisted mode laser performance to rotational orientation of the intracavity polarising elements a new laser cavity was constructed. The two quarter wave plates, Nd:YAG rod and the Brewster's angle linear polarising plate were mounted in a nested arrangement of four concentric cylinders, each cylinder carrying

one of the optical components. The cylinders were close fitting to prevent any wobble but were otherwise free to rotate around the axis of the cavity. See figure 4.20.

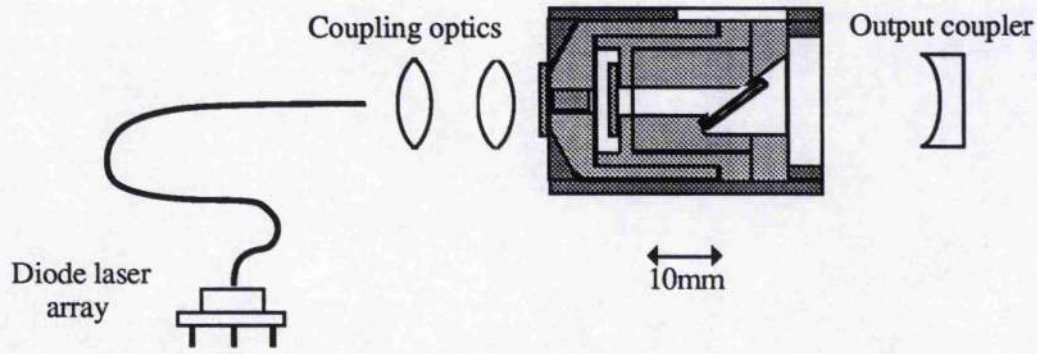

Figure 4.20 The new twisted mode laser cavity with rotatable optical components. The waveplates, Nd:YAG rod and Brewster plate are shown lightly shaded while the cross-hatched areas represent the brass cylinders on which they are mounted.

As in previous cavity designs the fibre optic pigtail of the diode laser array and the pump light coupling optics were clamped in an aluminium block. This time, however, the pump unit was mounted in a five axis gimbal mount (Newport M-LP-1) which gave 3 translational and 2 rotational degrees of freedom to the pump unit. The pump diode used to power this twisted mode laser was a fibre coupled 250mW device (Spectra Diode Labs model SDL-2432-P2) driven by a SDL820 high current (10Amps) stabilised diode laser power supply. The concave output coupler mirror was mounted in a Photon Control gimbal flexture mirror mount (Micropoint 25) to facilitate cavity alignment.

The three units of the twisted mode laser: pump, cylinders holding the intracavity elements, and the output coupler, were all secured to a common base plate. A photograph of the assembled laser system is shown in figure 4.21. The concentric cylinder section of the laser was positioned relative to the pump unit such that the dichroic laser cavity end mirror was located in the gimbal plane of the pump unit optical mount. In this way the angle of the pump beam could be optimised without causing significant displacement of the pump focus within the Nd:YAG rod.

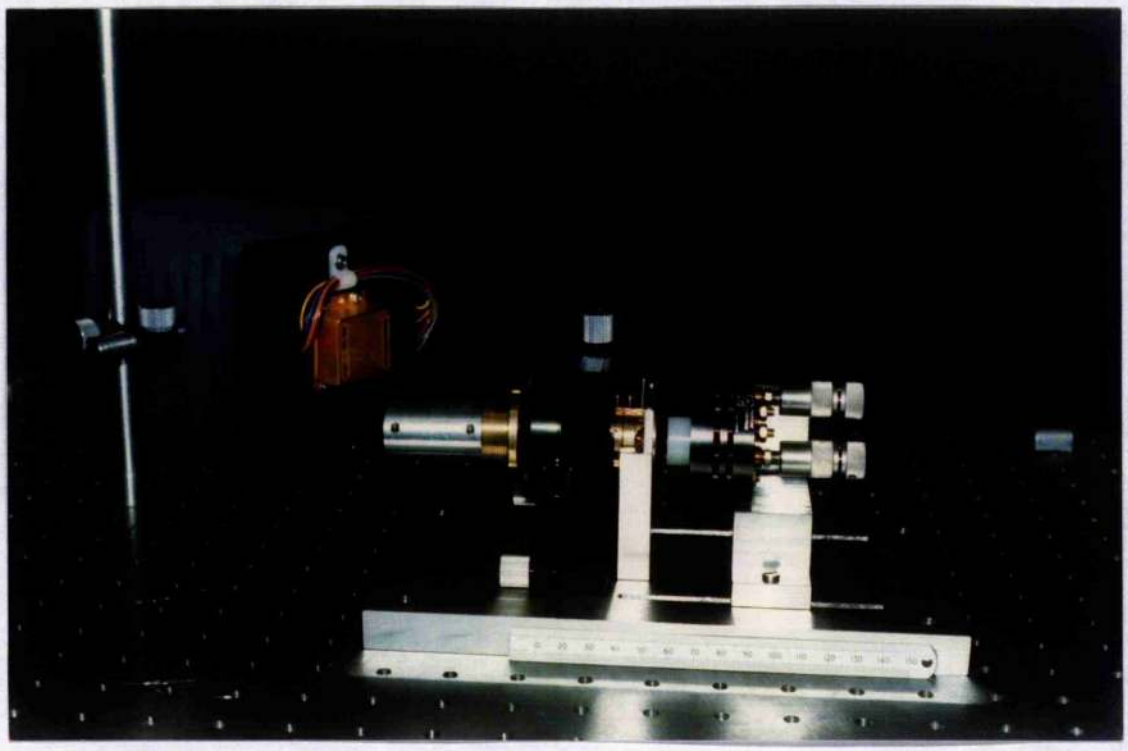

Figure 4.21. The assembled twisted mode laser. The fibre pigtail from the diode laser array enters from the left. 1064nm Nd:YAG laser emission exits to the right.

The Nd:YAG rod itself was made from high quality, birefringence free material. To avoid inducing any birefingence in the rod through mechanical stress the rod was lightly tacked in place using an acetone soluble rubber adhesive (Copydex®).

Performance of the New Twisted Mode Cavity

The pump optics for this laser consisted of a pair of aberration corrected compound lenses. An 8mm focal length compound lens with a numerical aperture (N.A.) of 0.5 (Melles Griot model 06-GLC002) was used to collect and collimate the divergent output beam from the fibre pigtail of the diode laser array. This was followed by a 14.5mm focal length, N.A. = 0.276 focusing element (Melles Griot model 06-GLC003). The overall magnification of this lens pair system was approximately 1.81 and so the 100μm diameter core of the fibre pigtail was transformed into a free space image approximately 181μm across.

A 50mm radius of curvature, concave mirror was selected for the output coupler of the laser resonator. For this curvature of output mirror the best mode overlap between pump and laser modes was achieved for an optical path length in the cavity of about 40mm.

Initially the laser was run using a 1.5% transmission output coupler similar to that used in the first twisted mode laser. The multimode output power from the laser was recorded by aligning the birefringence axes of the two waveplates with the plane of linear polarisation defined by the Brewster plate. In this way the quarter wave plates had no effect on the polarisation state of the lasing mode which remained linearly polarised throughout the length of the cavity. When pumped

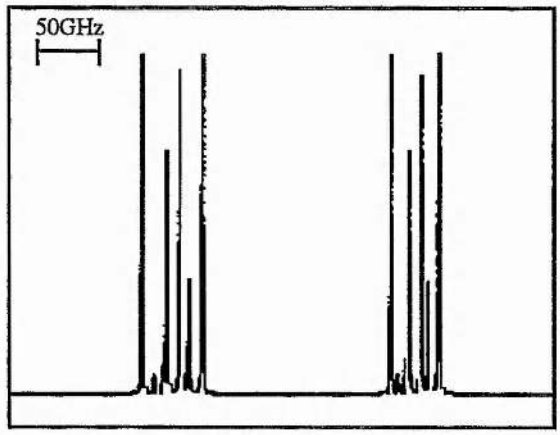

Figure 4.22. The multi-longitudinal mode output from the twisted mode laser with the fast axis of the two intracavity λ/4 wave plates collinear with the plane of polarization defined by the Brewster plate.

with the full 250mW output from the diode array the 1064nm Nd:YAG laser delivered 42mW distributed over 7 longitudinal cavity modes. Figure 4.22 shows a typical trace of the multi-longitudinal mode structure output from this laser observed using a 209GHz free spectral range scanning plane-parallel Fabry-Perot interferometer.

Having established the maximum output power potential of the laser under multi-longitudinal mode operation, the second quarter wave plate and the Brewster plate were rotated appropriately to give single longitudinal mode output. As expected single longitudinal mode operation could be achieved for any relative orientation of the two

quarter wave plates but was highly sensitive to the relative orientation of the Brewster plate to the second quarter wave plate. However, maximum single longitudinal mode output power was attained when the fast axis of the waveplates were perpendicular and the

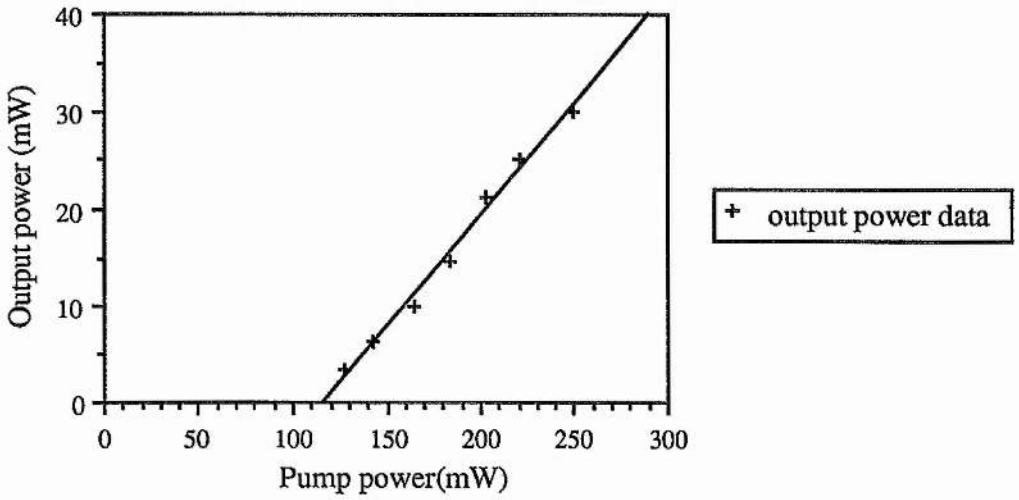

Figure 4.23. Single mode optical to optical slope efficiency for the redesigned twisted mode laser.

Brewster plate was carefully inclined at 45° to the fast axis of the waveplates. For this arrangement the laser exhibited an optical to optical slope efficiency of 23%, a threshold pump power of 116mW and a maximum single longitudinal mode output at λ=1064nm of 31mW as shown in figure 4.23.

Frequency tuning of the laser output was accomplished using a piezoceramic element mounted behind the output coupler mirror to vary the cavity length. Single longitudinal mode operation of the laser could be maintained over a frequency range of 650MHz before giving way to oscillation on two longitudinal modes. Using the scanning Fabry-Perot interferometer these two modes were found to be separated by about 10GHz corresponding to a spacing of 3 times the laser cavity free spectral range.

4.8 References

1 Zayhowski J. J., Mooradian A., "Single Frequency Microchip Nd Lasers", Opt. Lett. **14**(1) 24 (1989)

2 Zayhowski J. J., Mooradian A., "Frequency Modulated Nd:YAG Microchip Lasers", Opt. Lett. **14**(12) 618 (1989)

3 Zhou F., Ferguson A. I., "Tunable Single Frequency Operation of a Diode Laser Pumped Nd:YAG Microchip at 1.3μm", Elect. Lett. **26**(7) 490 (1990)

4 Zhou F., Ferguson A. I., "Frequency Stability of a Diode Laser Pumped Microchip Nd:YAG Laser", Opt. Lett. **16** 79 (1991)

5 Zhou B., Kane T. J., Dixon G. J., Byer R. L., "Efficient Frequency Stable Laser Diode Pumped Nd:YAG Laser", Opt. Lett. **10** 62 (1985)

6 Zayhowski J. J., "Limits Imposed By Spatial Hole Burning on the Single Mode Operation of Standing Wave Laser Cavities", Opt. Lett. **15**(8) 431 (1990)

7 Smith P. W., "Stabilized, Single Frequency Output from a Long Laser Cavity", IEEE J. Quant. Electron. QE-1(8) 343 (1965)

8 Smith P.W., "Mode Selection in Lasers", Proc. IEEE **60**(4) 422 (1972)

9 Hecht E., Zajac A., "Optics", Addison-Wesley Publishing Inc. 1974

10 Hercher M., "Tunable Single Mode Operation of Gas Lasers Using Intracavity Tilted etalons", Appl. Opt. **8**(6) 1103 (1969)

11 Leeb W. R., "Losses Introduced by Tilting Intracavity Etalons", Appl. Phys. **6** 267 (1975)

12 Danielmeyer H. G., "Stabilized Efficient Single-Frequency Nd:YAG Laser", IEEE J. Quant. Electron. **QE-6**(2) 101 (1970)

13 Danielmeyer H. G., Leibolt W. N., "Stable Tunable Single-Frequency Nd:YAG laser", Appl. Phys. **3** 193 (1974)

14 Danielmeyer H. G., Nilsen W. G., "Spontaneous single-Frequency Output from a Spatially Homogeneous Nd:YAG Laser", Appl. Phys. Letts. **16**(3) 124 (1970)

15 Danielmeyer H. G., Turner E. H., "Electro-optic Elimination of Spatial Hole Burning in Lasers", Appl. Phys. Letts. **17**(12) 519 (1970)

16 Evtuhov V., Siegman A. E., "A twisted-Mode Technique for Obtaining Axially Uniform Energy Density in a Laser Cavity", Appl. Opt. **4**(1) 142 (1965)

17 Draegert D. A., "Efficient Single-Longitudinal-Mode Nd:YAG Laser", IEEE J. Quant. Electr. **QE-8**(2) 235 (1972)

18 Wallmeroth K., Peuser P., "High Power CW Single-Frequency TEM_{00} Diode-Laser-Pumped Nd:YAG Laser", Electr. Lett. **24**(17) 1086 (1988)

19 Wallmeroth K., "Monolithic Integrated Nd:YAG laser", Opt. Lett. **15**(16) 903 (1990)

20 Hercher M., Young M., Smoyer C. B., "Travelling-wave Ruby Laser with a Passive Optical Isolator", J. Appl. Phys. **36**(10) 3351 (1965)

21 Neez J., Kowalski F. V., "Unidirectional Device for a Ring Laser Using an Acousto Optic Modulator", Opt. Lett. **13** 375 (1988)

22 Bromley L. J., Hanna D. C., "Single-Frequency Q-Swiched Operation of a Diode Laser Pumped Nd:YAG Ring Laser Using an Acousto-Optic Modulator", Opt. Lett. **16**(6) 378 (1991)

23 Koechner W., "Solid-State Laser Engineering", Springer-Verlag (1988)

24 Siegman A. E., "Lasers", University Science Books (1986)

25 Harrison J., Rines G. A., Moulton P. F., "Coherent Summation of Injection-Locked, Diode-Pumped Nd:YAG Lasers", Opt. Lett. **13**(2) 111 (1988)

26 Scheps R., Hyers J., "A Single Frequency Nd:YAG Ring Laser Pumped by Laser Diodes", IEEE J. Quant. Elec. **26**(3) 413 (1990)

27 Clarkson W. A., Hanna D. C., "Single Frequency Q-Switched Operation of a Laser Diode-Pumped Nd:YAG Laser", Opt. Comm. 73(6) 469 (1989)

28 Kane T. J., Byer R. L., " Monolithic, Unidirectional Single-Mode Nd:YAG Laser", Opt. Lett. **10**(2) 65 (1985)

29 Trutna W. R., Donald D. K., Nazarathy M., "Unidirectional Diode Laser Pumped Nd:YAG Ring Laser with a Small Magnetic Field", Opt. Lett. 12(4) 248 (1987)

30 Nilsson A. C., Kane T. J., Byer R. L., "Monolithic Nonplanar Ring Lasers: Resistance to Optical Feedback", SPIE Vol.**912** Pulsed Single Frequency Lasers: Technology and Applications (1988)

31 Nilsson A. C., Gustafson E. K., Byer R. L., "Eigenpolarization Theory of Monolithic Nonplanar Ring Oscillators", IEEE J. Quant. Elec. **25**(4) 767 (1989)

32 Cheng E. A. P., Kane T. J., "High Power Single Mode Diode Pumped Nd:YAG Laser Using a Monolithic Nonplanar Ring Resonator"' Opt. Lett. **16**(7) 478 (1991)

33 Kane T. J., Nilsson A. C., Byer R. L., "Frequency Stability and Offset Locking of a Laser Diode Pumped Nd:YAG Monolithic Nonplanar Ring Oscillator", Opt. Lett. **12**(3) 175 (1987)

34 Bush S. P., Gungor A., Davis C. C., "Studies of the Coherence Properties of a Diode Pumped Nd:YAG Ring Laser", Appl. Phys. Lett. **53**(8) 646 (1988)

35 Series 200, 500mW output power diode pumped ring laser - Lightwave Electronics, California, USA (1990).

36 Kane T. J., Cheng E. A. P., "Fast Frequency Tuning and Phase Locking of Diode Pumped Nd:YAG Ring Laser", Opt. Lett. **13**(11) 970 (1988)

37 Trutna W. R., Donald D. K., "Two-Piece Piezoelectrically Tuned Single Mode Nd:YAG Ring Laser", Opt. Lett. **15**(7) 369 (1990)

38 Day T., Nilsson A. C., Fejer M. M., Farinas A. D., Gustafson E. K., Nabors C. D., Byer R. L., "30Hz Linewidth, Diode Laser Pumped, Nd:GGG Nonplanar Ring Oscillators by Active Stabilization", Elec. Lett. **25**(13) 810 (1989)

39 Esherick P., Owyoung A. "Polarization Feedback Stabilization of an Injection-Seeded Nd:YAG Laser for Spectroscopic Applications" J. Opt. Soc. Am. B **4**(1) 41 (1987)

40 Esherick P., Owyoung A. "Stress-Induced Tuning of a Diode-Laser-Excited Monolithic Nd:YAG Laser" Opt. Lett. **12**(12) 999 (1987)

41 Ferguson A., "Frequency Doubled Countinuous Wave Dye Lasers", Ph.D. Thesis (1977), University of St. Andrews, Scotland

42 Man C. N., Centre National de la Recherche Scientifique, Laboratoire de l'Horloge Atomique, Orsay, France. Private communication.

43 Zverev G. M., Golyaev Y. D., Shalaev E. A., Shokin A. A., "Neodymium Activated Yitrium Aluminium Garnet (Nd:YAG) Lasers", J. Sov. Las. Res. **8**(3) (1987)

Chapter 5

PASSIVE STABILISATION

5.1 Noise Sources Affecting Laser Frequency

The most obvious approach to laser frequency stabilisation is to identify and eliminate, if possible, all the internal/external influences which contribute frequency noise to the free-running laser output.

The noise sources arising in a laser can be loosely classified into the following two groups; *technical noise* which refers to external noise sources and fluctuations in the environment which couple into the laser, and *fundamental noise* arising from quantum and thermodynamic fluctuations.

5.1.1 Technical noise.

Although these noise sources are numerous, it is possible through careful laser design and isolation, referred to here as passive stabilisation, to eliminate or at least reduce their contribution to frequency noise in the laser's output. Holosteric lasers are ideal systems for passive stabilisation since they are free from many of the noise source (such as electric discharge noise, vibration from flowing coolants, fast flowing dye jets, etc.) that plague more conventional laser systems. They can also be made extremely compact and so are more easily isolated from the environment.

In a laser oscillator because the resonance linewidth of the laser cavity is typically several orders of magnitude narrower than the atomic or molecular linewidth of the laser transition (~200GHz for Nd:YAG), the cavity resonance determines the precise frequency of the laser output. In turn, the cavity resonance frequency is set by the optical path length between the cavity mirrors. For a linear cavity of physical length L, containing a gain

medium of length d and refractive index n_1, and where the refractive index of the remainder of the cavity is n_2, the precise laser frequency (of the qth longitudinal mode of the cavity) is determined by ;

$$\nu = \frac{qc}{2(n_1 d + n_2(L-d))} \tag{5.1}$$

Obviously any fluctuations in n_1, n_2, d or L will result in changes of the laser frequency, ν. The exact spectral content of the frequency noise contributed by variations in any or all of these cavity parameters will of course depend on the design of the laser cavity and its immediate environment. However, certain commonly occurring environmental influences can be readily identified and loosely categorised as causing either short-term (of period < 1second say) fluctuations or longer term drifts in the laser frequency.

Long-Term Drifts.

Long-term drifts in laser frequency are mainly caused by slow variations in ambient temperature and pressure. To minimise long-term variation of cavity length due to thermal effects, the material comprising the mirror spacer should have a small thermal expansion coefficient. For example, materials such as Invar or Zerodur, which have extremely low coefficients of thermal expansion ($\alpha \sim 1\times10^{-6}$ °C^{-1} for Invar and $\alpha<0.1\times10^{-6}$ °C^{-1} for Zerodur) are frequently used. Even so, for a typical Invar cavity diode laser pumped Nd:YAG laser with a cavity approximately 5cm long, a temperature change of only 0.1°C would result in a frequency shift of around 25MHz.

Another source of long (and also short) term drift afflicting particularly external mirror cavities, is due to temperature and pressure induced fluctuations of the refractive index in intracavity air gaps. If a length x=(L-d), of the intracavity optical path is through air at some pressure P, then any change, ΔP, in the air pressure results in change of the round trip optical path length of

$$\Delta S = 2x(n-1)\frac{\Delta P}{P} \tag{5.2}$$

with $\frac{\Delta P}{P} = \frac{\Delta n}{(n-1)}$.

Again taking the diode pumped Nd:YAG laser as an example, with n=1.00027 and x=4.5cm we have, for a change in atmospheric pressure of $\Delta P \approx 300$Pa (due to wind turbulence around the building, air conditioning, doors opening, etc.)[1], a resultant laser frequency drift of ~20MHz. In a passively stabilised laser such pressure induced frequency drifts can only be reduced by enclosing the laser in a pressure tight container or by minimising intracavity air spaces.

For solid state lasers, because of the high refractive index and thermal expansion coefficients of the solid state materials, thermal expansions in the solid gain medium can cause large laser frequency shifts. For instance, Nd:YAG has a thermal expansion coefficient $\alpha \approx 1\times10^{-5}°C^{-1}$ and a refractive index n = 1.82, so for a 5mm long Nd:YAG rod in a 5cm long cavity a temperature change of 0.1°C will result in a 45MHz frequency shift caused by thermal expansion of the rod alone.

Short-Term Fluctuations.

As mentioned in the previous section, pressure fluctuations in any intracavity air spaces can give rise to both long term drifts in the laser frequency and also faster frequency fluctuations. These short term pressure fluctuations are due to acoustic pressure waves and tend to be smaller in magnitude compared with the slower effects caused by draughts and background pressure changes. For example, the pressure change ΔP (also termed the sound pressure level) associated with sound levels in a quiet laboratory[2] may be of the order of 10mPa. (For reference the sound pressure level at the threshold of hearing is around 20μPa.) Using this value for ΔP in equation (5.2) implies a change in the laser frequency in the region of 700Hz.

Another significant contribution to short-term laser frequency noise comes from airborne acoustic noise and mechanical vibrations coupling into the cavity structure. Using the familiar expression relating the tensile or compressive stress of a material to the applied strain

$$\frac{\Delta L}{L} = \frac{1}{Y} \cdot \frac{F}{A} \tag{5.3}$$

where Y is Young's Modulus, F is the applied force and A is the cross-sectional area of the material, the fractional deformation of a solid metal bar ($Y \sim 10^{11}$Pa) subjected to a pressure of 10mPa typical of low sound levels, will be of the order of 10^{-13}. This fractional length change in the mirror spacer material of a laser cavity would contribute about 60Hz to the laser linewidth. In practice, mechanical resonances in the cavity structure can lead to sizeable magnification of these vibrational changes in the cavity length resulting in peaks in the Fourier spectrum of the laser frequency noise.

Microphonic sensitivity of the laser to acoustic pressure waves and mechanical vibrations can be difficult, but not impossible, to eliminate. For instance, mechanical cavity resonances can sometimes be located with an acoustic probe and removed by proper damping (eg. by increasing the mass of the structure at various points). Isolation from building vibrations can be achieved, to a degree, by using a massive base plate resting on a sand bed mounted on low pressure air filled supports.

5.1.2 Fundamental Noise.

Even if the laser can be totally isolate from all external disturbances, there still remain two fundamental and inescapable sources of frequency noise affecting the free-running laser output spectrum. The first of these noise sources is due to the thermodynamic limit imposed on the mechanical stability of the cavity . This noise source, analogous to Johnson noise or Brownian motion, is caused by the presence of thermal energy in each vibrational mode of the laser structure. The principal contribution to the laser linewidth from this noise

source will normally derive from the lowest vibrational mode of the mirror spacers and can be calculated from[3]

$$\frac{\Delta\nu_{th}}{\nu} = \sqrt{\frac{2kT}{YV}} \tag{5.4}$$

where T=temperature of the spacer material, V=volume of spacer material and Y=Young's Modulus of the spacer material (~149×10^{9}Nm^{-2} for Invar). $\Delta\nu_{th}$ is of the order of 1Hz for an Invar cavity of a few centimetres in length at room temperature. The frequency spectrum of this noise source will show maxima at frequencies corresponding to mechanical resonances of the cavity structure.

The second fundamental contribution to the free running laser linewidth is inherent in the light generation mechanism itself. In the laser, light is emitted through two processes; stimulated emission and spontaneous emission. Stimulated emission is responsible for the dominant coherent amplification process producing light identical in phase, frequency, polarisation and direction to that in the stimulating radiation. In contrast, spontaneous emission requires no stimulating field and produces light with essentially random phases, directions and frequencies (within the bandwidth of the laser transition). A fraction of this spontaneously emitted light will propagate within the same resonator mode as the laser beam adding a small incoherent portion to the laser field resulting in an irreducible fluctuation in the laser frequency. In the case of a single mode, homogeneously broadened laser system operating above oscillation threshold, theory predicts a spontaneous emission noise limited linewidth given by

$$\Delta\nu = \frac{2\pi h\nu(\Delta\nu_{cav})^2}{P}\left(\frac{g_1N_2}{g_1N_2-g_2N_1}\right) \tag{5.5}$$

where h, ν, P and $\Delta\nu_{cav}$ are respectively, Planck's constant, the laser frequency, the laser output power and the cold cavity bandwidth. N_1 and N_2 are the population densities in the lower and upper laser levels respectively and g_1 and g_2 describe the degeneracies of these levels. This expression was originally proposed (all be it with an additional factor of 4) by

Schawlow and Townes in their original theoretical paper on the characteristics of the laser[4] and has since become known as the Schawlow-Townes linewidth limit. The spectral content of the noise fluctuations is essentially white in nature with a constant frequency fluctuation spectral density, ϖ (in Hz/$\sqrt{}$Hz) given by[5]

$$\varpi = \sqrt{\frac{\Delta\nu}{\pi}} \tag{5.6}$$

Consider once again the end pumped, diode laser pumped, single mode Nd:YAG laser used in this work. Taking typical values for the output power and net loss (including output coupling and parasitic losses) of 5mW and 3% respectively, the predicted Schawlow-Townes linewidth limit is of the order of 50-60mHz giving a spectral density in the laser frequency fluctuations of around 130mHz/$\sqrt{}$Hz.

5.2 Passive Stabilisation of the CW End-Pumped Nd:YAG Holosteric Lasers

This section charts the gradual improvement in the passive, relative frequency stability of two cw end-pumped single mode holosteric lasers through modifications in cavity design and acoustic isolation. The emphasis here was on reducing the short term laser linewidth in order to ease the demands on bandwidth and gain of any electronic servo loop to be used for further active frequency stabilisation. Although longer term frequency stability is an important issue in narrow linewidth lasers it was felt that this problem could be addressed, if need be, at a later stage with appropriate implementation of tight temperature control of the laser cavity and the use of low expansion materials in a thermal expansion compensating cavity design.

As a starting point the relative stability between the two first holosteric lasers built was measured. These two lasers were both open cavity systems constructed simply by clamping the three major building blocks (pump section, Nd:YAG rod holder and output coupler mount) of each laser straight on to the optical table. One of the lasers had its output mirror

mounted on a three channel piezo ceramic cube (Photon Control ASM18) and its intracavity mode selecting etalon mounted on a galvanometer to enable the single mode output frequency to be manually scanned. The second laser was of a fixed cavity length and contained an intracavity etalon mounted on a manual rotation stage for single longitudinal mode selection. Each laser cavity was enclosed in thin plastic film (Clingfilm®) to reduce pressure fluctuations in the intracavity air spaces.

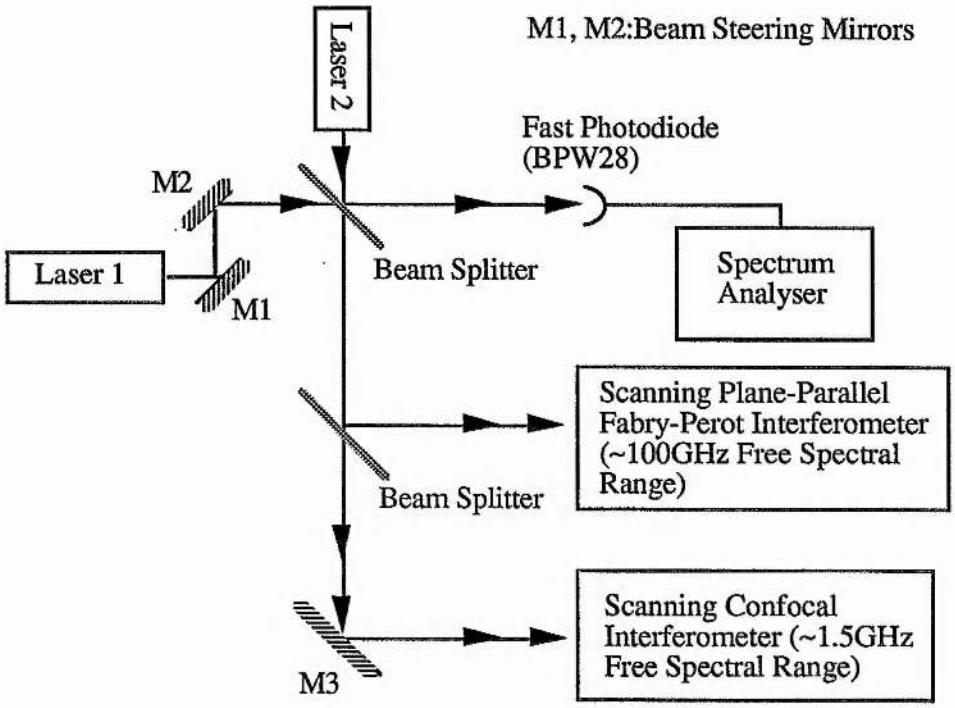

Figure 5.1 Schematic of the optical heterodyne experiment

The short term relative frequency stability of these two lasers was evaluated in an optical heterodyne experiment as shown in figure 5.1. The unpolarized output beam from each laser was roughly collimated using appropriate lenses and then the two beams were combined on a 50% power reflectivity beam splitter via beam steering mirrors. To ensure good spatial overlap of the laser beams the combined beams were projected on to a screen positioned several metres from the beam splitter. The tilt angles of the beam splitter and steering mirrors were adjusted so that the combined beams overlapped along the entire propagation path to the screen. The now collinear beams from one output port of the beam splitter were tightly focused onto the 200μm diameter active area of a 3GHz bandwidth BPW28 silicon avalanche photodiode. A Hewlett-Packard HP8566B radio frequency

spectrum analyser was used to monitor the spectrum of the photodiode output signal. The colinear beams exiting from the second output port of the beam splitter were passed through scanning plane parallel Fabry-Perot and scanning confocal interferometers so that the spectral overlap of the outputs from the two lasers could be monitored. The Fabry-Perot interferometer with its ~100GHz free spectral range gave an unambiguous display of the laser spectra and allowed the laser output frequencies to be overlapped to within a few gigahertz. The higher resolution of the 1.5GHz free spectral range scanning confocal interferometer could then be used for monitoring the final reduction in the frequency difference between the laser outputs to within the 3GHz response bandwidth of the photodiode and spectrum analyser. Using this experimental arrangement the heterodyne beat signals shown in figure 5.2 were recorded. Confirmation that the signal seen on the spectrum analyser was due to beating between the two lasers was given by blocking each laser beam in turn and observing that the spectrum analyser signal vanished in both cases. The frequency of the heterodyne beat note between the two lasers was, perhaps not surprisingly, found to be very unstable. Any movement near the optical table caused violent swings in the beat signal frequency and the 25MHz jitter and 5.4MHz jitter in the beat note illustrated in figures 5.2(a) and (b) should be regarded as the smallest linewidth results recorded from these lasers.

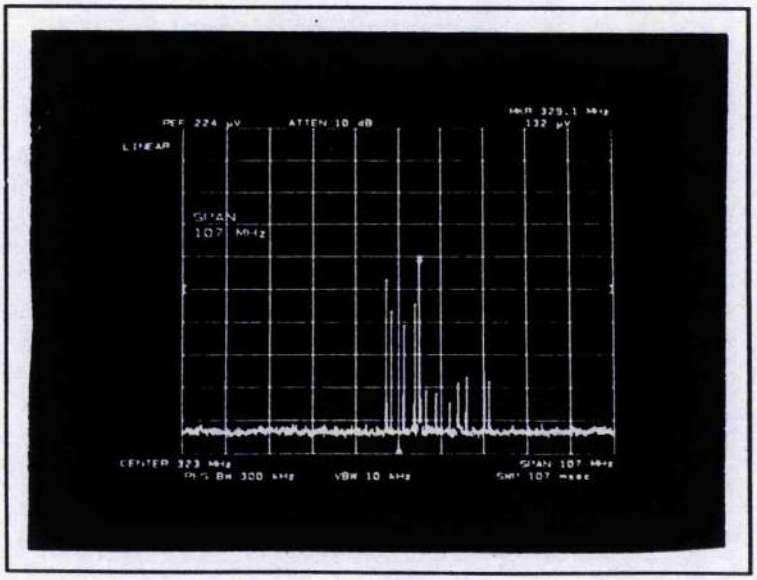

(a)

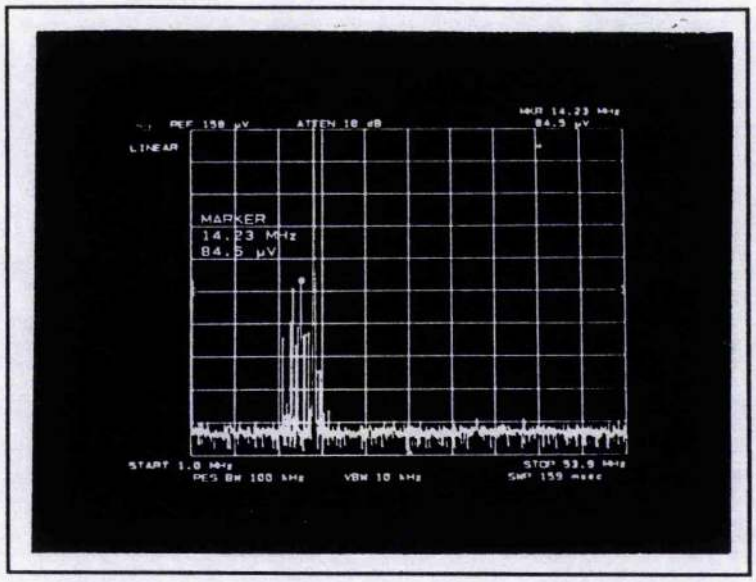

(b)

Figure 5.2. Heterodyne beat signals between two holosteric Nd:YAG lasers captured on a radio frequency spectrum analyser. Trace (a) shows a 25MHz frequency jitter in beat note over the 107ms analyser sweep time whilst (b) shows a 5.4MHz jitter in an analyser sweep time of 159ms.

These results were recorded under fairly hostile environmental conditions. The laboratory contained an industrial, discharge lamp pumped Nd:YAG lasers which was a major source of broad-band acoustic noise and generated enough heat to raise the air temperature by around 5°C over the course of the day. The laboratory also formed a main thoroughfare between two other rooms and so the opening and closing of doors was a frequent source of air pressure fluctuations and impact noise bursts. Mechanical vibrations and acoustic noise were also coupled into the lasers cavities from other experiments being conducted on the same optical table and from the department's Mechanical Workshop close by on the floor below.

The first modification to be made to the lasers was to remove their constituent parts from the optical table and build them into dedicated, mechanically rigid cavity structures. One of the laser cavities was built into a metal tube made from the low expansion alloy Invar. This cavity is shown in cross-section in figure 5.3. The output end of the aluminium block holding the pump fibre and focusing lens was centred down the bore of the invar

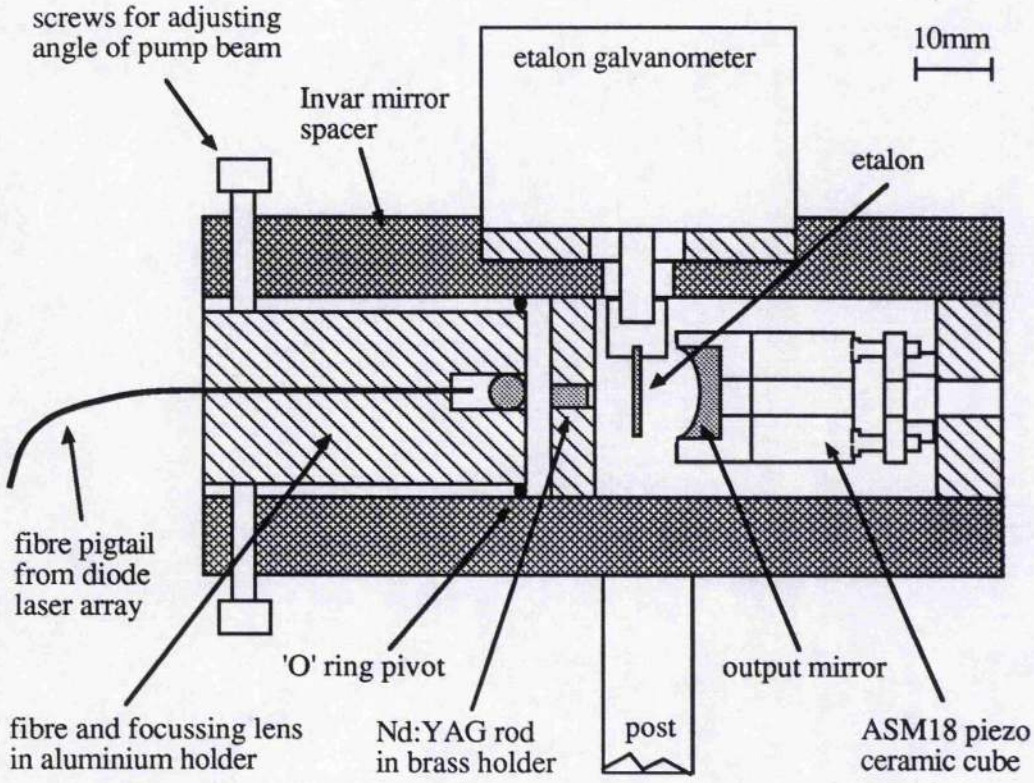

Figure 5.3. The end-pumped Nd:YAG holosteric laser built into a low expansion invar cavity.

cylinder by means of a tight fitting rubber 'O' ring glued round the end of the cylindrical aluminium block. The 'O' ring also acted as a universal joint around which this pump unit could be tilted. The output coupler mirror was mounted on a low voltage three channel piezo ceramic mirror mount (Photon Control ASM 18) as before. Three set screws in this mount provided coarse angular adjustment of the mirror while fine optimization of the cavity alignment was achieved by controlling the voltages applied to the three piezo ceramic pushers. To prevent fluctuations in the optical path length through instabilities in the angular position of the intracavity etalon a galvanometer with integral angular stabilisation servo circuitry was used.

Since the lasers themselves were still very much in the developmental stage the second laser cavity was kept as a bread-boarded system as this offered more flexibility in terms of ease of alignment and modifications to the cavity. This bread-boarded laser was built onto

its own steel base plate. A vertical side plate attached to the base plate was also used as an additional anchor point for each of the cavity components to improve mechanical stability of the bread-boarded design. The whole laser could be covered by a metal lid to form a rigid, closed box construction.

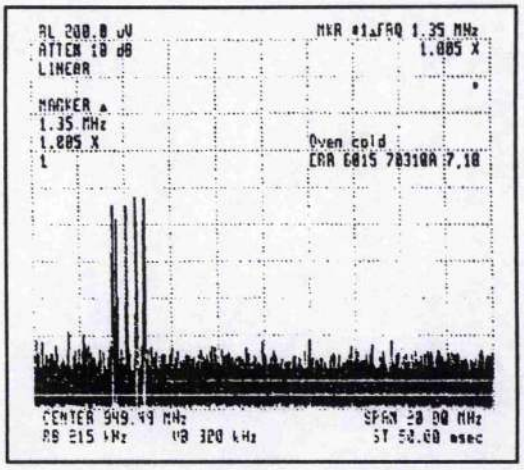

Figure 5.4. 1.52MHz jitter in the optical beat signal recorded between the invar cavity and bread-boarded holosteric lasers.

With the lid removed from the bread-boarded laser an optical heterodyne experiment between these to lasers revealed a short term relative frequency jitter of 1.52MHz recorded

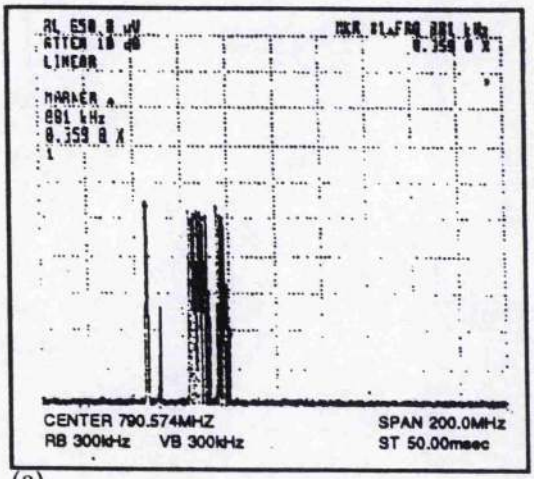

(a)

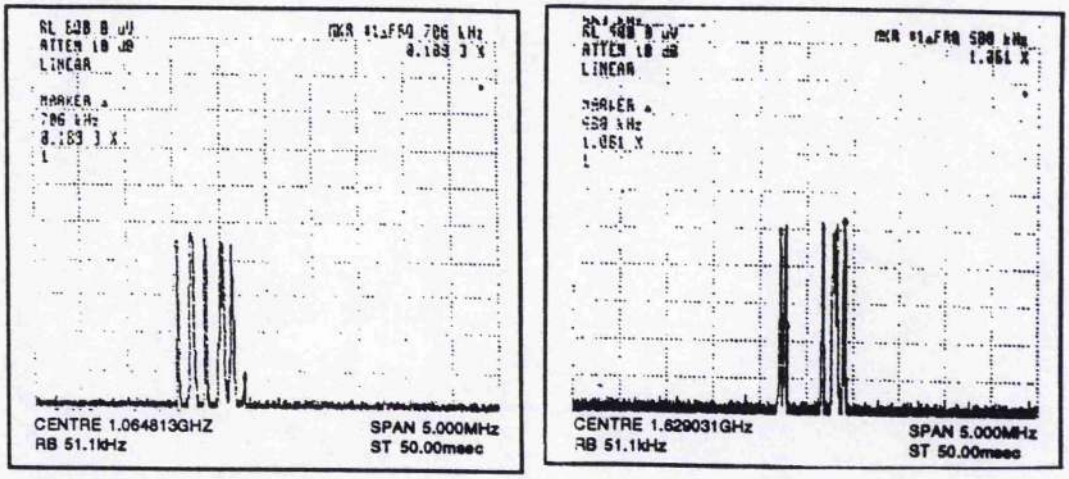

(b) (c)

Figure 5.5. Typical beat signals.

over the 50ms spectrum analyser sweep time under typically noisy laboratory conditions. See figure 5.4. Adding the lid to the bread-boarded laser box and surrounding the invar cavity laser by a foam filled enclosure reduced the effects of acoustic noise on the laser cavities resulting in optical beat signals of around 700-900kHz drift being observed on the spectrum analyser as shown in figure 5.5.

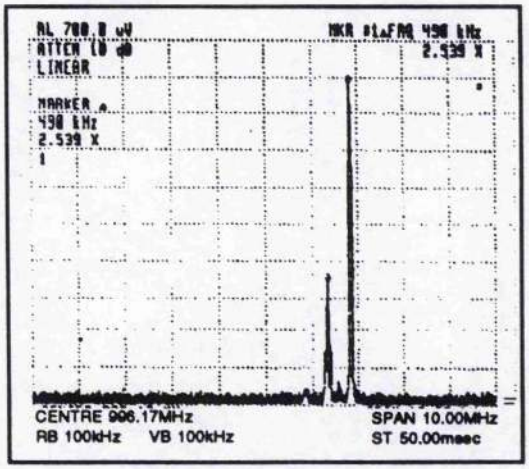

Figure 5.6. Beat signal recorded between the bread-boarded laser and the invar cavity with both lasers surrounded by acoustic damping foam. The jitter in this beat signal is 490kHz over the 50ms sweep time of the spectrum analyser.

The inclusion of foam acoustic damping material inside the metal box of the bread-boarded laser reduced the jitter in the heterodyne signal to around 490kHz as illustrated in

figure 5.6. The beat signals shown above were as far as possible typical of the relative frequency stability of the two lasers but because of fluctuations in the background environmental noise levels large variations in the frequency jitter of the heterodyne signal ranging from a few megahertz down to a few tens of kilohertz were observed.

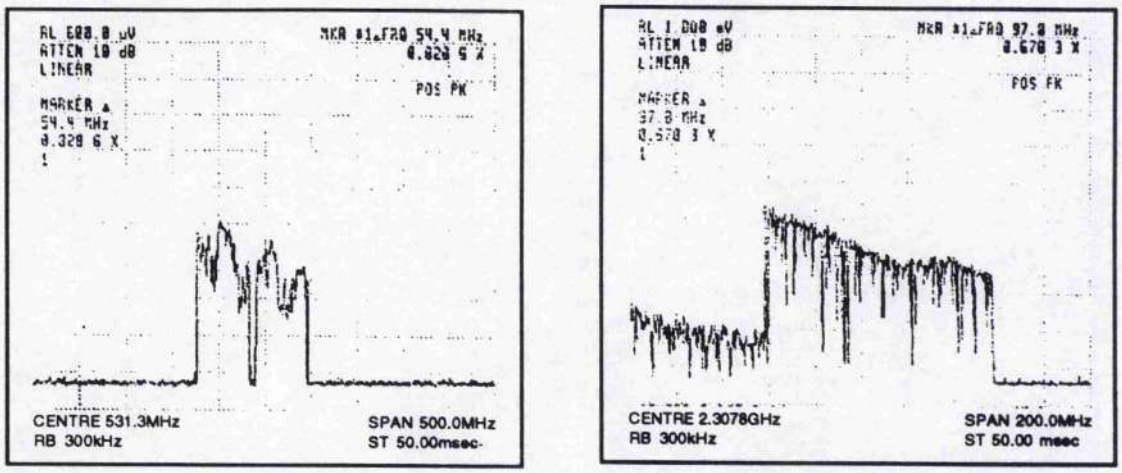

(a) (b)

Figure 5.7. Spectrum analyser displays of the optical heterodyne signal stored over 60 seconds. This shows a relative frequency drift of (a) 54.4MHz and (b) 97.8MHz. The two separate peaks visible in (a) are separated by 64.8MHz and were probability caused by polarisation splitting in one of the lasers.

Using the peak-hold function of the rf spectrum analyser the drift in the optical heterodyne signal frequency was measured over a period of 60 seconds. See figure 5.7. Figure 5.7(a) shows the presence of two beat signals drifting concurrently. The frequency separation of these two beats was measure from the spectrum analyser trace to be 64.8MHz. Since the free spectral ranges of the two laser cavities were greater than 3GHz, this frequency difference was too small to be accounted for by the presence of a second longitudinal mode in one of the lasers. However, the magnitude of the frequency difference was consistent with polarisation splitting of the longitudinal modes in the Nd:YAG laser as discussed earlier in section 4.6.3. Neither of the lasers contained any intracavity polarising elements and so this is the most likely explanation for the presence of the two heterodyne signals in figure 5.7(a).

One major drawback with this method of measuring laser frequency drift was that it only provided relative drift data. To be able to compare the longer term frequency stability of the two different cavity designs (invar cavity and bread-boarded laser) it was necessary to have an independent frequency reference to compare each laser against. For this purpose a low finesse, 100mm static confocal interferometer was built. To give the device good thermal and mechanical stability the interferometer mirrors were housed in a thick walled, tubular mirror spacer made from a solid piece of low expansion invar alloy. The whole unit was then placed in an expanded polystyrene enclosure for thermal insulation from the lab environment. The mirrors used for the interferometer were low reflectivity, broad band mirrors borrowed from a tunable dye laser system. There power transmission, T, and reflectivity, R, at 1064nm of these aluminium coated mirrors were measured using the output beam from one of the Nd:YAG holosteric lasers to be T=4.6% and R=62% respectively giving a reflectivity based interferometer finesse of $\mathcal{F}$=6.5. By scanning the output frequency of one of the single longitudinal mode Nd:YAG lasers the transmission characteristics of the interferometer were recorded as illustrated in figure 5.8.

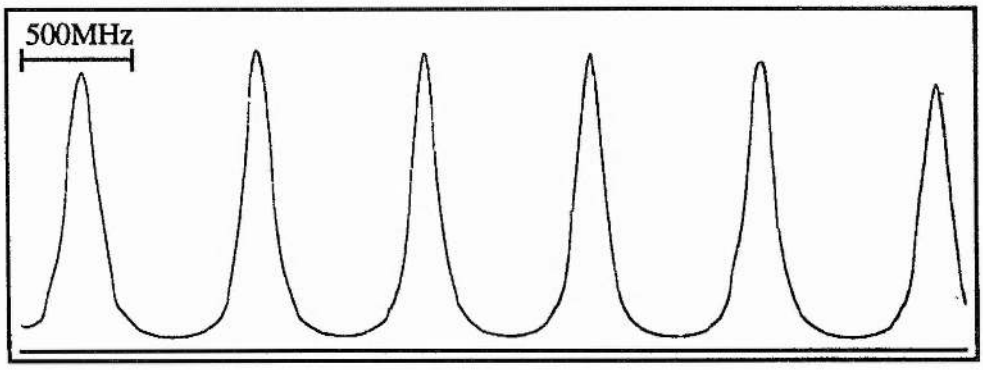

Figure 5.8. Transmission function of the static 100mm confocal reference interferometer.

From this transmission the instrumental finesse of the interferometer was measured to be $\mathcal{F}$=5.8. The interferometer free spectral range was $\Delta\nu_{fsr}$=750MHz and the full width at half maximum intensity transmission was 129.3MHz. To assess the laser frequency drift the output beam from both lasers was passed through the 100mm confocal interferometer in

turn and the time taken for the interferometer transmission to drift between its maximum and minimum levels was recorded. This time then corresponded to the time taken for the laser output frequency to change by half the free spectral range frequency (i.e. 375MHz) of the static interferometer. These interferometer transmissions for the invar cavity laser and the bread-boarded laser are presented in figure 5.9 (a) and (b) respectively. These measurements were taken in quick succession during a time of day when the laboratory air temperature was at its most stable. Rather disappointingly the frequency drift rate of 9.6MHz/minute for the invar cavity laser was found to be slightly larger than the 8.5MHz/minute drift rate observed for the steel bread-boarded laser. Assuming the thermal environment was the same for both lasers during each measurement, the larger than expected frequency drift rate of the invar cavity may have resulted from the following two causes. Firstly, the intracavity controlling galvanometer bolted to the invar spacer grew noticeably warm to the touch during its operation and so must have caused localised heating of the invar cavity spacer and Nd:YAG rod. This heating would have been compounded by thermal insulation effect of the acoustic damping foam surrounding the laser cavity. Secondly, the free spectral range of the short invar cavity was around double that of the longer bread-boarded laser and consequently, for the same change in optical path length in the two lasers the invar cavity laser would show a frequency shift twice that of the bread-boarded laser system.

Whilst the longer term frequency stability of the two different laser cavity designs appeared to be comparable, the results of figure 5.9 suggested that the invar cavity had superior mechanical stability. The small scale frequency fluctuations superimposed on the frequency drift curve in figure 5.9(b) for the bread-boarded laser were caused by acoustic noise and mechanical vibrations from machinery in the workshop on the floor below the laboratory. The same noise source was present during the recording of figure 5.9(a) for the invar laser cavity but its output frequency fluctuations were less.

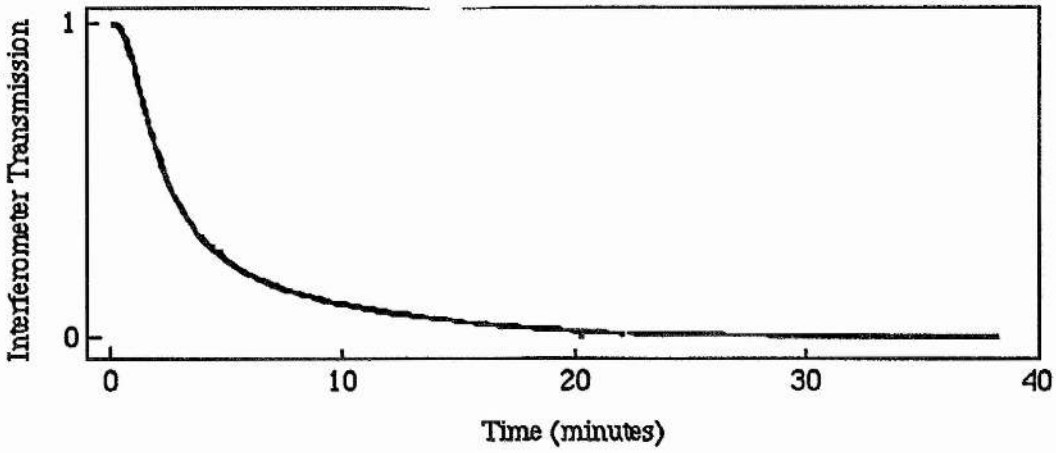

(a)

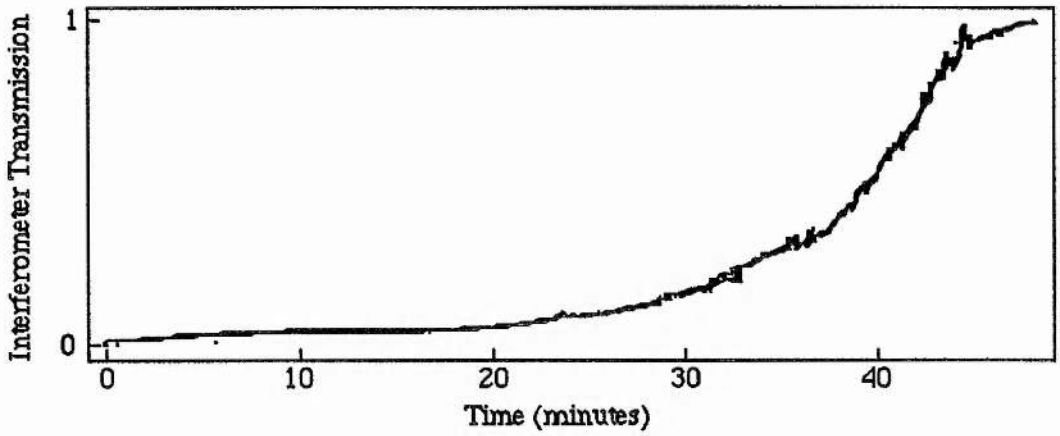

(b)

Figure 5.9. Transmission curves of the low finesse confocal interferometer showing the drift in the output frequency of (a) the invar cavity holosteric laser and (b) the bread-boarded holosteric laser.

5.2.1 The Small Anechoic Laser Enclosure

Since the major source of short term laser frequency instability is environmental noise it is desirable to isolate the lasers from such mechanical and acoustic noise sources as much as is practical. To this end a miniature anechoic chamber was built to house the two holosteric lasers as illustrated in figure 5.10.

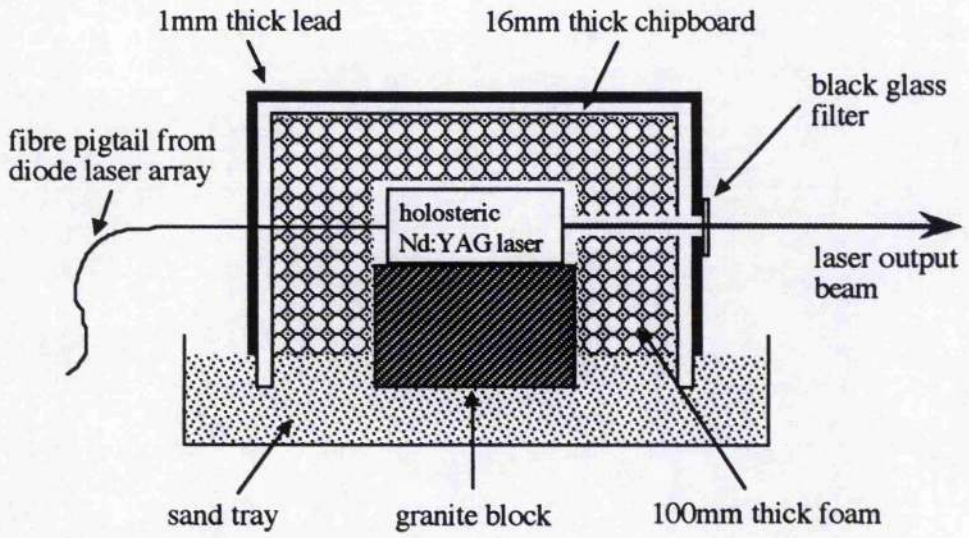

Figure 5.10. Schematic of the anechoic chamber built to house two frequency stable cw Nd:YAG holosteric lasers.

The lasers were bolted to a granite block (250×200×150mm) embedded in a few centimetres of sand. This provided insulation from impact generated sounds transmitted through the steel optical table top whilst giving a mechanically stable base for the lasers. Isolation of the lasers from airborne sound was in the form of an enclosure made from 16mm thick wooden chipboard covered with a cladding layer of lead 1mm thick. The high density and low stiffness of these materials, particularly in the case of lead, gave the structure good acoustic damping properties across a wide frequency range and particularly towards the upper end of the acoustic frequency spectrum[2]. The internal cavity of the box was lined with acoustic damping foam to a thickness of around 100mm. Air pressure waves passing through the many small pores in the foam experience large frictional forces resulting in energy being dissipated from the sound wave as heat in the damping foam. This effect is particularly acute for standing waves of the resonant modes of the box with wavelengths shorter than four times the thickness of the foam. These standing waves will have at least one pressure antinode lying within the foam and so will experience the most damping. Thus a 100mm thickness of damping foam should attenuate airborne sounds with wavelengths less than 400mm or equivalently frequencies over 825Hz. The laser beam exit holes in the side of the enclosure were covered using RG1000 infrared filter glass. This

served the dual purposes of plugging the acoustic leak caused by the holes through the enclosure walls and also blocking any residual pump light emanating from the lasers.

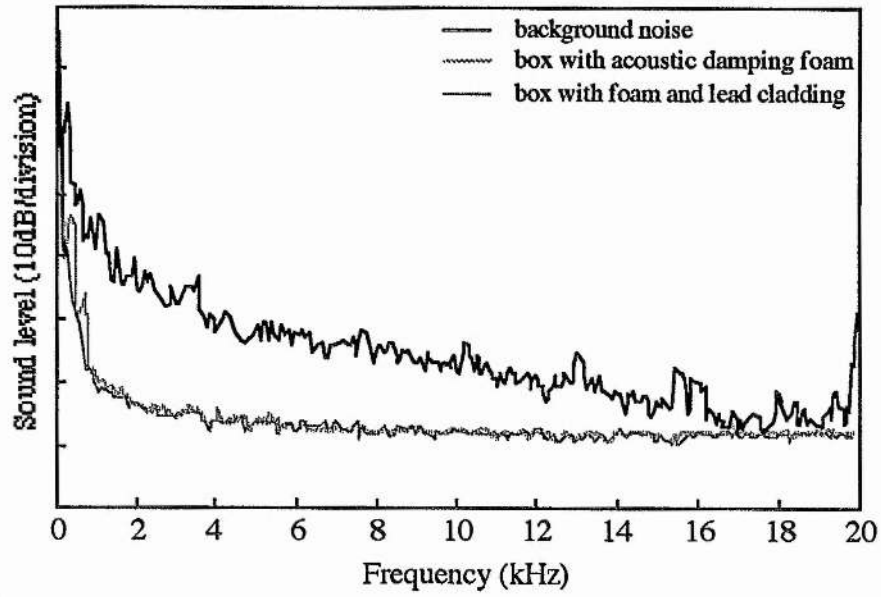

(a)

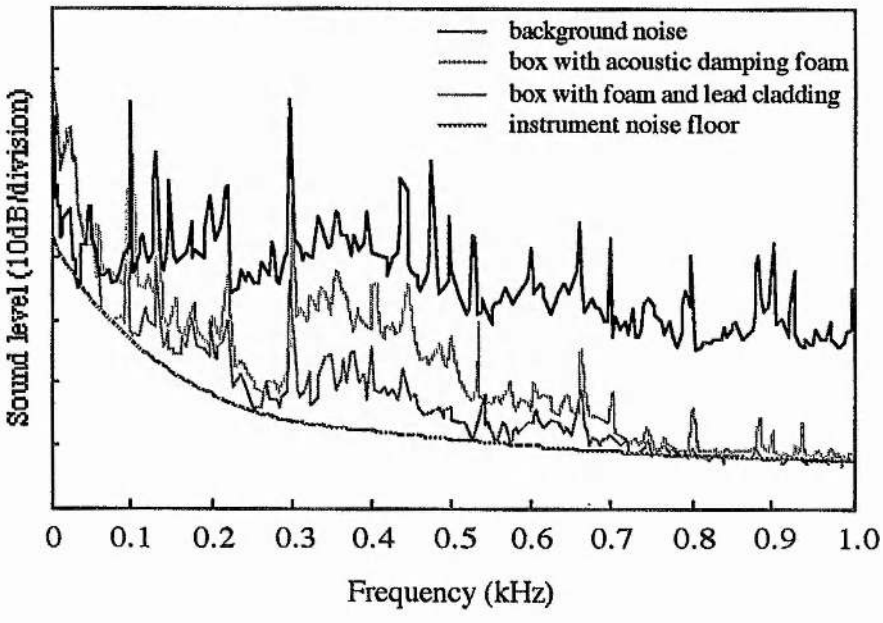

(b)

Figure 5.11. Acoustic noise spectra over (a) 0-20kHz and (b) 0-1kHz illustrating the sound attenuation achieved by the anechoic laser enclosure.

To measure the sound attenuation characteristics of the complete chamber a microphone was located on the granite block inside the chamber and coupled to a 0-20kHz fast Fourier transform spectrum analyser (Bruel and Kjaer type 2033). The frequency response of the Bruel and Kjaer condenser microphone, type 4134 used was flat to within ±2dB from 3Hz to 20kHz. First of all the background noise spectrum was recorded with the microphone in the box but with the box lid, damping foam and lead cladding removed. Noise spectra were then recorded with the damping foam added and then with both foam and lead in place to see the effect of these materials. See figure 5.11. The sound reduction of the foam, chipboard and lead enclosure was found to be so effective over the spectral range from 800Hz to 20kHz that the measurement of the attenuated sound level was limited by the noise floor of the detection system. A more detailed examination of the noise spectrum below 1kHz showed that the enclosure was providing between 10 and 20dB of attenuation of the background acoustic noise for frequencies greater than about 200Hz. Interestingly for frequencies less than 100Hz the acoustic enclosure actually enhanced the noise level by about 10dB over the previously measured background level possibly through some resonance effect of the structure. This raised low frequency noise level did not cause undue concern since its contribution to instabilities in the laser output frequency could be controlled using a small bandwidth active laser frequency servo loop.

The real test of the anechoic chamber was to see its effect on the short term laser frequency stability. One of the lasers used was the invar cavity system as before. Because of the apparently good mechanical stability of this design, the bread-boarded laser was replaced by a cavity similar to that of the invar cavity laser shown in figure 5.3. In this new cavity the long term thermal stability was sacrificed for ease and speed of machining by making the outer mirror spacer tube from aluminium instead of invar. Other modifications to the earlier laser design included lengthening the cavity to allow a Brewster angle plate to be inserted into the cavity and the replacement of the piezo ceramic cube mirror mount with a mechanically more stable and more easily aligned gimbal mount carved from a solid of piece of spring steel (Photon Control Flexture Mount model Micropoint 25)).

The output beams from the two lasers were combined on a beam splitter and the optical heterodyne signal monitored using the fast photodiode and rf spectrum analyser as before. To establish some kind of bench mark the jitter in the optical heterodyne beat signal was measured with the lid and acoustic damping foam removed from the laser enclosure. At this stage the lead clad chipboard enclosure itself could not be removed without risking serious damage to the lasers. Under these conditions the jitter of the heterodyne signal was measured as 1.25MHz over the 50ms spectrum analyser sweep time. See figure 5.12(a).

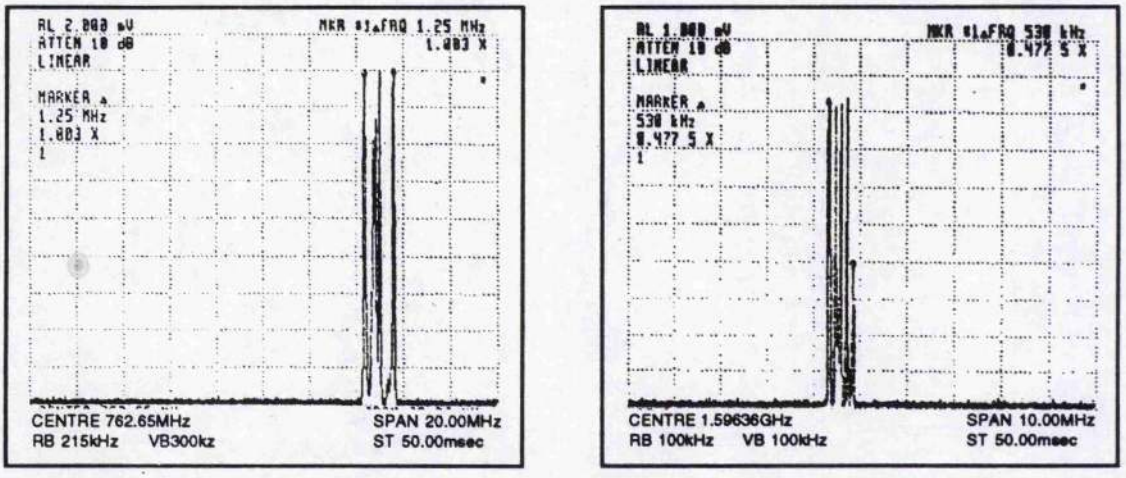

(a) (b)

Figure 5.12. Typical optical beat signals recorded between the two holosteric lasers located inside the anechoic enclosure. In (a) a 1.25MHz frequency jitter in the optical heterodyne signal was measured with both the lid and damping foam removed from the lasers enclosure. (b) With the foam and lid in place on the laser enclosure the beat signal frequency jitter was 530kHz.

When the damping foam and lid were replaced on the enclosure the jitter in the optical beat signal fell to around 500kHz over the same 50ms sweep time. Again this was found to be very reproducible. See figure 5.12(b). Frequency drifts in the heterodyne signal were found to be around 40 to 50MHz measured over 1 minute as shown in figure 5.13.

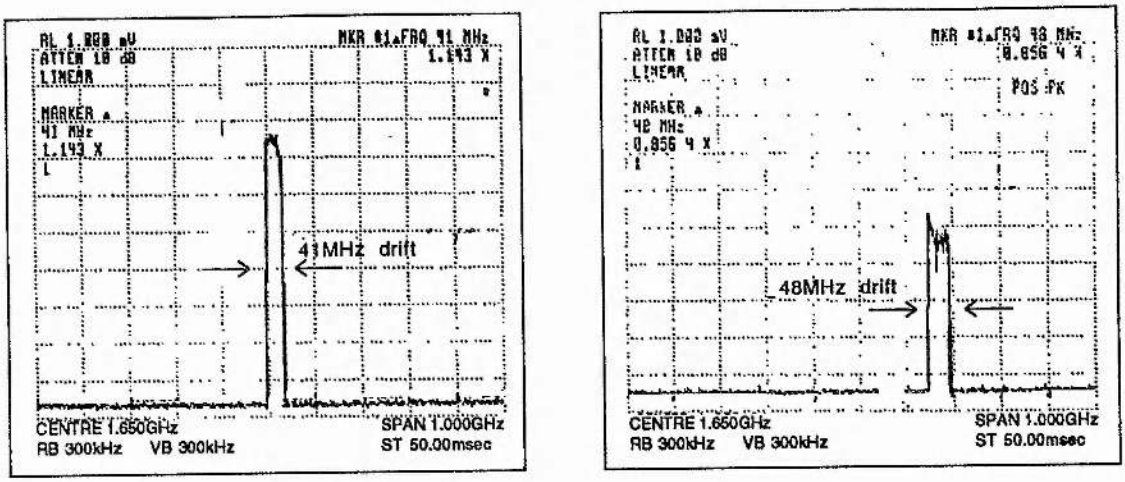

(a) (b)

Figure 5.13. Typical frequency drifts in the optical heterodyne signal from the lasers in the anechoic enclosure recorded in a 1 minute time interval.

5.2.2 Relative Frequency Stability Between The Etalon And Twisted Mode Nd:YAG Lasers in a New Laboratory Environment.

Following the construction and characterisation of the twisted mode, single longitudinal mode Nd:YAG laser described in section 4.7 and the relocation of the narrow linewidth laser experiments to a much quieter ground floor laboratory on solid foundations the short term relative frequency stability of the Nd:YAG lasers was measured once more. The two lasers used in this heterodyne experiment were the pre-aligned twisted mode laser (which replaced the old invar cavity laser with intracavity etalon) and the redesigned aluminium laser with intracavity mode selecting etalon described above. Again, for maximum acoustic noise isolation both lasers were mounted inside the anechoic enclosure. With these changes to the system the optical beat signal generated between the two combined laser outputs showed a relative frequency stability typically less than 20kHz and frequently below the 10kHz resolution bandwidth of the rf spectrum analyser (figure 5.14(a)) over the 50msec measurement time. Measurement of the relative frequency drift between the two lasers was

recorded using the peak hold function of the spectrum analyser and found to be 24.25MHz over 1 minute.

This measured value for the short term linewidth in the beat signal between the two diode pumped lasers compares well with published results from both monolithic[6,7,8,9] and open cavity[10] diode laser pumped solid state lasers.

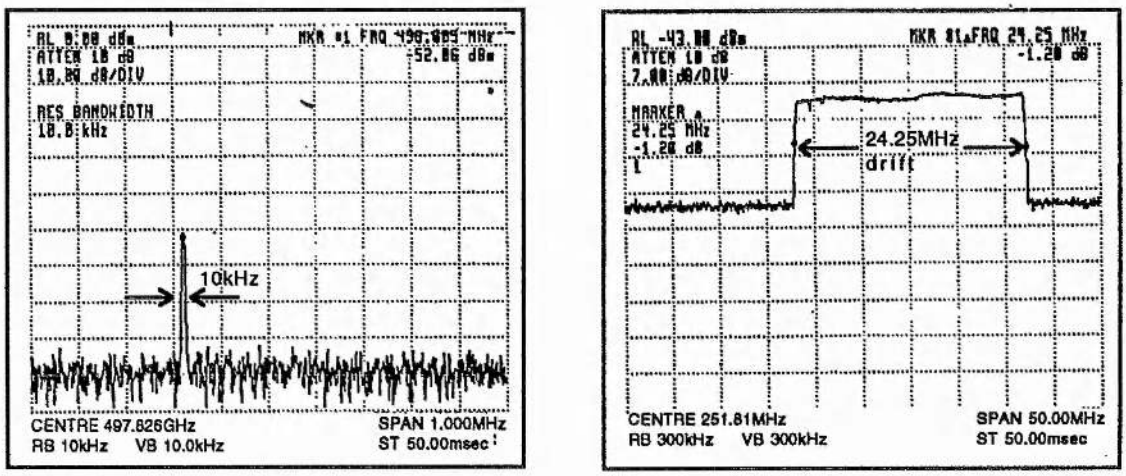

(a) (b)

Figure 5.14. (a) Commonly observed sub 10kHz frequency linewidth of the optical heterodyne signal. Measurement of the true jitter linewidth was limited by the 10kHz resolution bandwidth of the spectrum analyser. (b) 24.25MHz frequency drift in the heterodyne signal over 1 minute.

5.3 Measurement of Frequency Noise Spectral Density

The technique of optical heterodyning described above not only provides useful information on the relative short term frequency stability between two lasers but can also give information about the spectral content of this frequency jitter. This spectral density data is in the form of frequency modulation (FM) side bands around the main carrier frequency of the heterodyne signal[11]. However, this information can be very difficult to extract as the noise side bands of interest are often weak and lie close in to the carrier. To attain the level of frequency resolution required necessitates the use of long sampling times on the rf spectrum analyser. This in turn places stringent requirements on the longer term

frequency stability of the heterodyne signal. Furthermore, to allow unambiguous interpretation of the spectral density data one of the lasers would have to be extremely stable to act as a pure reference frequency local oscillator against which the test laser could be compared.

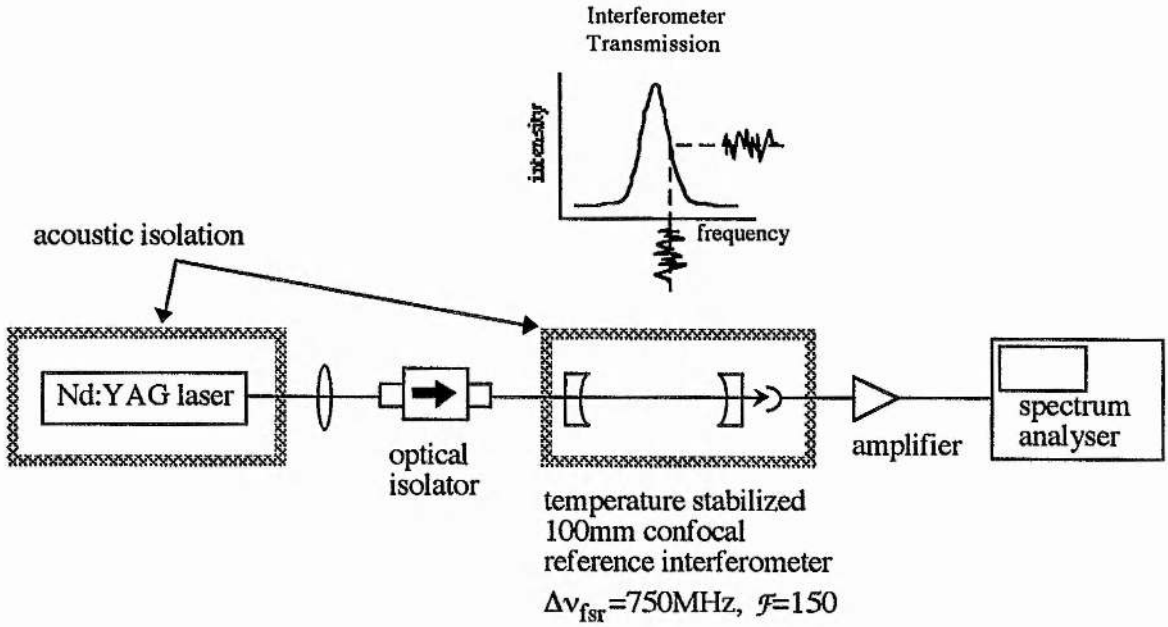

Figure 5.15. The optical layout used for measuring the frequency noise spectral density present in the Nd:YAG holosteric laser output.

A more convenient method for measuring the spectral density of frequency fluctuations from an individual laser is to use the slope of the transmission curve of a static interferometer as an optical frequency noise to optical intensity noise converter (figure 5.15). The laser output frequency is normally adjusted to match the inflection point in the interferometer transmission curve. Around this frequency the interferometer frequency to intensity conversion is at its most linear and providing that the laser frequency fluctuations are small (« interferometer half width at half maximum linewidth) then this method generates an intensity signal proportional to the instantaneous frequency of the laser output. The intensity modulated light beam can be detected by a photodiode and the frequency spectrum of the resulting electrical signal subsequently sampled and analysed using a fast Fourier Transform spectrum analyser. From knowledge of the frequency to photodiode voltage slope of the reference interferometer and the resolution bandwidth of the spectrum

analyser, the root mean squared (rms) voltage spectrum can be recalibrated in terms of the rms laser frequency fluctuations per √(unit sampling bandwidth).

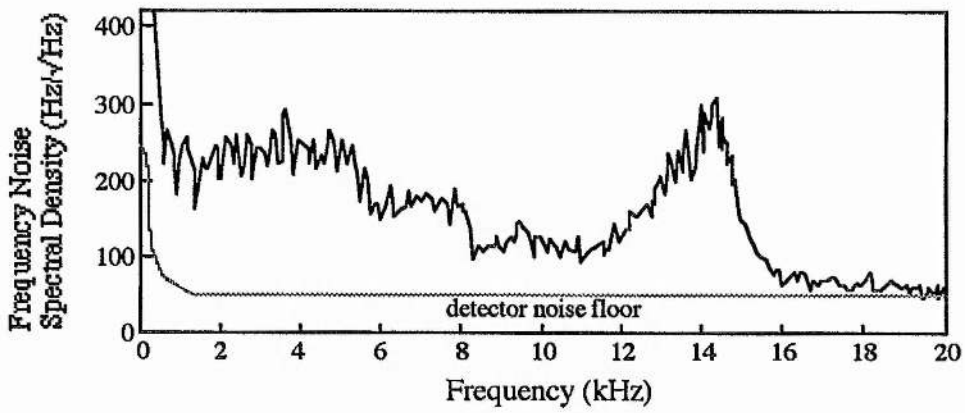

(a)

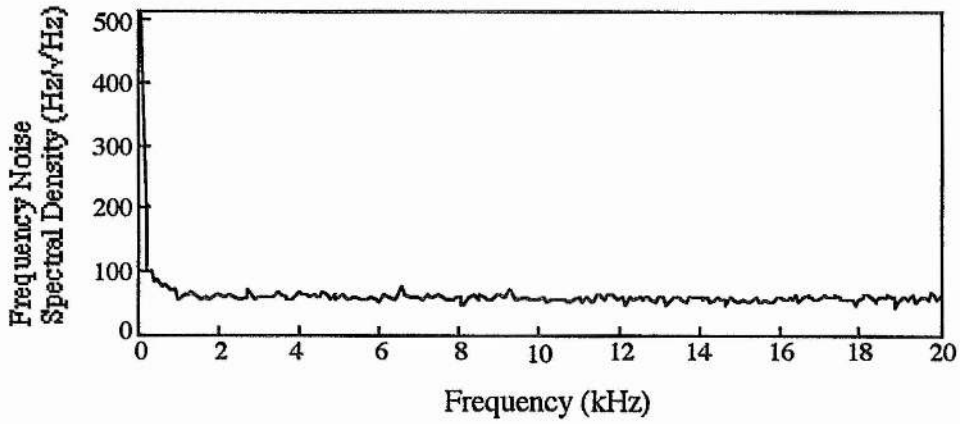

(b)

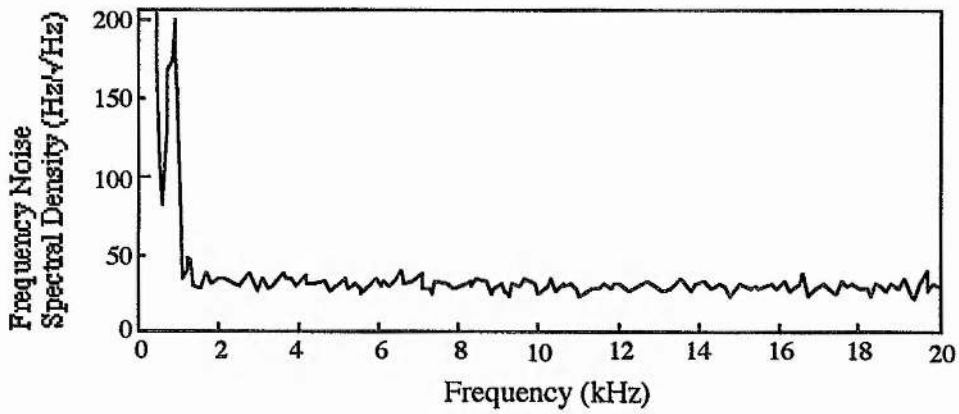

(c)

Figure 5.16. Frequency noise spectral density plots for (a) twisted mode laser with mains powered, high voltage piezo transducer driver, (b) twisted mode laser with battery powered high voltage piezo driver and (c) the Nd:YAG laser with intracavity mode selecting etalon.

Referring to the experimental arrangement in figure 5.15 the static reference confocal interferometer had a free spectral range $\Delta\nu_{fsr}$=750MHz and a FWHM instrumental linewidth of 5MHz giving the device a finesse of $\mathcal{F}$=150. Optical power transmission was measured to be 1%. For good long term stability the interferometer was made from a thick walled invar tube and was temperature stabilised by means of a CAL9000 (CAL Controls Inc, Illinois, USA). The interferometer was securely fixed inside an acoustic isolation chamber of similar design to the laser enclosure shown in figure 5.10. Light transmitted through the interferometer was detected by a BPX65 silicon photodiode connected to a 45kHz bandwidth, battery powered amplifier. A 0-20kHz, high resolution Bruel and Kjaer spectrum analyser type 2033 was used to process the resulting electrical signal.

Figure 5.16 (a) shows the frequency noise spectrum of the twisted mode laser recorded using this experimental arrangement. The noise spectrum shows laser frequency noise at levels several times the detector noise floor of (47±10)Hz/√Hz over the 0-16kHz spectral region. Above 16kHz the laser frequency noise tends towards the detection noise floor limit. It was suspected that much of this frequency noise was caused by electrical noise from the mains driven high voltage power supply used to activate the piezo ceramic laser frequency tuner. This suspicion was confirmed when the high voltage power supply was replaced by a high voltage battery pack resulting in the laser frequency noise spectral density being reduced to a level indistinguishable from the system noise floor, figure 5.16(b).

A similar noise measurement was made on the laser containing the intracavity mode selecting etalon, with the battery high voltage power supply being used as before. See figure 5.16(c). Below 2kHz there is some observable laser frequency noise with a distinct peak of 200 Hz/√Hz at a frequency of 1kHz. This low frequency noise may be due to electrical noise on the etalon galvanometer power supply. For frequencies over 2kHz the recorded spectral density plot is lost in the detection noise floor.

The poor signal to noise ratio limiting these spectral density experiments was primarily due to the 1% transmission efficiency of the reference interferometer. The resulting low light levels at the detector meant that the spectrum of the electrical signal was dominated by amplifier noise. The contribution to this level by the photocurrent generated shot noise was calculated to be negligible at only ~0.3Hz/√Hz for the light levels involved.

One failing of the simple experimental arrangement of figure 5.15 is that any laser intensity noise would be interpreted as frequency noise on passing through the reference interferometer. To check the intensity noise contribution to the frequency spectral density data of figures 5.16 (a), (b) and (c) the intensity noise spectra of both lasers were recorded with the same photodiode, amplifier and spectrum analyser used previously. The lasers were in turn run at full power and a fraction of the beam directed to the photodiode. A variable optical attenuator placed in front of the photodiode was adjusted to match the d.c. voltage level produced from the amplifier to that used during the frequency noise experiments. Under these conditions no intensity noise was measurable over the detection system noise.

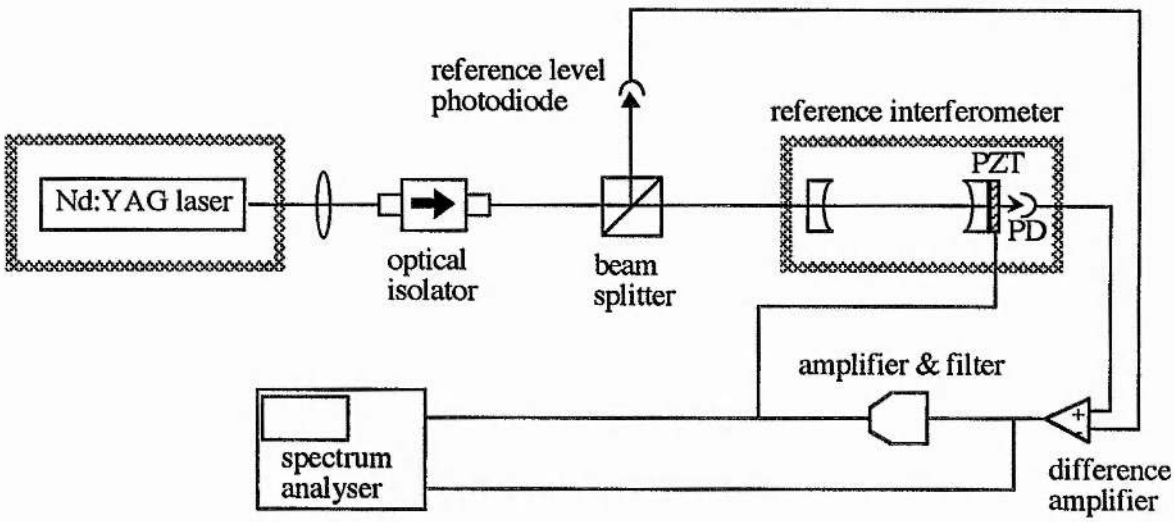

Figure 5.17. A side-of-fringe locking scheme for measuring the spectral density of the laser frequency noise.

An alternative experimental arrangement for measuring frequency noise spectral densities is shown in figure 5.17[12,13] . This variant on the side-of-fringe locking technique

eliminates the problem of laser frequency drift by actively locking the transmission frequency of the reference interferometer to the laser output frequency. Effects due to fluctuations in laser intensity are also partly suppressed by monitoring the laser intensity noise on a separate photodiode and subtracting this signal from the reference interferometer transmission signal. This difference voltage, after appropriate amplification and filtering, forms the feedback error signal to the piezo electric frequency tuner on the reference interferometer. By varying the light intensity falling on the intensity monitoring photodiode the lock point on the interferometer transmission curve can be selected. The point of inflection on the interferometer transmission curve is normally chosen as the lock point as this has the greatest frequency to intensity gradient and so gives the greatest frequency noise sensitivity. For error signal frequencies below the unity gain point of the servo loop, the error signal applied to the piezo transducer is a measure of the laser frequency noise. For error signal frequencies above the unity gain point of the servo loop, the interferometer no longer tracks the laser frequency fluctuations and so the spectral density data should be taken directly from the difference amplifier. One draw back of this measurement system is that active movement of the reference interferometer length can excite mechanical resonances of the interferometer structure giving spurious noise data.

5.4 References

1 Demtröder W., "Laser Spectroscopy", Springer-Verlog, 1st Edition (1981)

2 Ginn K. B., "Architectural Acoustics", Bruel and Kjaer (1978)

3 Jasaja T. S., Townes C. H., "Frequency Stability of HeNe Masers and Measurements of Length", Phys. Rev. Lett. **10**(5) 165 (1963)

4 Schawlow A. L., Townes C. H., "Infrared and Optical Masers", Phys. Rev. **112**(6), 1940 (1958)

5 Elliott D. S., Roy R., Smith S. J., "Extracavity Laser Band-Shape and Bandwidth Modification", Phys. Rev. A **26** (1), 12 (1982)

6 Zhou B., Kane T. J., Dixon G. J., Byer R. L., "Efficient, Frequency Stable Laser Diode Pumped Nd:YAG Laser", Opt. Lett. **10**(2) 62 (1985)

7 Kane T. J., Nilsson A. C., Byer R. L., "Frequency Stability and Offset Locking of a Laser Diode Pumped Nd:YAG Monolithic Nonplanar Ring Oscillator", Opt. Lett. **12**(3) 175 (1987)

8 Kane T. J., Kozlovsky W. J., Byer R. L., "Coherent Laser Radar at 1.06μm Using Nd:YAG Lasers", Opt. Lett. **12**(4) 239 (1987)

9 Bush S. P., Güngör A., Davis C. C., "Studies of the Coherence Properties of a Diode Pumped Nd:YAG Ring Laser", Appl. Phys. Lett. **53**(8) 646 (1988)

10 Nachman P., Munch J., Yee R., "Diode Pumped, Frequency Stable, Tunable, Continuous Wave Nd:Glass Laser", IEEE J. Quant. Elect. **26**(2) 317 (1990)

11 Manes K. R., Siegman A. E, "Observation of Quantum Phase Fluctuations in Infrared Gas Lasers", Phys. Rev. A **4**(1) 373 (1971)

12 Kerr G. A., " Experimental Developments Towards a Long-Baseline Laser Interferometometric Gravitational Radiation Detector", Ph.D. thesis, University of Glasgow (1986)

13 Fritschel P., Jeffries A., Kane T. J., "Frequency Fluctuations of a Diode-Pumped Nd:YAG Ring Laser", Opt. Lett. **14**(18) 993 (1989)

Chapter 6

ACTIVE FREQUENCY STABILISATION

Once a particular laser system has been passively stabilised, to a degree where it still remains a practical and usable system, active frequency stabilisation can be used to remove any residual frequency fluctuations from the laser output. In this chapter an overview of active laser frequency stabilisation is given indicating its limitations and capabilities. Particular emphasis is given to the Pound-Drever locking system as this was the stabilisation method applied to the diode pumped Nd:YAG laser in this work.

6.1 Basic Principles of Active Frequency Stabilisation

The design criteria for an active stabilisation servo system will vary depending not only on the noise sources (e.g. due to fast flowing dye jets, flowing coolants, etc.) present in the laser and in its immediate environment but also on the level of passive stablisation achieved. The magnitude of the task of the servo control will depend on the magnitude and spectral distribution of these remaining noise components. The smaller the magnitude and frequency bandwidth of the noise, the easier will be the task of the stabilisation servo.

Although frequency servo systems differ in detail they are all composed of the same basic building blocks namely;

a) A *stable frequency discriminant* which generates a zero crossing electrical signal directly proportional to the instantaneous frequency difference between the laser output and some fixed reference.

b) An *electronic control system* which processes the signal generated by the discriminant into an error signal to apply to the transducer to return the laser frequency to the desired frequency as fast as possible.

c) A *transducer* which responds to the error signal from the electronic control system to vary one (or more) of the parameters determining the precise laser output frequency.

Each of these elements will be discussed in more detail in the following sections.

6.1.1 References For Laser Stabilisation - Frequency Discriminants

The purpose of the frequency discriminant element of the laser frequency stabilisation loop is to sense departures of the laser frequency from the desired value and to generate an electrical signal proportional to that change. Many techniques can be used to generate suitable frequency disriminants for laser stabilisation such as comparing the intensity of orthogonally polarised, adjacent longitudinal modes used in HeNe laser stabilisation[1,2], interference fringes between the output of two lasers for direct laser phase locking[3,4,5,6,7,8,9], or intensity fluctuations in the interference fringes produced by a two beam Michelson interferometer[10,11]. The most commonly used and arguably the most effective laser stabilisation schemes, however, use frequency discriminants based on passive resonant optical cavities or spectroscopic features of atomic or molecular species.

Passive Optical Cavities

The frequency dependent intensity transmission or reflection characteristics, or even the phase shifting properties of passive optical resonators can be exploited to form highly stable and sensitive optical frequency discriminants. Since passive optical cavities can be made very compact and require no intracavity elements or external control

systems they usually suffer less technical noise than the original laser and are more easily isolated from the environment.

For instance, Richard et al[12] constructed a passive reference cavity for operation at λ = 633nm in which the mirror spacer was formed by a 1.6kg single crystal of silicon. The interferometer was carefully mounted in a vacuum chamber to isolate it from mechanical and acoustic noise and was also cooled to 4.2K in liquid Helium. Cooling to these cryogenic temperatures allowed tight temperature control and reduced the already small temperature expansion coefficient of the mirror spacer to an almost negligible level. Residual fractional cavity length changes and consequently fractional frequency changes of the cavity resonance were measured to be less than 5×10^{-15} for this cavity.

It is also possible to construct a completely solid reference cavity from a suitably transparent material and deposit the mirror coatings directly onto the polished surfaces as demonstrated by Tsuchida et al[13]. Such cavities should have good mechanical stability although their efficiency and Finesse may be limited by scattering sites within the solid. Ultra compact and so easily isolated, narrow linewidth cavities in the form of fibre optic resonators[14,15] may also prove useful as references for laser stabilisation.

As well as their potential for good mechanical stability, passive optical cavities can now be constructed which exhibit high transmission efficiency and very high finesses of the order of 10^4 resulting in narrow resonance linewidths a few tens or hundreds of kilohertz wide[16,17,18]. Such narrow resonances provide the basis for optical frequency discriminants with good sensitivity and signal to noise ratio, features which are important in determining the ultimate stability level reached through active stabilisation. Crucial to the development of such narrow linewidth optical resonators have been the advances made in ultra low loss, high reflectivity mirror technology. Cleaning and polishing methods are now available which can produce mirror substrates smooth to within a few Ångstroms. This, coupled with improved dielectric mirror coatings applied by ion beam sputtering, has lead to the production of mirrors with losses below 20 parts per million and optical power reflectivities in excess of 99.995%[19].

Spectroscopic Absorption and Emission Lines.

Absorption or emission lines of atomic or molecular species are attractive candidates as laser frequency discriminants because they provide an exact and highly reproducible frequency reference. A common stabilisation scheme employing an absorption reference is by saturated absorption[20]. The technique involves placing inside the laser cavity, a tube containing a low pressure vapour which has an absorption line falling within the gain bandwidth of the laser. The strong standing wave electric field inside the cavity gives rise to saturation of this absorption for the velocity group of absorbing atoms or molecules having a zero longitudinal velocity component. Thus a Lorentzian shaped, non Doppler broadened dip forms at the centre of the absorption line. This dip in absorption produces a corresponding increase in laser output power at the absorption line centre frequency. The width of the absorption feature, virtually free from Doppler broadening, is determined by the natural width of the line. Since lasers are very sensitive to the small changes in cavity gain and loss parameters such as these occurring in the region of the saturated absorption, suitable absorption effects can be produced with low pressure vapour cells. This means that pressure broadening of the absorption line can be minimised. The most suitable molecules for saturated absorption stabilisation are those with symmetry giving small dipole moments since they are insensitive to Stark or Zeeman frequency shifts.

Providing a molecular vapour can be found with an absorption line falling within the laser gain profile, the main limitation to laser stability is imposed by the absorption linewidth which is typically a few megahertz.

One of the most common laser to be stabilised to a saturated absorption feature has been the HeNe laser operating at 633nm or 3.39μm utilising low pressure I_2 [21,22,23,24] or CH_4 [25,26,27] as the intracavity absorber respectively. In the case of the Nd:YAG laser, the application of the saturated absorption stabilisation technique has been hampered by the sad lack of absorption lines coinciding with the fundamental laser frequency. One solution to this problem has been to generate the second harmonic of the laser frequency

and then use the strong absorption lines of molecular Iodine as the frequency reference[28,29]. As an alternative, absorption features around 1064nm in molecular Caesium have been proposed as possible frequency references[30] although this necessitated the use of a Caesium vapour heat pipe.

As an alternative to stabilisation by saturated absorption, the optogalvanic effect in spectroscopic discharges can also be used as a laser frequency reference. The optogalvanic effect manifests itself as sharp changes in electrical impedance of a low pressure gas discharge when the discharge is illuminated by light of frequency corresponding to an allowed transition of the gaseous species. If a low pressure discharge cell is placed inside the laser cavity, the laser frequency can be servo locked to the Doppler free Lamb dip in the optogalvanic signal from the discharge lamp[31,32,33].

Several other methods for generating frequency locking discriminants are also available such as using the Lamb dip[34,35] in the gain curve of a gas laser, or Zeeman splitting[36,37,38] in an intracavity or external absorption cell. An extensive review of these and other discriminants based on spectroscopic features has been presented by Baird and Hanes[39].

6.1.2 Servo Control Electronics.

The purpose of the control electronics is to suitably process the signal from the frequency discriminator into an appropriate error signal that, when fed to the frequency control transducer, reduces the frequency difference between the laser and the reference point. Generally, the use of a servo or feedback system minimises the discrepancy between the laser and reference frequencies by a factor proportional to the gain around the servo loop. Therefore, very large gains are desirable for maximum noise suppression. However, in any practical systems the gain cannot be made arbitrarily large due to time delays inherent in the feedback network. In the frequency domain, the time delay, T, will manifest itself as a frequency (f) dependent phase shift of magnitude $2\pi fT$. For very low frequency components of the laser noise spectrum, the closed loop phase shifts will be

negligible and so the negative feedback will effectively cancel the original noise input. However, for higher frequency components, the loop phase shifts approach $\pi/2$ and so the servo will become less and less effective at reducing their amplitudes. At still higher frequencies, the time delay induced phase shifts will exceed $\pi/2$ and tend towards π. In this frequency region the resulting error signal will start to augment rather than suppress the initial noise terms causing the system to go into self-sustained oscillation. To prevent such oscillations from building up on successive passes of the servo loop, the loop gain must be reduced to unity (or less) for noise frequency terms which experience phase shifts in excess of $\pi/2$. This then sets an upper limit, f_{max}, on the effective bandwidth of the servo, where $f_{max}=\frac{1}{4T}$. The frequency at which the gain must reach unity is termed the unity gain point.

The need to reduce, or roll-off, the loop gain towards higher frequencies brings, in itself, additional problems in the system design. Associated with every frequency dependent voltage gain function is an intrinsic, inescapable frequency dependent phase shift. Usually, the steeper the gain versus frequency curve, the larger the accompanying phase shift. As a consequence of this, there is a maximum safe rate at which the gain can be increased from the unity gain point with decreasing frequency. In turn, this governs the maximum attainable gain at lower frequencies. The addition of this gain dependent phase shift to that arising from finite loop time delays requires that the unity gain frequency be reduced further in order to maintain the total loop phase shifts at or below $\pi/2$. Assuming that the unity gain frequency is lowered to a point where the time delay phase shift contribution can be neglected then the maximum tolerable phase shift due to gain roll-off alone is again ~ $\pi/2$ near the unity gain point. The slope of the voltage gain curve associated with such a $\pi/2$ phase shift is ~ -6dB/octave. Commonly, these gain and phase shift characteristics are achieved using an electronic integrator circuit. For low frequencies, well removed from the oscillation danger zone near the unity gain point, larger phase shifts can be accommodated and so it is often possible to increase the slope of the gain curve to ~ -12dB/octave over approximately a decade in frequency usually by adding another integrator stage. Thus it is only really feasible to achieve the desired high

servo loop gains at low frequencies. These features of a "typical" laser frequency servo are shown schematically in figure6.1.

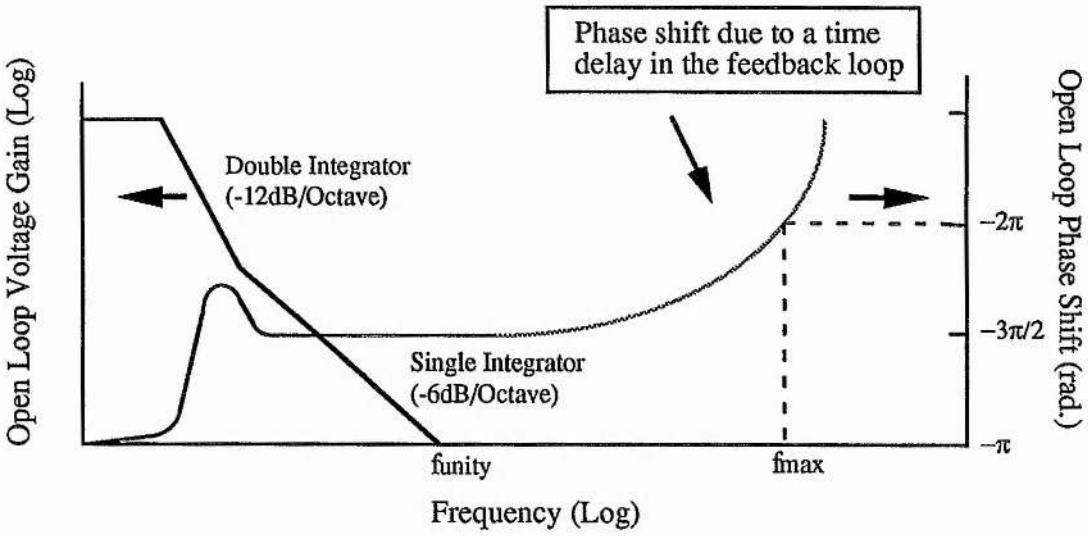

Figure 6.1 Gain and phase shift in a typical laser frequency servo system.

Various tricks are available in servo loop design which enable more bandwidth and consequently higher gains to be squeezed from a particular servo system. One such circuit scheme, commonly employed to keep loop time delays to a minimum whilst retaining a large servo bandwidth, is to include a bypass circuit which splits the input signal into its high and low frequency components. These components once separated , are fed through separate amplifier chains thus reducing propagation delays through the servo electronics. The two separate error signals derived from the high and low frequency components are then applied to separate frequency control transducers on the laser. For instance, the low frequency error signal could be sent to a piezo mounted cavity mirror while the high frequency signal could control an intra or extra-cavity electro-optic modulators. The crossover frequency between the two transducers is normally fixed by the bandwidth of the low frequency transducer[40].

6.1.3 Frequency Control Transducers.

Frequency control of the laser output is most commonly performed by varying the optical path length of the resonator (by controlling the mirror separation or intracavity

refractive index) or by extra-cavity phase modulation. In open cavity lasers, the cavity length can be simply varied over a few microns by mounting one of the laser mirrors on a piezoceramic element. This amount of movement means that such piezoceramic translators have good dynamic range in terms of the size of frequency shift they can impart to the laser output. However, their useful frequency response tends to be limited to only a few tens of kilohertz due to mechanical resonances of the moving mirror/piezo system. If low mass mirrors and carefully selected and damped piezos are used, it is possible to extend the bandwidth of a piezoceramic laser frequency transducer up to 200-300kHz[41,42].

Still higher frequency responses are possible by using an intracavity electro-optic crystal such as KDP, to modulate the intracavity refractive index. Unfortunately crystals which show electro-optic activity are also piezoelectric and so can exhibit undesirable mechanical resonance similar to the piezoceramic translators. However, by careful damping of these mechanical resonances and by judicious choice of crystal cut (for instance, the cut which makes use of the r_{41} electro-optic coefficient in AD*P has negligible piezoelectric effects[43]), the laser's output frequency can be controled over a bandwidth of hundreds of megahertz[44,45]. The upper limit to the frequency response of an intracavity electro-optic device is usually set by the ability of the electrical drive circuitry to develop the necessary voltage across the purely capacitive load of the modulator. Although the electro-optic modulator has an excellent bandwidth, its use as an intracavity laser frequency transducer is often limited because of its small dynamic range and because of the large parasitic loss it introduces into the laser cavity.

In the case of the piezoceramic mounted cavity mirror or the intracavity electro-optic modulator type of frequency transducer, the frequency of the laser output is corrected before it leaves the laser cavity. Alternatively, it is possible to modify the frequency of the laser beam outside the laser cavity by using an acousto-optic frequency shifter or an electro-optic phase modulator.

With the acousto-optic modulator, the frequency of the laser beam is Doppler shifted upon Bragg scattering from the travelling acoustic density wave in the modulator. The light frequency is shifted by an amount equal to the frequency of the acoustic wave and so for stabilisation purposes the modulator can be driven by a voltage controlled oscillator taking the error signal voltage as its input. The maximum frequency response of the acousto-optic frequency shifter is typically in the region of a few hundreds of kilohertz, limited by the finite propagation time of the acoustic wave. One difficulty encountered with the acousto-optic frequency shifter is the introduction of spatial noise into the laser beam because of the dependence of the Bragg deflection angle on the acoustic wave frequency. This addition of spatial noise can be avoided, however, by retroreflecting the laser beam back through the acousto-optic modulator for a second pass[46,47].

For faster frequency response an external electro-optic phase modulator can be used as an extracavity frequency shifter. To understand the principle of operation of this frequency transducer it is useful to represent the time varying, instantaneous frequency, $\nu(t)$, by

$$\nu(t) = \nu_0 + \frac{1}{2\pi}\frac{d\phi(t)}{dt} \tag{6.1}$$

where ν_0 is a constant centre frequency and $\phi(t)$ is some time dependent phase term. An electro-optic modulator can be used to generate such a time varying phase, $\phi(t)$ of the form

$$\phi(t) = \frac{U(t)}{U_{1/2}} \cdot \frac{\pi}{2} \tag{6.2}$$

$U(t)$ is the voltage applied to the modulator and $U_{1/2}$ is the modulator half wave voltage (voltage which produces a retardation of π radians). The resulting shift, $\Delta\nu$, in the laser frequency is thus

$$\Delta\nu = \frac{1}{4U_{1/2}} \cdot \frac{dU(t)}{dt} \tag{6.3}$$

Ideally this frequency shift should be proportional to the error signal voltage, V(t), generated by the frequency stabilisation servo electronics and so the voltage applied to the modulator must be of the form

$$U(t) \propto 4U_{1/2} \int V(t)dt \tag{6.4}$$

Therefore, the appropriate electro-optic modulator drive voltage can be derived by passing the error signal voltage through an electronic integrator.

The maximum frequency shift attainable with this type of transducer is dependent on the slew rate (rate of change of voltage with time (dU/dt)max) of the integrator, whilst the maximum output voltage of the integrator determines the time period over which this shift can be sustained. In practice the dynamic range of this device is very restricted and it is usually necessary to use it in conjunction with a slower frequency transducer capable of larger frequency shifts such as the piezo mounted mirror[40,41] or the extracavity acousto-optic modulator[47].

6.2 Laser Frequency Stabilisation Schemes Based on Passive Optical Reference Cavities

Laser stabilisation schemes utilising passive optical cavities as frequency references are among the most widely used and have in some cases achieved unprecedented levels of frequency stability. In the following section some of the most popular and successful techniques for laser frequency stabilisation are described.

6.2.1 Side-Of-Fringe Locking

In this stabilisation technique the locking discriminant is formed directly from one of the sloping sides of a transmission fringe of a passive optical cavity. The laser frequency

is set to lie near the half maximum intensity transmission point of the cavity resonance. Any small changes in laser frequency relative to the cavity resonance will be converted into fluctuations in the light intensity transmitted by the cavity. A photodiode monitoring this transmitted light produces an electrical signal, the amplitude of which corresponds to the frequency of the laser output.

To be useful as a frequency locking discriminant this electrical signal must be biased around zero volts so that its sign indicates whether the instantaneous laser frequency is on the high or low frequency side of the desired lock point. Biasing can be performed simply by subtracting a constant reference voltage level from the photodiode signal using a fast difference amplifier. The frequency lock point on the cavity fringe can then be set by adjusting the reference voltage level into the difference amplifier.

Unfortunately this method of generating the locking discriminant cannot distinguish between intensity noise and frequency noise in the laser output. To prevent this mapping of intensity noise into the frequency domain, it is common practice to derive the reference voltage for the difference amplifier from a second photodiode monitoring a suitably attenuated portion of the laser beam directly, as shown in figure 6.2. With a tight frequency lock the system exhibits strong rejection of laser intensity noise.

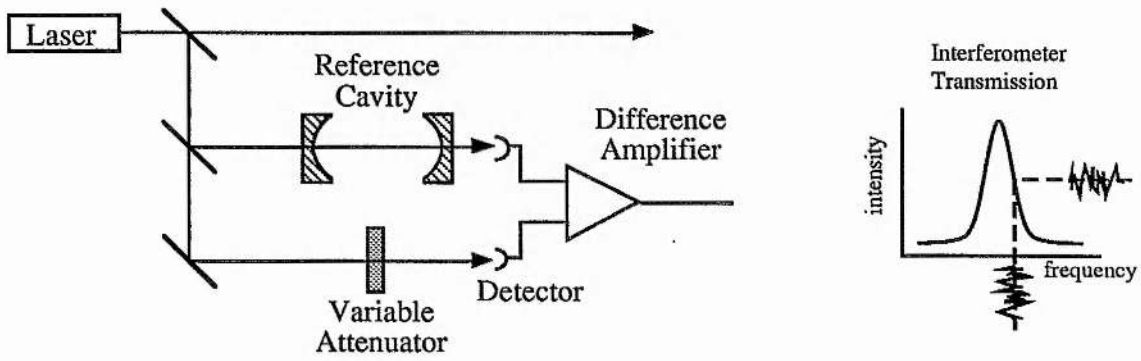

Figure 6.2. The side-of-fringe locking discriminant for laser frequency stabilisation.

This stabilisation scheme is however, not without its problems. Non exact matching of the photodetectors may result in small electrical imbalances between the two arms of

the detection circuit giving rise to long term frequency drift of the laser. Side-of-Fringe locking also displays a low tolerance to large laser frequency excursions. A frequency jump of as little as half the reference cavity linewidth is enough to throw the system out of frequency lock. This obviously becomes a severe problem when narrow linewidth cavities are used for high sensitivity.

Despite these short comings, this popular stabilisation technique has been successfully used on a wide variety of lasers ranging from dye to diode lasers[44,48,49,50,51]. For example, Helmcke et al[45] stabilised a jet stream dye laser to a reference cavity with a finesse of 450 and a free spectral range of 900MHz and observed a short term rms linewidth of 1.8kHz relative to the frequency lock point.

6.2.2 Phase Sensitive Detection Locking.

The experimental arrangement for this system is illustrated in figure 6.3. A small sinusoidal modulation, or "dither", is imposed on the fundamental laser frequency by, for example, a piezo mounted laser cavity mirror or an extra cavity phase modulator. Transmission through the reference cavity converts this frequency modulation into an intensity modulation which is detected by a photodiode. The amplitude of the resulting a.c. component of the photodiode output current depends on the magnitude of the slope of the interferometer transmission curve while its phase, relative to the original imposed laser modulation, depends on the sign of this slope. By processing this amplitude and phase information in a phase sensitive detector (P.S.D.) a zero crossing discriminant curve, approximately equal to the derivative of the reference cavity transmission function is formed. See figure 6.3. The servo electronics supply an appropriate error signal to the laser frequency transducer to maintain the P.S.D. output at the zero crossing point on the discriminant curve. This zero crossing point corresponds to the transmission peak of the reference cavity.

To obtain a large signal to noise ratio with this system it is desirable to use as large a frequency modulation depth as possible on the laser. However, if this modulation is too

large , distortion of the discriminant can occur. For a high finesse optical cavity which displays an approximately Lorentzian transmission line shape Nakazawa[52] has shown that the maximum discriminator sensitivity can be obtained when the amplitude of the applied frequency modulation is $\frac{1}{4\sqrt{2}}$ times the cavity linewidth. The frequency of the applied modulation sets the upper limit on the bandwidth of the servo.

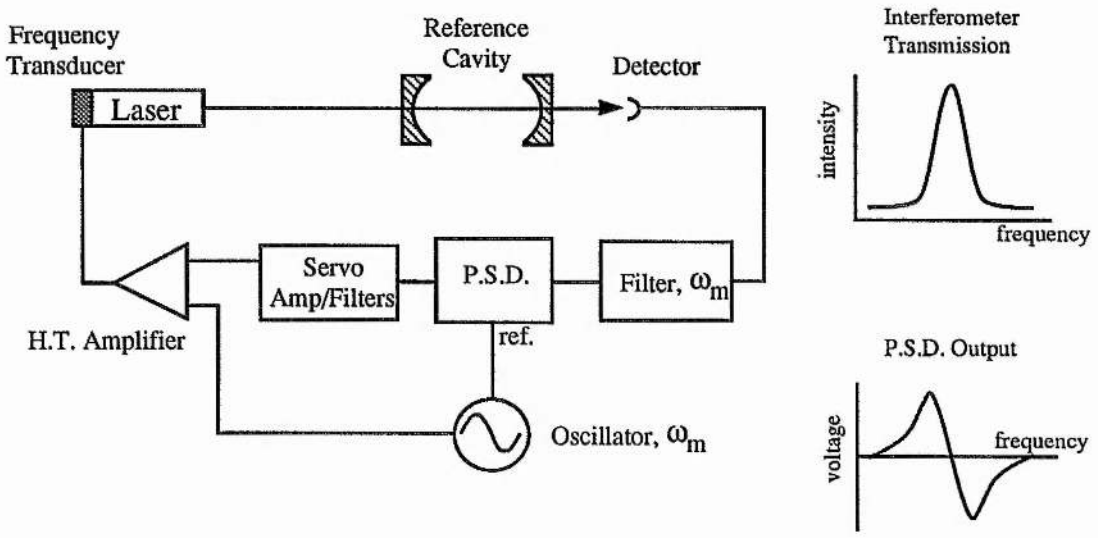

Figure 6.3. Schematic of the dither system for laser frequency stabilisation

Impressive stabilisation results have been demonstrated with this dither technique by Salomon et al[53]. In their experiments two HeNe laser were stabilised to a high finesse reference cavity and were shown to have short term, relative linewidths of ~50mHz.

6.2.3 Limitations of Reference Cavities Used in Transmission Mode

The two main requirements for a high performance laser frequency servo system are that the frequency discriminant has a large slope to give a good signal to noise ratio and that the feedback gain and hence the servo bandwidth are as large as possible to achieve maximum suppression of the laser frequency noise. For frequency discriminants based on transmission through passive optical cavities these two requirements cannot be satisfied simultaneously due to the finite cavity response time. In the extreme case where

the frequency of the laser field incident on the reference cavity is fluctuating on a time scale much smaller than the cavity response time, changes in the intensity of the light transmitted through the cavity will not be a true representation of the fluctuations in the incident light frequency but instead will be some time average of these fluctuations. Viewed in the frequency domain, the laser frequency noise sidebands lie outside the transmission bandwidth of the reference cavity and so will be blocked by the reference cavity. Since this high frequency noise information is not transmitted by the cavity, there is little to be gained by using a feedback loop with a bandwidth very much greater than the reference cavity linewidth and in fact the use of larger loop bandwidths only includes more noise in the feedback signal. Even with servo bandwidths similar to the reference cavity linewidth, problems still occur in maintaining servo loop stability because of the significant time delays (or equivalently phase shifts) introduced on transmission through the cavity at the upper end of the frequency response. This situation has been analysed in detail by Helmcke et al[45] for both side-of-fringe and dither locking techniques. They showed that even with carefully designed electronics to compensate for these cavity transmission time delays, the largest servo bandwidth which could usefully be employed was around a factor of three greater than the reference cavity linewidth for side-of-fringe locking.

If instead, the frequency locking discriminant is derived from the reflection response of the reference cavity, the finite cavity response time need not limit the servo bandwidth. The signal reflected from the reference cavity is made up from two field components, one directly reflected from the cavity input mirror and the second due to leakage of the resonant circulating field within the cavity. Although for fast frequency fluctuations in the incident laser beam the circulating cavity field cannot respond, the frequency noise information is still contained within the component directly reflected from the cavity input mirror. Therefore, an error signal can still be produced by comparing the instantaneous phase of the direct reflection field to that of the time averaged cavity leakage field. Although the side-of-fringe and dither discriminants can be produced from the cavity reflection response they are not capable of extracting noise

information from this high frequency "phase storage" domain of the cavity reflection. The only benefit to be gained by using these techniques in reflection mode is perhaps an improvement in signal to noise ratio[54]. To fully exploit the phase storage mode of cavities in reflection, other techniques have been developed such as Pound-Drever locking[55] (which is analysed in detail in the following section) and a polarisation sensitive reference cavity method designed by Hansch et al[56].

6.2.4 Pound-Drever Locking

In 1983 R.V.P. Drever and co-workers[55] introduced an extremely powerful laser phase and frequency stabilisation scheme based on an earlier microwave stabiliser proposed by R. V. Pound[57]. This Pound-Drever system, which uses the interaction of rf (radio frequency) phase modulated light with a resonant optical reference cavity in reflection mode, offers many clear advantages over more conventional stabilisation schemes. The most significant of these is the system's potential for very wide bandwidth control. With careful electronic design, the laser frequency correcting servo loop can be operated with a bandwidth approaching that of the imposed rf modulation frequency. By comparison, in frequency stabilisation schemes based on optical reference cavities in transmission mode, the servo loop bandwidth is limited by the response time of the reference cavity.

In addition to this wide bandwidth capability, the frequency discriminant generated by the Pound-Drever stabiliser provides a large "pull in" or "capture" range for the servo control. The size of this capture range is independent of the linewidth of the reference cavity and is defined only by the rf modulation frequency. Thus ultra-narrow linewidth reference cavities can be used to improve the sensitivity and hence the signal to noise ratio of the locking discriminant without adversely affecting the ease with which locking can be accomplished.

The signal to noise ratio of the Pound-Drever system is further enhanced through the use of phase sensitive detection at the rf modulation frequency to recover the error

signal. This gives the system excellent resistance to any low frequency intensity noise present in the laser output.

Ultimately the level of frequency stabilisation achieved by any laser frequency servo will be limited by photon generated shot noise in the photodetection stage. In Pound-Drever locking this noise source is minimised since the servo system locks the laser frequency to the minimum in the intensity reflection response (one minus the Airy function) of the reference cavity.

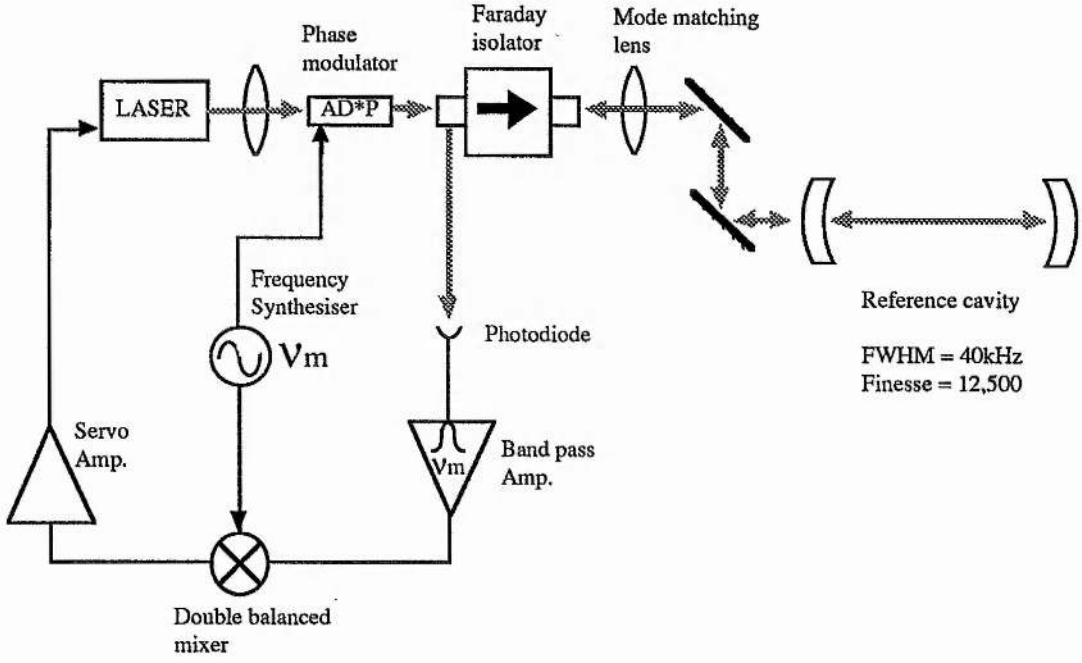

Figure 6.4. A schematic representation of the Pound-Drever laser frequency stabilisation system.

The main components of the Pound-Drever locking scheme are shown in figure 6.4. The laser output at frequency ν, passes through an optical phase modulator which is used to impose a sinusoidal phase modulation at some rf frequency, ν_m, (typically several megahertz) on the optical carrier field. The instantaneous phase, Φ_i, of the optical phase modulated wave is thus

$$\Phi_i = 2\pi\nu t + M \sin 2\pi\nu_m t$$

$$= \omega t + M \sin \omega_m t \qquad (6.5)$$

where ω is the optical carrier angular frequency and ω_m is the angular frequency of the applied modulation. M represents the peak deviation of the carrier phase and is called the modulation index. Defining $M = \Delta\nu_m/\nu_m$, means that the instantaneous frequency, ν_i, of the optical field is

$$\nu_i = \frac{1}{2\pi}\frac{d\Phi_i}{dt} = \nu + \Delta\nu_m \cos \omega_m t \tag{6.6}$$

where $\Delta\nu_m$ is the maximum deviation of the optical frequency from ν. Using the above expression for the instantaneous phase, the optical field emerging from the phase modulator can be written in the form

$$E = E_o e^{j(\omega t + M \sin \omega_m t)} \tag{6.7}$$

where E_o is the field amplitude. Using the Bessel function identities ;

$$e^{j(M \sin \omega_m t)} = \sum_{n=-\infty}^{\infty} J_n(M) e^{j(n\omega_m t)}$$

$$J_n(M) = J_{-n}(M) \quad \text{for even n}$$

$$J_n(M) = -J_{-n}(M) \quad \text{for odd n} \tag{6.8}$$

where $J_n(M)$ are Bessel functions of the first kind of order n, equation (6.7) becomes

$$E = E_o e^{j(\omega t)}\Big\{J_o(M) + J_1(M)\left[e^{j(\omega_m t)} - e^{-j(\omega_m t)}\right] + J_2(M)\left[e^{j(2\omega_m t)} + e^{-j(2\omega_m t)}\right]$$

$$+ J_3(M)\left[e^{j(3\omega_m t)} - e^{-j(3\omega_m t)}\right] + \ldots.\Big\} \tag{6.9}$$

From this it can be seen that phase modulated light contains an infinite set of frequency components, or sidebands, symmetrically distributed around the optical carrier

frequency, ω. In practice, however, most of the power of the optical field will be contained within a finite number of spectral components and so only these significant sidebands need be considered.

For the purposes of the Pound-Drever locking scheme the modulation index, M, of the imposed rf signal is kept small (M<1). Under this condition over 99% of the optical power is contained within the carrier frequency, ω, and the first two rf modulation sidebands at frequencies $\omega-\omega_m$ and $\omega+\omega_m$ respectively[58]. The phase modulated optical field is thus given by

$$E \approx E_o e^{j(\omega t)}\left[J_o(M) + J_1(M)e^{j(\omega_m t)} - J_1(M)e^{-j(\omega_m t)}\right] \qquad (6.10)$$

The frequency spectrum of this phase modulated light beam is shown schematically in figure 6.5.

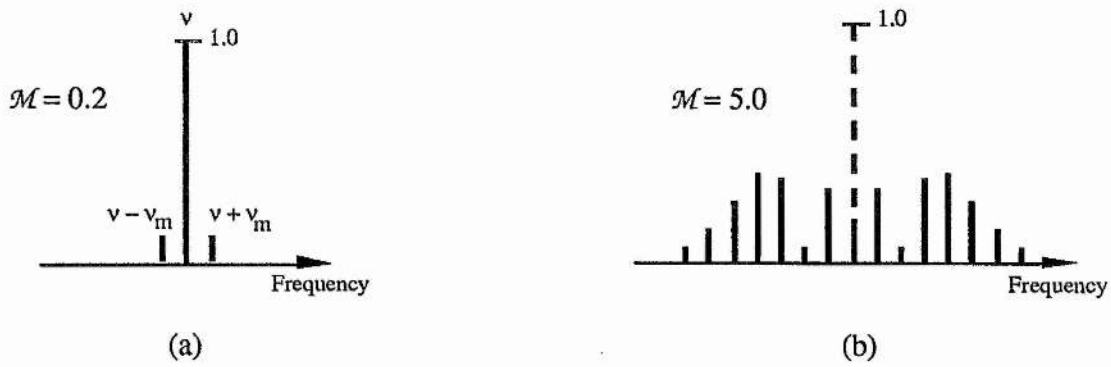

Figure 6.5. Examples of frequency spectra for a signal sinusoidally phase modulated at frequency ν_m and with modulation index M (a) small, (b) large.

A key feature of this stabilisation technique is that the rf modulation frequency, ν_m, is chosen to be greater than the linewidth of the reference cavity. If the optical carrier is tuned to line centre of the reference cavity, the rf sidebands of the optical signal will be located spectrally well outside the cavity resonance and so will be unaltered on reflection from the cavity input mirror. However, the cavity does modify the phase and amplitude of the optical carrier signal, disrupting the delicately balanced phase

relationship between the carrier and modulation sidebands. This introduces an amplitude modulated (AM) component into the optical field retro-reflected from the reference cavity. Detection of this AM signal on a photodiode and subsequent demodulation of the resulting photodiode output generates the error signal for the system.

A Phasor Description

An appreciation of how the error signal is generated and of the overall system response can be gained by considering the interaction of the rf modulated laser output field with the reference cavity in terms of phasor diagrams.

The initial rf phase modulated optical field of equation (6.10) can be depicted in phase space as a composite of the carrier phasor of magnitude $E_oJ_o(M)$ and two counter rotating phasors, each rotating at ω_m and of magnitude $E_oJ_1(M)$, representing the upper

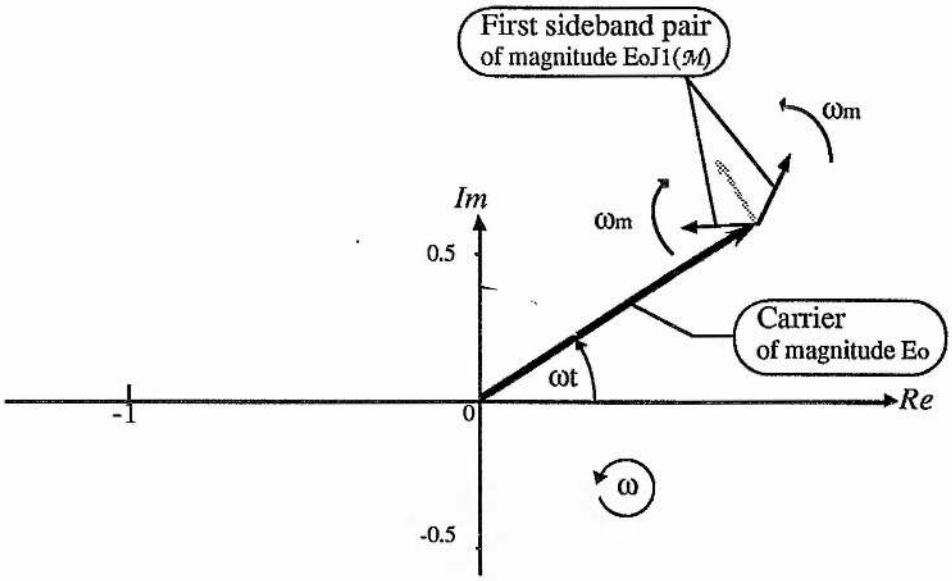

Figure 6.6. A phasor representation for a frequency/phase modulated signal (carrier) where the modulation angular frequency is ω_m and the modulation index M is small (M<1). Note that the resultant (⟿) of the two sideband phasors is of magnitude $2E_oJ_1(M)\sin\omega_m t$ and is always $\pi/2$ out of phase with the carrier. This whole system of phasors is rotating at the angular frequency of the carrier, ω.

and lower modulation sidebands. The resultant of these two sideband phasors is always $\pi/2$ out of phase with the carrier phasor. This whole system of phasors is of course rotating about the origin at ω, the angular frequency of the optical carrier (See figure 6.6).

Reflection of this light from the reference cavity gives rise to a resultant optical signal composed of two field components. One component, E_{refl}, is just the incident optical field directly reflected from the input mirror of the reference cavity and is given by rE where r is the amplitude reflectivity of the cavity mirror. The second field, E_{leak}, is due to leakage through the cavity input mirror of any circulating field within the cavity, shown in figure 6.7.

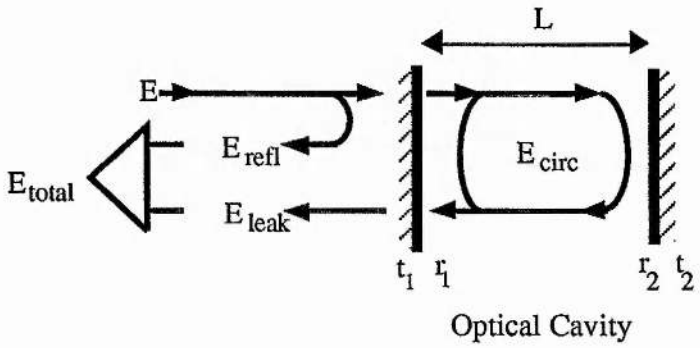

Figure 6.7. The optical fields returning from the reference interferometer.

The total optical field returning from the cavity for a monochromatic wave of frequency ω is thus

$$E_{total} = E_{refl} + E_{leak} = E_o e^{j(\omega t)} \left[r_1 - \frac{t_1^2 r_2 e^{-j(\omega\tau)}}{1 - r_1 r_2 e^{-j(\omega\tau)}} \right] \qquad (6.11)$$

where;

$\tau = \frac{2L}{c}$ = Cavity round trip time for cavity of optical path length L

r_1, r_2 = Cavity mirror field amplitude reflectivities

t_1 =Cavity mirror field amplitude transmission. Assuming no losses then $t^2 = (1-r^2)$.

If $r_1=r_2=r$ and if the mirrors are lossless then

$$E_{total} = E_o e^{j(\omega t)}\left[\frac{(r+r^3)(1-\cos\omega\tau)}{1+r^4-2r^2\cos\omega\tau} + j\frac{(r-r^3)\sin\omega\tau}{1+r^4-2r^2\cos\omega\tau}\right] \tag{6.12}$$

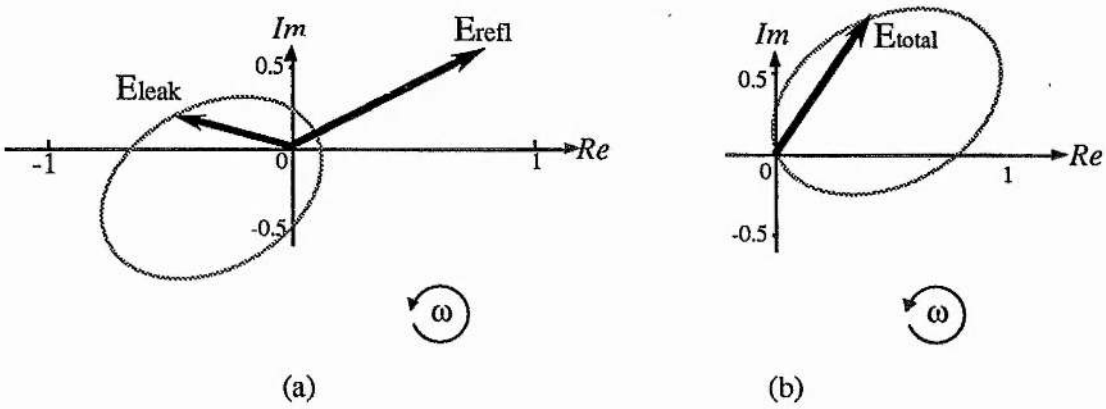

Figure 6.8. A phasor diagram of equation (6.11) describing the optical fields returning from a passive optical cavity. The ellipse shown in (a) represents the locus for the E_{leak} phasor as the frequency of the input optical field is swept through a free spectral range of the reference cavity. (b) shows the resultant, E_{total}, of the E_{leak} and E_{refl} phasors. Again the ellipse indicates the locus for E_{total} as the input field frequency is swept through the reference cavity free spectral range.

A phasor representation of equation (6.11) is shown in figure 6.8 for the case of non phase modulated light. The locus swept out in phase space by the E_{leak} phasor, as the input optical frequency is varied, is also indicated on the diagram.

Figure 6.9 shows the same situation but this time with the phase modulation present. Remembering that the rf sidebands lie outside the cavity resonance the resultant field returning from the cavity may be written as

$$E = E_o e^{j(\omega t)}\left\{\frac{(r+r^3)(1-\cos\omega\tau)}{1+r^4-2r^2\cos\omega\tau} + j\left[\frac{(r-r^3)\sin\omega\tau}{1+r^4-2r^2\cos\omega\tau} + 2J_1(M)\sin\omega_m t\right]\right\} \tag{6.13}$$

The photodiode receiving this signal is sensitive to the irradiance, I, of this signal

$$I \propto \frac{EE^*}{2} = \frac{E_o^2}{2}\left\{\left[\frac{(r+r^3)(1-\cos\omega\tau)}{1+r^4-2r^2\cos\omega\tau}\right]^2+\left[\frac{(r-r^3)\sin\omega\tau}{1+r^4-2r^2\cos\omega\tau}\right]^2\right.$$

$$\left.+\,4J_1(M)^2\sin^2\omega_m t+\frac{4J_1(M)\sin\omega_m t\cdot(r-r^3)\sin\omega\tau}{1+r^4-2r^2\cos\omega\tau}\right\} \qquad (6.14)$$

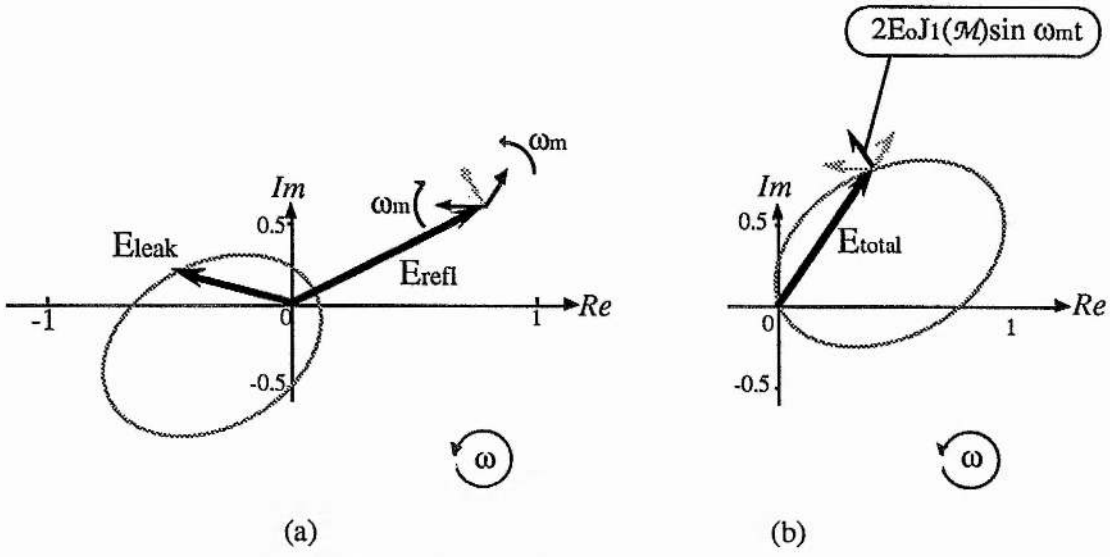

Figure 6.9. This diagram illustrates the reflection response of the optical reference cavity to phase modulated light. The Modulation frequency, ν_m, is set to be larger than the linewidth of the reference cavity and so the modulation sidebands are reflected from the cavity input mirror unaltered.(b) shows the resultant, E_{total}, of the phasors illustrated in (a). See also figures 6.6 & 6.8.

A bandpass filter centred on frequency ω_m filters the photodiode output to remove unwanted components at DC and $2\omega_m$. This filtered output, containing only signals at ω_m, is passed to the double balanced mixer where it is mixed with sin $\omega_m t$ to generated sum frequency ($2\omega_m$) and difference frequency (DC) terms. Only resulting DC terms need be considered since higher frequency terms do not contribute to the useful error signal and can be removed by appropriate filters. The error signal output from the balanced mixer is thus

$$\text{BALANCED MIXER OUTPUT} \propto \frac{(r-r^3)\sin\omega\tau}{1+r^4-2r^2\cos\omega\tau} \qquad (6.15)$$

This function has been plotted in figure 6.10 for various values of mirror reflectivity. As can be seen from the form of this curve, the error signal is an approximately linear function of frequency between the two turning points occurring at values of $\omega\tau$ of

$$\omega\tau(\text{turning point}) = \cos^{-1}\left(\frac{2r^2}{1+r^4}\right) \tag{6.16}$$

For frequency excursions outside this range it can be seen from the graph that the error signal becomes nonlinear but still retains the appropriate sign to enable the servo system to return the laser frequency to the centre of the cavity resonance.

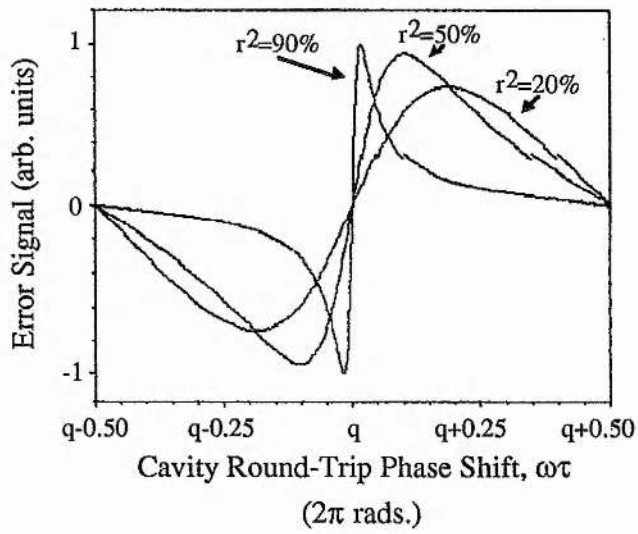

Figure 6.10. The error signal described by equation (6.15) for various values of reference cavity mirror reflectivity.

The gradient of the error signal in the vicinity of cavity resonance ($\omega\tau = q2\pi$: q=large integer) is a measure of the frequency sensitivity of the system and increases with increasing cavity mirror reflectivity. This gradient is given by the differential of equation (6.15) evaluated at $\omega\tau = q2\pi$

$$\left.\frac{d(\text{Mixer Output})}{d(\omega\tau)}\right|_{\omega\tau=q2\pi} \propto \frac{(r-r^3)}{(1+r^4-2r^2)} \tag{6.17}$$

The above analysis assumes that the frequency of the light incident on the reference cavity is changing on a time scale greater than the cavity build-up time. For a more

complete understanding of the behaviour of this locking scheme the response of the system to frequency fluctuations of the incident optical field on time scales shorter than the reference cavity build-up time must also be considered.

In considering the system response to "fast" frequency fluctuations the assumption may be made that the optical carrier frequency is coincident with line-centre of the reference cavity. This assumption is valid since for "slow" frequency fluctuations the system can generate an appropriate error signal for the servo system to maintain the optical carrier on resonance with the cavity. Without loss of generality, the fast frequency fluctuations can be represented by an FM component of frequency ν_n and of maximum frequency excursion, $\Delta\nu_n$, from the carrier frequency. Combining this FM noise term with the original rf phase modulated carrier (see equation 6.6) gives the instantaneous frequency of the optical wave as

$$\nu_i = \nu + \Delta\nu_m \cos \omega_m t + \Delta\nu_n \cos \omega_n t \tag{6.18}$$

where $\omega_n = 2\pi\nu_n$ = angular frequency of the FM noise. Since the instantaneous phase, Φ_i, is related to ν_i through

$$\frac{1}{2\pi}\frac{d\Phi_i}{dt} = \nu_i \tag{6.19}$$

integration of equation (6.18) produces

$$\Phi_i = \omega t + \frac{\Delta\nu_m}{\nu_m} \sin \omega_m t + \frac{\Delta\nu_n}{\nu_n} \sin \omega_n t \tag{6.20}$$

and so the complex representation of the wave is

$$E = E_o e^{j(\omega t + M \sin \omega_m t + N \sin \omega_n t)} \tag{6.21}$$

As before, $M = \frac{\Delta\nu_m}{\nu_m}$ is the modulation index of the rf phase modulation and similarly, $N = \frac{\Delta\nu_n}{\nu_n}$ is the modulation index of the noise frequency modulation.

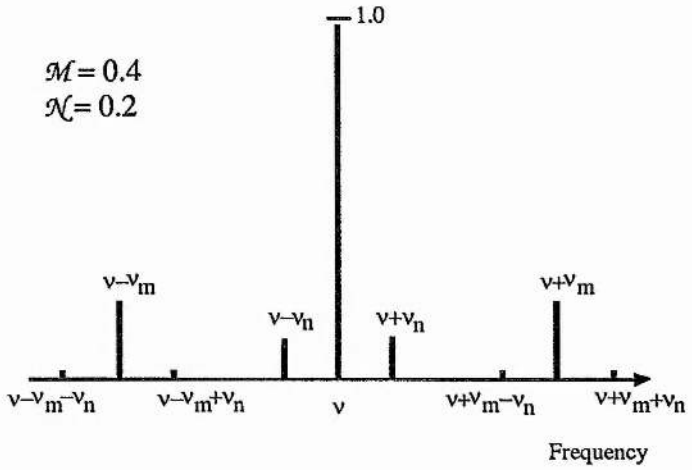

Figure 6.11. Frequency spectrum of a signal (of fundamental frequency ν) under the influence of two small sinusoidal phase/frequency modulations at frequencies ν_m, ν_n and of modulation index M, N respectively.

Using the Bessel function identities of equation (6.8) and restricting N<1 so that only the first two noise sidebands are significant, then equation (6.21) becomes

$$E = E_o \Big\{ J_o(M)J_o(N)\, e^{j\omega t} + J_o(M)J_1(N)\, e^{j(\omega+\omega_n)t} - J_o(M)J_1(N)\, e^{j(\omega-\omega_n)t}$$

$$+ J_o(N)J_1(M)\, e^{j(\omega+\omega_m)t} + J_1(M)J_1(N) e^{j(\omega+\omega_m+\omega_n)t} - J_1(M)J_1(N)\, e^{j(\omega+\omega_m-\omega_n)t}$$

$$- J_o(N)J_1(M)\, e^{j(\omega-\omega_m)t} - J_1(M)J_1(N)\, e^{j(\omega-\omega_m+\omega_n)t} + J_1(M)J_1(N)\, e^{j(\omega-\omega_m-\omega_n)t} \Big\} \quad (6.22)$$

Figure 6.11 shows the frequency spectrum described by equation (6.22). The phasor representation of equation (6.22) is illustrated in figure 6.12. Also shown on this diagram is the phasor for the leakage field, E_{leak}, from the reference cavity when the laser carrier frequency, ν, matches a resonance frequency of the cavity.

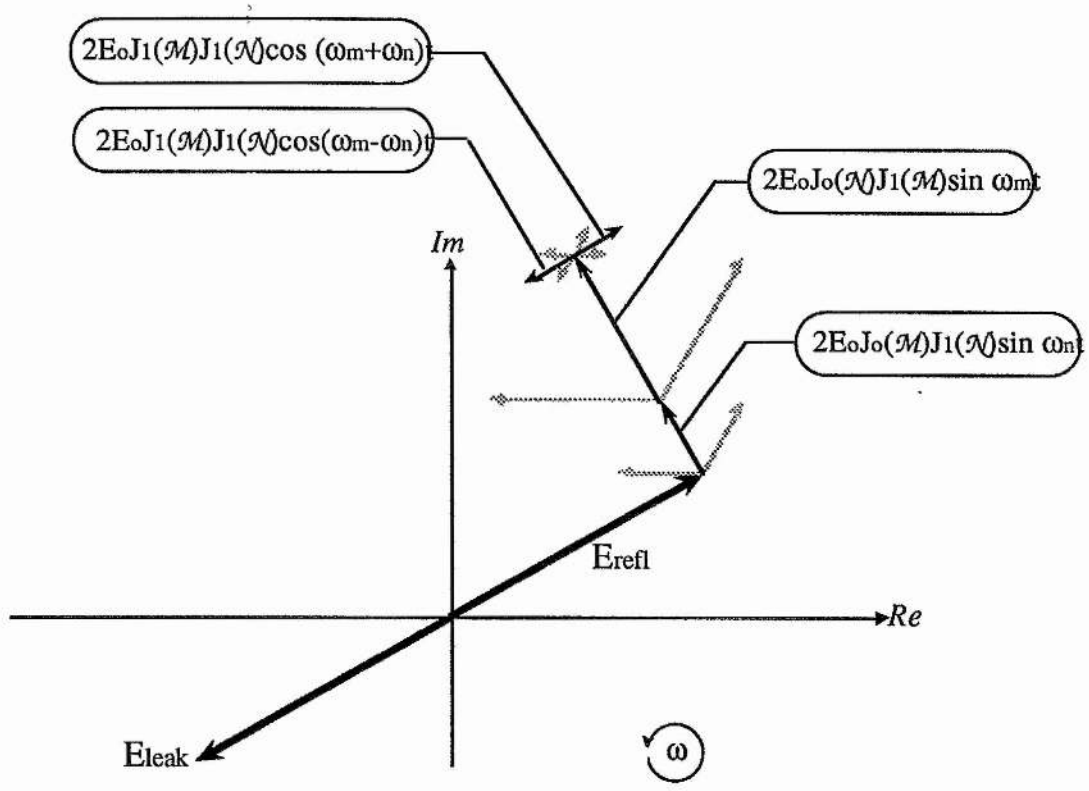

Figure 6.12. A phasor picture of the optical field of Equation (6.22) after the field has been reflected from the reference cavity. The frequency of the input optical field is chosen to match a resonance of the reference cavity. Assuming no losses in the cavity then E_{leak} cancels with E_{refl} leaving only the sideband phasors.

Assuming, for simplicity, that there are no losses in the system, the leakage field from the cavity, E_{leak}, and the reflected carrier field, E_{refl}, will cancel each other completely on resonance. From the phasor diagram of figure 6.12 the residual field returning from the reference cavity will be

$$E = E_o e^{j(\omega t)} \{ 2J_1(M)J_1(N)[\cos(\omega_m+\omega_n)t - \cos(\omega_m-\omega_n)t] + j\cdot 2\,[J_o(M)J_1(N)\sin\omega_n t + J_o(N)J_1(M)\sin\omega_m t]\} \quad (6.23)$$

As before, the photodiode generates a current proportional to the intensity, I, of this optical wave.

$$I \propto \frac{EE^*}{2}$$

$$= E_o^2 \left\{ 2J_1(M)^2 J_1(N)^2 \left[\cos 2(\omega_m+\omega_n)t - \cos 2(\omega_m-\omega_n)t - \cos 2\omega_m t - \cos 2\omega_n t\right] \right.$$

$$+ 4 \left[J_o(M)^2 J_1(N)^2 \sin^2\omega_n t + J_o(N)^2 J_1(M)^2 \sin^2\omega_m t \right.$$

$$\left. \left. + 2J_o(M)J_o(N)J_1(M)J_1(N) \sin\omega_m t \cdot \sin\omega_n t \right] \right\} \qquad (6.24)$$

As before, the bandpass filter centred at ω_m selects only those components of this photodiode output which have frequencies close to ω_m. Providing that ω_n is small enough so that $\omega_m+\omega_n$ is not blocked by the bandpass filter, then subsequent demodulation of this signal with $\sin(\omega_m t)$ in the double balanced mixer followed by low pass filtering (to reject $2\omega_m$) results in an output of the form

$$\text{MIXER OUTPUT} \propto E_o^2 J_o(M)J_o(N)J_1(M)J_1(N) \sin\omega_n t \qquad (6.25)$$

If N is very small («1) then the Bessel functions $J_o(N)$ and $J_1(N)$ can be approximated by their first order expansions ;

$$J_o(N) \approx 1 \text{ and } J_1(N) \approx \frac{N}{2} \qquad (6.26)$$

and so

$$\text{MIXER OUTPUT} \propto N \sin\omega_n t$$

$$\propto \frac{\Delta\nu_n}{\nu_n} \sin\omega_n t \qquad (6.27)$$

This is just the instantaneous phase of the original FM noise modulating the laser output. See equation (6.20). So, in this operating regime, where the frequency noise sidebands lie outside the cavity resonance, the system behaves as an optical phase detector. The error signal generated is proportional to the instantaneous phase difference between the light incident on the reference cavity and the light field (at the optical

carrier frequency) leaking from the resonant cavity. Since the instantaneous phase of the optical wave is proportional to the time integral of the instantaneous frequency, the system can alternatively be thought of as an optical integrator.

This "optical integrator" effect must be taken into consideration when designing the electronic feedback network. If the full bandwidth of the system is to be exploited then it may be necessary to compensate for the $\pi/2$ phase shift associated with the optical integration behaviour in order to avoid servo loop oscillation due to excessive closed loop phase shifts.

From the above phasor analysis the overall system response to an optical field of instantaneous frequency

$$\nu_i = \nu + \Delta\nu_n \cos \omega_n t \tag{6.28}$$

containing a single FM noise component of frequency ν_n, can be summarised by the following table.

	$\Delta\nu_n < \Delta\nu_{HWHM}$	$\Delta\nu_n > \Delta\nu_{HWHM}$
$\nu_n < \Delta\nu_{HWHM}$	ERROR SIGNAL $\propto$ FREQUENCY OF NOISE COMPONENT $\Delta\nu_n \cos(\omega_n t)$	NONLINEAR RESPONSE
$\nu_n > \Delta\nu_{HWHM}$	ERROR SIGNAL $\propto$ PHASE OF NOISE COMPONENT $\frac{\Delta\nu_n}{\nu_n} \sin(\omega_n t)$	NONLINEAR RESPONSE

$\Delta\nu_{HWHM}$ refers to the reference cavity half width at half maximum linewidth.

A Mathematical Description

The previously outlined phasor analysis of the Pound-Drever locking system gives the form of the error signal for the two extreme cases:

1) laser FM noise frequency « cavity linewidth,

2) laser FM noise frequency » cavity linewidth.

A more comprehensive description of the error signal for laser frequency/phase noise of small modulation index (N<1) can be obtained by combining the expression for the modulated optical field, equation (6.22), with the cavity reflection response given by equation (6.11). Calculating the intensity of the resulting field retro-reflected from the reference cavity and then demodulating this signal with $\sin\omega_m t$ gives an error signal of the form:

$$I \propto E_o^2 J_o(M)\, J_o^2(N)\, J_1(M)\, t_1^2 r_1 r_2 \left[\frac{2\sin\omega\tau}{D} - \frac{\sin(\omega+\omega_m)\tau}{D^+} - \frac{\sin(\omega-\omega_m)\tau}{D^-}\right]$$

$$+ E_o^2 J_o(M)\, J_o(N)\, J_1(M)\, J_1(N)\, t_1^2 r_1 r_2 \left\{ 2\frac{r_1 r_2}{D^+}\sin(\omega_n t) + 2\frac{r_1 r_2}{D^-}\sin(\omega_n t) \right.$$

$$-\frac{1}{D^+}\sin\left[(\omega+\omega_m)\tau+\omega_n t\right] + \frac{1}{D^+}\sin\left[(\omega+\omega_m)\tau-\omega_n t\right] - \frac{1}{D^-}\sin\left[(\omega-\omega_m)\tau+\omega_n t\right]$$

$$+\frac{1}{D^-}\sin\left[(\omega-\omega_m)\tau-\omega_n t\right] + 2\frac{r_1 r_2}{D^{n+}}\sin(\omega_n t) + 2\frac{r_1 r_2}{D^{n-}}\sin(\omega_n t)$$

$$+ 2\frac{1}{D^{n+}}\sin\left[(\omega+\omega_n)\tau-\omega_n t\right] - 2\frac{1}{D^{n-}}\sin\left[(\omega-\omega_n)\tau+\omega_n t\right]$$

$$- r_1 r_2\left(\frac{1}{D^{++}}+\frac{1}{D^{+-}}+\frac{1}{D^{-+}}+\frac{1}{D^{++}}\right)\sin(\omega_n t)$$

$$-\frac{1}{D^{++}}\sin\left[(\omega+\omega_m+\omega_n)\tau-\omega_n t\right] + \frac{1}{D^{+-}}\sin\left[(\omega+\omega_m-\omega_n)\tau+\omega_n t\right]$$

$$-\frac{1}{D^{-+}}\sin\left[(\omega-\omega_m+\omega_n)\tau-\omega_n t\right] + \frac{1}{D^{--}}\sin\left[(\omega-\omega_m-\omega_n)\tau+\omega_n t\right]$$

$$\left. + 2\frac{1}{D}\sin\left[\omega\tau+\omega_n t\right] - 2\frac{1}{D}\sin\left[\omega\tau-\omega_n t\right] - 4\frac{r_1 r_2}{D}\sin(\omega_n t)\right\}$$

$$+ \text{higher order terms} \qquad (6.29)$$

where

$$D = 1 + r_1^2 r_2^2 - 2r_1 r_2 \cos(\omega\tau),$$

$$D^{+} = 1 + r_1^2 r_2^2 - 2r_1 r_2 \cos(\omega+\omega_m)\tau,$$

$$D^{-} = 1 + r_1^2 r_2^2 - 2r_1 r_2 \cos(\omega-\omega_m)\tau,$$

$$D^{n+} = 1 + r_1^2 r_2^2 - 2r_1 r_2 \cos(\omega+\omega_n)\tau,$$

$$D^{n-} = 1 + r_1^2 r_2^2 - 2r_1 r_2 \cos(\omega-\omega_n)\tau,$$

$$D^{++} = 1 + r_1^2 r_2^2 - 2r_1 r_2 \cos(\omega+\omega_m+\omega_n)\tau,$$

$$D^{+-} = 1 + r_1^2 r_2^2 - 2r_1 r_2 \cos(\omega+\omega_m-\omega_n)\tau,$$

$$D^{-+} = 1 + r_1^2 r_2^2 - 2r_1 r_2 \cos(\omega-\omega_m+\omega_n)\tau,$$

$$D^{--} = 1 + r_1^2 r_2^2 - 2r_1 r_2 \cos(\omega-\omega_m-\omega_n))\tau$$

A full derivation of this equation can be found in Appendix A. The behaviour of the error signal described by equation (6.29) is best understood by considering the following three cases.

Case 1 - Error signal as a function of optical carrier frequency.

By setting $\Delta\nu_n=0$ (i.e. modulation index N=0 and so $J_0(N)=1$, $J_1(N)=0$) the contribution to the error signal from the noise component can be removed. In this case, equation (6.29) simplifies to

$$I \propto E_o^2 J_o(M) J_1(M) t_1^2 r_1 r_2 \left[\frac{2 \sin \omega\tau}{D} - \frac{\sin(\omega+\omega_m)\tau}{D^{+}} - \frac{\sin(\omega-\omega_m)\tau}{D^{-}}\right] \qquad (6.30)$$

which is the error signal due purely to detuning of the laser frequency, ν, from the resonance frequency of the reference cavity. The first term in the above expression is the error signal generated when the laser carrier frequency, ν, is in the vicinity of the reference cavity resonance frequency. This term is of the same form as equation (6.15) derived earlier. The second and third terms of equation (6.30) are contributions to the error signal due to interaction of the upper and lower sidebands of the optical signal with the reference cavity respectively.

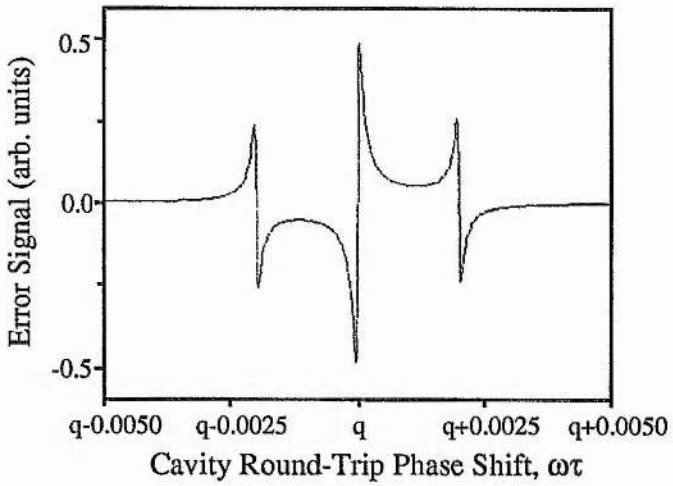

Figure 6.13. Theoretical calculation of the Pound-Drever error signal as a function of detuning between the laser frequency and the resonance frequency of the reference interferometer.

mirror amplitude reflectivity, r_1, $r_2 = r$	0.99987
mirror amplitude transmission, t_1^2	$(1-r^2)$
cavity length, L	0.3m
free spectral range, $\Delta\nu_{fsr}=\frac{c}{2L}$	500MHz
finesse, $\mathcal{F}=\frac{\pi r}{1-r^2}$	12,500
cavity resonance FWHM	40kHz
rf modulation frequency, ν_m	1MHz

In figure 6.13, equation (6.30) has been plotted as a function of laser carrier angular frequency, ω, (or equivalently as a function of reference cavity round trip phase shift, $\omega\tau$) for an ultra high finesse reference cavity having parameters as listed above.

Figure 6.13 illustrates the "ideal" nature of the locking discriminant, or rf fringe, generated by this locking technique. The curve has a zero-crossing, high slope region centred on the cavity resonance giving high sensitivity to frequency off-sets between the laser frequency and the reference cavity resonance. This frequency discriminant also provides a signal of appropriate sign over a range of $2\nu_m$ around cavity resonance to enable the frequency servo system to pull the laser frequency into resonance with the reference cavity from any frequency off-set within this $2\nu_m$ frequency range.

Case 2 - Frequency Modulation (FM), $\Delta\omega_n$=const.

In studying the effect of a small FM noise component on the error signal, the laser carrier frequency, ν, can be assumed to be coincident with line centre of the reference cavity resonance through the action of the error signal described in Case 1. Under this condition $\omega\tau=q2\pi$: q=integer and so the error signal described by equation (6.29) reduces to

$$I \propto E_o^2\, J_o(M)\, J_o(N)\, J_1(M)\, J_1(N)\, 2t_1^2 r_1\, r_2 \Bigg\{ \sin(\omega_n t)\Bigg[r_1 r_2 \left(\frac{2}{D^+} + \frac{2}{D^{n+}} - \frac{2}{D} - \frac{1}{D^{++}} - \frac{1}{D^{+-}}\right) + \frac{2}{D} - \frac{2}{D^+}\cos(\omega_m\tau) - \frac{2}{D^{n+}}\cos(\omega_n\tau) + \frac{1}{D^{++}}\cos(\omega_m+\omega_n)\tau + \frac{1}{D^{+-}}\cos(\omega_m-\omega_n)\tau\Bigg] + \cos(\omega_n t)\Bigg[\frac{2}{D^{n+}}\sin(\omega_n\tau) - \frac{1}{D^{++}}\sin(\omega_m+\omega_n)\tau + \frac{1}{D^{+-}}\sin(\omega_m-\omega_n)\tau\Bigg]\Bigg\} \tag{6.31}$$

This expression indicates that the error signal is composed of two components. The $\cos(\omega_n t)$ term is in phase with the original FM noise signal while the other component in $\sin(\omega_n t)$ represents a contribution to the error signal in phase quadrature. The

coefficients of these two components have been plotted as a function of noise frequency, ν_n, for $\Delta\nu_n$=100Hz and $N=\frac{\Delta\nu_n}{\nu_n}$ «1. See figure 6.14.

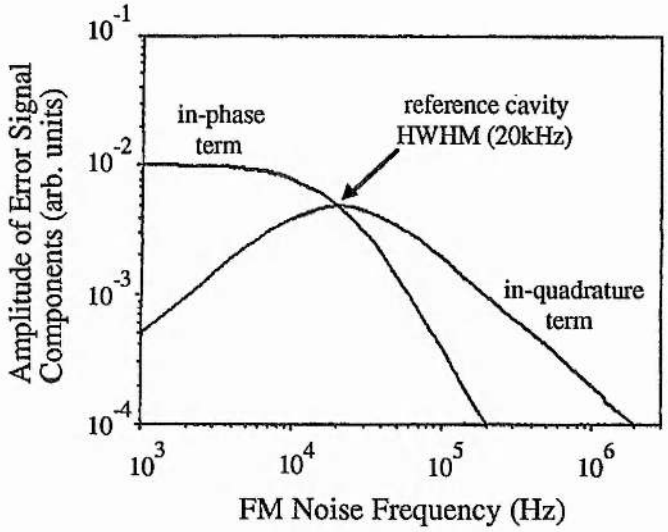

Figure 6.14. The in-phase and in-quadrature terms in the Pound-Drever error signal generated in response to FM noise.

This log - log plot shows that for noise frequencies less than the half width at half maximum (HWHM) frequency of the reference cavity (20kHz in this case), the error signal is dominated by the in-phase, $\cos(\omega_n t)$ term which is initially constant. For noise frequencies much greater than the cavity half width this in-phase term rolls off with a gradient of -2 (or equivalently -12dB/octave) and is superseded by the in-quadrature, $\sin(\omega_n t)$, term which rolls off with a slope of only -1 (-6dB/octave). The cross over between these two components occurs at the HWHM of the cavity resonance (20kHz in this example).

Figures 6.15(a)&(b) show the magnitude and phase respectively of the overall error signal as a function of FM noise frequency. The form of this error signal can be understood in the following way. For noise frequencies much less than the reference cavity HWHM resonance the optical field circulating within the cavity is able to follow the frequency fluctuations of the input field and so the resulting error signal from the system is in phase with the original disturbance. Because the maximum frequency

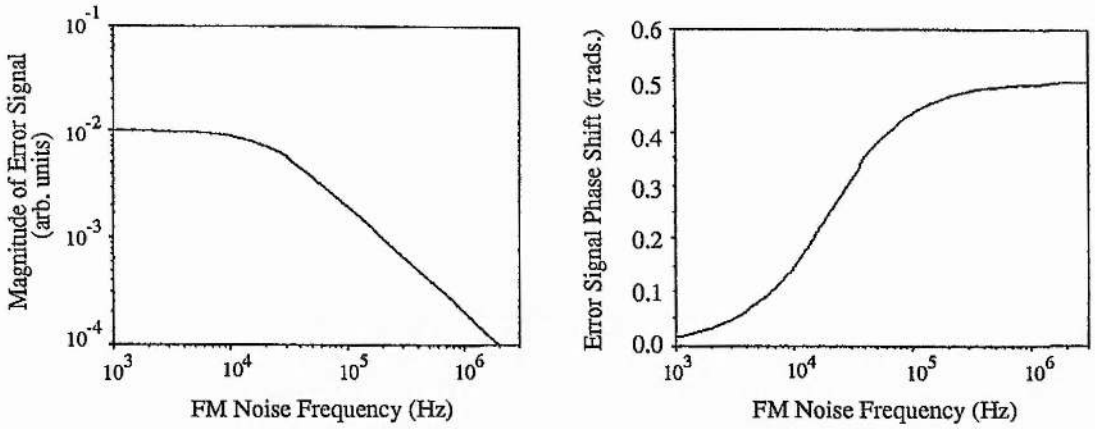

Figure 6.15. (a) Magnitude and (b) phase of the Pound-Drever error signal as functions of FM noise frequency.

excursion, $\Delta\nu_n$, is constant the magnitude of the error signal also remains constant as the noise frequency changes. However, for noise frequencies much greater than the cavity resonance half width the circulating field in the cavity is no longer able to track variations in the incident field. The field circulating in the cavity now represents a time average of the input field where the averaging time is of the order of the cavity response time. In this regime the error signal generated represents the instantaneous phase difference between the time averaged field stored in the cavity and the input field. Provided that N«1 so that to first order $J_0(N) \approx 1$ and $J_1(N) \approx \frac{N}{2}$, the system now acts as an optical phase detector giving an error signal

$$I \propto N \sin(\omega_n t) \tag{6.32}$$

as shown previously in equation (6.27). The dependence of N on $1/\nu_n$ in equation (6.32) causes the error signal to roll off with a slope of -1 in the log - log plot of figure 6.15(a).

Case 3 - Phase Modulation (PM), N=const.

The form of the error signal generated by phase noise on the laser output can easily be studied using equation (6.31) by setting the noise modulation index N=const (<1). In figure 6.16 the coefficients of the cos $\omega_n t$ and sin $\omega_n t$ components have been plotted as

functions of noise frequency, ν_n, for N=0.1 over the noise frequency range1kHz - 300kHz. For noise frequencies below the reference cavity HWHM (20kHz) the cavity reflection response is sensitive to the instantaneous frequency of the laser output and so the error signal is dominated by the cos $\omega_n t$ (frequency) component of equation (6.31). This frequency component rolls on with a slope of +1 on the log - log plot of figure 6.16 due to the linear dependence of $\Delta\nu_n$ on ν_n for phase noise.

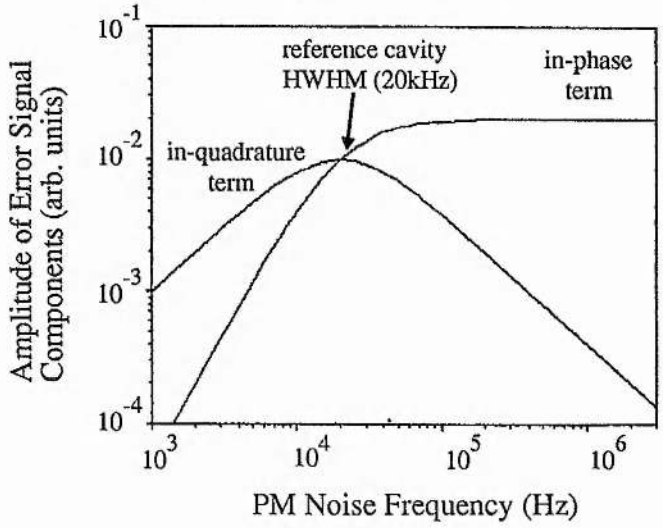

Figure 6.16. The in-phase and in-quadrature terms in the Pound-Drever error signal generated in response to PM noise.

For noise frequencies above the HWHM linewidth of the reference cavity the system crosses over to its phase detector mode of operation and so the error signal becomes constant as a function of phase noise frequency. Figure 6.16 shows that the cross over between the cos $\omega_n t$ (frequency) and the sin $\omega_n t$ (phase) components of the error signal of equation (6.31) occurs at the cavity HWHM frequency of 20kHz.

Figures 6.17(a)&(b) illustrate the overall magnitude and phase of the error signal due to the two components plotted in figure 6.16. As with Case 2, there is a smooth transition in both the error signal's phase and magnitude as the system moves between its frequency sensitive and its phase sensitive operating regimes.

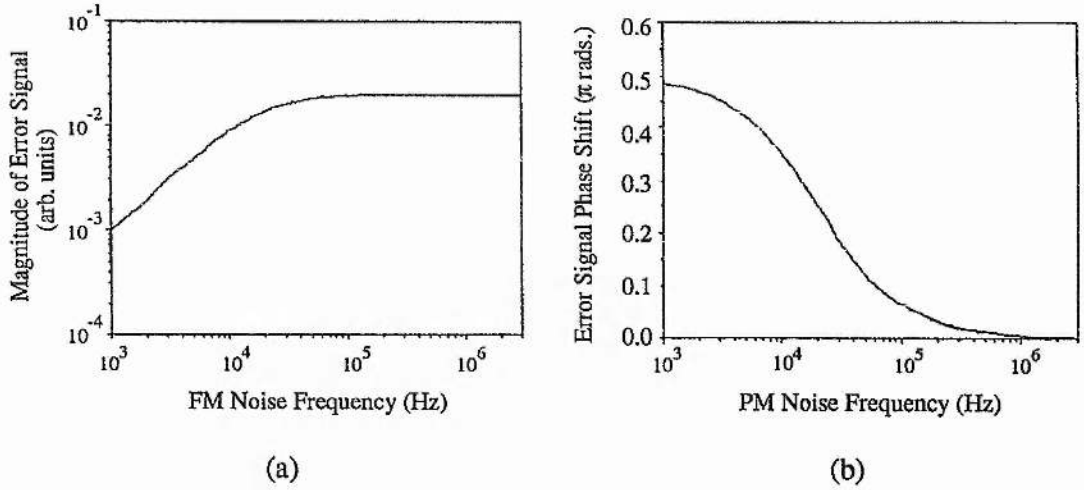

Figure 6.17. (a) Magnitude and (b) phase of the Pound-Drever error signal as functions of FM noise frequency.

Pound-Drever locking and Absolute Frequency Referencing

The technique of Pound-Drever locking may be easily extended to enable lasers to be frequency locked and referenced to rf or microwave standards. A scheme to implement this absolute referencing was realised in 1984 by De Voe and Brewer[16] and consists of two Pound-Drever locking systems operating in tandem. See figure 6.18.

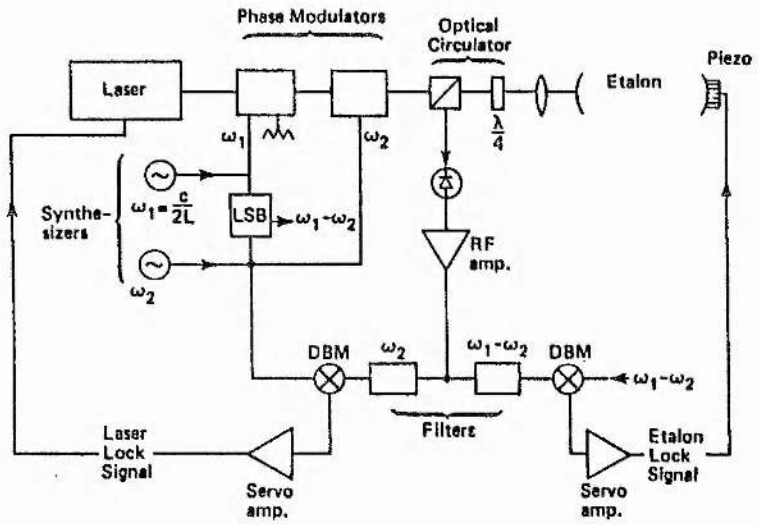

Figure 6.18. Block diagram of an optical-frequency divider showing two servo loops where the laser is locked to a reference cavity and the cavity to a radio frequency standard. LSB denotes a mixer and filter and DBM is a double balanced mixer. (Diagram from ref. 16)

As with the conventional rf locking technique, the laser output at frequency ω_o is passed through a phase modulator driven at frequency ω_1. This generates sideband components in the optical frequency domain which lie outside the reference cavity linewidth. The light beam reflected from the reference cavity is detected on a photodiode and the resulting photocurrent signal is demodulated with ω_1 to yield the familiar error signal of the Pound-Drever locking scheme. In this absolute referencing system, however, the laser output passes through a second phase modulator driven by the rf/microwave standard at frequency ω_2 . This leads to the generation of sidebands (in the lowest order) at frequencies $\omega_o \pm \omega_2$, $\omega_o \pm \omega_1 \pm \omega_2$ in addition to the first set of sidebands at $\omega_o \pm \omega_1$. The length, L, of the reference cavity is chosen so that the cavity's free spectral range, c/(2L), equals some sub-multiple of frequency ω_2. By detecting the reflected light beam from the cavity and this time demodulating in a balanced mixer with the frequency $\omega_1+\omega_2$ or $\omega_1-\omega_2$ an error signal is generated which depends on the detuning of the reference cavity free spectral range from the rf/microwave standard frequency ω_2. Thus the reference cavity length can be servo locked via this error signal to the rf/microwave standard. Locking the laser output frequency in turn to this reference cavity by means of the first Pound-Drever locking loop means that the optical frequency is related to the frequency of the rf/microwave source by the expression

$$\omega_o = n\omega_2 \tag{6.33}$$

where n is the order of the cavity fringe to which the laser frequency is locked.

With optimised servo loop design this technique should allow lasers to be absolutely frequency referenced with an accuracy approaching that of the rf/microwave standard. Conversely, the technique will enable rf or microwave sources to be frequency referenced to future high precision optical frequency standards.

6.3 Laser Linewidth Limit Under Servo Control

An estimate of the laser linewidth limit under active servo control has been carried out by Day et al[59] using the schematic representation of a laser frequency stabilisation loop shown in figure 6.19.

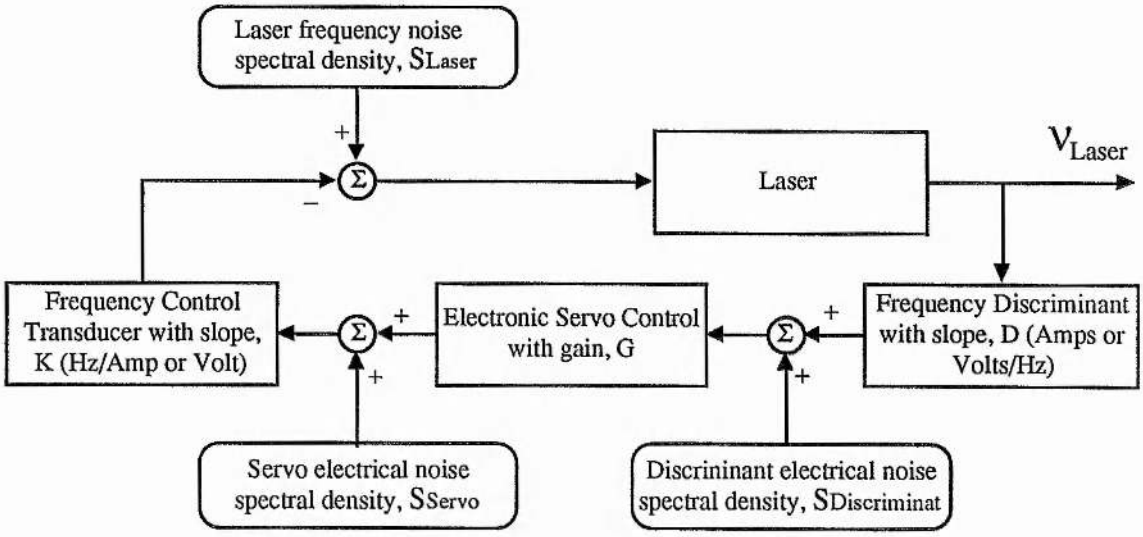

Figure 6.19. Block diagram representation of a general active laser frequency stabilisation feedback loop.

In figure 6.19 the frequency to electrical conversion slope of the discriminant is D (in units of volts/Hertz or Amps/Hertz), the gain of the servo is G and the electrical to frequency slope of the frequency transducer is given by K (Hertz/Volt or Hertz/Amp). To model the various noise sources within the loop (i.e. the laser frequency noise and electrical noise in the discriminant, servo amplifiers and frequency transducer), the appropriate noise spectral density terms S_{laser}, $S_{discriminant}$, S_{servo}, are added at the relevant points around the loop. The noise spectral density terms for the frequency transducer and the laser itself can be combined in the one term, S_{laser}, since noise added by the transducer manifests itself directly as frequency noise in the laser.

Using standard control systems theory[60] the closed loop linear spectral density of the laser frequency noise can be shown to be

$$S_{closed\text{-}loop} = \frac{\sqrt{S_{laser}^2 + (KS_{servo})^2 + (KGS_{discriminant})^2}}{1+KGD} \tag{6.34}$$

(Note: the linear spectral density is equal to the square root of the sum of the individual power spectral densities). If the gain, G, of the servo loop can be made large enough, equation (6.34) is reduced to

$$S_{closed\text{-}loop} = \frac{S_{discriminant}}{D} \tag{6.35}$$

indicating that the intrinsic frequency noise of the laser, together with any contribution from electrical noise in the servo have been completely suppressed over the servo bandwidth. Thus, under maximum active control, the laser noise is determined by the noise and slope of the discriminant.

Under ideal conditions the only inescapable noise source in the discriminant is due to photocurrent generated shot noise in the output of the photodetector and so this determines the fundamental limit to the laser linewidth reached through active control. If, under locked conditions, a fraction α, of the laser output power P, is incident on the photodetector then a photocurrent i_p is created such that

$$i_p = \frac{\eta e \alpha P}{h\nu_L} \tag{6.36}$$

where η is the detector quantum efficiency, e is the electronic charge and ν_L is the laser output frequency. This photocurrent leads to a shot noise current with a spectral density $S_{discriminant}$

$$S_{discriminant} = \sqrt{2ei_p}$$

$$= \sqrt{\frac{2e^2h\alpha P}{h\nu_L}} \tag{6.37}$$

For a discriminant based on a resonance feature of say a passive optical cavity or an atomic species, the frequency to electrical signal slope of the discriminant will in general be proportional to the laser output power and inversely proportional to the resonance linewidth, $\Delta\nu_{res}$. So for such a discriminant the frequency to current conversion, D, can be represented by

$$D = \beta \cdot \frac{e\eta\alpha P}{\Delta\nu_{res}\, h\nu_L} \tag{6.38}$$

β is a constant of proportionality and depends on the stabilisation technique used.

The lower limit to the laser frequency noise spectral density can now be calculated by substituting (6.37) and (6.38) into (6.35) to get

$$S_{closed\text{-}loop} = \frac{\Delta\nu_{res}}{\beta} \cdot \sqrt{\frac{2h\nu_L}{\eta\alpha P}} \tag{6.39}$$

Elliott et al[61] have shown that if the root-mean square (rms) of the frequency deviations due to a white noise source are large compared to the measurement bandwidth, then the observed laser spectrum has a Gaussian profile with a linewidth, $\delta\nu$, proportional to the rms frequency deviations. Under this condition, the shot noise limited linewidth will be

$$\delta\nu \propto \frac{\Delta\nu_{res}}{\beta} \cdot \sqrt{\frac{2h\nu_L B}{\eta\alpha P}} \tag{6.40}$$

where the relevant bandwidth, B, is the bandwidth of the servo loop. This is the commonly quoted form of the shot noise limited laser linewidth under servo control[11,45,62]. For a high performance laser frequency servo, however, a more realistic situation would be where the rms frequency deviations due to shot noise are small compared to the servo bandwidth. In this case the spectral lineshape of the laser emission is Lorentzian with a linewidth given by (Elliott et al[61])

$$\delta\nu_L = \pi S^2 \tag{6.41}$$

where S is the spectral density of the white noise. So the ultimate shot noise limited laser linewidth under active stabilisation will be

$$\delta\nu_{min} = \frac{2\pi h\nu_L}{\beta^2 P\alpha\eta} \cdot \Delta\nu_{res}^2 \qquad (6.42)$$

The dependence of the shot noise limited laser linewidth on $(\Delta\nu)^2$ highlights the importance of using a discriminant based on a narrow resonance feature.

In a well designed laser stabilisation system the shot noise limit to the laser linewidth may be in the region of only a few millihertz, often well below the Schawlow-Townes limit. In some recent laser frequency stabilisation experiments staggering levels of laser stability have been achieved with laser linewidths approaching their shot noise limit. For instance, by using phase sensitive detection locking (see section 6.2.2) to lock two HeNe lasers to adjacent transmission orders of a high finesse optical cavity, Salomon et al[53] measured a relative frequency stability between the two lasers which corresponded to a linewidth of only ~50mHz for each laser. In a similar type of experiment by Day et al[59], a heterodyne linewidth of 330mHz was recorded between two diode laser pumped Nd:YAG lasers locked to a high finesse reference cavity using the Pound-Drever technique. This linewidth value was only about an order of magnitude greater than the estimated limit due to electronic noise in the system. Shoemaker et al[63] also used Pound-Drever locking to lock their diode pumped Nd:YAG laser to a high finesse cavity. By measuring the noise spectral density of the output signal from the frequency discriminant they calculated the linewidth of their laser to be of the order of 1mHz, close to the expected shot noise limit for their system and over two orders of magnitude lower than the predicted Schawlow-Townes limited linewidth.

6.4 References

1 Balhorn R., Kunzmann H., Lebowsky F., "Frequency Stabilisation of internal-Mirror Helium-Neon Lasers", Appl. Opt. **11**(4) 742 (1972)

2 Niebaur T. M., Faller J. E., Godwin H. M., Hall J. L., Barger R. L., "Frequency Stability Measurements on a Polarisation Stabilised HeNe Laser", Appl. Opt. **27**(7) 1285 (1988)

3 Enloe L. H., Rodda J. L., "Laser Phase Locked Loop" Proc. IEEE **53**(2) 165 (1965)

4 SooHoo J., Hayes C. L., "Phase Locking of a Multimode to a Single mode HeNe Laser", Opt. Lett. **4**(7) 202 (1979)

5 Leeb W. R., Philipp H. K., Scholtz A. L., Bonek E., "Frequency Synchronisation and Phase Locking of CO_2 Lasers", Appl. Phys. Lett. **41**(7) 592 (1982)

6 Hall J. L., Long-Sheng M., Kramer G., "Principles of Optical Phase Locking: Application to Internal Mirror HeNe Lasers Phase Locked Via Fast Control of the Discharge Currents", IEEE J. Quant. Elec. **QE-23**(4) 427 (1987)

7 Williams K. J., Goldberg L., Esman R. D., Dagenais M., Weller J. F., "6-34GHz Offset Phase Locking of Nd:YAG 1319nm Nonplanar Ring Lasers", Elec. Lett. **25**(18) 1242 (1989)

8 Day T., Farinas A. D., Byer R. L., "Demonstration of a Low Bandwidth 1.06μm Optical Phase Locked Loop For Coherent Homodyne Communications", IEEE Photon. Tech. Lett. **2**(4) (1990)

9 Ramos R. T., Seed A. J., "Delay, Linewidth and Bandwidth Limitations in Optical Phase Locked Loop Design", Elec. Lett. **26**(6) 389 (1990)

10 Ballik E. A., "Optical Maser Frequency Stabilisation and Precise Wavelength Measurements", Phys. Lett. **4**(3) 173 (1963)

11 White A. D., "Frequency Stabilisation of Gas Lasers", IEEE J. Quant. Elec. **QE-1**(8) 349 (1965)

12 Richard J. P., Hamilton J. J., "Cryogenic Monocrystalline Silicon Fabry-Perot Cavity For the Stabilisation of Laser Frequency", Rev. Sci. Instrum., **62**(10) 2375 (1991)

13 Tsuchida H., Mitsuhashi Y., "Novel Ring Interferometer For Frequency Stabilisation of Semiconductor Lasers", Appl. Opt. **27**(2) 302 (1988)

14 Franzen D. L., Kim E. M. "Long Optical Fibre Fabry-Perot Interferometer", Appl. Opt. **20**(23) 3991 (1981)

15 Yue C. Y., Peng J. D., Liao Y. B., Zhou B. K., "Fibre Ring Resonator With Finesse of 1260", Elec. Lett. **24**(10) 622 (1988)

16 De Voe R. G., Brewer R. G., "Laser Frequency Division and Stabilisation", Phys. Rev. A. **30**(5) 2827 (1984)

17 Fabre C., De Voe R. G., Brewer R. G., " Ultrahigh Finesse Optical Cavities", Opt. Lett. **11**(6) 365 (1986)

18 Newport Product Catalogue, Newport Corporation (U. S. A.) (1992)

19 Amaya P., Masser C., "Ultra-Low-Loss Optics", Lasers and Optronics **11**(6) 7 (1992)

20 Shimoda K., "High Resolution Laser Spectroscopy", Topics in Applied Physics **13** Springer-Verlag (1976)

21 Wallard A. J., "Frequency Stabilisation of the Helium-Neon Laser by Saturated Absorption in Iodine", J. Phys. E: Sci. Instrum. **5** 926 (1972)

22 Rowley W. R. C., Wallard A. J., "Wavelength Values of the 633nm Laser Stabilised with $^{127}I_2$ Saturated Absorption", J. Phys. E: Sci. Instrum. **6** 647 (1973)

23 Hanes G. R., Baird K. M., De Remigis J., "Stability, Reproducibility and Absolute Wavelength of a 633nm HeNe Laser Stabilised to an Iodine Hyperfine Component", Appl. Opt. **12**(7) 1600 (1973)

24 Wallard A. J., "A Practical Approach to the Design and Construction of Iodine Stabilised Lasers", National Physical Laboratory, U. K., report QU51 (1979)

25 Berger R. L., Hall J. L., "Pressure Shift and Broadening of Methane Line at 3.39μm Studied by Laser Saturated Molecular Absorption", Phys. Rev. Lett. **22**(1) 4 (1969)

26 Gnativskii A. V., "Concerning the Reproducibility of the Frequency of the Laser Stabilised to the Transition of the Absorbing Gas", JETP Lett. **19**(6), 205 (1974)

27 Belenov E. M., "Spectroscopic Investigation of Power Resonances in a Ring HeNe/CH_4 Laser", Sov. J. Quant. Electon. **9**(7), 876 (1979)

28 Kruzhalov S. V., Parfenov V. A., Pakhomov L. N., Petrun'kin V. Y., "Frequency Stabilisation of a Nd:YAG Laser by Means of $^{127}I_2$ Absorption Lines", Sov. Tech. Phys. Lett. **11**(3) 111 (1985)

29 Arie A., Schiller S., Gustafson E. K., Byer R. L., "Absolute Frequency Stabilisation of Diode Laser Pumped Nd:YAG Lasers to Hyperfine Transitions in Molecular Iodine", Opt. Lett. **17**(17) 1204 (1992)

30 Orlov O. A., Ustyugov V. I., "Molecular Caesium Reference Point For Frequency Stabilisation of the Nd:YAG Laser at 1.06μm", Sov. Tech. Phys. Lett. **12**(3) 120 (1986)

31 Walsh C. J., "Optogalvanic Fluctuations in a Waveguide CO_2 Laser", J. Phys. D: Appl. Phys. **18** 789 (1985)

32 Kapoor R., Suri B. M., Saksena G. D., "Wavelength Control for a Pulsed Dye Laser Using the Optogalvanic Effect", J. Phys. E: Sci. Instrum. **18** 930 (1985)

33 Shy J. T., Yen T. C., "Optogalvanic Lamb Dip Frequency Stabilisation of a CO_2 Laser", Opt. Comm. **60**(5) 306 (1986)

34 McFarlane R. A., Bennett W. R., Lamb W. E., "Single Mode Tuning Dip in the Power Output of a HeNe Optical Maser", Appl. Phys. Lett. **2**(10) 189 (1963)

35 Shimoda K., Javan A., "Stabilisation of the HeNe Laser on the Resonance Line Centre", J. Appl. Phys. **36**(3) 718 (1965)

36 White A. D., Gordon E. I., Labuda E. F., "Frequency Stabilisation of Single Mode Gas Lasers", Appl. Phys. Lett. **5**(5) 97 (1964)

37 Tobias I. Skolnick M. L., Wallace R. A., Rolanti T. G., "Deviation of a Frequency Sensitive Signal From a Gas Laser in an Axial Magnetic Field", Appl. Phys. Lett. **6**(10) 198 (1965)

38 Weis A., Derler S., "Doppler Modulation and Zeeman Modulation: Laser Frequency Stabilisation Without Direct Frequency Modulation", Appl. Opt. **27**(13) 2662 (1988)

39 Baird K. M., Hanes G. R., "Stabilisation of Wavelengths From Gas Lasers", Rep. Prog. Phys. **37** 927 (1974)

40 Kerr A. G., "Experimental Development Towards a Long-Baseline Laser Interferometer Gravitational Radiation Detector", Ph. D. Thesis, University of Glasgow, U. K., (1986)

41 Kerr G. A., Robertson N. A., Hough J., Man C. N., "The Fast Frequency Stabilisation of an Argon Laser to an Optical Resonator Using An Extra-Cavity Electro-Optic Modulator", Appl. Phys. B **37** 11 (1985)

42 Jitschin W., Meisel G., "Fast Frequency Control of a CW Dye Jet Laser", Appl. Phys. **19** 181 (1979)

43 Enscoe R. F., Kocka R. J., "Electro-Optic Modulation: Systems and Applications", Lasers and Applications pp91-95 June 1984

44 Barger R. L., West J. B., English T. C., "Fast Frequency Stabilisation of a CW Dye Laser", Appl. Phys. Lett. **27**(1) 31 (1975)

45 Helmcke J., Lee S. A., Hall J. L., "Dye Laser Spectrometer for UltraHigh Spectral Resolution: Design and Performance", Appl. Opt. **21**(9) 1686 (1982)

46 Hall J. L., Layer H. P., Deslattes R. D., "An Acoustooptic Frequency and Intensity Control System for CW Lasers", IEEE J. Quant. Elec. **QE-13** 45D (1977)

47 Hall J. L., Hänsch T. W., "External Dye Laser Frequency Stabiliser", Opt. Lett. **9**(11) 502 (1984)

48 Barger R. L., Sorem M. S., Hall J. L., "Frequency Stabilisation of a CW Dye Laser", Appl. Phys. Lett. 22(11) 573 (1973)

49 Gerhardt H., Tittel F. K., "A Frequency Stabilised CW Dye Laser for High Resolution Spectroscopy", Opt. Comm. **16**(3) 307 (1976)

50 Vassen W., Zimmermann C., Kallenback R., Hansch T. W., "A Frequency Stabilised Titanium Sapphire Laser for High Resolution Spectroscopy", Opt. Comm. **75**(5,6) 435 (1990)

51 Yeo S. P., Ang A. L., "Optical Frequency Stabilisation and Linewidth Reduction of a Multielectrode DFB Laser with Current Feedback", Elec. Lett. **23**(21) 1161 (1987)

52 Nakazawa M., "Phase-Sensitive Detection on Lorentzian Line Shape and its Application to Frequency Stabilisation of Lasers", J. Appl. Phys. **59**(7) 2297 (1986)

53 Salomon Ch., Hils D., Hall J. L., "Laser Stabilisation at the millihertz Level", J. Opt. Soc. Am. B **5**(8) 1576 (1988)

54 Troitskii Y. V., "Optimization and Comparison of The Characteristics of Optical Interference Discriminators", Sov. J. Quant. Elec. **8**(5) 628 (1978)

55 Drever R. W. P., Hall J. L., Kowalski F. V., Hough J., Ford G. M., Munley A. J., Ward H., "Laser Phase and Frequency Stabilisation Using an Optical Resonator", Appl. Phys. B **31** 97 (1983)

56 Hänsch T. W., Coullaud B., "Laser Frequency Stabilisation by Polarisation Spectroscopy of a Reflecting Reference Cavity", Opt. Comm. **35**(3) 441 (1980)

57 Pound R. V., "Electronic Frequency Stabilisation of Microwave Oscillators", Rev. Sci. Instrum. **17** 490 (1946)

58 Taub H., Schilling D. L., "Principles of Communication Systems", McGraw-Hill (1971)

59 Day T., Gustafson E. K., Byer R. L., "Sub-Hertz Relative Frequency Stabilisation of Two Diode Laser Pumped Nd:YAG Lasers Locked to a Fabry-Perot Interferometer", IEEE J. Quant. Elec. **28**(4) 1106 (1992)

60 Hostetter G. H., Savant Jr C. J., Stefani R. T., "Design of Feedback Control Systems", Holt-Saunders International Editions (1982)

61 Elliott D. S., Roy R., Smith S. J., "Extracavity Laser Band-Shape and Bandwidth Modification", Phys. Rev. A **26**(1) 12 (1982)

62 Polanyi T. G., Tobias I., "The Frequency Stabilisation of Gas Lasers", Lasers Volume 2, Ed: Levine A. K., Pub: Edward Arnold Ltd., London (1968)

63 Shoemaker D., Brillet A., Nary Man C., Crégut O., Kerr G., "Frequency Stabilised Laser Diode Pumped Nd:YAG Laser", Opt. Lett. **14**(12) 609 (1989)

Chapter 7

EXPERIMENTAL IMPLEMENTATION OF POUND-DREVER LOCKING

7.1 Experimental Details

Using the Pound-Drever locking system described in Chapter 6 and illustrated in figure 6.4, the diode pumped, twisted mode Nd:YAG laser was frequency stabilised to a custom built ultranarrow linewidth (FWHM~40kHz) optical reference cavity. The following sections detail the various elements of the stabilisation experiment and the level of laser frequency stability achieved using this system.

7.1.1 Phase Modulation of the Laser Output

The compressed and collimated output beam from the laser was phase modulated at approximately 1MHz via a four crystal, AD*P, transverse field electro-optic (EO) modulator (Gsänger model LM0202-IR). The choice of modulation frequency in this case was mainly determined by the frequency limitations of the rf oscillator used. Ideally, phase modulation should be added at a frequency where the laser output intensity is shot noise limited because the Pound-Drever system is susceptible to intensity noise around the phase modulation frequency. Work by T. J. Kane[1] on intensity noise in monolithic diode pumped single frequency Nd:YAG lasers has indicated that for such lasers the photoelectric shot noise limit is reached at frequencies greater than 20MHz for photodetector currents up to 4.4mA. So for optimum performance of this locking technique in diode pumped Nd:YAG laser systems, phase modulation frequencies of at least a few tens of megahertz should be use.

An indication of the amplitude of the voltage signal required to drive the EO modulator can be calculated from

$$\frac{V}{V_\pi} \times \frac{\pi}{2} = M \tag{7.1}$$

where V is the drive voltage amplitude, V_π is the modulator half wave voltage (voltage required to produce a π phase shift between the components of the optical field along the fast and slow axes of the modulator) and M is the desired phase modulation index. For instance, the phase modulator used in these experiments had a measured half wave voltage of (321± 4)V and so to achieve a modulation index of 0.5 would require a drive signal with an amplitude of about 100V. Drive voltages up to this level were conveniently generated by multiplying the output voltage from a conventional low voltage (10V amplitude into 1MΩ load) rf oscillator using a hand wound step-up transformer. With this arrangement however, the almost purely capacitive load of the EO modulator, in conjunction with the inductance of the transformer secondary coil, forms a tuned LC circuit which must be made to resonate in order to develop the maximum voltage across the modulator. Through a process of trial and error a transformer was wound with suitable secondary inductance to cause resonance at around 1MHz, whilst providing adequate voltage multiplication (~10:1). Fine tuning of the LC resonance frequency was accomplished by varying the insertion depth of a ferrite core into the cylindrical coil former of the transformer. Using this phase modulator drive circuitry a phase modulation index of between 0.4 and 0.5 could be applied to the laser beam with modulation frequencies tuneable from 470kHz to 1.055MHz.

Careful alignment of the EO modulator was found to be critical in order to prevent the modulator contributing any intensity modulation to the laser beam. The presence of intensity modulation added in this way leads to undesirable offsets in the demodulated error signal. To align the modulator, the device was initially set up as an intensity modulator between crossed linear polarisers and then rotated about its optical axis until

the intensity modulation was minimised. Any residual intensity modulation could then be removed by small angular adjustments of the modulator axis.

7.1.2 The Optical Isolator

After the phase modulation had been added to the laser beam, the beam was passed through a Faraday effect optical isolator before finally being mode matched into the ultrahigh finesse optical reference cavity. The isolator served the dual functions of protecting the laser from the perturbing effects of optical feedback and also redirecting the retro-reflection from the on axis reference cavity towards the fast photodetector at the input stage of the frequency stabilisation electronics.

7.1.3 The Ultra-Narrow Linewidth Reference Cavity

One of the benefits of the Pound-Drever laser frequency locking technique is its ability to easily lock on to the very sharp resonance features of high finesse reference cavities. As discussed previously in section 6.3 the use of very sharp frequency references in laser frequency stabilisation schemes is highly desirable since the fundamental shot noise limited laser linewidth possible under active control is proportional to the square of the optical reference cavity linewidth[2,3]. To take advantage of this property, an ultra-narrow linewidth optical reference cavity was constructed which displayed a finesse of ~12,500 and a full width at half maximum instrumental linewidth of only 40kHz. The specialised mirrors, supplied by Newport Corporation (Fountain Valley, California, U.S.A.), used to attain such a high cavity finesse are manufactured using advanced substrate polishing techniques and ion beam sputter coating to achieve mirror reflectivities in excess of 99.99% and losses of the order of 50 parts per million[4].

Cavity Geometry

The two concave mirrors forming this symmetric high finesse reference interferometer were mounted on top of a 50mm diameter invar bar which functioned as an optical rail. This mechanical design enabled the mirror separation to be easily altered whilst providing adequate mechanical stability. Coarse adjustment of the cavity length was accomplished simply by sliding the gimbal mount holding the cavity output mirror along the invar rail. For finer control over the mirror spacing the bracket supporting the cavity input mirror was mounted on a linear translation stage which had a positioning resolution of 0.5μm. The steel bracket holding the cavity input mirror was designed such that it, in conjunction with the steel translation stage, gave some thermal compensation for temperature induced length changes in the invar bar. Angular alignment of the resonator was provided by the two-axes gimbal mirror mount.

To simplify beam alignment into such a high finesse optical cavity, the cavity was initially set up in the confocal geometry with the two 300mm radius of curvature mirrors spaced 300mm apart on the invar bar. The transverse modes of such a cavity are degenerate in frequency and so the requirement for selectively exciting only one transverse mode (mode matching) is greatly relaxed[5]. This freedom from mode matching is however at the expense of precise setting of the mirror spacing. The amount of mismatch, ε, from exact confocal mirror spacing which can be tolerated before transverse mode frequency degeneracy is noticeably lost can be calculated from the standard resonance expression for a symmetric spherical mirror cavity;

$$\nu_{mnq} = \frac{c}{2L} \cdot \left\{ q + \frac{(1+m+n)}{\pi} \cdot \cos^{-1}\left(1 - \frac{L}{r}\right) \right\} \tag{7.1}$$

where ν_{mnq} is the resonance frequency of the TEM_{mnq} cavity mode with q being the longitudinal mode number and m and n being the transverse mode numbers. L is the mirror separation and r the mirror radius of curvature. For an exactly confocal cavity

(L=r) the resonance frequency for a general TEM_{mnq} cavity mode can be expressed in terms of the lowest order transverse mode frequencies as

$$\begin{aligned} \nu_{mnq} &= \nu_{00(q+\frac{m+n}{2})} && \text{for (m+n) even} \\ \nu_{mnq} &= \nu_{01(q-1+\frac{m+n}{2})} && \text{for (m+n) odd} \end{aligned} \tag{7.2}$$

and so the interferometer is said to be two-fold mode degenerate. If the mirror spacing is then adjusted off exact confocallity by a small amount ε, such that L=r±ε, the equalities of equation (7.2) will no longer hold and a small frequency difference, Δν, will be introduced. Providing that Δν does not exceed the minimum resolvable frequency interval of the interferometer the cavity will remain mode degenerate. This sets an upper limit on the amount of cavity detuning, ε, which can be tolerated. If, for convenience, the minimum resolvable frequency interval of the interferometer is defined as the transmission FWHM (this is similar to the Rayleigh criterion) then the maximum permissible detuning of the cavity length is

$$\begin{aligned} |\varepsilon|_{max} &= \frac{r\pi}{(m+n)\mathcal{F}} && \text{for (m+n) even} \\ |\varepsilon|_{max} &= \frac{r\pi}{(m+n-1)\mathcal{F}} && \text{for (m+n) odd} \end{aligned} \tag{7.3}$$

where $\mathcal{F}$ is the cavity finesse defined by $\mathcal{F}= (c/2L)/\Delta\nu_{FWHM}$. In the case of the ultra-high finesse reference cavity with L≈300mm and $\mathcal{F}$=12,500, if the input beam excites transverse modes up to say (m+n)=10 then the cavity length must be within $|\varepsilon|_{max}$ = 7.5μm of the exact confocal mirror spacing. This degree of alignment should be possible given the positioning resolution of the translation stage on the interferometer.

In practice it was found that the transverse mode frequencies of the interferometer would not collapse to the mode degenerate regime. This was possibly due to a mis -

match in the radius of curvature of the two mirrors rather than an error in the mirror spacing. Unfortunately tolerance data on the mirror curvatures were not available from the suppliers to allow confirmation of this. This inability to reach mode degeneracy dictated that the interferometer had to be operated in a non-confocal geometry and that the input beam was mode matched to the fundamental cavity mode. The cavity length was extended to 310mm giving a transverse mode frequency splitting of 10MHz. This frequency separation was large enough so that higher order transverse mode resonances of the reference cavity did not interfere with the rf phase modulated sidebands imposed on the frequency of the input beam.

Mode-Matching

Mode-matching of the input Gaussian beam to the fundamental mode of the reference cavity requires that the position and size of the laser beam waist matches the position and size of the reference cavity TEM_{00} mode and that the optical axes of both beam and cavity are collinear. Kogelnik[6] showed that the appropriate transformation of a beam of waist size w_1 into a beam of waist size w_2 could be accomplished by a single thin lens as illustrated in

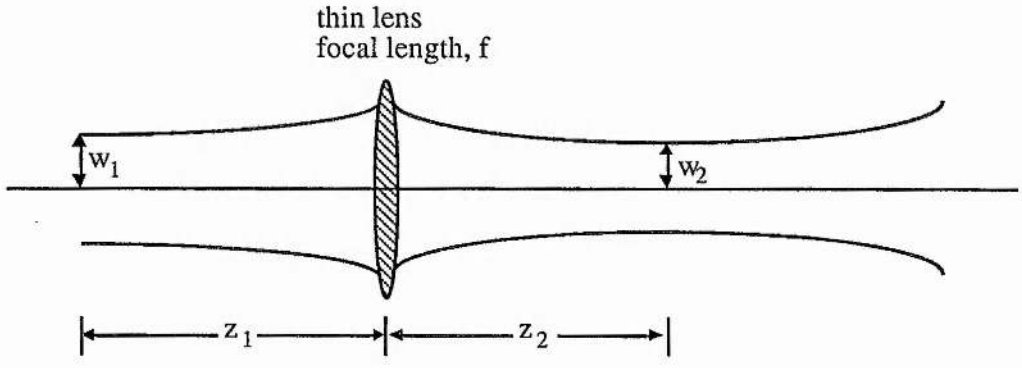

Figure 7.1. Gaussian beam transformation by a thin lens

figure 7.1. For matching to be possible the focal length, f, of the lens must exceed a characteristic length, f_o, defined by

$$f_o = \frac{\pi w_1 w_2}{\lambda} \tag{7.4}$$

Having chosen f, the distances of the initial and transformed waists from the lens, z1 and z2 respectively, can be calculated from the matching formulae

$$z_1 = f \pm \frac{w_1}{w_2}\sqrt{f^2 - f_o^2}$$

$$z_2 = f \pm \frac{w_2}{w_1}\sqrt{f^2 - f_o^2} \tag{7.5}$$

In the particular optical layout used, the location of the input beam waist, w_1, was taken to lie at the output lens of the beam collimating telescope. The beam radius at this point was measured using a scanning pinhole to be w_1=750μm. The beam waist in the 310mm long reference cavity was calculated to be w_2=225.33μm as shown in figure 7.2 giving a characteristic

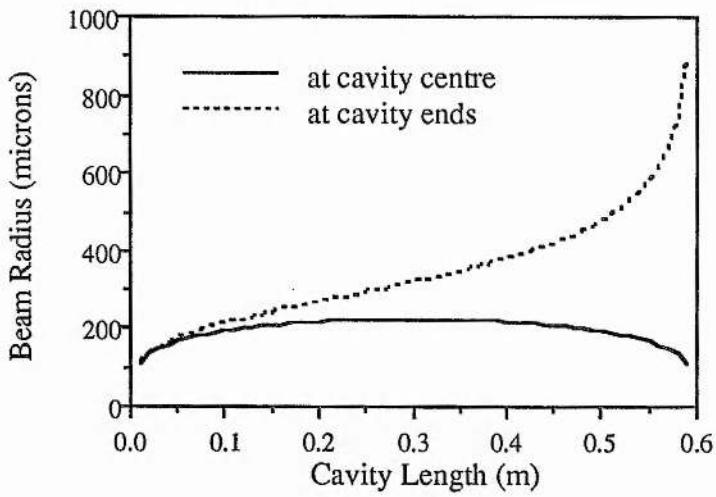

Figure 7.2. Curves showing the calculated radius of the TEM_{00} mode at the cavity mirrors and at the mode waist for a symmetric spherical mirror cavity (mirror curvature=0.3m).

length, f_o of 0.499m. For mode matching to be possible the focal length of the matching lens must be greater than this characteristic length. A lens with a focal length of 0.571m

was selected and the distances d_1 and d_2 were then calculated from equations (7.5) as 1.49m and 0.65m respectively. In practice these separations between w_1 and the matching lens and from the lens to w_2 could only be set at best to the nearest centimetre. Nontheless reasonable mode matching was achieved using this arrangement. A variety of other matching lenses with focal lengths in the vicinity of the calculated value of 0.571m were also tested. The best mode matching results were obtained using a 0.5m focal length lens located 1.67m from the input beam waist and 0.49m from the reference cavity waist.

Cavity Alignment Procedure

Since the reflectivity of the ultra-high finesse reference cavity mirrors was so large (R>99.99%) the input beam had to be reasonably well aligned to the cavity axis before any measurable transmission through the cavity could be observed. Preliminary alignment of the beam was performed by replacing the cavity input and output mirrors by a pinhole and a centred target respectively. The spatial position and angle of the input beam was then manipulated by means of two beam steering mirrors so that the beam lay along the axis defined by the pinhole and target. The cavity output mirror was substituted for the target and its tilt angle adjusted (via the gimbal mount) to maximise the beam transmission back through the pinhole. Finally the cavity input mirror was put in position and its tilt angle set to retro-reflect the input laser beam. If this alignment procedure was followed with care reasonable levels of optical transmission through the cavity were recorded when the laser frequency was scanned through a resonance of the reference cavity.

Due to residual alignment errors between the input beam and cavity axes, several higher order transverse modes of the cavity were usually excited. This meant that the near confocal cavity displayed a free spectral range of approximately c/4L after this initial alignment procedure. To aid the final optimisation of beam alignment and mode matching, the laser frequency was repeatedly scanned through a few free spectral ranges

of the reference cavity and the transmission of the cavity was synchronously displayed on an oscilloscope. Whilst monitoring this cavity transmission, small angular adjustments were then made to the beam steering mirrors guiding the beam into the cavity. As the beam axis was brought into alignment with the cavity axis, fewer higher order transverse modes were excited and so the amplitude of alternate transmission maxima diminished while the amplitude of the remaining transmission peaks grew. This effect is illustrated in figure 7.3. Eventually the cavity free spectral range became c/2L indicating that good matching of the input beam to the fundamental mode of the cavity had been achieved.

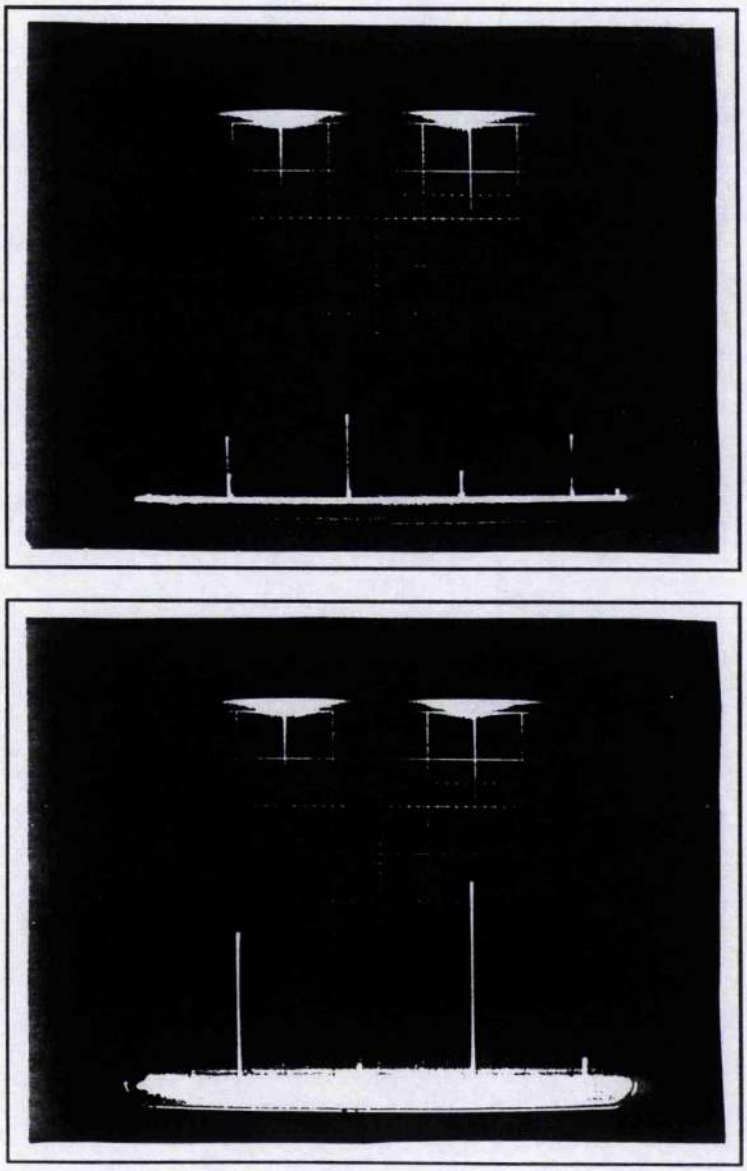

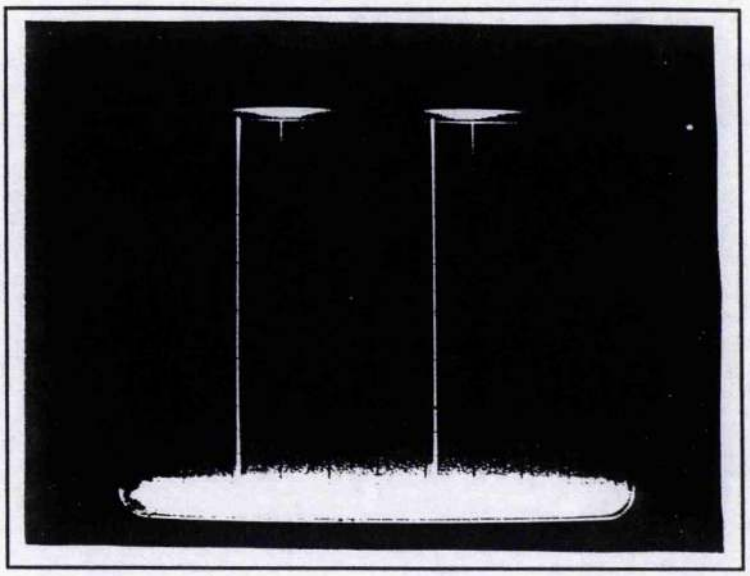

Figure 7.3. The output spectrum of the single frequency Nd:YAG laser viewed on the ultra-high finesse reference cavity as the cavity mode matching condition is approached. The amplitude of every other transmission peak decreases until the c/4L free spectral range becomes c/2L for perfect mode matching.

Performance

After careful alignment and mode matching, the cavity transmission showed at most three other resonances due to excitation of higher order transverse modes. The amplitudes of these modes, however, were small at around -20dB relative to the transmission of the TEM_{00} mode.

The overall transmission efficiency, defined as the ratio of the input optical power to the peak output power in the TEM_{00} mode of the reference cavity, was measured to be between 3% and 8% depending on the mirror set used. Similarly the reflection efficiency (ratio of the on resonance reflected power in the TEM_{00} mode to the total power reflected from the cavity off resonance) was measured to be typically around 72%.

Calibration of the reference cavity linewidth was performed by phase modulating the laser beam at a known frequency and then linearly scanning the frequency of the laser carrier and accompanying modulation sidebands through a resonance of the reference

cavity. The resulting cavity transmission of the laser carrier and its symmetrically spaced phase modulation sidebands was displayed on an oscilloscope (see figure 7.4) enabling the cavity transmission linewidth to be measured as a function of the imposed modulation sideband spacing.

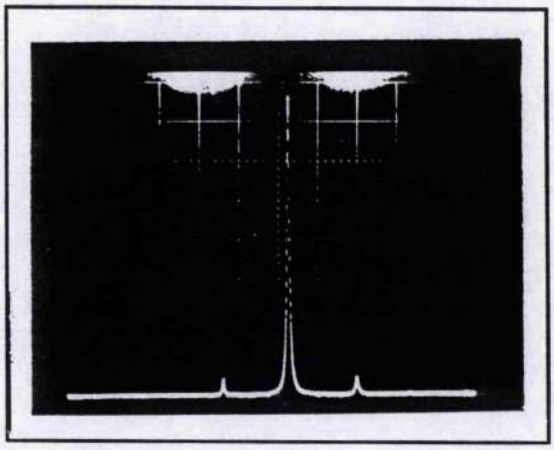

Figure 7.4 Ultra high finesse reference cavity transmission showing imposed modulation sidebands on either side of the laser carrier frequency. Sideband spacing is ± 1.053MHz from the carrier.

7.1.4 Characterisation of the Laser Frequency Transducer

For the diode laser pumped Nd:YAG lasers used in this work, the laser cavity length and hence laser output frequency was controlled by mounting the output coupler mirror on a piezoceramic translator. This frequency transducer unit is shown in cross-section in figure 7.5.

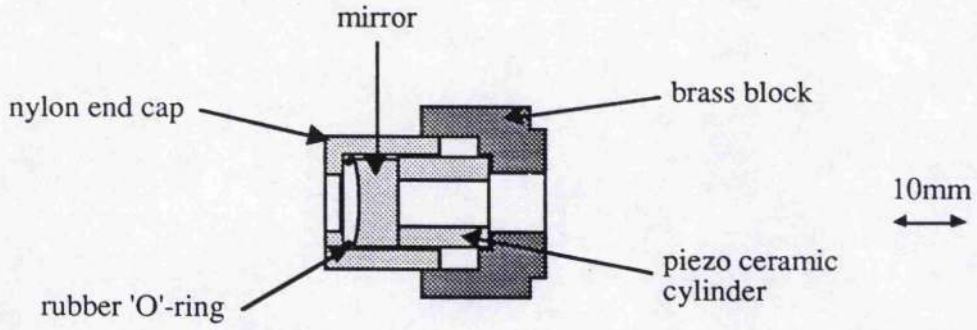

Figure 7.5. The diode laser pumped Nd:YAG laser frequency transducer.

The piezo material used in the transducer was a modified lead zirconate titanate ceramic (Vernitron type PZT-5H) in the form of a cylinder 12.7mm long × 12.7mm in diameter and with a wall thickness of 3.18mm. A standard 12.7mm diameter × 6.4mm thick fused silica substrate (supplied and coated by Laser Optik, Germany) with a mass of ~1.8grams was used for the laser output coupler mirror. To help reduce hysteresis in the displacement versus applied voltage characteristics of the piezoceramic and also to eliminate any unwanted mechanical movement between the various transducer components, the transducer was preloaded[7]. The preload was applied by clamping the mirror and piezoceramic between the brass block and the threaded nylon end cap. A rubber 'O'-ring, placed between the mirror and the nylon end cap protected the mirror from damage and acted as a stiff spring against which the piezoceramic could push.

An important consideration in the design of an active laser frequency servo is the bandwidth of the frequency transducer. In the case of the piezoceramic transducer, the maximum frequency response is limited by the first mechanical resonance. A mechanical resonance in the transducer is accompanied by a sharp change in the electrical impedance of the piezoceramic and so the resonance behaviour of the piezo can be analysed simply by monitoring its electrical characteristics[8,9]. The test circuit used to analyse this resonant behaviour is shown in figure 7.6.

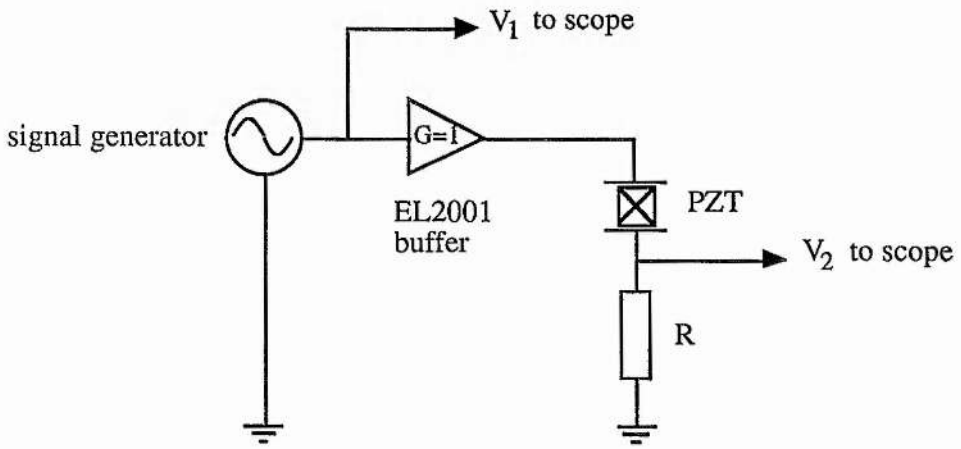

Figure 7.6. Series impedance circuit for measuring resonances in the piezo frequency transducer.

On resonance it was found that the impedance of the piezo dropped to a small value. So, to prevent loading of the signal generator and to maintain a constant voltage amplitude across the piezo-R combination, it was necessary to isolate the signal generator from the piezo by means of a low output impedance, large drive current, unity gain buffer amplifier (Elantec EL2001). The frequency dependent impedance of the transducer was monitored by measuring the phase (relative to the output voltage signal) and amplitude of the current flowing in the circuit. A small resistor, R, acted as a current to voltage converter and the voltage developed across R was displayed on an oscilloscope. To prevent resistor R from influencing this current measurement its resistance value was kept small compared to the impedance of the piezoceramic. The transducer impedance and the phase of the current relative to the supply voltage, V_2 are shown as a function of frequency in figure 7.7.

The straight line portion of the log-log impedance versus frequency plot of figure 7.7(a) and the corresponding 90° phase lag between the current and the drive voltage shown in figure 7.7(b) indicate that at low drive frequencies the transducer exhibits a purely capacitive electrical load. From the slope of the impedance graph the transducer capacitance was calculated to be (2.77±0.07)nF. The first electrical resonance (and therefore mechanical resonance) was centred around ~140kHz and can clearly seen in

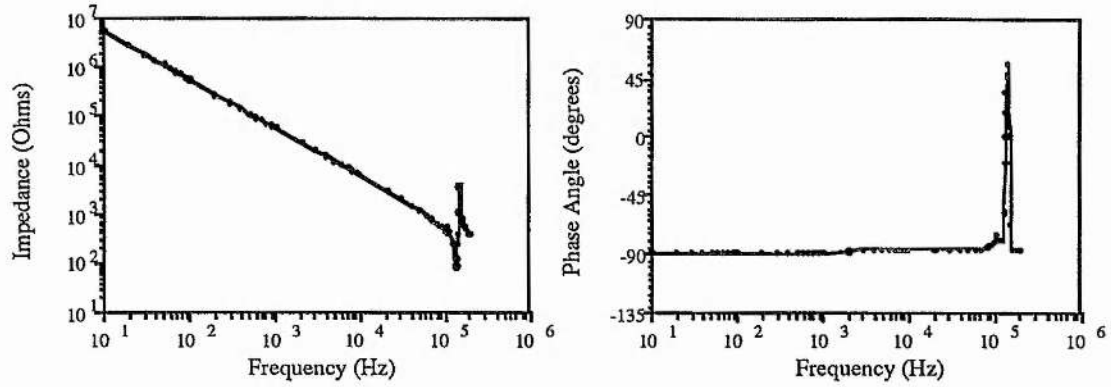

Figure 7.7. (a) Transducer impedance and (b) phase of the current through the transducer relative to the drive voltage.

figure 7.7 as a sharp change in both the impedance of the transducer and the phase of the current. Therefore, this particular laser frequency transducer had a relatively large, safe usable bandwidth of ~100kHz.

The voltage to frequency sensitivity of the transducer was measured by using the transducer to linearly sweep the laser frequency through a free spectral range of the calibrated ultrahigh finesse reference cavity. In this way a value of 4.2MHz/volt was obtained.

7.1.5 The Stabilisation circuitry

A simplified block diagram of the detection and servo control electronics used in the Pound-Drever locking experiment is given in figure 7.8.

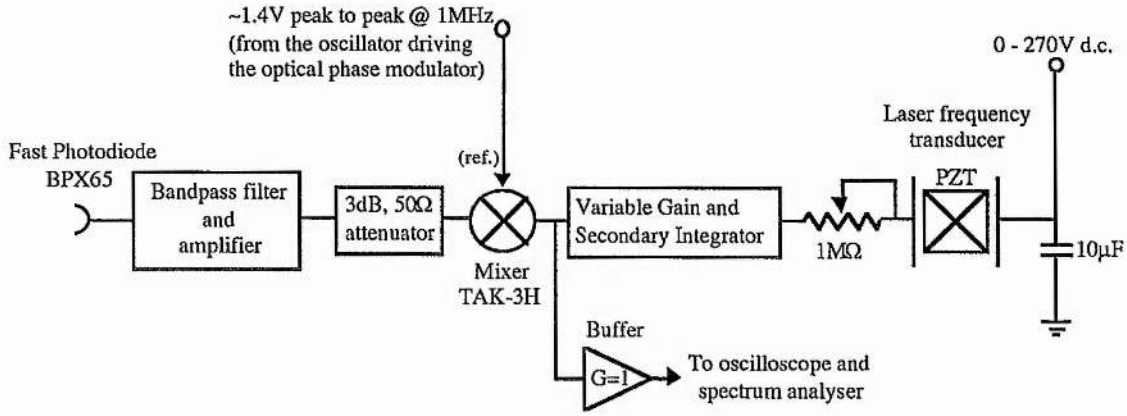

Figure 7.8. Block diagram of the Pound-Drever electronics.

Interaction of the phase modulated laser beam with the on or near resonance reference cavity encoded the error signal information on the beam retro-reflected from the reference cavity in the form of an intensity modulation around the original phase modulation frequency. This intensity modulation was picked up using the sensitive band pass optical detector shown in figure 7.9. A tuned LC load on the fast photodiode output provided the band pass effect together with resonant enhancement of the small detected signal. The increased signal circulating in the tuned LC circuit was accessed via a

capacitive tap and further amplified by a factor of 200 in a fast ac coupled video amplifier.

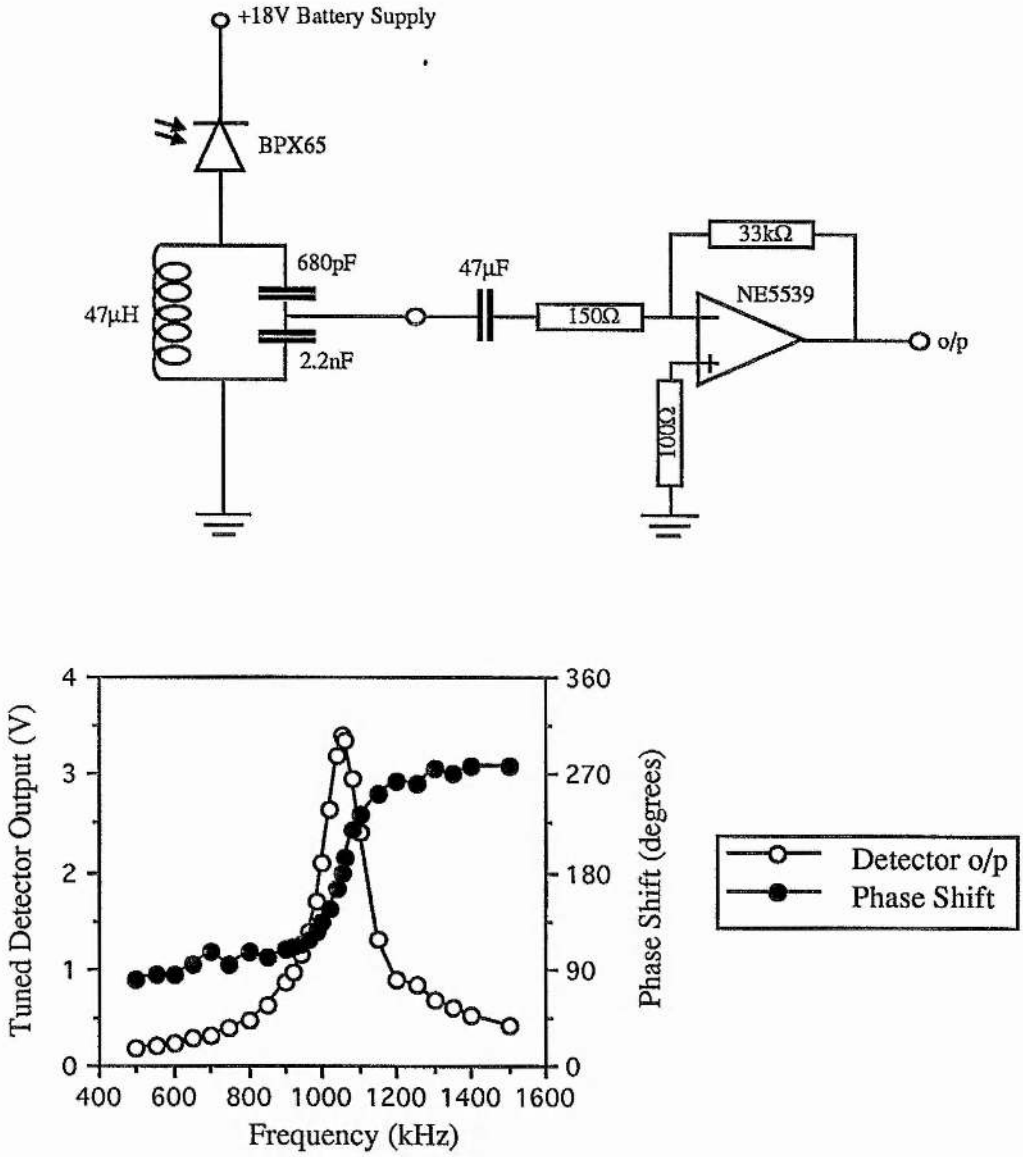

Figure 7.9. The circuit diagram of the tuned photodetector and fast video amplifier together with the circuits frequency and phase response to intensity modulated light. This band pass detector has a centre frequency of 1.050MHz, a FWHM bandwidth of 150kHz and a phase shift of 123° across this bandwidth.

Demodulation of the amplifier output against a portion of the original rf phase modulator drive source then took place in a double balanced mixer (Minicircuits model TAK-3H) to extract the "rf fringe" locking discriminant for the laser frequency servo

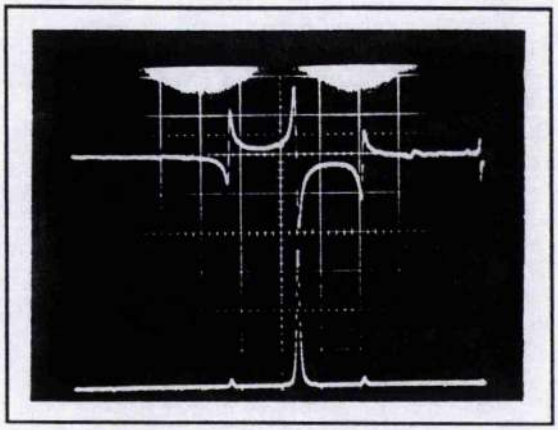

Figure 7.10. The lower trace shows the reference cavity transmission as the laser frequency is swept through one of the cavity resonances. The small rf sidebands produced by phase modulation of the laser output are clearly visible on either side of the main carrier peak. The upper trace is the corresponding locking discriminant recorded from the output of the double balanced mixer.

system. A typical example of the discriminant obtained from the mixer output is shown in figure 7.10. It is worth noting at this point that the function of the 3dB, 50Ω attenuator on the output of the bandpass detector (see figure 7.8) was to prevent the resonance frequency and output level of the tuned detector from being influenced by back reflected signal from the mixer. Far from reducing the signal level at the mixer input, the inclusion of the attenuator actually gave a 20 fold increase in this signal level compared to either direct coupling or coupling through a 50Ω terminator between the detector and the mixer.

The servo electronics used to process the discriminant signal from the mixer output were based on an NPL circuit for an I_2 stabilised HeNe laser system. The modified circuit, illustrated in figure 7.11, provides a variable voltage gain ranging from 0.04 up to 1200 with a flat frequency response from D.C. to just over 1kHz. Above 1kHz the gain curve of the amplifier response rolls-off at 6dB/Octave.

As discussed in section 6.1.2, it is necessary to alter this flat gain vs frequency response such that the gain rolls-off to the unity gain point at a slope of -6dB/octave. This primary integration effect is achieved by a passive RC integrator/low pass filter network formed by placing a variable resistor in series with the purely capacitive load of

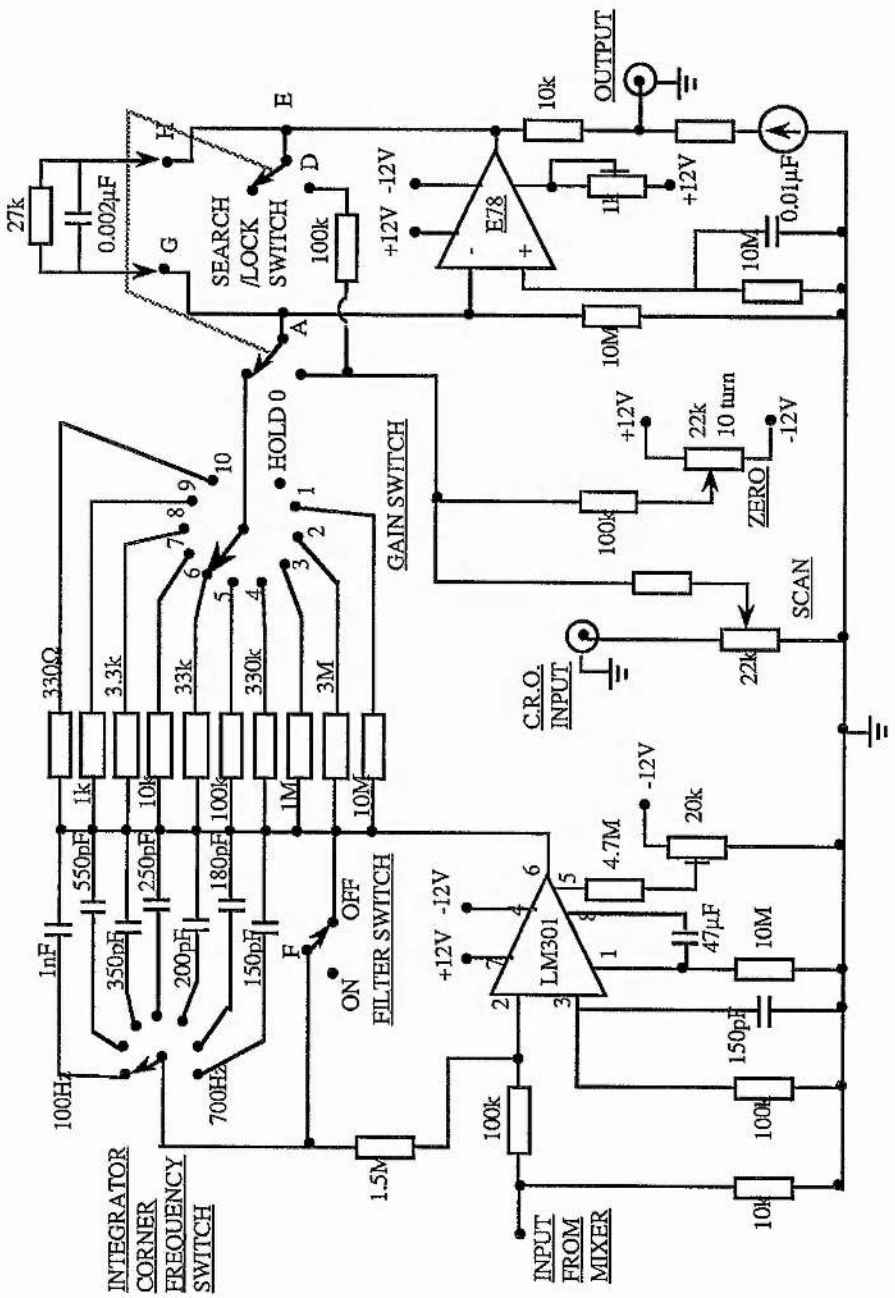

Figure 7.11. The amplifier/integrator circuit for the laser frequency servo.

the PZT laser frequency transducer. When operating the servo system in practice it was necessary to set the series resistance to 970kΩ giving a 3dB corner frequency for the integrator of ~50Hz.

An additional active OP-AMP integrator could be switched into the circuit in order to increase the slope of the gain vs frequency curve to 12dB/Octave at low frequency to achieve larger loop gains. The 3dB crossover frequency from the -12dB/Octave slope of the double integrator to the -6dB/Octave slope of the single integrator could be varied from 100 - 700HZ in steps of 100Hz.

7.2 Pound-Drever Locking Servo Loop Performance.

To obtain a true indication of the level of frequency stabilisation achieved under active control the closed loop spectral density, $S_{CL}^{(LASER)}$, of frequency fluctuations of the laser output beam should be measured. Referring back to the block diagram of the laser frequency servo system shown in section 6.3, $S_{CL}^{(LASER)}$ has the form

$$S_{CL}^{(LASER)} = \frac{\sqrt{(S_L)^2 + (KS_S)^2 + (KGS_D)^2}}{1 + KGD} \tag{7.6}$$

where D = discriminant sensitivity in (V/Hz)

K = frequency transducer sensitivity in (Hz/V)

G = gain of the servo amplifier and integrator

S_L = linear spectral density of the free-running laser frequency noise in ($Hz/\sqrt{Hz}$)

S_S = linear spectral density of servo amplifier voltage noise in ($V/\sqrt{Hz}$)

S_D = linear spectral density of the discriminant voltage noise in ($V/\sqrt{Hz}$).

In practice, however, the measurement of this parameter can be extremely difficult, since it requires a more stable frequency reference, such as another laser or passive

cavity against which the frequency of the test laser can be compared. In the absence of such a frequency reference, a common alternative is to measure the closed loop spectral density of the voltage generated by the frequency discriminant, $S_{CL}^{(DISCRIM)}$. By using the frequency to voltage conversion factor of the discriminant, $S_{CL}^{(DISCRIM)}$ can be converted from a voltage spectral density, in $V/\sqrt{Hz}$, into a frequency spectral density, in $Hz/\sqrt{Hz}$. Once again referring to the servo block diagram (see figure 6.18), this frequency spectral density has the form

$$\frac{S_{CL}^{(DISCRIM)}}{D} = \frac{\sqrt{(S_L)^2 + (KS_S)^2 + (S_D/D)^2}}{1 + KGD} \tag{7.7}$$

As can be seen from equation (7.7) this measurement only gives a true representation of the actual frequency noise of the stabilised laser when the loop gain, G, is small and the discriminant noise, S_D, is negligible. In contrast, under conditions of very large loop gain, $S_{CL}^{(DISCRIM)}/D$ will approach zero as the feedback loop imposes additional frequency fluctuations on the laser output in order to null the servo's own internal noise. In this high loop gain limit, the real laser frequency noise is thus determined by the servo discriminant's own noise and will have a value given by equation (7.6) of S_D/D. Despite these difficulties in interpreting $S_{CL}^{(DISCRIM)}$, measurement of this quantity does provide some useful insight into the performance of the frequency stabilisation system.

Figure 7.12 shows a typical example of the closed loop error signal voltage recorded at the output of the frequency discriminant (double balanced mixer output) together with the optical transmission through the reference cavity. The cavity transmission was at its maximum indicating that the laser frequency was indeed locked to the centre of the reference cavity resonance. The residual error signal voltage was calibrated in terms of the apparent fluctuations in the laser output frequency relative to the reference cavity resonance using the gradient (in Hz/V) of the central zero-crossing portion of the rf-fringe discriminant. From this calculation the maximum peak-to-peak deviation of the laser frequency from the reference cavity line centre was typically no greater than 2kHz.

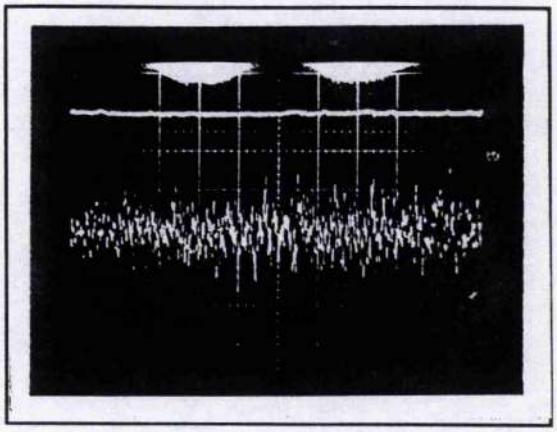

Figure 7.12. The upper trace shows the transmission through the reference cavity when the laser frequency is locked to the centre of the reference cavity resonance using the Pound-Drever stabiliser. The lower trace is the corresponding error point signal measured at the balanced mixer output. The time duration of the recording was 100 sec.

Spectral density measurements of this discriminant signal were also made over the frequency range 0-20kHz using a Brüel & Kjær fast Fourier transform spectrum analyser. Three examples of spectral density plots of $S_{CL}^{(DISCRIM)}$ are shown in figure 7.13

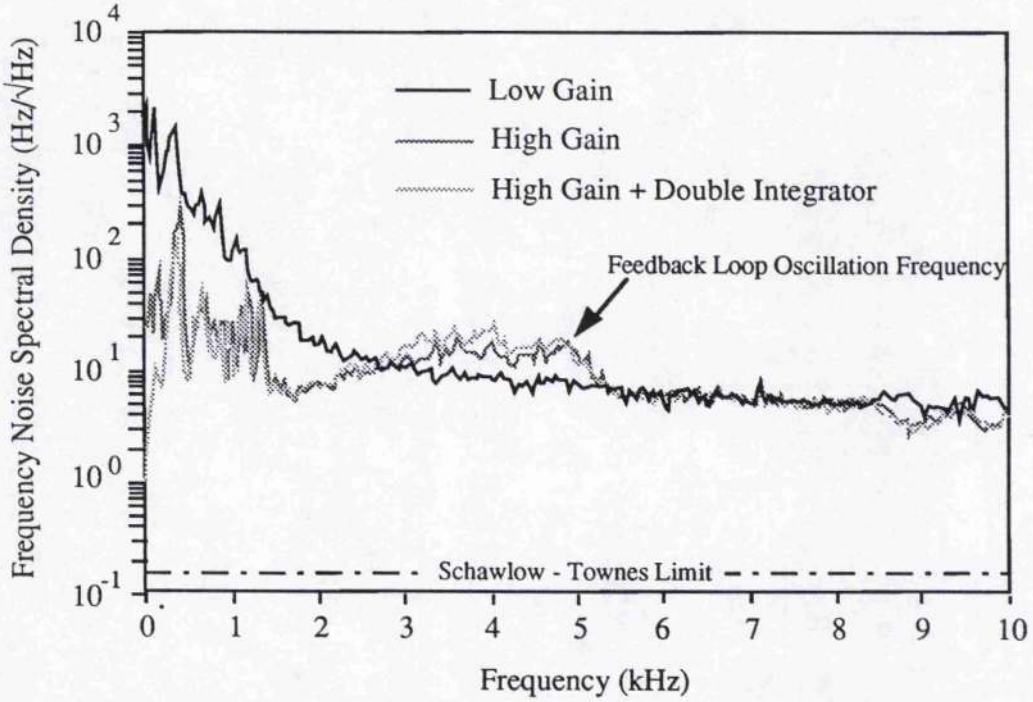

Figure 7.13. Spectral density plots of the Pound-Drever error signal measured at the output of the balanced mixer for a) low servo loop gain and b) high servo loop gain.

for different gain settings of the servo loop. For reference, the Schawlow-Townes limit for this laser of 130mHz/$\sqrt{\text{Hz}}$ is also indicated. From this figure the effect of changing the gain on the performance of the servo loop can be clearly seen. The low gain curve shown in this figure corresponds to the minimum loop gain required to keep the laser frequency locked to the reference cavity. For this gain setting the servo's unity gain point was at approximately 30Hz. The high gain curve was obtained using the maximum loop bandwidth (~5kHz) and gain possible before oscillation of the feedback network occurred. In both these cases only the single integration effect of the low pass RC filter was used to roll off the gain to the unity.

For small loop gain the error signal was dominated by low frequency (<1kHz) components. Increasing the loop gain to its maximum value, before loop oscillation occurred, suppressed these low frequency fluctuations by ~13dB for frequencies around 1kHz and by as much as 30dB for frequency components of a few tens of Hertz. However, this quietening of the low frequency laser noise was accompanied by an increase in the error signal spectral density components in the range 2-5kHz by as much as 10dB. This behaviour is indicative of the feedback loop approaching instability. Indeed any further increase in servo loop gain resulted in the loop becoming unstable and oscillating at a frequency of approximately 5kHz.

The benefits of increasing the low frequency gain through the use of an additional stage of electronic integration in the feedback network is clearly demonstrated in the third spectral density curve shown in figure 7.13. In this case activating the second integrator decreased the sub 100Hz noise components by a further 30dB compared to the high gain, single integrator curve. The cross-over frequency from double to single integration was set at 500Hz.

The cause of the loop instability at ~5kHz was investigated by measuring the open loop gain and phase shift characteristics of the amplifier and integrator stage of the servo electronics as a function of frequency. To do this the signal from the balanced mixer output was replaced by a signal generator and the amplitude and phase of the open loop

voltage generated across the PZT of the laser frequency transducer was recorded for various gain settings. These data are displayed in figure 7.14 In the graph of the gain data the contributions from the frequency discriminant and the frequency transducer have been included to convert the measured voltage gains into values of the total open loop gain of the servo.

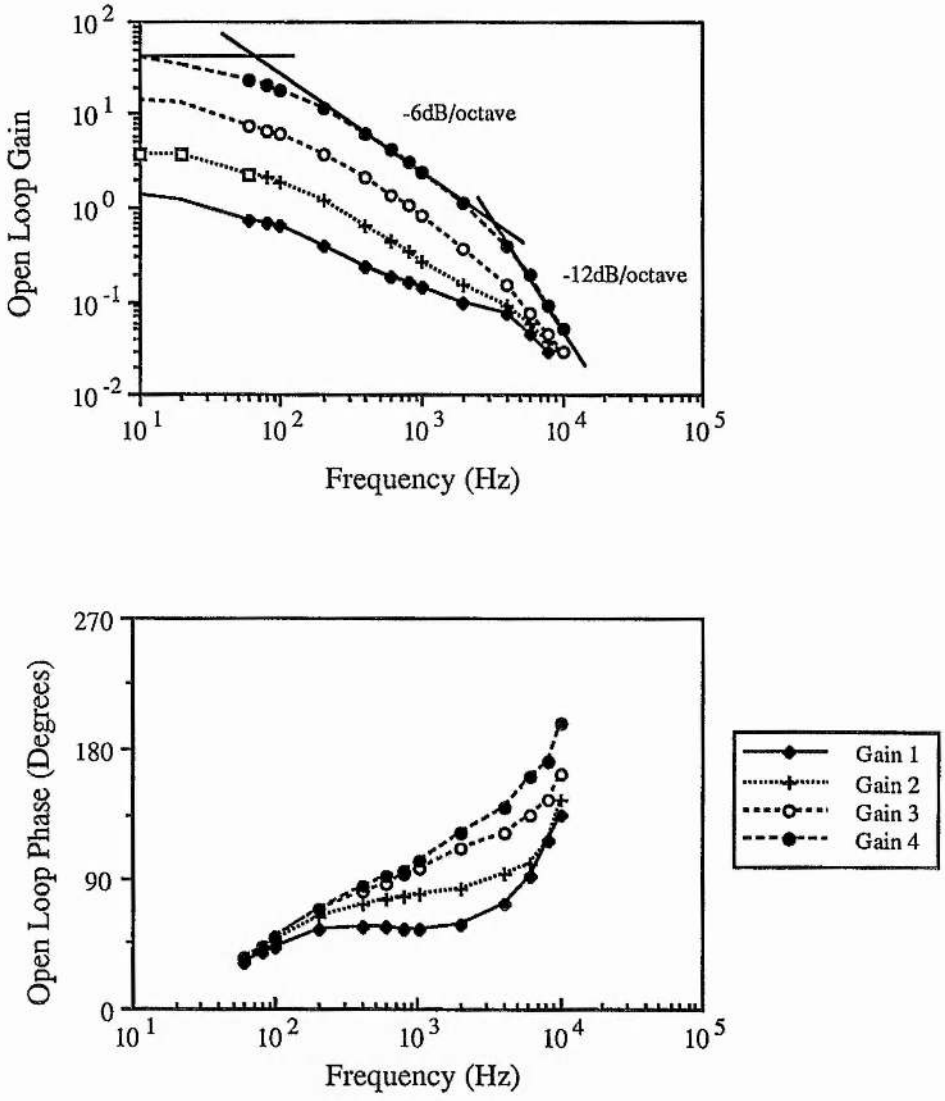

Figure 7.14. Open loop gain and phase shift characteristics of the servo amplifier/integrator.

For frequencies above the 3dB point (f_{3dB}~50Hz) of the RC integrator formed by the frequency transducer and series resistor the slope of the gain versus frequency curve

shown in figure 7.14 displays the characteristic 6dB/Octave gain roll off. However, for frequencies over approximately 3.5kHz the gain curve slope increases to -12dB/Octave. Associated with this increased slope is an undesirable large phase shift which, in the case of the highest gain setting, exceeds 180°. Clearly it is this large phase shift in the electronics of the amplifier/integrator which is restricting the maximum frequency of the unity gain point and consequently the maximum low frequency gain attainable with this circuit. Modest improvements to the maximum loop gain of this system could be obtained by making the following modifications; The use of wider bandwidth OP-AMPS would help to avoid these unintentional phase shifts in the circuitry whilst replacing the passive RC integrator by a more "ideal" active OP-AMP integrator could extend the -6dB/Octave gain slope to much lower frequencies enabling larger gains to be achieved. However, to extend the unity gain frequency much beyond its current 5kHz level the electronics would have to be carefully designed to accommodate the additional optical integration effect of the reference cavity with its 3dB corner frequency of 20kHz. If the unity gain point could be extended up to the operating limit of the laser frequency transducer of 100kHz then significantly larger loop gains of say 10^3-10^4 at 10Hz could be achieved with just a single level of integration.

The potential of this system for generating ultra-narrow linewidth laser output can perhaps be appreciated from the excellent results of Shoemaker et al[10], Day et al[11] and more recently by Uehara et al[12] on similar Pound-Drever stabilised, diode laser pumped Nd:YAG systems. For instance, Shoemaker et al locked an open cavity Nd:YAG laser, containing an intracavity mode-selecting etalon, to a 1.1MHz linewidth reference cavity using a very wide bandwidth (120kHz) servo loop. This wide bandwidth was achieved using two nested feedback loops, one controlling a piezoceramic frequency transducer over the frequency range 0-300Hz and the other driving an external acousto-optic modulator up to frequencies of 120kHz. The loop could provide gains in excess of 10^9 at 10 Hz and 10^6 at 1kHz. These huge servo loop gains suppressed the laser noise power spectral density to around 14.3mHz/$\sqrt{\text{Hz}}$, a factor of 14 less than the Schawlow-Townes limit for their laser. The systems operated by Day et al and Uehara et al were very

similar with both making use of commercial (Lightwave Electronics) Nd:YAG Non-Planar Ring Oscillators and ultrahigh finesse (F~20,000) reference cavities. The feedback loop used by Uehara had a gain of greater than 10^6 at dc and 10^2 at 1kHz. The unity gain frequency was 30kHz. With this system a spectral density of 10mHz/$\sqrt{\text{Hz}}$ and a measured heterodyne beat linewidth of 193mHz between two lasers locked to the same reference cavity were obtained. This measured linewidth was again below the calculated Schawlow-Townes limit by a factor of 1.4. The heterodyne linewidth recorded by Day et al was at best 330mHz, limited by electronic noise and acoustic pickup in the reference and laser cavities. If the loop gain of our electronic servo system could be increased substantially so that it approaches the levels used in the examples above, there is no reason why our system performance should not be comparable to the impressive levels of frequency stability achieved by these other systems..

7.2.1 Calculation of the Free-Running Frequency Noise Spectral Density

It is interesting to note that from knowledge of the open loop gain of the frequency servo together with the closed loop spectral density data from the discriminant signal, it is possible to infer the spectral density of the free-running laser frequency noise by using the relation shown in equation 7.7. The contribution to equation 7.7 due to the voltage noise spectral density, S_S, from the servo amplifier was measured using a spectrum analyser and found to be 0.14μV/$\sqrt{\text{Hz}}$. Since the corresponding frequency spectral density, KS_S, of 0.6Hz/$\sqrt{\text{Hz}}$ was small compared to those values measured for $S_{CL}^{(DISCRIM)}/D$ the noise contribution from S_S could be neglected. Thus, in equation (7.7) the only remaining unknowns were S_L and S_D. By making the assumption that $S_D=0$, equation (7.7) simplifies to

$$S_L = \frac{S_{CL}}{D}(1 + KGD) \tag{7.8}$$

giving an upper limit to the free-running laser frequency noise spectral density. Using this equation, the spectral density data from the closed loop discriminant signal (some of which are shown in figure 7.13) was combined with the servo loop gain data from figure 7.14 to generate values for S_L at specific Fourier frequencies in the range 100Hz - 20kHz. This information is tabulated in table 7.1.

Table 7.1

FOURIER FREQUENCY = 100Hz			
SERVO GAIN SETTING	1 + KGD	$S_{CL}^{(discrim.)}/D$ (Hz/√Hz)	S_L (Hz/√Hz)
1	1.63	572.4	933.0
2	2.84	255.7	726.2
3	7.20	72.1	519.1
4	19.44	22.8	443.2
FOURIER FREQUENCY = 200Hz			
SERVO GAIN SETTING	1 + KGD	$S_{CL}^{(discrim.)}/D$ (Hz/√Hz)	S_L (Hz/√Hz)
1	1.40	361.1	505.5
2	2.18	181.0	394.8
3	4.80	60.6	293.3
4	11.65	18.1	210.9
FOURIER FREQUENCY = 400Hz			
SERVO GAIN SETTING	1 + KGD	$S_{CL}^{(discrim.)}/D$ (Hz/√Hz)	S_L (Hz/√Hz)
1	1.23	181.0	222.6
2	2.63	114.2	186.15
3	3.07	45.5	139.7
4	7.20	14.4	103.68

FOURIER FREQUENCY = 600Hz			
SERVO GAIN SETTING	1 + KGD	$S_{CL}^{(discrim.)}/D$ (Hz/√Hz)	S_L (Hz/√Hz)
1	1.18	114.2	134.8
2	1.44	76.3	109.9
3	2.40	34.1	81.8
4	5.20	12.10	62.9
FOURIER FREQUENCY = 800Hz			
SERVO GAIN SETTING	1 + KGD	$S_{CL}^{(discrim.)}/D$ (Hz/√Hz)	S_L (Hz/√Hz)
1	1.16	64.2	74.5
2	1.34	54.0	72.4
3	2.03	27.1	55.0
4	4.10	10.2	41.8
FOURIER FREQUENCY = 1kHz			
SERVO GAIN SETTING	1 + KGD	$S_{CL}^{(discrim.)}/D$ (Hz/√Hz)	S_L (Hz/√Hz)
1	1.14	45.5	51.9
2	1.27	36.1	45.8
3	1.81	21.5	38.9
4	3.43	8.7	29.8
FOURIER FREQUENCY = 2kHz			
SERVO GAIN SETTING	1 + KGD	$S_{CL}^{(discrim.)}/D$ (Hz/√Hz)	S_L (Hz/√Hz)
1	1.10	12.8	14.0
2	1.15	10.2	11.7
3	1.37	10.8	14.8
4	2.11	8.1	17.1

It can be seen that for any given frequency, the values for S_L calculated for each of the four gain settings are not constant as anticipated but instead show an approximately two

fold increase in going from the highest to the lowest gain setting. The exact cause of this inconsistency in the calculated S_L values is unclear but may be related to variations in the servo loop phase shift experienced at different loop gains.

To gauge the free-running frequency stability performance of this laser, the S_L data from table 7.1 was plotted together with spectral density data on other diode laser pumped solid state laser systems compiled from publications in the open research literature. The lasers used by Day et al[11] and Fritschel et al[13] were Nd:YAG Non-Planar Ring Oscillator (NPRO) operating at 1.064μm. An Nd:YAG NPRO laser was also used by Williams et al[14] but this time operating on the 1.3μm transition. Shoemaker et al[10] made their measurements on an open cavity Nd:YAG laser (1.064μm) containing an intracavity etalon longitudinal mode selector. See figure 7.15.

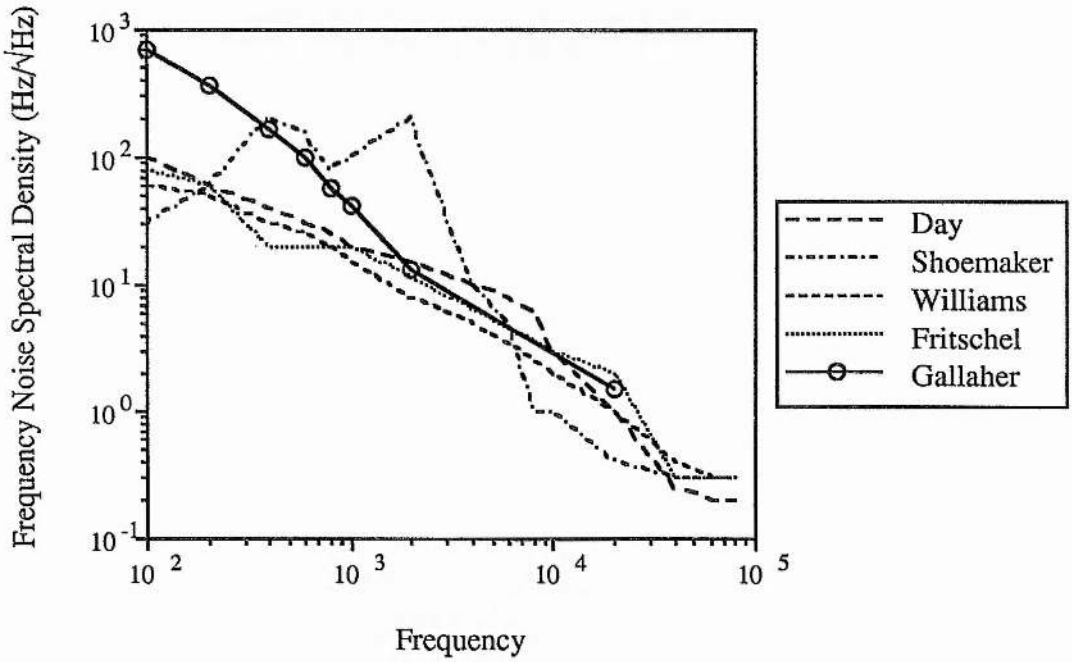

Figure 7.15. Comparison of the linear spectral density of frequency fluctuations of various free-running diode pumped solid state lasers.

Bearing in mind that the frequency noise spectral density data calculated for the laser in this work are an upper estimate, figure 7.15 shows that the free-running frequency stability of this laser compares favourably with the diode pumped laser

systems produced by other researchers. To put these spectral density figures on the diode pumped systems into perspective, an Argon ion laser displays frequency fluctuations of the order of 10^3 Hz/$\sqrt{\text{Hz}}$ at 1kHz[11] and a "quiet" semiconductor diode laser exhibits frequency noise of about 10^4 Hz/$\sqrt{\text{Hz}}$ at 1kHz[12]. In contrast a typical diode pumped solid state laser has a frequency noise spectral density of only ~50 Hz/$\sqrt{\text{Hz}}$ at 1kHz.

7.3 References

1 Kane T. J., "Intensity Noise in Diode Pumped Single Frequency Nd:YAG Lasers and its Control by Electronic Feedback", IEEE Photon. Tech. Lett. **2** 244 (1990)

2 Salomom C., Hils D., Hall J. L., "Laser Stabilisation at the millihertz Level", J. Opt. Soc. Am. **5** 1576 (1988)

3 Day T., Nilsson A. C., Fejer M. M., Farinas A. D., Gustafson E. K., Nabors C. D., Byer R. L., "30Hz Linewidth, Diode-Laser-Pumped, Nd:GGG Nonplanar Ring Oscillators By Active Frequency Stabilisation", Electron. Lett. **25**(13) 810 (1989)

4 Amaya P., "Ultra-Low-Loss Optics", Lasers and Optronics **11**(6) 7 (1992)

5 Munnerlyn C. R., Balliett J. W., "Alignment Requirements for Mode Matching in a Confocal Fabry-Perot Interferometer", Appl. Opt. **9**(11) 2535 (1970)

6 Kogelnik H., "Imaging of Optical Modes - Resonators With Internal Lenses", Bell Sys. Tech. J. 455 March(1965)

7 "The Piezo Book", Burleigh Instruments (1988)

8 Cady W. G., "Piezoelectricity", McGraw-Hill (1946)

9 Piezoceramics Catalogue - Pyzotec Ltd., Warwickshire, England (1988)

10 Shoemaker D., Brillet A., Nary Man C., Crégut O., Kerr G., "Frequency Stabilised Laser Diode Pumped Nd:YAG Laser", Opt. Lett. **14**(12) 609 (1989)

11 Day T., Gustafson E. K., Byer R. L., "Sub-Hertz Relative Frequency Stabilisation of Two Diode Laser Pumped Nd:YAG Lasers Locked to a Fabry-Perot Interferometer", IEEE J. Quant. Elec. **28**(4) 1106 (1992)

12 Uehara N., Ueda K., "193mHz Beat Linewidth Of Frequency Stabilised Laser-Diode-Pumped Nd:YAG Ring Lasers", Opt. Lett. **18**(7) 505 (1993)

13 Fritschel P., "Frequency Fluctuations of a Diode Pumped Nd:YAG Laser", Opt. Lett. 14(18) 993 (1989)

14 Williams K.J., Dandridge A., Kersey A. D., Weller J. F., Yurek A. M., Tveten A. B., "Interferometric Measurement of Low-Frequency Phase Noise Characteristics of Diode Laser Pumped Nd:YAG Ring Laser", Elec. Lett. **25**(12) 774 (1989)

Chapter 8

INJECTION SEEDING AND LOCKING OF HOLOSTERIC LASERS

8.1 Introduction

One area where frequency stabilised CW lasers are used is in axial mode selection (injection seeding) and frequency control (injection locking) of higher power pulsed and CW laser oscillators by injected signal. This chapter describes experimental work in the use of the narrow linewidth, CW, end-pumped holosteric laser as a "master oscillator" for injection seeding a Q-switched transversely pumped holosteric laser and some preliminary studies of the injection locking of a second CW, end pumped holosteric laser.

8.2 Injection Seeding

Certain applications, such as laser radar (or LIDAR), high resolution spectroscopy or nonlinear optics, demand short, single axial mode, high peak power laser light pulses. Optical pulses with the required high peak powers and short durations can readily be generated using the well established technique of cavity Q-switching but single axial mode selection in such lasers can be a challenging problem.

In a Q-switched laser the initial population inversion present at the start of the pulse build up process is so large that mode competition through gain saturation is insignificant until well into the pulse evolution. Thus, during the initial build up stages of the Q-switched pulse, a few of the lower loss longitudinal cavity modes may experience similar large amounts of gain and grow rapidly. Because of this reduced mode competition, high levels of intracavity round trip loss, often in excess of 10%, are required to suppress unwanted cavity modes. Conventional axial mode selecting methods transposed from CW lasers such as intracavity etalons or thin film absorbers, often cannot provide such large

levels of differential intracavity loss and so more sophisticated mode selection techniques have been developed.

One highly successful technique for single longitudinal mode selection in short pulse and Q-switched lasers is injection seeding. This process involves injecting a small amount of light from a single frequency, CW laser, referred to as the "master oscillator", into the cavity of the Q-switched "slave" laser at a frequency close to a resonant mode of the slave. In the pre Q-switched below threshold state the injected beam reaches a steady state regeneratively amplified intensity inside the slave cavity which is well above the spontaneous emission noise. When the Q of the slave laser cavity is suddenly switched to a high state the amplitude of this initial intracavity signal grows exponentially and its frequency is pulled rapidly in to the nearest cavity mode of the slave laser. This cavity mode thus experiences a significant head start over other cavity modes which grow initially from the spontaneous noise level and so dominates the pulse output.

8.2.1 Transversely Pumped Q-Switched Nd:YAG Holosteric Laser

The pulsed, high power, transversely pumped Nd:YAG holosteric laser used as the slave oscillator in the injection seeding experiments was designed and built by C. Norrie at the University of St. Andrews. A brief description of this laser is included here for completeness but a more detailed description of its construction and characterisation can be found in reference (1).

The pump source for the Q-Switched laser was a model SDL-3220-J quasi-CW diode laser bar from Spectra Diode Labs driven by a SDL-922 high current pulse generator. This diode laser had an emitting aperture 10mm long by 1μm thick containing a linear array of 1000 laser active stripes. These 1000 emitters were arranged into 40 groups of 25 emitters evenly distributed along the laser bar. The output beam was highly astigmatic because of the dimensions of the emitting aperture with full width at half maximum beam divergences of 40° and 10° perpendicular and parallel to the diode junction respectively. Due to the

difficulty of removing waste heat from the large number of emitters, the diode laser bar could only be operated in a pulsed mode with a maximum output pulse width of 200μs at a repetition rate of up to 100Hz. The maximum pulse energy available from the device was 5mJ corresponding to a maximum peak power of 25W and an average power 500mW.

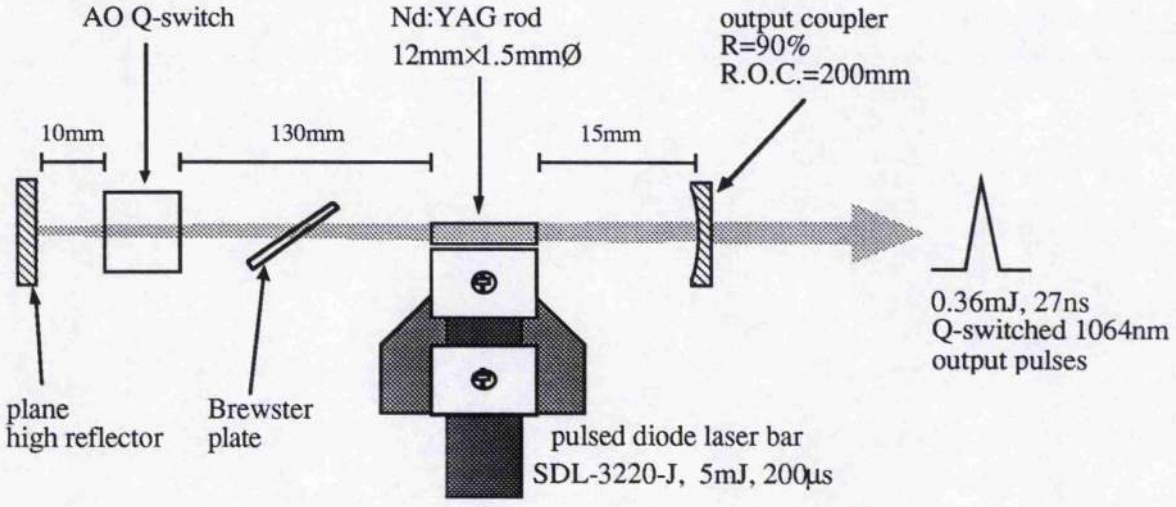

Figure 8.1. The transversely pumped, acousto-optically Q-switched Nd:YAG holosteric laser.

The plano-concave open resonator of the Nd:YAG laser contained a 12mm long × 1.5mm diameter plano-plano Nd:YAG rod and a lead molybdate acousto-optic Q-switch, as illustrated in figure 8.1. Each surface of the intracavity components was antireflection coated for the laser wavelength of 1064nm to keep the intracavity losses to a minimum. Efficient absorption of pump light in the transverse pumped laser geometry is difficult because of the short interaction length available to the pump light crossing the small diameter Nd:YAG rod, a problem which is compounded by the large (relative to the Nd:YAG absorption bands) 5nm wavelength chirp of the diode laser array output during the pump pulse[2]. In order to combat this problem a YAG gain medium containing a high (1.3%) Nd ion dopant density was chosen to increase the pump light absorption. Pumping efficiency was further enhanced by placing the Nd:YAG rod inside a close fitting, polished brass, cylindrical housing which acted as a back reflector for any pump light transmitted through the Nd:YAG rod.

Pump light from the diode laser bar was coupled into the Nd:YAG rod by positioning the output facet of the laser bar within 200μm of the polished cylindrical surface of the crystal. This made use of the large numerical aperture lens effect of the high refractive index, cylindrical Nd:YAG rod for efficient collection of the highly divergent pump light.

The optical cavity of the Nd:YAG laser was formed between a high reflector plane mirror and a 90% reflectivity, 200mm radius of curvature concave output coupler mirror. For efficient Q-switching of the laser the rise time of the Q-switch was required to be short compared to the ~130ns build up time of the Q-switched laser pulse. Since the opening time of the acousto-optic Q-switch was dependent on the laser beam radius, the cavity was set to be close to hemispherical to provide a small beam size in the acousto-optic Q-switch. With the cavity geometry shown in figure 8.1 the beam radius in the Q-switch was 145μm corresponding to a Q-switch rise time of 90ns, well below the Q-switched pulse build up time as required.

The laser was restricted to oscillation on the fundamental transverse mode of the cavity by using the small diameter of the gain medium as an intracavity TEM_{00} mode selecting aperture. Maximum TEM_{00} output power was obtained from the laser with the rod positioned in the cavity where the laser beam radius was 425μm.

In the absence of the acousto-optic Q-switch the transverse pumped Nd:YAG laser operating long-pulse displayed a pump threshold of 1.84mJ and an optical to optical slope efficiency of 21.8%. Under optimum Q-switching conditions the laser threshold was increased to 2.83mJ with a Q-switched pulse slope efficiency of 15%. The maximum Q-switched output pulse energy from the laser was 0.36mJ in 27ns corresponding to a pulse peak power of 13kW at a wavelength of 1064nm. The Q-switched performance of the laser is summarised in figure 8.2 below.

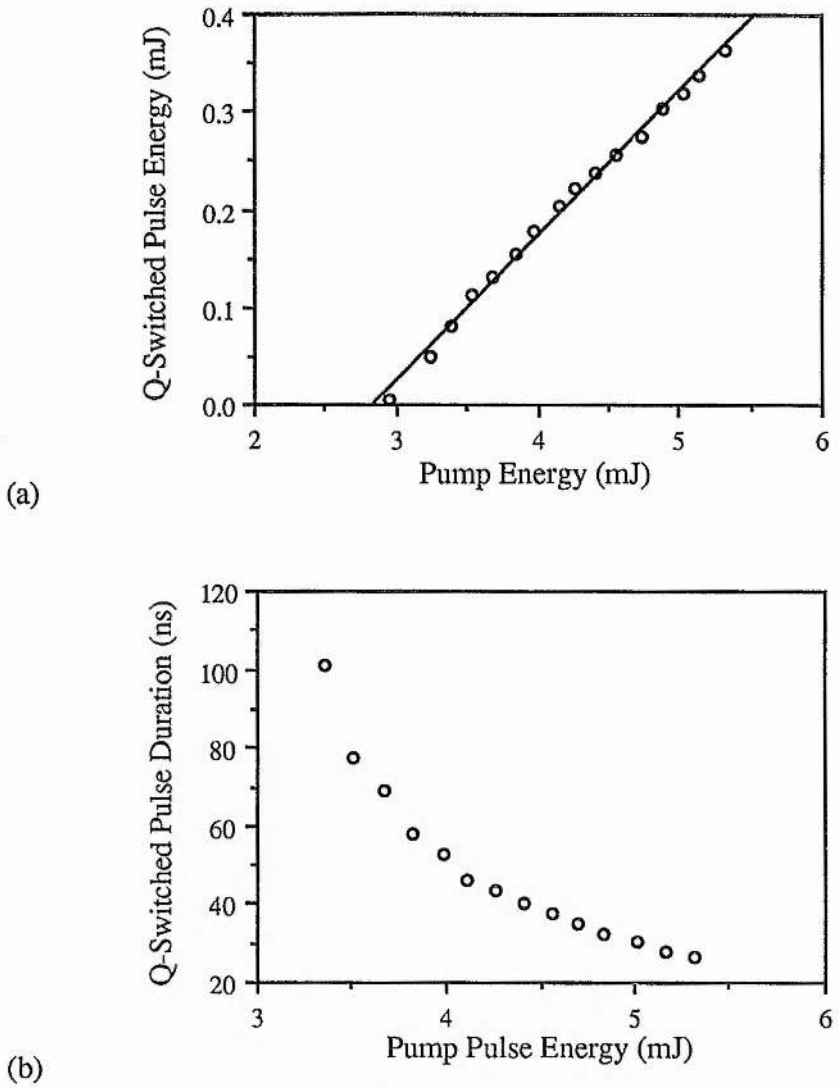

Figure 8.2. Output pulse characteristics of the transversely pumped, Q-switched Nd:YAG holosteric laser. (a) Optical to optical slope efficiency, (b) Q-switched pulse duration (FWHM) as a function of pump pulse energy.

Longitudinal Mode Structure

Examination of the temporal profile of the Q-switched laser pulse using a wide bandwidth digital oscilloscope (Hewlett Packard 54111D) and a fast avalanche photodiode (BPW28) revealed the presence of an intensity modulation superimposed on the Q-switched pulse envelope as illustrated in figure 8.3. This type of behaviour is characteristic of multi-longitudinal mode Q-switched lasers and is caused by beating

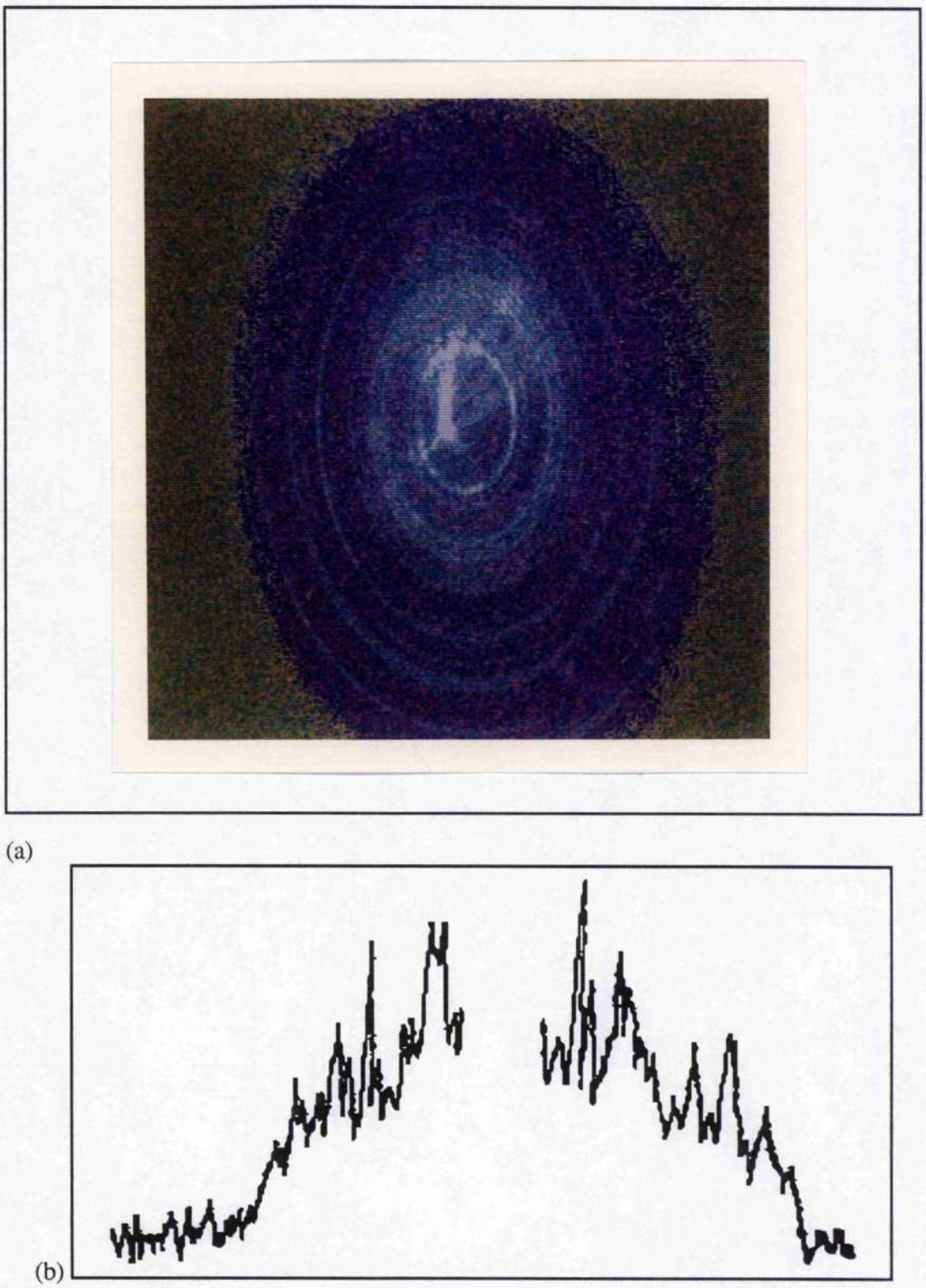

Figure 8.4. (a) False colour image showing the multiple frequency components of the unseeded Q-switched laser pulse as viewed through the 14.6GHz free spectral range Fabry-Perot interferometer. (b) A linear intensity scan through the centre of the ring pattern shown in (a) above.

between simultaneously oscillating longitudinal laser modes. In the particular case shown in figure 8.3 the intermode beat frequency was 684MHz corresponding to an optical path length in the laser cavity of 219mm.

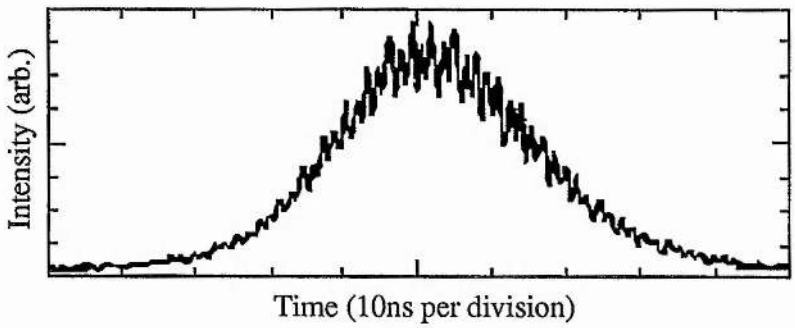

Figure 8.3. The temporal profile of the Q-switched laser pulse showing the presence of mode beating caused by multilongitudinal mode laser operation.

Further evidence for the multilongitudinal mode output of the transversely pumped laser was obtained by observing the optical spectrum of the Q-switched pulse on a static plane-parallel Fabry-Perot interferometer. The Fabry-Perot ring pattern generated by the interferometer was viewed using a CCD camera connected to an electronic frame grabber and a micro computer. The electronic frame grabber was synchronously gated to the Q-switched pulse train to produce static images of the interferometer transmission. These images could be down loaded into the computer for analysis. Figure 8.4 shows a false colour image of a representative interferometer transmission for a Q-switched output pulse from the transversely pumped laser. The image contains just over two free spectral ranges of the Fabry-Perot interferometer. The multiple rings visible in figure 8.4 clearly indicate laser operation on many longitudinal modes during the Q-switched pulse duration. The number of modes oscillating at any one instant during the output pulse cannot however, be ascertained from this analysis as the spectral data from the CCD image of the interferometer transmission is averaged over the sampling time of the camera-frame grabber system.

8.2.2 Injection Seeding Results

The injection seeding experiments on the transversely pumped Nd:YAG holosteric laser were carried out using the arrangement depicted in figure 8.5. The seeding beam was provided by the passively stabilised, end-pumped, single frequency Nd:YAG holosteric master oscillator described in Chapter 5. This master oscillator contained a 1mm thick uncoated intracavity fused silica etalon for single longitudinal mode selection and could generate 7-10mW single mode 1064nm laser output with a short term linewidth of 40kHz. Contained within the seeding beam path between the master and slave oscillators was a Faraday rotator optical isolator, a $\lambda/2$ waveplate and a mode matching lens. The

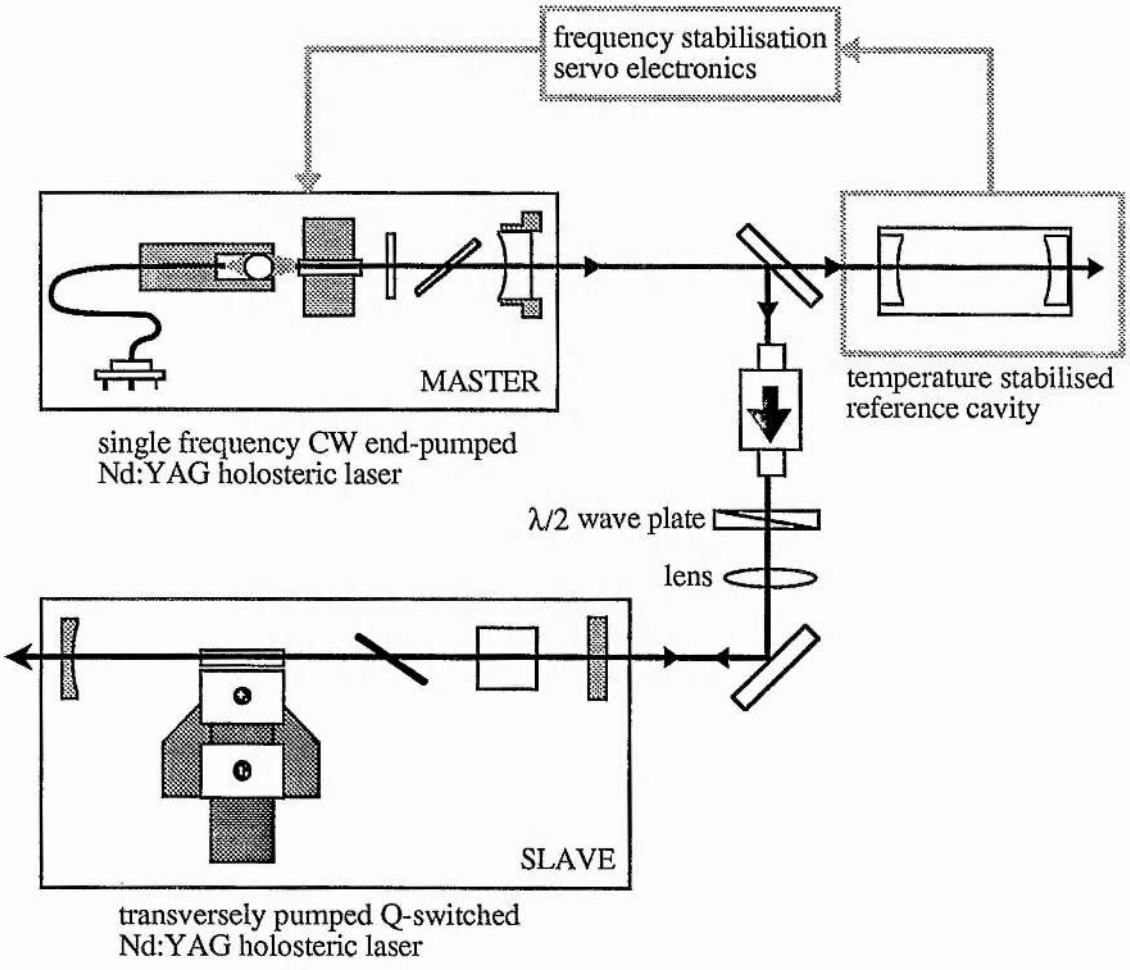

Figure 8.5. The optical arrangement used for the injection seeding experiments.

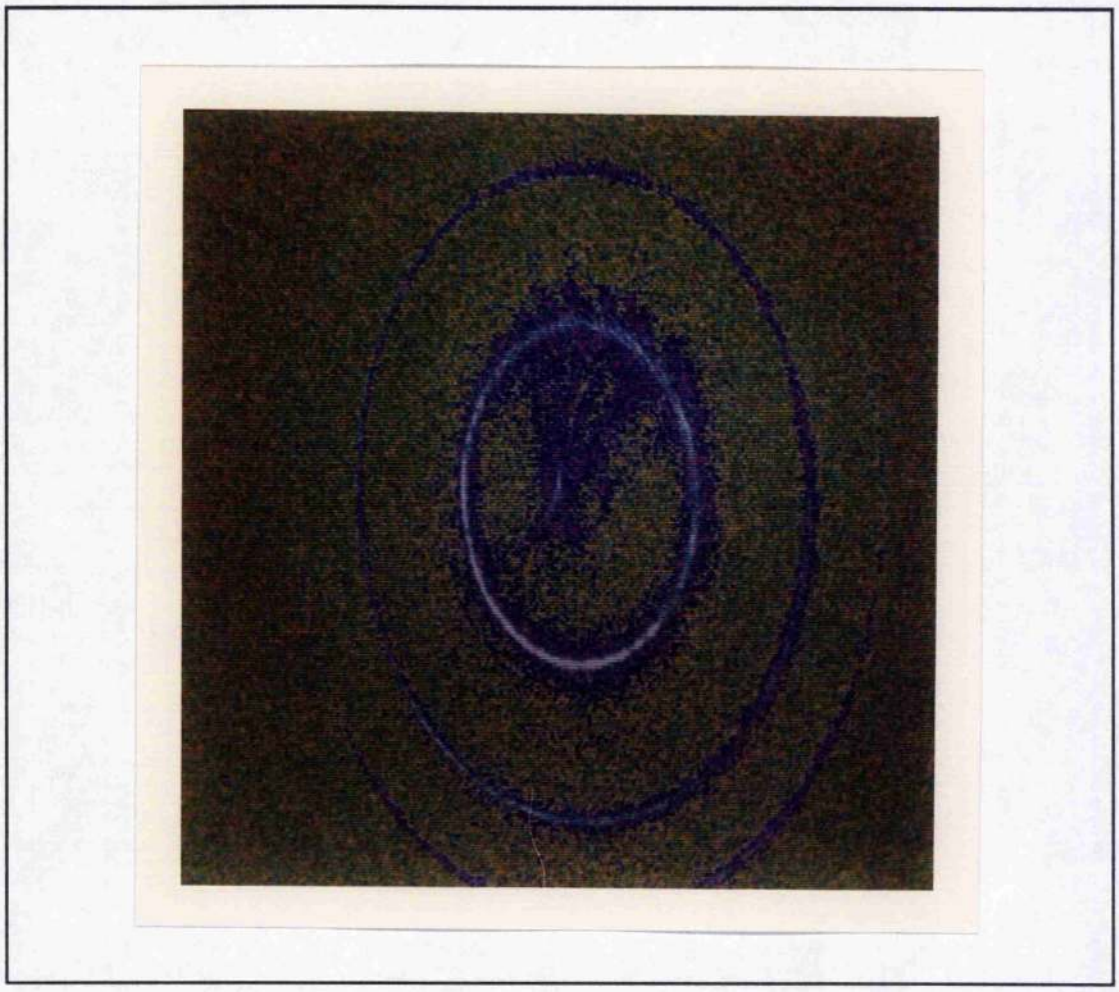

(a)

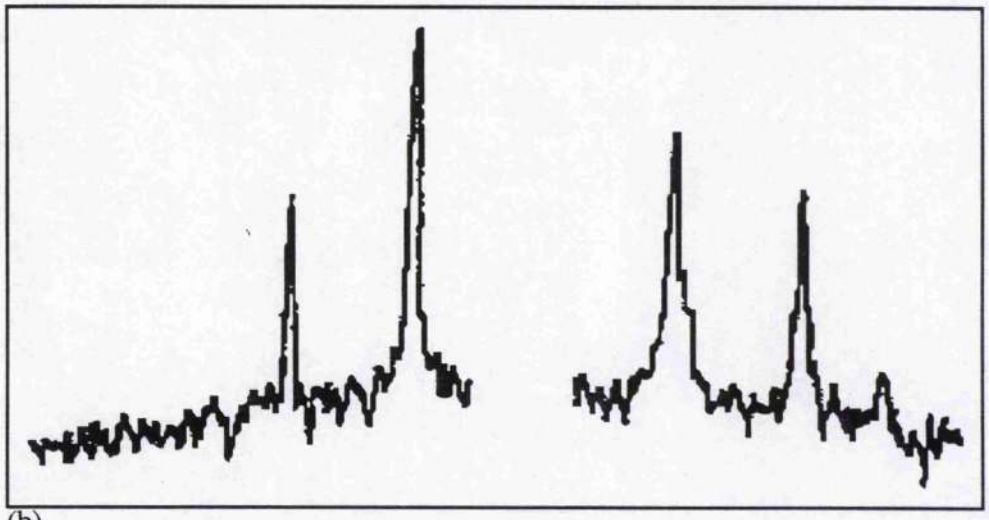

(b)

Figure 8.6. (a) False colour image of the 14.6GHz Fabry-Perot interferometer transmission showing the injection seeded Q-switched laser operating on a single longitudinal mode. (b) A linear intensity scan through the centre of the ring pattern shown in (a) above.

unidirectional Faraday optical isolator protected the master oscillator from any frequency pulling effects caused by small amounts of the Q-switched laser emission entering the master oscillator by providing up to 40dB attenuation of any slave oscillator output heading back along the seeding beam. The rotatable $\lambda/2$ waveplate and the mode matching lens allowed the seeding efficiency to be optimised by enabling the linear polarisation states and the spatial profiles of the seeding beam and the Q-switched cavity mode to be matched respectively.

With the seeding beam turned on, the resonance frequency of the slave oscillator was scanned by altering the cavity length via its piezo mounted output coupler mirror. A fast photodiode and the static Fabry-Perot interferometer were used to monitor the temporal and spectral output of the Q-switched slave oscillator for any evidence of injection seeding behaviour. With as little as 0.2mW of optical power from the master oscillator incident on the high reflectivity (~0.02% transmission at λ=1064nm) plane mirror of the slave cavity dramatic changes in the temporal and spectral character of the Q-switched pulse output of the slave laser were observed when injection seeding occurred. Transmission of the output beam from the seeded Q-switched laser through the interferometer generated a "clean" Fabry-Perot ring pattern indicative of single longitudinal mode laser operation. See figure 8.6.

A typical example of the seeded Q-switched pulse profile, as observed using the fast photodiode and oscilloscope, is presented in figure 8.7(a). The temporal power profile of the pulse was smooth, showing no sign of any mode beating modulation. By accumulating traces of 100 injection seeded Q-switched laser shots in the digital store of the oscilloscope, the pulse to pulse power stability of the seeded pulses was found to be better than ±6%, limited only by noise in the detector. This data is shown in figure 8.7(b).

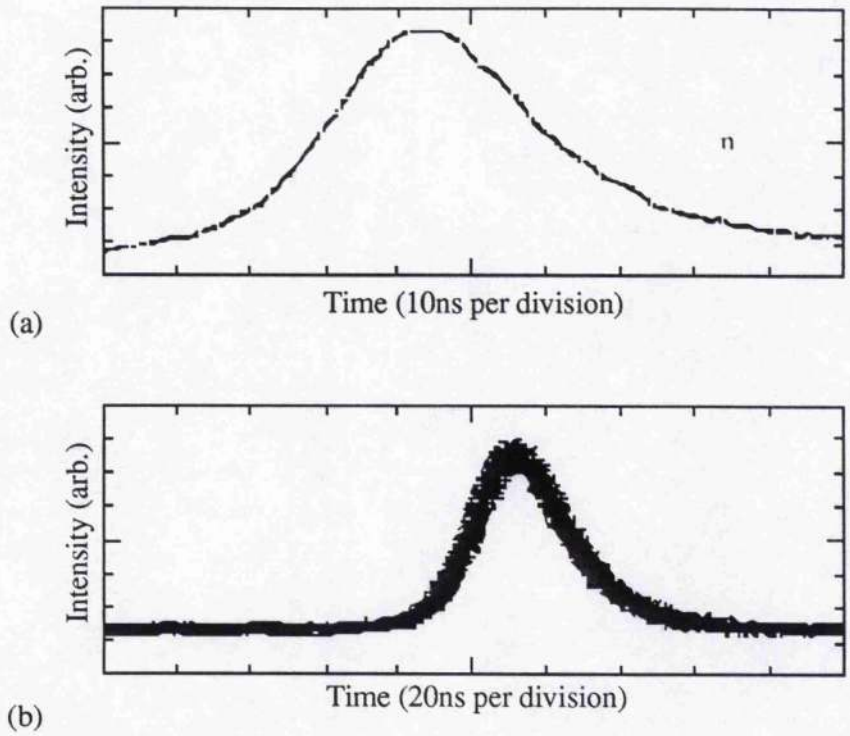

Figure 8.7. (a) A typical example of the smooth temporal profile of one injection seeded Q-switched pulse from the transversely pumped holosteric laser. (b) An overlay of 100 consecutive seeded Q-switched pulses showing an intensity stability of better than 6%.

A direct comparison between the time evolution of the seeded and unseeded Q-switched pulses profiles is given in figure 8.8. This composite image was formed by

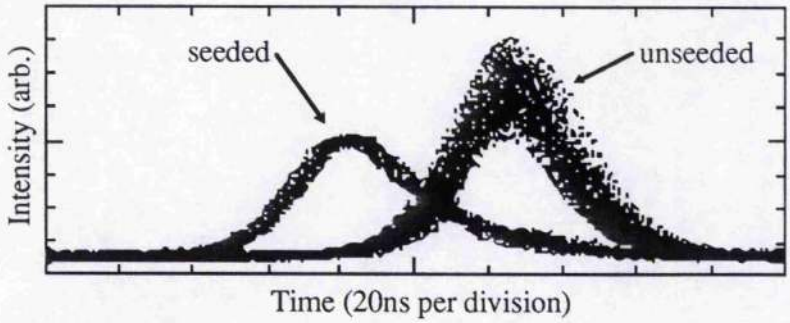

Figure 8.8. Direct comparison of the seeded and unseeded Q-switched pulse output. Each trace is formed from an overlay of 100 consecutive pulses

storing a number of consecutive unseeded Q-switched pulses and then overlaying a similar number of seeded pulses. The trigger pulse to the acousto-optic Q-switch defined the time origin for both groups of pulses. Figure 8.8 clearly illustrates three major differences

between the seeded and unseeded pulses. Firstly, the intensity noise of the seeded pulses is much reduced in comparison with the pulses in the unseeded cases. This reduction in intensity noise is due to the absence of mode beating in the single longitudinal mode seeded Q-switched pulse. The mode beating intensity modulation responsible for the noisy profile of the unseeded pulse is unresolved because of the limited sampling rate of the digital oscilloscope.

The second observable difference between the seeded and unseeded pulses is that the 0.36mJ energy of the unseeded pulses drops to 0.25mJ when injection seeding occurs. This reduction in pulse energy was due to spatial hole burning effects which left the regions of gain, inaccessible to the seeded single longitudinal mode cavity mode, unused. To eliminate spatial hole burning the twisted mode technique was implemented on the slave oscillator by placing quarter wave plates on either side of the Nd:YAG rod. However, due to the extra intracavity loss introduced by the addition of the waveplates no increase in output pulse energy was obtained from the laser.

Thirdly, the time delay from the switching of the cavity Q to the emergence of the seeded pulse is less than that for the unseeded case. Siegman[3] for instance has shown that the build up time T_b of a Q-switched pulse has the following dependence on the initial photon density (photons per mode) inside the laser cavity;

$$T_b = \frac{\tau_c}{r-1} \times \log_e\left(\frac{n_{ss}}{n_i}\right) \tag{8.1}$$

where τ_c = cold cavity decay time

r = pumping ratio (ratio of the population inversion just after opening the Q-switch to the population inversion at laser threshold)

n_{ss} = steady state photon density that would result if the laser was CW with a pumping ratio r

n_i = initial cavity photon density.

In the unseeded case the pulse builds up from the initial spontaneous emission noise in the cavity ($n_i \approx 1$). However, the presence of an externally injected coherent light beam into the resonant mode of the cavity provides an initial photon density many times greater than the spontaneous emission noise level from which the seeded Q-switched pulse can grow. To show the influence of injected signal level on pulse build up time for the injection seeded holosteric laser system equation (8.1) was re-expressed in terms of the change in pulse build up time for various intracavity injected power levels, P_{inj}, relative to the build up time for $P_{inj} = 1nW$.

$$T_b(P_{inj}=1nW) - T_b(P_{inj}) = \frac{\tau_c}{r-1} \times \log_e\left(\frac{P_{inj}}{1nW}\right) \tag{8.2}$$

In figure 8.9 $T_b(P_{inj}=1nW) - T_b(P_{inj})$ has been plotted as a function of $\log_e\left(\frac{P_{inj}}{1nW}\right)$ for the case of the Q-swiched laser operating 1.65 (r=1.65) times above threshold. Using a value for the cavity decay time τ_c of 5.1ns (see ref. 1), the predicted value for $\tau_c/(r-1)$ is 7.85ns. From figure 8.9 the gradient of the best-fit-line to the data is (7.7±0.8)ns in good agreement with this predicted value.

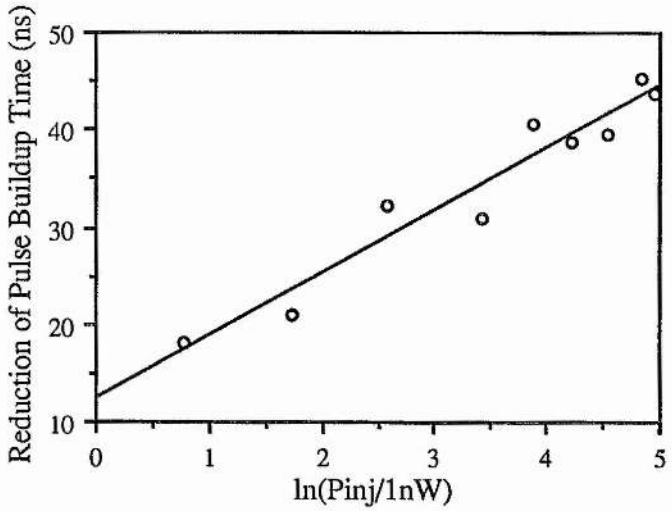

Figure 8.9. Dependence of seeded pulse build build up time on injected intracavity power.

With a seeding beam power of 0.2mW incident on the high reflectivity (0.02% power transmission) mirror of the slave laser, a frequency difference of up to ±150MHz between the slave and master oscillator frequencies could be tolerated before multilongitudinal mode operation of the slave laser occurred. It is worth noting that, in contrast to steady state injection locking to be described in section 8.3, no convenient analytical expression exists which defines the frequency offset range over which injection seeding occurs. In the transient injection seeding case the unwanted axial modes of the slave cavity still exist inside the resonator, all be it at a very much reduced level compared to the seeded mode. Therefore, an injection seeding range can only be defined somewhat arbitrarily as the frequency detuning range over which the output power ratio between the seeded axial mode and the unseeded adjacent mode always exceeds some preset value[4,5]. Detailed investigations of mode competition, frequency output and pulse build-up under various conditions of injection seeding have, however, been carried out by various research groups for specific laser systems using numerical techniques to solve the coupled equations describing the oscillating fields of the axial modes and the population density in the gain medium[6,5,7].

The passive stability of this all solid state laser system was such that stable injection seeding behaviour could be maintained for periods of several minutes before thermal expansion of the laser cavities pushed their cavity mode frequencies outside the 300MHz seeding range. For longer term seeding stability some form of active laser cavity length control would be required. Several techniques for active stabilisation of injection seeded laser systems are available such as locking the master and slave cavity frequencies to a passive reference cavity[5], controlling the slave laser cavity length to transmission of the seeding beam through the slave cavity[8], using a polarization sensitive feedback system to maintain cavity matching[9], minimizing the Q-switched pulse build up time[10] and locking the cavities using a fast phase locked loop[11].

8.3 Injection Locking

In the injection seeding process described above the small injected signal from the master laser merely preferentially assists pulse build up of one of the slave laser's own axial modes. Injection locking may be regarded as a refinement of this process where by the injected signal from the master oscillator completely suppresses the free running oscillation frequency of the slave cavity, forcing the slave to operate at the master oscillator frequency. True injection locking of Q-switched lasers has been demonstrated by Buczek et al[12] and Lachambre et al[7] but Lachambre showed both theoretically and experimentally that injection locking of such high gain, short pulse lasers required prohibitively large injection signal levels and could tolerate only small frequency detuning between master and slave oscillators.

Injection locking of CW laser oscillators has also been successfully demonstrated as far back as 1966 when, in a heroic experiment, Stover and Steier injection locked two He-Ne gas lasers[13]. The ability to precisely define the output phase and frequency of a high power CW laser oscillator by injecting a small, high purity signal from a low power, frequency stable master oscillator opens up a host of exciting possibilities. For instance a number, N, of high power oscillators each with output power P, could be injection locked by a common master oscillator and their outputs coherently combined to give a total output power of N^2P. This high power output beam would essentially have the same spectral and spatial purity of the original master oscillator beam[14,15,16,17].

Another possibility is to steer the output beam from a parallel array of phase locked lasers. By altering the phase offset between individual lasers the maxima in the far field interference pattern can be steered. This is analogous to beam steering in radio frequency and microwave phased array radar. At present beam steering of phase locked arrays in the optical domain is limited to low power semiconductor diode laser arrays consisting of only a few active stripes[18,19]. Multiple injection locked bulk holosteric lasers could perhaps provide a higher power phase steerable beam with better spatial quality.

Finally the possibility exists for creating an optical Fourier synthesizer. The desired phase locked Fourier components could be generated by sum- and difference-frequency mixing the outputs from a group of phase coherent, injection locked lasers. By controlling the relative phases and frequencies spacings of the combined beams optical pulses could be created with tailored temporal shapes and durations. Hansch[20] has proposed an optical Fourier synthesizer which combines six optical frequency harmonics to generate sub-femtosecond optical pulses. Recently work carried out by his research group (Mukai et al[21])in Germany has demonstrated the feasibility of this proposal by synthesizing 8.4ns and 5ns pulses from combs of 3 and 5 Fourier components respectively with an intercomponent frequency spacing of 38MHz.

8.3.1 Basic Injection Locking Theory

An understanding of the injection locking mechanism can be obtained by considering the regenerative amplifier model of the laser oscillator shown in figure 8.10. Although a linear cavity is illustrated here the analysis applies equally well to ring resonators.

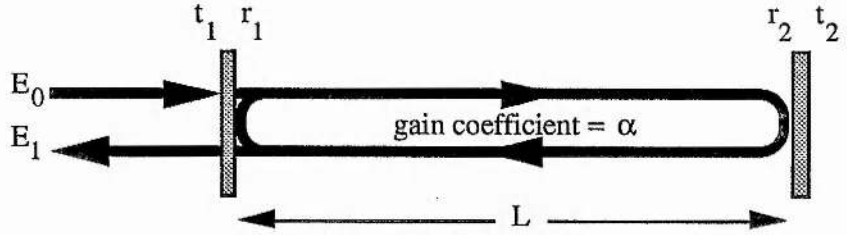

Figure 8.10 A simple model of a linear cavity regenerative optical amplifier. The field amplitude reflectivities and transmissions of the two mirror are represented by r and t respectively. E_0 is the injected field and E_1 is the net output field from the amplifier.

The output field, E_1, from the regenerative amplifier is composed of two portions, namely the reflection of the input field from the first mirror and a leakage component of the intracavity circulating field. This can be expressed mathematically as[22]

$$\frac{E_1}{E_0} = \frac{r_1 - r_2 e^{2\alpha L} e^{-i\phi}}{1 - r_1 r_2 e^{2\alpha L} e^{-i\phi}} = \frac{1}{r_1} \times \frac{r_2^2 - r_1 r_2 e^{2\alpha L} e^{-i\phi}}{1 - r_1 r_2 e^{2\alpha L} e^{-i\phi}} \qquad (8.3)$$

where $\phi = 4\pi L/\lambda = 4\pi L\nu/c$ is the cavity round trip phase shift. The frequency of the input field can be rewritten in terms of the resonance frequency, ν_q, of the q-th cavity mode and so the phase shift becomes

$$\phi = 2\pi \times \frac{2L}{c}(\nu_q + \Delta\nu) = q2\pi + 2\pi \frac{\Delta\nu}{\Delta\nu_{fsr}} \tag{8.4}$$

where $\Delta\nu$ is the frequency difference between the input field frequency and the resonance frequency of the q-th cavity mode, and $\Delta\nu_{fsr}$ is the cavity free spectral range. Substituting now for ϕ in equation (8.3) gives

$$\frac{E_1}{E_0} = \frac{1}{r_1} \times \frac{r_2^2 - r_1 r_2 e^{2\alpha L} \exp(-i2\pi\Delta\nu/\Delta\nu_{fsr})}{1 - r_1 r_2 e^{2\alpha L} \exp(-i2\pi\Delta\nu/\Delta\nu_{fsr})} \tag{8.5}$$

For very small detunings, $\Delta\nu$, of the input field's frequency from the resonance frequency of the amplifier cavity, equation (8.5) simplifies to

$$\frac{E_1}{E_0} = \frac{1}{r_1} \times \frac{r_2^2 - r_1 r_2 e^{2\alpha L}(1 - i2\pi\Delta\nu/\Delta\nu_{fsr})}{1 - r_1 r_2 e^{2\alpha L}(1 - i2\pi\Delta\nu/\Delta\nu_{fsr})} \tag{8.6}$$

This is the regenerative amplitude gain experienced by a small injected signal oscillating close to a resonant mode of the cavity. However, under injection locking conditions, the regenerative amplifier gain is such that oscillation threshold has been passed. Thus the question to be addressed is what is the residual regenerative amplitude gain experienced by a small externally injected signal of frequency close to the frequency of the lasing cavity mode ? Under steady state oscillation conditions the overall cavity round trip gain, $r_1 r_2 e^{2\alpha L}$, clamps at a value of unity and so this "saturated" regenerative amplitude gain for the small injected signal is

$$\frac{E_1}{E_0} = \frac{1}{r_1} - i\frac{\Delta\nu_{fsr}}{2\pi\Delta\nu} \cdot \frac{r_2^2 - 1}{r_1} \tag{8.7}$$

giving a "saturated" regenerative power gain for the injected signal of

$$\frac{I_1}{I_0} = \left(\frac{1}{r_1}\right)^2 + \left(\frac{\Delta\nu_{fsr}}{2\pi\Delta\nu}\right)^2 \cdot \left(\frac{r_2^2 - 1}{r_1}\right)^2 \tag{8.8}$$

As the injected signal frequency is tuned closer and closer to the laser oscillation frequency ($\Delta\nu \rightarrow 0$) the regenerative gain increases rapidly. At some small but finite value of detuning, $\Delta\nu$, the regeneratively amplified intensity of the injected signal will approach the intensity of the free running oscillator. This now large amplified injected signal begins to steal gain from the free running mode until the free running laser mode is eventually driven below threshold. At this point the laser is said to be injection locked. Just as gain saturation effects limited the intensity of the free running laser mode these same effects limit the regeneratively amplified injected signal to a similar intensity value over the injection locked regime.

The frequency bandwidth or "locking range" over which injection locking occurs can be estimated from equation (8.8). If I_{osc} is the free running laser intensity measured outside the cavity then from the above argument, locking will occur when $I_1 \geq I_{osc}$. From equation (8.8) this is

$$I_0\left\{\left(\frac{1}{r_1}\right)^2 + \left(\frac{\Delta\nu_{fsr}}{\Delta\omega}\right)^2 \cdot \left(\frac{r_1^2 - 1}{r_1}\right)^2\right\} \geq I_{osc} \tag{8.9}$$

$$\Rightarrow \left|\frac{\Delta\nu_{fsr}}{\Delta\omega} \cdot \left(\frac{1-r_1^2}{r_1}\right)\right| \geq \sqrt{\left(\frac{I_{osc}}{I_0} - \frac{1}{r_1^2}\right)}$$

$$\Rightarrow |\Delta\omega| \leq \Delta\nu_{fsr} \cdot \left(\frac{1-r_1^2}{r_1}\right) \cdot \sqrt{\frac{I_0 r_1^2}{(I_{osc} r_1^2 - I_0)}} \tag{8.10}$$

This amount of detuning can be tolerated on either side of cavity resonance and so the full injection locking capture range is twice equation (8.10)

$$\text{Injection Locking Bandwidth (FWHM)} \quad |\Delta\nu| \leq \frac{\Delta\nu_{fsr}}{\pi}\left(\frac{1-r_1^2}{r_1}\right)\cdot\sqrt{\frac{I_0 r_1^2}{(I_{osc}r_1^2 - I_0)}} \qquad (8.11)$$

If the reflectivities of the two cavity mirrors are the same ($r_1=r_2=r$) then using the following expression for the cold cavity FWHM linewidth[23], $\Delta\nu_{1/2}$

$$\Delta\nu_{1/2} = \frac{\Delta\nu_{fsr}}{\pi}\cdot\frac{1 - r^2}{r} \qquad (8.12)$$

the FWHM injection locking range given by equation (8.11) reduces to

$$\text{Injection Locking Bandwidth (FWHM)}\ \Delta\nu \leq \Delta\nu_{1/2}\sqrt{\frac{I_0 r^2}{(I_{osc}r^2 - I_0)}} \qquad (8.13)$$

To gain an idea of the magnitude of the locking range for practical laser systems, consider the following two examples

	He-Ne GAS LASER	HOLOSTERIC Nd:YAG LASER
cavity length	50cm	5cm
free spectral range, $\Delta\nu_{fsr}$	300MHz	3GHz
mirror amplitude reflectivity r_1	$\sqrt{0.99}$	$\sqrt{0.99}$
mirror amplitude reflectivity, r_2	1	1
oscillator output power, I_{osc}	10mW	10mW
injected signal power, I_0	1mW	1mW
injection locking range, $\Delta\nu$	**320kHz**	**3.2MHz**

The small size of these practical injection locking ranges places stringent demands on laser stability and highlights the main difficulty which has until now prevented the technique of injection locking from being exploited. However, with the advent of holosteric lasers with their inherent frequency stability and larger injection locking ranges by virtue of their short, high Q cavities, laser injection locking of bulk lasers is becoming a more attractive proposition[24,25].

8.3.2 Initial Work on Injection Locking of Two CW Holosteric Nd:YAG Lasers

The relative frequency stability of a few MHz recorded between the two semi-breadboarded CW, end pumped, intracavity etalon holosteric lasers indicated that it might be possible to injection lock these two laser under optimum conditions. A simple injection locking experiment was constructed in which the output beam of one laser was passed through an optical isolator and directed through the output coupler of the second laser via a 50% beam splitter. The frequencies of these combined beams were monitored using the scanning confocal interferometer. Working at night when the acoustic noise in the laboratory was at a minimum, the frequency of the slave laser was slowly scanned by means of its piezo mounted output mirror. Occasionally fleeting glimpses of interference fringes between the two combined laser beams were observed when the laser mode frequencies monitored on the scanning confocal interferometer were seen to coincide. Although the presence of observable interference fringes between the two beams is not conclusive proof of injection locking it is very unlikely, given the relative frequency stability of the two separate lasers, that static interference fringes could be generated in the absence of injection locking.

After moving to a laboratory which had a more stable and quieter environment and improving the passive stability of the two lasers, a second injection locking experiment was set up as illustrated in figure 8.11. In this experiment the radio frequency beat signal generated between the two lasers outputs was detected using a 3GHz bandwidth avalanche

photodiode (BPW28). This time when the output frequency of the slave laser frequency was altered to reduce the frequency difference between the two lasers, the heterodyne beat signal was seen to decrease steadily and then abruptly vanish at around 3MHz. Continuing

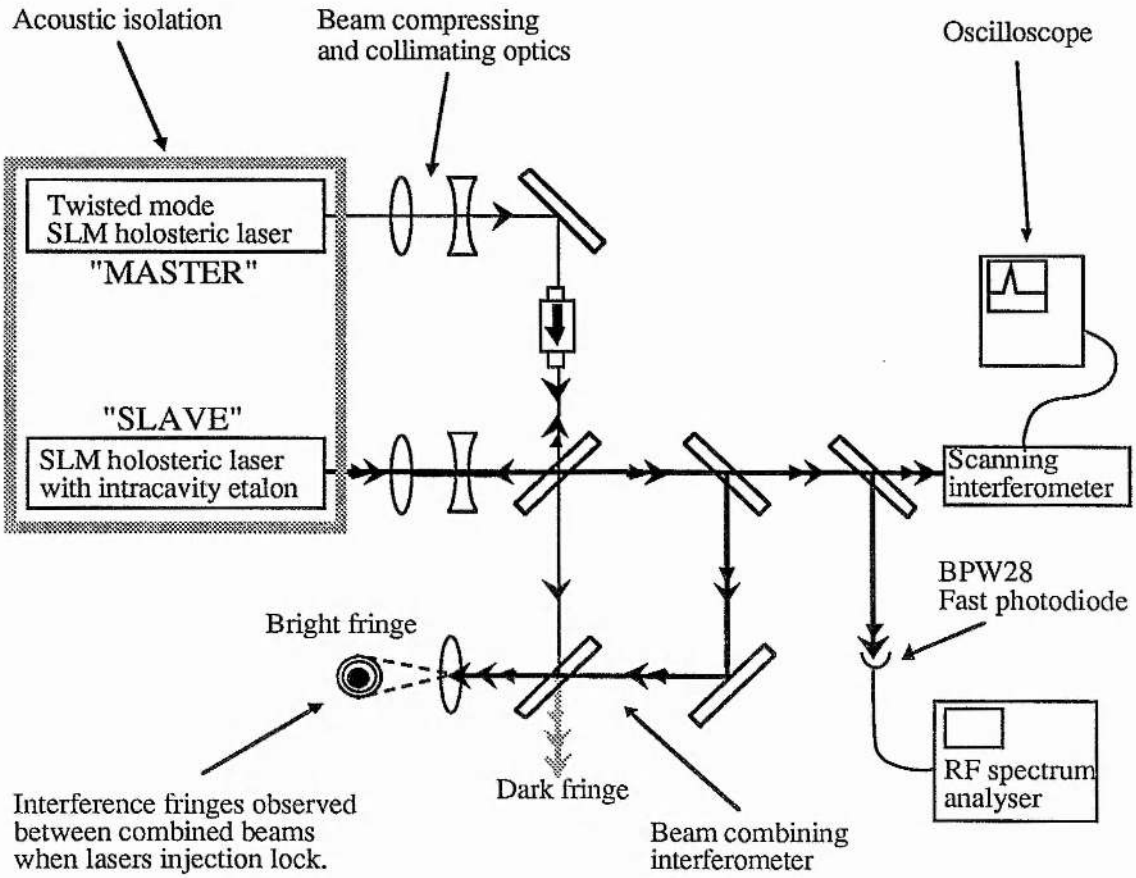

Figure 8.11. Schematic representation of the injection locking experiment.

to adjust the slave frequency in the same direction brought a sudden reappearance of the heterodyne beat signal again starting at 3MHz. During the frequency scanning process no mode hopping was observed on the scanning confocal interferometer display. Coincident with the disappearance of the heterodyne signal interference fringes could be seen in the combined beam output. This evidence strongly suggests that the lasers were injection locked. Injection locking could be sustained for one or two seconds before laser frequencies drifted apart due to thermal expansion of the laser cavities.

Using the following parameters for the slave laser and injected power the injection locking range was calculated from equation (8.11) to be 11.1MHz. The discrepancy between this theoretical prediction and the experimentally measured value of 6MHz may be due to poor spatial mode matching of the injection beam into the slave cavity mode. Although this initial injection locking work looks promising the experiment requires

cavity length	5cm
cavity free spectral range, $\Delta\nu$	3GHz
Output coupler amplitude reflectivity, r_1	$\sqrt{0.985}$
slave output power, I_{osc}	7mW
master injected power, I_o	2.8mW

significant improvements such as better long term laser frequency stability and the development of an active servo systems to maintain the lasers within the injection locking range and to stabilise the optical path lengths in the beam combining interferometer.

8.4 Frequency Stabilisation By Resonant Optical Feedback.

In conventional injection locking, described in the previous section, frequency control and linewidth reduction of the slave laser emission is achieved by injecting the slave cavity with a weak, narrow linewidth signal from a master laser. An interesting alternative to this scheme was proposed and demonstrated by D. Hjelme and co-workers[26] in 1987, for frequency stabilising semiconductor diode lasers, in which the laser is self-injection locked by a spectrally filtered portion of its own output beam. This technique, known as resonant optical feedback locking, has proved to be easily implemented and very effective for frequency stabilising semiconductor diode lasers, producing linewidths in the region of a few tens of kilohertz[27,28,29,30].

In resonant optical feedback locking, the weak, spectrally filtered optical feedback is provided by an on resonance, narrow linewidth (relative to the cold cavity linewidth of the laser), passive optical resonator. There are several possible optical geometries which can be used to provide the desired feedback characteristics of optical feedback only over a narrow frequency range. The most commonly used scheme, shown in figure 8.12, employs an off-axis confocal optical cavity. This arrangement gives automatic mode matching between the laser cavity and passive resonator and allows only the leakage field from the on resonance cavity to be fed back. Thus the laser sees optical feedback only when the laser frequency matches the reference cavity resonance and so the laser 'optically self-locks' to the resonance of the feedback cavity. For stable operation of this system it is also necessary to control the phase of the optical feedback signal relative to the phase of the laser output beam. This can be simply achieved by varying the optical path length between laser and feedback cavity by means of a beam steering mirror mounted on a piezoceramic element or a tiltable glass plate inserted into the beam.

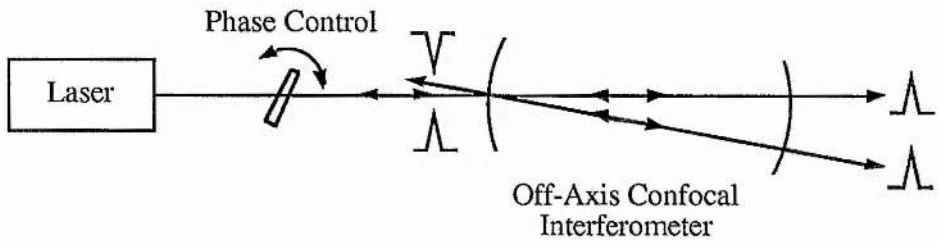

Figure 8.12. Off-axis confocal interferometer used for resonant optical feedback locking.

For resonant optical feedback to achieve line narrowing of the source laser, the linewidth of the feedback cavity should be smaller than that of the laser cavity[31,32].,This requirement has so far limited the application of the technique to semiconductor diode lasers. These lasers tend to have very low finesse cavities and so it is simple to construct an external passive cavity of much higher finesse to provide the optical feedback. However, with the development of the ultra high finesse optical resonator used in this work and the inherent frequency stability of diode laser pumped solid state lasers, we are

now in the novel position of being able to apply the resonant optical feedback technique to a solid state laser system.

As mentioned in section 7.1.3 our ultrahigh finesse optical cavity is non-confocal and so must be used on axis for mode matching purposes. Thus an alternative geometry to the conventional off axis feedback cavity scheme must be used. The novel optical layout developed to overcome this difficulty is shown in figure 8.13. A third mirror, M3 (identical to M1), and a 50% beam splitter, BS, are added to the optical cavity to form a Michelson interferometer in conjunction with the input mirror, M1, of the cavity. With the cavity in the off-resonance state the optical path length of Michelson arm M3-BS is adjusted by means of the piezo transducer, to null the output from port I (i.e.. the directly reflected signal from the cavity input mirror now appears at port II) of the Michelson interferometer. When the optical cavity is now brought into resonance (by changing the laser frequency appropriately) only the leakage field from the cavity emerges at port I of the Michelson interferometer to be returned to the laser.

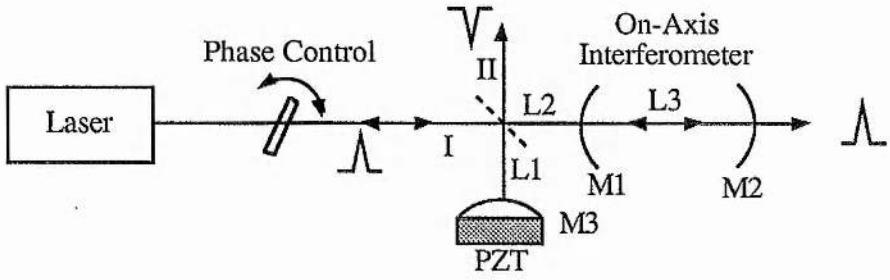

Figure 8.13. Combined Michelson/Fabry-Perot interferometer to enable on-axis, non-confocal interferometers to be used for resonant optical feedback locking.

The theoretical reflection response of this coupled Michelson/Fabry-Perot interferometer was determined using flow diagram analysis[33] and found to be

$$\frac{I_{refl}}{I_{in}} = \left[2A^2 + B^2 + R^2B^2 - 2A^2\cos(\delta) + 2AB\cos(\Delta) - 2RAB\cos(\Delta-\delta) - 2AB\cos(\Delta+\delta) + 2RAB\cos(\Delta) - 2RB^2\cos(\delta)\right] / \left[1 + R^2 - 2R\cos(\delta)\right] \quad (8.14)$$

where R = mirror power reflectivity

R_{bs} = beamsplitter power reflectivity

$A = \sqrt{R}(1-R_{bs})$

$B = \sqrt{R}R_{bs}$

δ = round trip phase shift off-set from resonance of Fabry-Perot cavity

$= 2kL_3$

Δ = phase difference between the two arms of the Michelson interferometer.

$= 2k(L_2 - L_1)$

$k = 2\pi/\lambda$

In figure 8.14, equation (8.14) has been plotted as a function of the round trip phase shift off-set from resonance of the Fabry-Perot cavity, δ, for various phase differences, Δ, between the two arms of the Michelson interferometer. As can be seen from this figure,

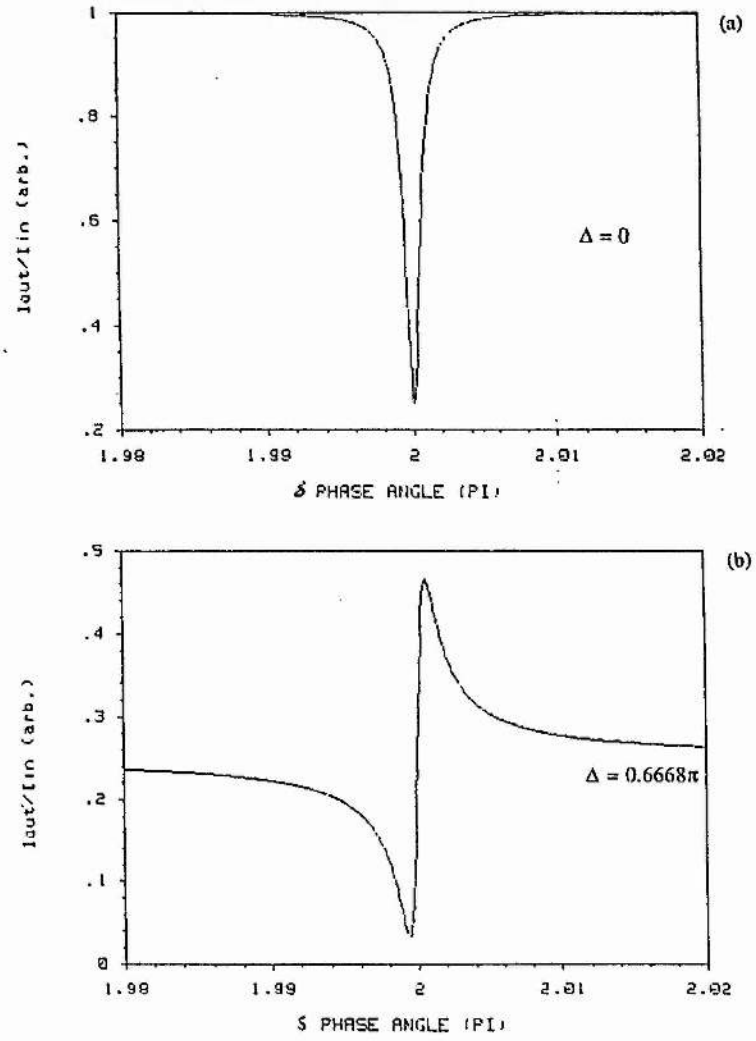

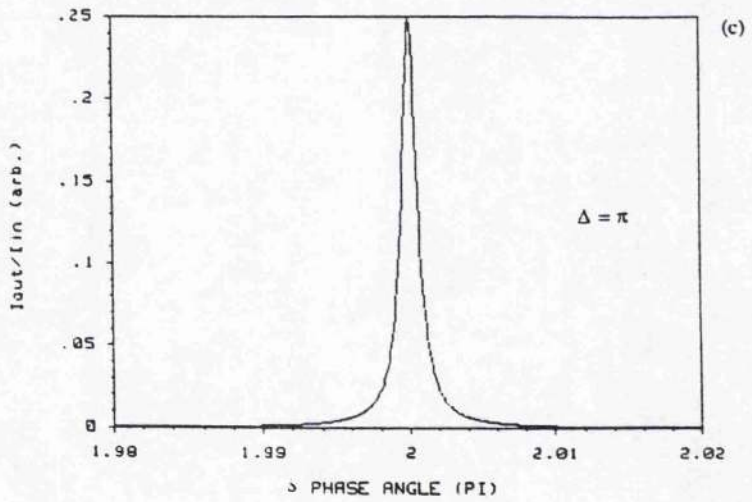

Figure 8.14. The calculated reflection response of the coupled Michelson/Fabry-Perot interferometer as a function of the round trip phase shift off-set from resonance of the Fabry-Perot cavity, δ, for various phase differences, Δ, between the two arms of the Michelson interferometer. (a) $\Delta=0$, (b) $\Delta=0.6668\pi$, (c) $\Delta=\pi$.

when the phase difference between the two arms of the Michelson interferometer is π radians, the combined Michelson/Fabry-Perot interferometer does indeed display the desired reflection characteristic of feedback signal only on resonance.

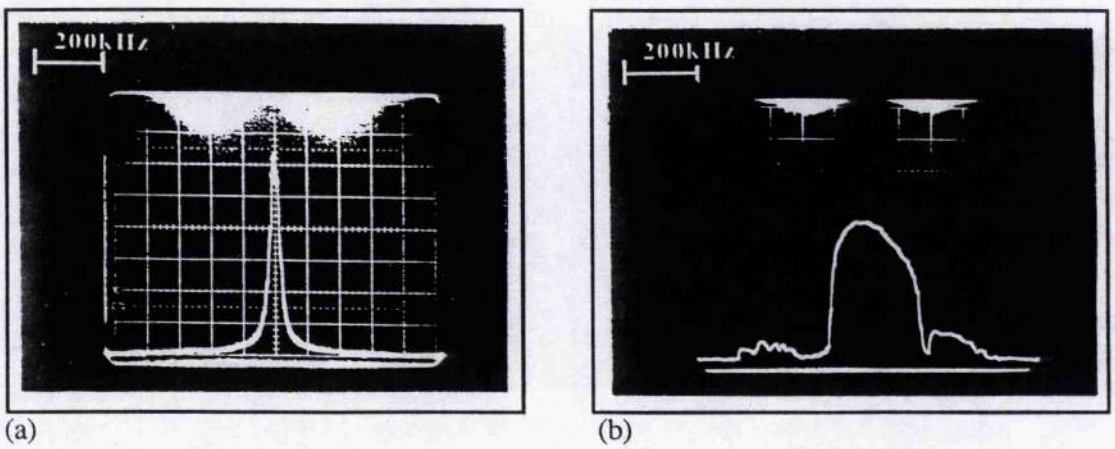

(a) (b)

Figure 8.15. The transmission function of the reference cavity as a function of laser frequency for (a) no optical feedback and (b) resonant optical feedback.

Using this arrangement a preliminary investigation of the effect of resonant optical feedback on a single longitudinal mode, diode laser pumped Nd:YAG laser has been carried out. To show the existence of some form of optical locking effect, the transmission characteristics of the reference cavity were recorded as the laser frequency was scanned through a resonance of the reference cavity. Frequency scanning was accomplished by applying a ramp voltage to the piezoceramic mount of laser output coupler. Figure 8.15(a) shows the characteristic Airy transmission function of the reference cavity obtained with no optical feedback present. The full-width-at-half-maximum frequency width of this fringe was calculated to be 38kHz. With optical feedback applied to the laser an apparently much broader reference cavity transmission fringe was obtained. See figure 8.15(b). This indicates that for a portion of the frequency scan, the laser frequency stopped changing with applied voltage to the frequency transducer and became locked to the resonance frequency of the reference cavity. In this case, the full-width-at-half-maximum of the transmission fringe was found to be 223kHz, a factor of 5.9 greater than the no feedback case, indicating that the laser frequency was indeed locked to the cavity resonance over some finite locking range.

Two difficulties have been encountered with this system which have so far prevented controlled, long term resonant optical feedback frequency locking of the diode pumped Nd:YAG laser. Firstly, the phase and intensity of the signal reflected from the reference cavity are very dependent on the phase difference between the arms of the Michelson interferometer. Any instabilities in the arm lengths of the Michelson interferometer will therefore have a profound effect on the stability of the optical feedback locking process. Secondly, the optical locking range is small being only 100-200kHz wide. Although the free running linewidth and frequency drift of the diode pumped Nd:YAG laser are small it is still extremely difficult to maintain the laser frequency within this narrow frequency locking range for longer than a second. The first difficulty may be overcome by using a different feedback geometry which dispenses with the Michelson interferometer section and makes use of the reference cavity transmission signal as shown in figure 8.16.

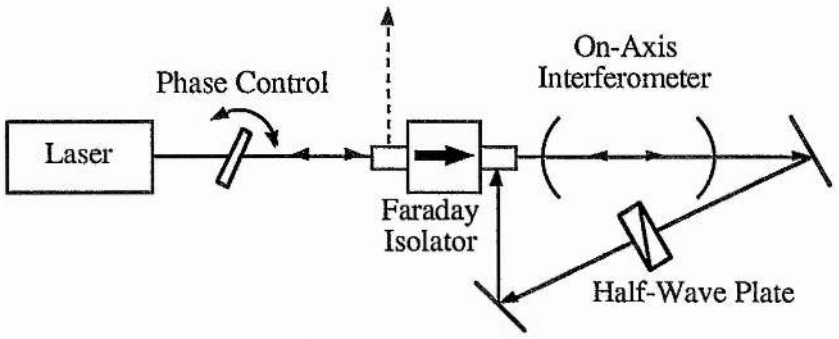

Figure 8.16. An alternative geometry for optical feedback locking using the transmission signal of a resonant cavity.

To maintain the laser frequency within the feedback locking range a hybrid locking scheme, combining both optical feedback and convention electronic feedback, could be used. For instance, Pound-Drever locking could provide a loose frequency lock to the centre of the reference cavity resonance. The addition of optical feedback to the system may reduce the bandwidth requirements of the electronic servo. Such a double feedback method has been applied to an AlGaAs diode laser by Shin and Ohtsu[34]. In their system the diode laser was electronically servoed to a high finesse cavity using side-of-fringe locking, whilst resonant optical feedback was provided by a separate, off-axis confocal cavity. With optical feedback alone the laser linewidth was measured to be a few kilohertz. This was further reduced to 7Hz when electronic locking was added to the feedback network.

Whether or not resonant optical feedback locking will prove to be a useful complementary technique for frequency stabilisation of solid state lasers, such as diode pumped solid state lasers, remains to be shown. For these lasers, much work still requires to be done to investigate self-locking ranges and the frequency and intensity noise spectra of the laser output under the influence of resonant optical feedback for different levels of feedback and for reference cavities of various linewidths.

8.5 References

1 Norrie C. J., "Holosteric Nd:YAG Lasers", Ph.D. Thesis, University of St. Andrews, (1990)

2 Norrie C. J., Sinclair B. D., Gallaher N., Sibbett W., Dunn M. H., "Measurement of Frequency Sweep in a Quasi-CW Diode Laser Array and its Implications for Pumping Solid State Lasers", J. Mod. Opt. **36**(1) 1 (1989)

3 Siegman A. E., "Lasers", University Science Books, chap 26, p.1012 (1986)

4 Park Y. K., Giuliani G., Byer R. L., "Stable Single Axial Mode Operation of an Unstable Resonator Nd:YAG Oscillator by Injection Locking", Opt. Lett. **5**(3) 96 (1980)

5 Park Y. K., Giuliani G., Byer R. L., "Single Axial Mode Operation of a Q-Switched Nd:YAG Oscillator by Injection Seeding", IEEE J. Quant. Elec. **QE-20**(2) 117 (1984)

6 Ganiel U., Hardy A., Treves D., "Analysis of Injection Locking in Pulsed Dye Laser Systems", IEEE J. Quant. Elec. **QE-12**(11) 704 (1976)

7 Lachambre J. L., Lavigne P., Otis G., Noel M., "Injection Locking and Mode Selection in TEA-CO_2 Laser Oscillators", IEEE. J. Quant. Elec. **QE-12** 756 (1976)

8 Teets R. E., "Feedback to Maintain Injection Locking of Nd:YAG Lasers", IEEE. J. Quant. Elec. **QE-20** 326 (1984)

9 Esherick P., Owyoung A., "Polarization Feedback Stabilization of an Injection Seeded Nd:YAG Laser", J. Opt. Soc. Am. B **4** 41 (1987)

10 Rahn L. A., "Feedback Stabilization of an Injection Seeded Nd:YAG Laser", Appl. Opt. **24** 940 (1985)

11 Fry E. S., Hu Q., Li X., "Single Frequency Operation of an Injection Seeded Nd:YAG Laser in High Noise and Vibration Environments", Appl. Opt. **30** 1015 (1991)

12 Buczek C. J., Freiberg J., Skolnik M. L., "Laser Injection-Locking", Proc. IEEE. **61** 1411 (1973)

13 Stover H. L., Steier W. H., "Locking of Laser Oscillators by Injected Light", Appl. Phys. Lett. **8** 91 (1966)

14 Chow W. W., "Phase Locking of Lasers by an Injected Signal", Opt. Lett. **7**(9) 417 (1982)

15 Man C. N., Brillet A., "Injection Locking of Argon-Ion Lasers", Opt. Lett. **9**(8) 333 (1984)

16 Veldkamp W. B., Leger J. R., Swanson G. J., "Coherent Summation of Laser Beams Using Binary Phase Gratings", Opt. Lett. **11**(5) 303 (1986)

17 Kerr G. A., Hough J., "Coherent Addition of Laser Oscillators for use in Gravitational Wave Antennas", Appl. Phys. B **49**(5) 491 (1989)

18 Scifres D. R., Streifer W., Burnham R. D., "Beam Scanning and Wavelength Modulation with Branching Waveguide Stripe Injection Lasers", Appl. Phys. Lett. **33** 616 (1978)

19 Moriki K., Ohnishi Y., Hattori T., "Seering Operation of Optical Beam Scanner With Semiconductor Waveguides", Elec. Lett. **27**(5) 450 (1991)

20 Hansch T. W., "A Proposed Sub-Femtosecond Pulse Synthesizer Using Separate Phase-Locked Laser Oscillators", Opt. Comm. **80**(1) 71 (1990)

21 Mukai T., Wynands T. W., Hansch T. W., "Subfemtosecond Pulse Generation", QELS 1992

22 Siegman A. E., "Lasers", University Science Books, chap 11, p.422 (1986)

23 Verdayen J., "Laser Electronics", 2nd Edition (1989)

24 Harrison J., Rines G. A., Moulton P. F., Leger J. R., "Coherent Summation of Injection-Locked, Diode-Pumped Nd:YAG Lasers", Opt. Lett. **13**(2) 111 (1988)

25 Nabors C. D., Farinas A. D., Day T., Yang S. T., Gustafson E. K., Byer R. L., "Injection Locking of a 13W CW Nd:YAG Laser", Opt. Lett. **14**(21) 1189 (1989)

26 Hjelme D. R., Mickelson A. R., Hollberg L., Dahmani B., "Novel Optical Frequency Stabilisation of Semiconductor Lasers", Digest of Topical Meeting on Semiconductor Lasers (Optical Society of America, Washigton, DC, 1987), pp.15-18

27 Barwood G. P., Gill P., Rowley W. R. C., "Optically Narrowed Diode Laser For Rb Saturation Spectroscopy", J. Mod. Opt. **37**(4) (1990)

28 Hemmerich A., McIntyre D. H., Schropp D., Meschede D., Hansch T. W., "Optically Stabilised Narrow Linewidth Semiconductor Laser For High Resolution Spectroscopy", Opt. Comm. **75**(2) 118 (1990)

29 Lee W. D., Campbell J. C., Brecha R. J., Kimble H. J., "Frequency Stabilisation Of An External-Cavity Diode Laser", Appl. Phys. Lett. **57**(21) 2181 (1990)

30 Simonsen H. R., "Frequency Noise Reduction Of Visible InGaAlP Laser Diodes By Different Optical Feedback Methods", IEEE J. Quant. Elec. **29**(3) 877 (1993)

31 Li H., Telle H. R., "Efficient Frequency Noise Reduction of GaAlAs Semiconductor Lasers By Optical Feedback From An External High-Finesse Resonator", IEEE J. Quant. Elec. **25**(3) 257 (1989)

32 Laurent P. H., Clairon A., Bréant C. H., "Frequency Noise Analysis Of Optically Self-Locked Diode Lasers", IEEE J. Quant. Elec. **25**(6) 1131 (1989)

33 Dunn M. H., "Use Of Flow Graph Analysis Of Optical Cavities", Appl. Opt. **10**(6) 1393 (1971)

34 Sin C. H., Ohtsu M., "Stable Semiconductor Laser With A 7Hz Linewidth By An Optical-Electrical Double-Feedback Technique", Opt. Lett. **15**(24) 1455 (1990)

Chapter 9

GENERAL CONCLUSIONS

Diode laser pumped solid state lasers have now become a well established technology and have proved their worth in almost all facets of laser research. However, in the field of ultranarrow linewidth optical sources, the unique features of diode laser pumped solid state lasers have perhaps, had the most profound influence. For instance, commercial diode pumped solid state lasers are now available "off the shelf", with free running, short term linewidths in the region of a few kilohertz at power levels of hundreds of milliwatts. With the application of the advanced frequency stabilisation techniques, this already narrow linewidth can be dramatically reduced to the millihertz level, well below the Schawlow-Townes limit and approaching the ultimate, shot noise limit.

In this thesis the design, construction, evaluation and development of an all solid state, narrow linewidth laser source has been presented. The work has ranged from the initial characterisation of the fibre coupled, GaAlAs diode laser arrays used as the pump sources for the solid state Nd:YAG laser, through all the steps required to produce an actively stabilised, narrow linewidth laser and the application of the resulting frequency stabilised source to injection seeding and injection locking of other solid state lasers.

The rate equation based numerical model of the basic Nd:YAG laser proved an invaluable tool in the development and understanding of the end-pumped laser, allowing the effects of varying different cavity parameters on the laser performance to be explored without the expense and time involved in prototyping. The model enabled optimisation of the optical characteristics of the laser cavity and provided useful confirmation of the performance of the first experimental devices.

Two methods of longitudinal mode selection, namely the intracavity etalon and the twisted mode, were applied to the diode laser pumped Nd:YAG laser with equal success. In the case of the etalon mode selector it was shown that a simple, uncoated fused silica

etalon could provide just enough intracavity loss to allow only one longitudinal mode to oscillate in the laser. The design criteria for such etalons were presented and used to calculate the optimum etalon thickness and surface reflectivity for mode selection in the diode pumped laser.

Contrary to expectations the twisted mode laser brought no benefit in terms of increased output power compared to the etalon mode selector. This was thought to be due to the increased intracavity losses from the large number of additional intracavity surfaces introduced into the low gain laser cavity. It is expected however, that this technique should be more efficient than an etalon mode selector in higher gain laser systems. From the experimental analysis of the twisted mode laser it was apparent that the mode selecting ability of the technique was very sensitive to any residual birefringence in the gain medium. It is therefore important to the success of this method of mode control that high quality birefringence free gain crystals are used and that mechanical stress and internal thermal gradients are minimised to avoid stress induced birefringence effect in the gain medium.

The relative free running frequency stability between a pair of single longitudinal mode diode laser pumped Nd:YAG lasers was investigated. By carefully isolating these lasers from environmental noise using a small, custom built anechoic chamber the linewidth of the optical heterodyne signal between the two free running lasers was reduced from tens of megahertz to around 10kHz measured on a millisecond time scale. This narrow linewidth was comparable to those observed by other research groups in this field. Although these Nd:YAG lasers exhibited excellent short term frequency stability, their longer term frequency drift was significant. To reduce this frequency drift, future cavity designs should be constructed from low expansion materials, carefully thermally compensated and hermetically sealed. Active temperature of the lasers' environment could also be considered.

To achieve additional line narrowing of the diode laser pumped Nd:YAG laser output spectrum the active frequency stabilisation technique of Pound-Drever locking was applied

to one of the Nd:YAG lasers. A mathematical description of the Pound-Drever stabiliser was presented and a phasor model was developed which provided useful insight into the operation of this system. The ultimate limit of active stabilisation in reducing laser linewidth was also discussed.

One area where frequency stabilised CW lasers are increasingly being used is in axial mode selection (injection seeding) and frequency control (injection locking) of higher power pulsed and CW laser oscillators by injected signal. Having developed a practical narrow linewidth laser, the system was successfully used as a master oscillator to injection seed a 0.25mJ diode laser pumped Q-switched Nd:YAG slave laser.

The availability of compact, efficient lasers of exceptionally high spectral purity extends the opportunities for progress in many research areas such as coherent optical communications, LIDAR remote sensing, gravitational wave detectors, laser isotope separation and the next generation of optical frequency standards based on laser cooled atoms or ions. It is now conceivable that many of the more sophisticated and refined techniques, such as phase locked loops, phased array beam steering, wave form and pulse synthesis, etc. commonly used at radio and microwave frequencies will also be applied to the optical region of the spectrum.

APPENDIX A

DERIVATION OF POUND-DREVER DISCRIMINANT

Outlined in this appendix is a mathematically more rigorous derivation of the error signal produced by the Pound-Drever locking scheme and serves to complement the analysis described in Chapter 6. The analysis extends that of Houssin et al[1] to include a small frequency modulation (FM) noise component and derives an expression for the error signal resulting from this noise term.

Consider the instantaneous frequency, ν_i, of the optical field incident on the reference cavity as consisting of the fundamental laser frequency, ν and two FM contributions. One FM term is imposed on the laser beam by the extracavity optical phase modulator and is of the form

$$\Delta\nu_m \cos \omega_m t \tag{A1}$$

where $\Delta\nu_m$ = Maximum frequency excursion from ν. The other FM term represents a single frequency component of the laser noise spectrum and is given by

$$\Delta\nu_n \cos \omega_n t \tag{A2}$$

Thus the instantaneous frequency ν_i, of the laser output is

$$\nu_i = \nu + \Delta\nu_m \cos \omega_m t + \Delta\nu_n \cos \omega_n t \tag{A3}$$

The instantaneous phase , Φ_i, of the optical field is just

$$\frac{1}{2\pi}\frac{d\Phi_i}{dt} = \nu_i = \nu + \Delta\nu_m \cos \omega_m t + \Delta\nu_n \cos \omega_n t \tag{A4}$$

Φ_i is obtained through integration and is

$$\Phi_i = \omega t + \mathcal{M} \sin \omega_m t + \mathcal{N} \sin \omega_n t \tag{A5}$$

The terms $\mathcal{M} = \Delta\nu_m/\nu_m$ and $\mathcal{N} = \Delta\nu_n/\nu_n$ are the modulation indices for the imposed rf modulation and noise induced modulation respectively. Using this expression for instantaneous phase, the modulated laser field may be written in complex notation as

$$E = E_o e^{j(\omega t + \mathcal{M} \sin \omega_m t + \mathcal{N} \sin \omega_n t)} \tag{A6}$$

Expanding in terms of Bessel functions of the first kind of order p, equation A6 becomes

$$E = E_o e^{j\omega t} \left[\sum_{p=-\infty}^{\infty} J_p(\mathcal{M}) e^{jp\omega_m t} \right] \left[\sum_{p=-\infty}^{\infty} J_p(\mathcal{N}) e^{jp\omega_n t} \right] \tag{A7}$$

In laser stabilisation schemes involving rf reflection locking the amount of rf modulation is kept small such that its modulation index $\mathcal{M}<1$. In this circumstance the Bessel function expansion of the rf modulation may be replaced, to a good approximation, by the first three terms of the summation of order p = -1, 0, +1.

To keep the calculation within manageable proportions it is necessary at this stage to impose the limitation that the modulation index of the FM noise term $\mathcal{N}<1$. With this assumption the Bessel function of the FM noise term may also be replaced by the three terms p = -1, 0, +1 in the summation . With the aid of the Bessel function identity

$$J_{-1}(X) = -J_1(X) \tag{A8}$$

equation A7 becomes

$$E = E_o \Big\{ J_o(\mathcal{M})J_o(\mathcal{N})\, e^{j\omega t} + J_o(\mathcal{M})J_1(\mathcal{N})\, e^{j(\omega+\omega_n)t} - J_o(\mathcal{M})J_1(\mathcal{N})\, e^{j(\omega-\omega_n)t}$$

$$+J_o(\mathcal{N})J_1(\mathcal{M})\, e^{j(\omega+\omega_m)t} + J_1(\mathcal{M})J_1(\mathcal{N}) e^{j(\omega+\omega_m+\omega_n)t} - J_1(\mathcal{M})J_1(\mathcal{N})\, e^{j(\omega+\omega_m-\omega_n)t}$$

$$- J_o(\mathcal{N})J_1(\mathcal{M})\, e^{j(\omega-\omega_m)t} - J_1(\mathcal{M})J_1(\mathcal{N})\, e^{j(\omega-\omega_m+\omega_n)t} + J_1(\mathcal{M})J_1(\mathcal{N})\, e^{j(\omega-\omega_m-\omega_n)t} \Big\}$$

(A9)

After interacting with the reference cavity the optical field returning from the cavity will be

$$E = E_o \Big\{ J_o(\mathcal{M})J_o(\mathcal{N})g(\omega)\, e^{j\omega t} + J_o(\mathcal{M})J_1(\mathcal{N})g(\omega+\omega_n)\, e^{j(\omega+\omega_n)t}$$

$$- J_o(\mathcal{M})J_1(\mathcal{N})g(\omega-\omega_n)\, e^{j(\omega-\omega_n)t} + J_o(\mathcal{N})J_1(\mathcal{M})g(\omega+\omega_m)\, e^{j(\omega+\omega_m)t}$$

$$- J_o(\mathcal{N})J_1(\mathcal{M})g(\omega-\omega_m)\, e^{j(\omega-\omega_m)t} + J_1(\mathcal{M})J_1(\mathcal{N})g(\omega+\omega_m+\omega_n)\, e^{j(\omega+\omega_m+\omega_n)t}$$

$$- J_1(\mathcal{M})J_1(\mathcal{N})g(\omega+\omega_m-\omega_n)\, e^{j(\omega+\omega_m-\omega_n)t} - J_1(\mathcal{M})J_1(\mathcal{N})g(\omega-\omega_m+\omega_n)\, e^{j(\omega-\omega_m+\omega_n)t}$$

$$+ J_1(\mathcal{M})J_1(\mathcal{N})g(\omega-\omega_m-\omega_n)\, e^{j(\omega-\omega_m-\omega_n)t} \Big\}$$

A(10)

where

$$g(\omega) = r_1 - \frac{t_1^2 r_2\, e^{-j(\omega)\tau}}{1 - r_1 r_2 e^{-j(\omega)\tau}} \qquad \text{(A11)}$$

is the lineshape function of the optical cavity in reflection mode, with

r_1 , r_2 = amplitude reflectivities of cavity mirrors (assumed real),

t_1 = amplitude transmission of cavity input mirror (assumed real),

τ = cavity round trip time = 2L/c.

Detection of the optical field E_r by the photodiode produces an average photocurrent proportional to $E_r E_r^*$. Of this current, only components oscillating at or near ω_m contribute to the generation of the final error signal. In practice these terms may be selected by a suitable bandpass filter centred at ω_m. The output, I, for such a filter will be

$$I \propto E_o^2 J_o(\mathcal{M}) J_o^2(\mathcal{N}) J_1(\mathcal{M}) \left\{ g(\omega)\, g(\omega+\omega_m)^*\, e^{-j(\omega_m t)} - g(\omega)\, g(\omega-\omega_m)^*\, e^{j(\omega_m t)} \right\}$$

$$+ E_o^2 J_o(\mathcal{M}) J_o(\mathcal{N}) J_1(\mathcal{M}) J_1(\mathcal{N}) \left\{ g(\omega+\omega_n)\, g(\omega+\omega_m)^*\, e^{-j(\omega_m-\omega_n)t} \right.$$

$$- g(\omega+\omega_n)\, g(\omega-\omega_m)^*\, e^{j(\omega_m+\omega_n)t} - g(\omega-\omega_n)\, g(\omega+\omega_m)^*\, e^{-j(\omega_m+\omega_n)t}$$

$$+ g(\omega-\omega_n)\, g(\omega-\omega_m)^*\, e^{j(\omega_m-\omega_n)t} + g(\omega)\, g(\omega+\omega_m+\omega_n)^*\, e^{-j(\omega_m+\omega_n)t}$$

$$- g(\omega)\, g(\omega+\omega_m-\omega_n)^*\, e^{-j(\omega_m-\omega_n)t} - g(\omega)\, g(\omega-\omega_m+\omega_n)^*\, e^{j(\omega_m-\omega_n)t}$$

$$\left. + g(\omega)\, g(\omega-\omega_m-\omega_n)^*\, e^{j(\omega_m+\omega_n)t} \right\} + \text{complex conjugate} \qquad \text{(A12)}$$

Subsequent demodulation of this signal with $\sin \omega_m t$ in the double balanced mixer performs the function $\sin A \cos B = \frac{1}{2}[\sin(A-B) + \sin(A+B)]$. Again filtering of the balanced mixer output is used to reject signals at $2\omega_m t$ leaving only dc and low frequency terms. The error signal emanating from the filter output is thus

$$I \propto E_o^2 J_o(\mathcal{M}) J_o^2(\mathcal{N}) J_1(\mathcal{M})\, t_1^2\, r_1\, r_2 \left[\frac{2 \sin \omega\tau}{D} - \frac{\sin(\omega+\omega_m)\tau}{D^+} - \frac{\sin(\omega-\omega_m)\tau}{D^-} \right]$$

$$+ E_o^2 J_o(\mathcal{M}) J_o(\mathcal{N}) J_1(\mathcal{M}) J_1(\mathcal{N})\, t_1^2\, r_1\, r_2 \left\{ 2\frac{r_1\, r_2}{D^+} \sin(\omega_n t) + 2\frac{r_1\, r_2}{D^-} \sin(\omega_n t) \right.$$

$$-\frac{1}{D^{+}}\sin\left[(\omega+\omega_m)\tau+\omega_n t\right]+\frac{1}{D^{+}}\sin\left[(\omega+\omega_m)\tau-\omega_n t\right]$$

$$-\frac{1}{D^{-}}\sin\left[(\omega-\omega_m)\tau+\omega_n t\right]+\frac{1}{D^{-}}\sin\left[(\omega-\omega_m)\tau-\omega_n t\right]$$

$$+2\frac{r_1 r_2}{D^{n+}}\sin(\omega_n t)+2\frac{r_1 r_2}{D^{n-}}\sin(\omega_n t)$$

$$+2\frac{1}{D^{n+}}\sin\left[(\omega+\omega_n)\tau-\omega_n t\right]-2\frac{1}{D^{n-}}\sin\left[(\omega-\omega_n)\tau+\omega_n t\right]$$

$$-r_1 r_2\left(\frac{1}{D^{++}}+\frac{1}{D^{+-}}+\frac{1}{D^{-+}}+\frac{1}{D^{++}}\right)\sin(\omega_n t)$$

$$-\frac{1}{D^{++}}\sin\left[(\omega+\omega_m+\omega_n)\tau-\omega_n t\right]+\frac{1}{D^{+-}}\sin\left[(\omega+\omega_m-\omega_n)\tau+\omega_n t\right]$$

$$-\frac{1}{D^{-+}}\sin\left[(\omega-\omega_m+\omega_n)\tau-\omega_n t\right]+\frac{1}{D^{--}}\sin\left[(\omega-\omega_m-\omega_n)\tau+\omega_n t\right]$$

$$+2\frac{1}{D}\sin\left[\omega\tau+\omega_n t\right]-2\frac{1}{D}\sin\left[\omega\tau-\omega_n t\right]$$

$$-4\frac{r_1 r_2}{D}\sin(\omega_n t)\Big\}+\text{higher order terms} \qquad \text{(A13)}$$

where

$$D = 1+r_1^2 r_2^2 - 2r_1 r_2\cos(\omega\tau),$$

$$D^{+} = 1+r_1^2 r_2^2 - 2r_1 r_2\cos(\omega+\omega_m)\tau,$$

$$D^{-} = 1+r_1^2 r_2^2 - 2r_1 r_2\cos(\omega-\omega_n)\tau,$$

$$D^{n+} = 1+r_1^2 r_2^2 - 2r_1 r_2\cos(\omega+\omega_h)\tau,$$

$$D^{n-} = 1+r_1^2 r_2^2 - 2r_1 r_2\cos(\omega-\omega_h)\tau,$$

$$D^{++} = 1 + r_1^2 r_2^2 - 2r_1 r_2 \cos(\omega+\omega_m+\omega_n)\tau,$$

$$D^{+-} = 1 + r_1^2 r_2^2 - 2r_1 r_2 \cos(\omega+\omega_m-\omega_n)\tau,$$

$$D^{-+} = 1 + r_1^2 r_2^2 - 2r_1 r_2 \cos(\omega-\omega_m+\omega_n)\tau,$$

$$D^{--} = 1 + r_1^2 r_2^2 - 2r_1 r_2 \cos(\omega-\omega_m-\omega_n))\tau$$

An analysis of this system transfer function is given in Chapter 6.

References

1 Houssin M., Jardino M., Gely B., Desaintfuscien M., "Design and Performance of a Few-kiloHertz Linewidth Dye Laser Stabilised by Reflection in an Optical Resonator", Opt. Lett.**13** 823 (1988)

PUBLICATIONS

C. J. Norrie, B. D. Sinclair, N. Gallaher, W. Sibbett and M. H. Dunn, "Measurement of Frequency Sweep in a Quasi-CW Diode Laser Array and its Implications for Pumping Solid State Lasers.", J. Mod. Opt. 36(1) 1-6 (1989)

N. Gallaher, C. J. Norrie, B. D. Sinclair, M. H. Dunn and W. Sibbett, "All-Solid State Injection Seeded Pulsed Laser System", CLEO Conference Proceedings 1989, paper TUJ29

C. J. Norrie, B. D. Sinclair, N. Gallaher, M. H. Dunn and W. Sibbett, "Single Frequency Operation of a Diode Laser Array, Transverse Pumped, Q-Switched Nd:YAG Laser.", Electron. Letts. 25(17) 1115-1116 (1989)